

# Soils and Rocks

An International Journal of Geotechnical  
and Geoenvironmental Engineering



Volume 35, N. 1  
January-April 2012

**Soils and Rocks is an International Journal of Geotechnical and  
Geoenvironmental Engineering published by**

**ABMS - Brazilian Association for Soil Mechanics and Geotechnical Engineering  
Av. Prof. Almeida Prado, 532, - Prédio 11 - Térreo  
Cidade Universitária, 05508-901 São Paulo, SP  
Brazil**

**SPG - Portuguese Geotechnical Society  
LNEC, Avenida do Brasil, 101  
1700-066 Lisboa  
Portugal**



*Issue Date: June 2012*

*Issue: 350 copies and 2150 online-distributed copies*

*Manuscript Submission: For review criteria and manuscript submission information, see Instructions for Authors at the end.*

*Disclaimer:* The opinions and statements published in this journal are solely the author's and not necessarily reflect the views or opinions of the publishers (ABMS and SPG). The publishers do not accept any liability arising in any way from the opinions, statements and use of the information presented.

*Copyright:* Authors and ABMS-Brazilian Society of Soil Mechanics and Geotechnical Engineering

# ***SOILS and ROCKS***

An International Journal of Geotechnical and Geoenvironmental Engineering

**Editor** André Pacheco de Assis - University of Brasilia, Brazil

**Co-editor** Manuel Matos Fernandes - University of Porto, Portugal

## **Executive Board**

Márcio Muniz de Farias  
*University of Brasilia, Brazil*

João Maranhã  
*LNEC, Portugal*

Fernando Schnaid  
*Federal Univ. Rio Grande do Sul, Brazil*

Jorge Almeida e Sousa  
*University of Coimbra, Portugal*

## **Associate Editors**

H. Einstein  
*MIT, USA*

John A. Hudson  
*Imperial College, UK*

Kenji Ishihara  
*University of Tokyo, Japan*

Michele Jamiolkowski  
*Studio Geotecnico Italiano, Italy*

Willy A. Lacerda  
*COPPE/UFRRJ, Brazil*

E. Maranhã das Neves  
*Lisbon Technical University, Portugal*

Nielen van der Merve  
*University of Pretoria, South Africa*

Paul Marinos  
*NTUA, Greece*

James K. Mitchell  
*Virginia Tech., USA*

Lars Persson  
*SGU, Sweden*

Harry G. Poulos  
*University of Sidney, Australia*

Niek Rengers  
*ITC, The Netherlands*

Fumio Tatsuoka  
*Tokyo University of Science, Japan*

Luiz González de Vallejo  
*UCM, Spain*

## **Editorial Board Members**

Claudio P. Amaral  
*Pontifical Catholic University, Brazil*

Roberto F. Azevedo  
*Federal University of Viçosa, Brazil*

Nick Barton  
*Consultant, Norway*

Richard J. Bathurst  
*Royal Military College of Canada*

Frederick Baynes  
*Baynes Geologic Ltd., Australia*

Pierre Bérest  
*LCPC, France*

Omar Y. Bitar  
*IPT, Brazil*

Helmut Bock  
*Q+S Consult, Germany*

Laura Caldeira  
*LNEC, Portugal*

Tarcisio Celestino  
*University of São Paulo-SC, Brazil*

António S. Cardoso  
*University of Porto, Portugal*

Chris Clayton  
*University of Surrey, UK*

António G. Coelho  
*Consultant, Portugal*

Nilo C. Consoli  
*Federal Univ. Rio Grande do Sul, Brazil*

António G. Correia  
*University of Minho, Portugal*

Rui M. Correia  
*LNEC, Portugal*

Roberto Q. Coutinho  
*Federal Univ. of Pernambuco, Brazil*

António P. Cunha  
*LNEC, Portugal*

R. Jonathan Fannin  
*University of British Columbia, Canada*

Sérgio A.B. Fontoura  
*Pontifical Catholic University, Brazil*

Roger Frank  
*LCPC, France*

Maria H.B.O. Frascá  
*IPT, Brazil*

Carlos D. Gama  
*Lisbon Technical University, Portugal*

Vinod Garga  
*University of Ottawa, Canada*

Nuno Grossmann  
*LNEC, Portugal*

Richard J. Jardine  
*Imperial College, UK*

Milton Kanji  
*University of São Paulo, Brazil*

Peter Kaiser  
*Laurentian University, Canada*

Luís L. Lemos  
*University of Coimbra, Portugal*

José V. Lemos  
*LNEC, Portugal*

Serge Leroueil  
*University of Laval, Canada*

Robert Mair  
*University of Cambridge, UK*

Mario Manassero  
*Politécnico di Torino, Italy*

He Manchao  
*CUMT, China*

João Marcelino  
*LNEC, Portugal*

António C. Mineiro  
*New University of Lisbon, Portugal*

Teruo Nakai  
*Nagoya Inst. Technology, Japan*

Claudio Olalla  
*CEDEX, Spain*

Antonio M.S. Oliveira  
*University of Guarulhos, Brazil*

Ennio M. Palmeira  
*University of Brasilia, Brazil*

José D. Rodrigues  
*Consultant, Portugal*

R. Kerry Rowe  
*Queen's University, Canada*

Rodrigo Salgado  
*University of Purdue, USA*

Sandro S. Sandroni  
*Consultant, Brazil*

Luís R. Sousa  
*University of Porto, Portugal*

Fabio Taioli  
*University of São Paulo, Brazil*

Luis Valenzuela  
*Consultant, Chile*

Ricardo Vedovello  
*São Paulo Geological Institute, Brazil*

Andrew Whittle  
*MIT, USA*

Jorge G. Zornberg  
*University of Texas/Austin, USA*

Lázaro V. Zuquette  
*University of São Paulo, Brazil*

*Soils and Rocks* publishes papers in English in the broad fields of Geotechnical Engineering, Engineering Geology and Geo-environmental Engineering. The Journal is published in April, August and December. Subscription price is US\$ 90.00 per year. The journal, with the name “Solos e Rochas”, was first published in 1978 by the Graduate School of Engineering, Federal University of Rio de Janeiro (COPPE-UFRJ). In 1980 it became the official magazine of the Brazilian Association for Soil Mechanics and Geotechnical Engineering (ABMS), acquiring the national character that had been the intention of its founders. In 1986 it also became the official Journal of the Brazilian Association for Engineering Geology and the Environment (ABGE) and in 1999 became the Latin American Geotechnical Journal, following the support of Latin-American representatives gathered for the Pan-American Conference of Guadalajara (1996). In 2007 the journal acquired the status of an international journal under the name of Soils and Rocks, published by the Brazilian Association for Soil Mechanics and Geotechnical Engineering (ABMS), Brazilian Association for Engineering Geology and the Environment (ABGE) and Portuguese Geotechnical Society (SPG). In 2010, ABGE decided to publish its own journal and left the partnership.

*Soils and Rocks*

1978,	1 (1, 2)
1979,	1 (3), 2 (1,2)
1980-1983,	3-6 (1, 2, 3)
1984,	7 (single number)
1985-1987,	8-10 (1, 2, 3)
1988-1990,	11-13 (single number)
1991-1992,	14-15 (1, 2)
1993,	16 (1, 2, 3, 4)
1994-2010,	17-33 (1, 2, 3)
2011,	34 (1, 2, 3, 4)
<b>2012,</b>	<b>35 (1,</b>

ISSN 1980-9743

CDU 624.131.1

**SOILS and ROCKS**

An International Journal of Geotechnical and Geoenvironmental Engineering

**Publication of****ABMS - Brazilian Association for Soil Mechanics and Geotechnical Engineering****SPG - Portuguese Geotechnical Society****Volume 35, N. 1, January-April 2012****Table of Contents***XXVII MANUEL ROCHA LECTURE**Design with Geo-Hazards: An Integrated Approach from Engineering Geological Methods*

L.I. González de Vallejo

1

*ARTICLES**Considerations on the Probability of Failure of Mine Slopes*

A.S.F.J. Sayão, S.S. Sandroni, S.A.B. Fontoura, R.C.H. Ribeiro

31

*Electroosmosis in the Remediation of Tropical Soils Contaminated with Cadmium:**Effect of the Incubation Time*

R.Z. Velten, D.C. Lima, M.P.F. Fontes, C.A.B. Carvalho

39

*Modification of a Lateritic Soil with Lime and Cement:**An Economical Alternative for Flexible Pavement Layers*

F.H.M. Portelinha, D.C. Lima, M.P.F. Fontes, C.A.B. Carvalho

51

*Evaluation of Direct Shear Tests on Geogrid Reinforced Soil*

A.S.F.J. Sayão, A.C.C.F. Sieira

65

*Developing a System for Down-Hole Seismic Testing Together with the CPTU*

O.P.M. Vitali, R.A.A. Pedrini, L.P.R. Oliveira, H.L. Giacheti

75

*Estimating Young Moduli in Sands from the Normalized  $N_{60}$  Blow Count*

A. Conde de Freitas, M. Pacheco, B.R. Danziger

89

*The Influence of the Relative Density of Sands in SPT and CPT Correlations*

J.M.S. Souza, B.R. Danziger, F.A.B. Danziger

99



## **XXVII Manuel Rocha Lecture**



**Manuel Rocha** (1913-1981) was honoured by the Portuguese Geotechnical Society with the establishment of the Lecture Series bearing his name in 1984.

Having completed the Civil Engineering Degree at the Technical University of Lisbon (1938) he did post-graduate training at MIT. He was the driving force behind the creation of the research team in Civil Engineering that would lead to the foundation of the National Laboratory for Civil Engineering (LNEC), in Lisbon. He was Head of LNEC from 1954 to 1974 and led it to the cutting edge of research in Civil Engineering.

His research work had great impact in the area of concrete dams and rock mechanics. He was the 1<sup>st</sup> President of the International Society for Rock Mechanics and organized its 1<sup>st</sup> Congress in Lisbon (1966). He did consultancy work in numerous countries. He was Honorary President of the Portuguese Geotechnical Society, having promoted with great commitment the cooperation between Portugal and Brazil in the area of Civil Engineering, and member of the National Academy of Sciences of the USA. Recognized as a brilliant researcher, scientist and professor, with a sharp, discerning intellect allied to a prodigious capacity for work and management, he was truly a man of many talents.



Prof. **L.I. González de Vallejo**, Emeritus Professor of Geological Engineering at Universidad Complutense de Madrid (UCM). PhD (UCM) and MSc (Imperial College). Director of the MSc Courses in Geological Engineering at UCM (1990-2008). He has dedicated his professional career in geological engineering to teaching, research and consulting, and he has conducted a large number of geological and geotechnical investigations in Spain and Central and South America. Has written 150 scientific papers and five books. Past-Chairman of the JTC3 on Education and Training of FedGIS. He has been invited to present the 2<sup>nd</sup> Ing. Mariano Ruiz Vazquez Memorial Lecture at the Academy of Engineering of Mexico (2007) and the 27<sup>th</sup> Manuel Rocha Lecture at the Portuguese Geotechnical Society and the Associação de Geotécnicos Antigos Alunos da UNL (2010).

**Soils and Rocks**  
**v. 35, n. 1**



# Design with Geo-Hazards: An Integrated Approach from Engineering Geological Methods

L.I. González de Vallejo

**Abstract.** An engineering geological approach to analysed geo-hazards affecting engineering and planning design decisions is presented. The methodological procedures include hazard identification, hazard assessment, site vulnerability, economic cost, environmental impact, risk assessment, social acceptability, decision analysis and engineering design criteria. The practical application of the Engineering Geological Methodology (EGM) is shown in several case studies: dam safety problems due to slope instability and induced seismicity during reservoir filling; seismic hazard assessment in regions with insufficient seismic data and tectonic information; and large scale geo-hazards due to giant landslides and related tsunamis. The EGM approach can provide fundamental criteria for engineering decisions and territorial planning. Social acceptability should be included in the decision analysis being evaluated according with the hazard level of the geological process and the corresponding risk of the affected elements. Examples of geo-hazards and their social acceptability are presented.

**Keywords:** geological hazards, engineering geology, hazard assessment, risk assessment, Canary Islands, Tenerife.

## 1. Introduction

One of the first books to include geological factors as a conditioning parameter of urban and infrastructure planning was Ian McHarg's pioneering "Design with Nature" published in 1969. Now, more than 40 years later, these criteria are well established and concern for the environment has grown to the point where it is one of the most critical factors in any large engineering project. However, it is only in recent times that natural hazards have been properly accounted for in engineering design and infrastructure planning. This concern is reflected in the title of this lecture: "Design with Geo-Hazards".

The approach presented here is based on engineering geological methods to provide solutions to the geo-hazards problems involved in engineering design decisions. Engineering Geology (EG) helps to reduce risk effectively, to design and build safer and more economical infrastructure, and to ensure environmental compatibility.

The term geological hazards -or geo-hazards- usually refers to earthquakes, landslides, volcanic eruptions or tsunami because of their catastrophic effects. However, there are also other minor damaging geo-hazards that have to be considered, such as those listed in Table 1. The effects of geo-hazards are usually accompanied by other related phenomena. Earthquakes can induce a variety of associated hazards such as ground shaking, surface deformation and faulting, liquefaction, landslides, rockfalls and tsunamis. Hydrometeorological hazards, such as floods or heavy rain, can also cause landslides, rockfalls, earth and debris flows on slopes. The nature of the geo-hazards and their consequences at a particular site should always be considered

when a large engineering or land planning project is undertaken.

One of the main applications of EG, as the science applied to the study and solution of problems produced by the interaction of the geological environment and human activity, is the evaluation, prevention and mitigation of geological hazards. Problems arising from the interaction between human activities and the geological environment make appropriate actions to balance natural conditions and land use with geological hazard prevention and mitigation methods that are essential at the planning stage. These actions should have as their starting point an understanding of geodynamic active processes and of the geomechanical behaviour of the ground.

Damage related to specific geological processes depends on:

- The speed, magnitude and extent of the process.
- Whether actions can be taken to control the process or protect elements exposed to its effects.

The effects of ground movements may be direct or indirect, short or long term or permanent. Some tectonic or isostatic processes develop on a geological time scale, what means that their effects cannot be considered on a human scale. Only certain processes, when they occur on an engineering or geotechnical scale, can be controlled by human action, such as landslides or rockfalls, erosion, subsidence and floods. Others, such as earthquakes, tsunamis, volcanic eruptions and large scale landslides are outside the scope of human control. Here the importance of considering the influence of Earth dynamic processes on the design and safety of engineering works and installations. The follow-

**Table 1** - Geological and meteorological processes which may cause risk (González de Vallejo & Ferrer, 2011).

Processes	Risk
External geo-dynamic processes	- Landslides and rock falls - Collapse and subsidence - Erosion - Expansivity and collapsibility of soils
Internal geo-dynamic processes	- Earthquakes and tsunamis - Volcanic activity - Diapirism
Meteorological processes	- Torrential rain and intense precipitation - Flooding and flash floods - Gully erosion processes - Hurricanes - Tornados

ing sections present fundamental aspects related to the evaluation of geological hazards for engineering projects.

## 2. Hazard, Risk and Vulnerability

In hazard studies specific terminology is used to define hazard, risk and vulnerability. The term “hazard” refers to any more or less violent process which may affect people or property; it is often taken to be synonymous with “risk”, although the two concepts are not the same. Hazard refers to the geological process, risk to the losses and vulnerability to damage. These concepts will be defined, according to how they are generally used.

Hazard,  $H$ , refers to the frequency with which a process occurs and its location. It is defined as the probability of occurrence of a potentially damaging phenomenon at a specified level of intensity or severity for a given time within a specific area (Varnes, 1984). To evaluate hazard, the following information is needed:

- Where and when the processes occurred in the past.
- Their intensity and magnitude.
- The areas where future processes may occur.
- The frequency of the occurrence.

This last point can only be estimated if the process timeframe is known (*e.g.* the return period for earthquakes or floods, from historical or instrumental data series), or for the triggering factors (*e.g.* the return period for rainfall that triggers landslides in a certain area).

Hazards, as it has been explained, can be defined as the probability of occurrence of a phenomenon of specific intensity within a given period, but can also be expressed using the return period  $T$  (years elapsing between two events or processes of similar characteristics), which is the inverse of the annual exceedance probability,  $P(a)$ :

$$T = 1/P(a) \quad (1)$$

The probability  $p$  that a specific intensity value (*e.g.* an acceleration value in the case of earthquakes) corresponding to an average return period  $T$  (years) will be exceeded during a specific time period  $t$  is expressed as:

$$p = 1 - \left(1 - \frac{1}{T}\right)^t \quad (2)$$

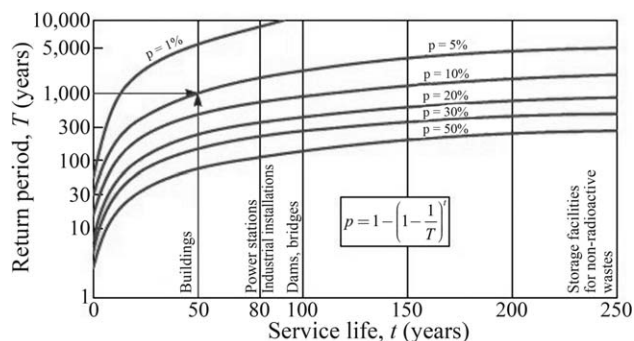
The time  $t$  (years) can be the service life of a dam or building, that is, the expected exposure time or useful life of the structure. Table 2 shows the service life of different installations; Fig. 1 gives the probability of exceedance curves as a function of this parameter and of the return period  $T$ .

The concept of risk,  $R$ , includes socio-economic considerations and is defined as the potential losses due to a specific natural phenomenon (human lives, direct and indirect economic losses, damage to buildings or structures, etc.). At the present time, the risk of earthquakes is the most widely developed. Seismic risk is defined as the expected losses that structures will suffer during the period they are exposed to seismic activity; this time period is known as the exposure time or service life of the structure, as has been mentioned above.

Risk is evaluated starting from the hazard corresponding to a particular process (cause) and the effects of this on the elements exposed to the hazard (consequences). These effects on the exposed elements (buildings, infrastructures, people, etc.) may be expressed by different pa-

**Table 2** - Service life of different installations ( $t$ ) (González de Vallejo & Ferrer, 2011).

Structure or installation	$t$ (years)
Storage of radioactive waste	10,000
Nuclear power stations	40-80
Dams	100-150
Bridges, tunnels and major infrastructure works	100
Storage of toxic waste	250
Conventional buildings and structures	50-70

**Figure 1** - Probability of exceedance ( $p$ ) of an event of known return period occurring in the service life of a structure (González de Vallejo & Ferrer, 2011).

parameters: vulnerability, losses, cost, exposure, etc. The risk and the hazard refer to a specified time period, and may be evaluated in either deterministic or probabilistic terms.

The risk can be calculated from the expression:

$$R = H \times V \times C \quad (3)$$

where  $H$  is the hazard of the process in question,  $V$  is the vulnerability of the elements exposed to the process (elements at risk) and  $C$  is the cost or value of these elements. As described above, the risk is expressed in losses (human or economic); in the expression above, these “unit” correspond to  $C$ , while  $H$  is a probability and  $V$  an adimensional parameter, as is explained below. The value of  $C$  can be expressed in either deterministic or probabilistic terms; if the latter, the risk will also be obtained in terms of probability.

If any of the factors is zero, the risk will be zero; this means that in a high hazard zone, the risk will be zero if there are no element exposed, or if the vulnerability of these is nil. People may increase the risk by occupying hazardous zones, affecting the intensity of the processes or triggering them and by constructing vulnerable buildings or structures. The risk can be reduced by reducing the hazard (acting on the process control factors where this is possible) or the vulnerability (acting on the elements exposed to the risk).

According to Smith (2001) risk can be defined as the probability that a hazard will occur and cause losses, and is evaluated from the expression:

$$R = P \times L_e \quad (4)$$

where  $P$  is the occurrence probability of the process, or hazard, and  $L_e$  the expected losses.

The product  $H \times V$  is known as specific risk and is defined as the level of losses expected during a given time period resulting from the occurrence of a specific process, expressed in terms of probability. In this case, a quantitative evaluation of losses cannot be made (Varnes, 1984). According to the UNESCO definitions, the risk can be evaluated as follows:

$$R = H \times V \times E \quad (5)$$

where  $E$  is the exposure of the elements at risk. Because of the difficulty of quantifying the variable  $E$  and considering that for some authors exposure is included in vulnerability (an element is not vulnerable if it is not exposed to risk), the expressions above are more appropriate, when the cost of either the exposed elements,  $C$ , or the expected losses,  $L_e$ , are considered directly for a specific occurrence.

Vulnerability,  $V$ , is the expected degree of damage or loss in an element or group of elements at risk resulting from the occurrence of a hazard of specific intensity or magnitude. It depends on the characteristics of the element considered (not on its economic value) and on the intensity of the phenomenon; it is usually evaluated on a scale from 0 (no damage) to 1 (total loss or destruction of the element) and from 0 to 100% damage.

In the case of seismic risk, the vulnerability of a structure or group of structures, or of whole urban area, is defined as its intrinsic predisposition to sustain damage if a seismic movement of a specific intensity occurs. This will depend on the structural design characteristic and on the intensity of the earthquake; it means that the vulnerability of a masonry building is higher than that of a concrete building during an earthquake. This parameter is usually defined through vulnerability functions that can be established from the damage or losses such processes have caused in the past and/or from the hypothetical potential damage these phenomena would cause were they to occur. In both cases, present-day measures to reduce or mitigate the potential damage have to be taken into account, as these reduce the vulnerability of the exposed elements.

### 3. Geological Engineering and Engineering Decisions

In geological engineering it is normal practice to estimate safety criteria by using a factor of safety  $FS$ , as a deterministic indicator of the relationship between the stabilizing and destabilizing forces (in a limit equilibrium situation  $FS = 1.00$ ). The factor of safety can be defined as the coefficient by which the ground shear strength must be reduced for a slope, excavation, foundation, etc. to reach a state of limit equilibrium (Morgenstern, 1991). The value chosen for this factor depends on how much is known about the ground strength parameters, hydrostatic pressures, potential shear surfaces and the magnitude of the external forces which act or may act on the ground (Hoek, 1991).

A satisfactory solution to the geological and geotechnical problems which may arise from interactions between the ground and the structures depends on the correct selection of geomechanical parameters, the application of the appropriate analytical tools and the choice of reasonable safety and acceptability criteria. Table 3 shows some acceptability criteria for different types of structures.

When geological processes may occur with potentially damaging results, these processes must be considered in the stability and safety of the project. Once the process has been identified (earthquake, flood, landslide, etc.) and the level of severity has been defined using parameters such as seismic acceleration, water height and speed, these parameters are integrated into the factor of safety calculation.

There are standards or regulations which specify the factor of safety, return period and other criteria that must be used depending on the project type and function. If there are no codes or specific safety requirements, the decision is usually left to the expert judgement or criteria of the designer. The following factors of safety are given as guidelines:

- For ground failure conditions:
  - Short-term engineering works with no structures involved (opencast mining, temporary slopes, etc. which do not form a supporting part of foundations or structures):  $1.2 \leq FS < 1.5$ .

- Long-term engineering works with no structures involved:  $FS \geq 1.5$ .
- Foundations and excavations involving structures:  $1.5 \leq FS \leq 3.0$ .
- The effects of a particular event that may affect an engineering structure due to a geo-hazard is usually related to the return period  $T$  of such an event. The following  $T$  values are suggested:
  - Conventional buildings and structures:  $100 \leq T \leq 500$  years.
  - Major structures, dams, bridges, significant buildings:  $T = 1,000$  years.
  - Critical facilities:  $1,000 \leq T \leq 10,000$  years or the equivalent of the recorded maximum historical intensity level.

When a geological process causing a potential hazard has been identified in terms of intensity and return period, then the probability  $p$  of this hazard being exceeded during the service life of the structure is calculated, using the following criteria:

- Major structures:  $p \leq 10\%$
- Critical facilities:  $p \leq 5\%$ .

Excluded from these criteria are some exceptional geological phenomena with extremely low probability, *e.g.* major tsunamis, large landslides or maximum potential earthquakes according to geological data.

#### 4. Geo-Hazard Assessment by Engineering Geological Methods

Engineering geology and geotechnical engineering are related terms that integrate knowledge from geological and engineering sciences and technologies with engineer-

ing and the environment in a wide range of activities. When a project has to be implemented in a particular region exposed to natural hazards, the engineering design has to consider a variety of concepts using the criteria needed to ensure safe and economical solutions.

Managing geological, statistical, social and engineering data is a complex task due to the different criteria, time and spatial scales used. Geological Engineering (GE) can provide a link between geo-scientific information and engineering requirements. This is possible because GE uses a language common to both engineers and geo-scientists and is based on a common geological and engineering background. A procedure based on practical experience that integrates geological and geo-engineering methods is described below to provide specific answers for engineering solutions when geo-hazards have to be considered. The procedure includes the following points:

1. Hazard identification: intensity, size and scale of the phenomenon.
2. Hazard assessment: frequency, probability and maximum potential event.
3. Site vulnerability evaluation.
4. Economic cost estimation.
5. Environmental impact assessment.
6. Risk assessment.
7. Social acceptability evaluation.
8. Decision analysis.
9. Engineering design criteria

Hazard assessment is usually carried out by deterministic and probabilistic methods. Deterministic methods conventionally adopt the maximum historical or characteristic event, which usually leads to a very conservative result. However, these methods do not provide the uncer-

**Table 3** - Acceptability criteria in relation to different types of engineering structures and excavations (modified from Hoek, 1991).

Engineering structures	Acceptability criteria
Soil slopes	$FS > 1.3$ for “temporary” slopes. $FS > 1.5$ for “permanent” slopes.
Rock slopes	$FS > 1.3$ for “temporary” slopes. $FS > 1.5$ with probability of failure of 10 to 15% may be acceptable for open pit mine slopes.
Earth dams	$FS > 1.5$ for full pool. $FS > 1.2$ for probable maximum flood with steady state seepage and $> 1.0$ for full pool with steady state seepage and maximum credible horizontal pseudostatic seismic loading.
Gravity dams	$FS$ against foundation failure $> 1.5$ for normal full pool operating conditions. $FS > 1.3$ for probable maximum flood. $FS > 1$ for extreme loading-maximum credible earthquake.
Arch dams	$FS$ against foundation failure $> 1.5$ for normal full pool operating conditions. $FS > 1.3$ for probable maximum flood.
Foundations	Bearing capacity failure should not be permitted for normal loading conditions. Differential settlement should be within limits specified by structural engineers.
Rock tunnels	$FS$ including the effects of reinforcement, should exceed 1.5 for sliding and 2.0 for falling wedges and blocks.

tainty or reliability of the characteristic event. Uncertainty evaluation is a high priority issue and also one of the main problems when dealing with geo-hazards.

Probabilistic methods can provide a quantitative value for uncertainties and there are different procedures available for probabilistic analysis. The Cornell method (Cornell, 1968) is widely used for probabilistic seismic hazard assessment (PSHA). An example of the application of this method is shown in Section 6.6. Other examples of PSHA applied to critical facilities in Spain are described by González de Vallejo (1994), and an example of its application to active fault hazard assessment for a dam in Portugal is given by Gomes Coelho (2005).

Logic tree methods can be a useful tool for hazard analysis quantification, giving a number of possible consequences resulting from an initial event. The sequence of subsequent events needs to be identified and the probability of occurrence quantified. An example of logic trees applied to uncertainty evaluation in slope stability analysis is shown in Fig. 26, Section 7.4 of this paper. Whitman (1984) presents several applications of this methodology and Bommer *et al.* (2005) apply logic trees to seismic hazard analysis.

The Monte Carlo simulation method is another useful probabilistic procedure for geo-hazard analysis. This simulates stochastic processes by repeated random sampling of inputs to an analysis model in proportion to their joint probability density function. A description and example applications of Monte Carlo simulation are shown in Nadim (2007). A comprehensive review of probabilistic methods for risk assessment and geotechnical applications is given by Fenton & Griffiths (2008).

Probabilistic and deterministic methods are both necessary for geo-hazard analysis. However, each of them has advantages and disadvantages as shown in Table 4. Although probabilistic methods are currently the most used, they are not a substitute for deterministic methods but are complementary to them (CETS, 1995).

The results of the hazard assessment can be used to evaluate site vulnerability of exposed elements, the economic and environmental consequences if failure occurs and for risk assessment.

Social acceptability can be expressed as the level of acceptance of risk from hazards which may cause loss of life and material or environmental damage in the short, medium or long term. Social acceptability is a subjective concept that depends on many different factors, including regional or country acceptability of risk in a particular project or facility. It can also be considerably affected if disasters occur such as dam failure or a nuclear power plant accident.

Given that social acceptance or rejection of the risks from natural hazards depends on multiple variables which may change over time in different circumstances, the level of social acceptability has to be quantified depending on parameters related to the hazard (probability) and their consequences. For example, the following descriptors for dam failure probability ( $p_f$ ) are used by the U.S. Bureau of Reclamation:

- Virtually certain  $p_f = 0.999$       Unlikely  $p_f = 0.1$
- Very likely  $p_f = 0.99$       Very unlikely  $p_f = 0.01$
- Likely  $p_f = 0.9$       Virtually impossible  $p_f = 0.001$
- Neutral  $p_f = 0.5$

These probability values do not include failure due to the effects of geo-hazards with probabilities lower than  $10^{-3}$ .

Whitman (1984) used annual probability of failure versus both costs and number of fatalities for a wide variety of project types, with the annual probability of failure of commercial aircraft around or lower than  $10^{-6}$ . Because people generally accept this type of transport as acceptable and safe, this threshold value can be considered as an acceptable risk by society.

On the other hand, in some European countries the probability of occurrence of a particular geo-hazard during the service life of the structure can be ranked in the following intervals:

**Table 4** - Some experts' opinions on using deterministic and probabilistic methods for seismic hazard assessment (modified from González de Vallejo, 1994).

	Deterministic	Probabilistic
Advantages	Appropriate if one has complete knowledge of the seismogenetic models. Recommendable for areas with high seismicity. Recommendable for top security installations.	Suitable for areas with low and moderate seismicity. The uncertainties can be incorporated and dealt with. The frequency of earthquakes can be dealt with.
Disadvantages	It requires good geological data. It may give unacceptable results from an economic point of view, it may be equivalent to a probability of $10^{-4}$ - $10^{-5}$ . It does not take the uncertainties into account. In "stable" regions the uncertainties may be so great that it should not be applied. The inclusion of new data ( <i>e.g.</i> : paleoseismicity) may substantially modify the result.	The Poisson model is not suitable either for major earthquakes or for the Gutenberg and Richter distribution. Prediction of earthquake magnitudes greater than 5.0 cannot be made by probabilistic methods with an accuracy that is meaningful for site specific evaluations in engineering.

- Low probability:  $10^{-2} > p \geq 10^{-3}$
- Very low probability:  $10^{-3} > p > 10^{-4}$
- Extremely low probability:  $p < 10^{-5}$
- Remote probability:  $p < 10^{-6}$

Therefore those geo-hazards with an occurrence probability lower than  $10^{-4}$  can be considered as acceptable in terms of risk according to some codes and regulations. But acceptability is also highly dependent on the consequences of failure. This is the case of nuclear power plants or radioactive waste repositories that require a geo-hazard occurrence probability much lower than  $10^{-6}$ . Although social acceptability is a difficult question to estimate, it is an increasingly important issue that should be considered and integrated into the decision analysis procedures when dealing with geo-hazards risk assessment.

Social acceptability criteria can be related to hazard, vulnerability and risk. Table 5 presents an example of acceptability criteria assessment for different types of infrastructures. Geo-hazard probability and vulnerability are related with the degree of losses, e.g. economic costs and fatalities, and environmental impacts. Risk is classified in 3 categories: I (acceptable), II (acceptable with restrictions) and III (unacceptable). Restrictions mean that the engineering solutions have to be improved to reach an acceptable level of risk, either by selecting an alternative site with lower level of hazard or by decreasing the vulnerability by engineering design solutions, or both.

Decision analysis is a necessary exercise for the analysis of the information described above. At this stage, logic tree methods are useful tools for integrating data to help decision-making. After this analysis process, design criteria have to be based on safety requirements, cost optimization and environmentally compatible solutions. A compromise solution between cost and safety should be agreed, keeping in mind that increased safety means exponentially increasing costs.

The following sections present three case studies of practical applications of engineering geological methods to

engineering and territorial planning with different types of geo-hazards.

### 5. Landslide and Seismic Hazards in Dam Safety: The Itoiz Dam Case Study

The Itoiz dam was designed with the opposition of the people living downstream who had been alerted by technical reports to the unsafe conditions of the dam due to landslide instability of the left slope of the reservoir close to the dam site. During the first reservoir filling, a series of earthquakes were felt near the dam and public opposition led to legal action demanding closure of the dam. An independent Commission was set up to report on the potential geological hazards affecting the dam safety (González de Vallejo *et al.*, 2005). New investigations were also carried out (González de Vallejo *et al.*, 2009). This gravity type dam (height: 122 m, length: 525 m, reservoir: 418 Hm<sup>3</sup>) is for irrigation and water supply and has been in operation since 2008. The dam is 22 km eastern of Pamplona, northern Spain (Fig. 2).



Figure 2 - Itoiz dam and reservoir, located 22 km east of Pamplona, northern Spain.

Table 5 - Social acceptability criteria in relation to hazard, vulnerability and risk.

Hazard probability $p_f$	Vulnerability: losses and environmental impacts in case of failure																			
	Conventional structures				Large infrastructures				Critical facilities											
	L	ST	M	ST	H	MT	VH	MT	L	ST	M	MT	H	LT	VH	LT				
$\leq 10^{-2}$	III																			
$\leq 10^{-3}$																				
$\leq 10^{-4}$													II							
$\leq 10^{-5}$													I							
$\leq 10^{-6}$																				

$p_f$  = Annual probability of failure.  
 Risk: I = Acceptable, II = Acceptable with restrictions, III = Unacceptable.  
 Losses: L = Low, M = Medium, H = High, VH = Very high.  
 Environmental impacts: ST = Short term, MT = Medium term, LT = Long term.

## 5.1. Engineering geological investigations

The main aim of the investigation carried out was to determine the slope stability conditions regarding possible earthquakes and precipitation for 500, 1,000 and 5,000 year return periods. The methodology used required the following investigations:

- Neotectonics and fault activity:
  - Identification and characterization of the seismogenic faults in the area.
  - Absolute dating of the Quaternary deposits affected by recent tectonic deformation.
  - Relationship between faults and seismicity.
- Seismic hazard:
  - Compilation of a joint Franco-Spanish unified seismic catalogue.
  - Characterization of possible seismogenic sources depending on seismic and tectonic information.
  - Probabilistic seismic hazard analysis for 500, 1,000 and 5,000 years return periods in terms of the horizontal peak ground acceleration (PGA).
  - Uniform hazard response spectra and compatible earthquake accelerograms.
- Hydrological and hydrogeological surveys:
  - Pluviometry, temperature and climate classification.
  - Surface run-off and water balance.
  - Groundwater flow models.
- Geological and geomechanical description:
  - Geological-geotechnical mapping.
  - Boreholes, in-situ tests, geophysical surveys and laboratory tests.
  - Evolution and absolute dating of landslides.
  - Hydrogeological characterization of materials.
  - Geotechnical classification of materials and their strength and deformational properties.
- Slope stability analysis:
  - Geological, hydrogeological and geomechanical models.
  - Stability analysis using limit equilibrium and stress-strain methods
  - Critical landslide surfaces, safety factors, maximum displacement and deformation for different hypotheses.
  - Influence on slope stability of strength properties, piezometric levels and seismicity.
- Slope instrumentation and monitoring:
  - Installation of piezometers, inclinometers, extensometers and surface movement control points.
  - Analysis and relationships between piezometers and inclinometers and surface movements.

## 5.2. Tectonic and seismicity studies

### 5.2.1. Fault activity

The results of the surveys carried out in the area within a 25 km radius of the Itoiz dam identified 3 faults with possible seismic potential. No morphological expressions were found in the area which display quaternary activity in the faults. The maximum potential seismicity associated with these faults has been estimated at around  $M = 6.5$  for a return period of over 6,000 years. The results of thermoluminescence dating show that the tectonic deformations associated with the faults are less than 125,000 years old, *i.e.* Upper Pleistocene.

### 5.2.2. Seismicity during the first reservoir filling

A large number of low magnitude earthquakes were recorded near the dam site during the first reservoir filling (2004), the largest of magnitude 4.6. (Figs. 3 and 4). Table 6 shows a summary of the criteria used following Simpson (1986), Gupta (2002) and McGarr *et al.* (2002), which show that the type of seismicity recorded in the area surrounding the dam responds to the concept of triggered seismicity, not induced seismicity (Boomer *et al.*, 2005). The earthquake triggering due to the reservoir filling would be what could occur in the future from natural, not induced causes. The maximum earthquake corresponding to this type of triggered seismicity could be associated with the normal faults present in the area with potential magnitude lower than 5.5 for 1,000 year return period.

### 5.2.3. Seismic hazard

The seismic actions of earthquakes corresponding to 500, 1,000 and 5,000 years return periods were characterized from the seismic hazard curve obtained for the dam site, expressed as the PGA. The PGA value obtained for a 500 year return period was 0.08 g; for a 1,000 years return

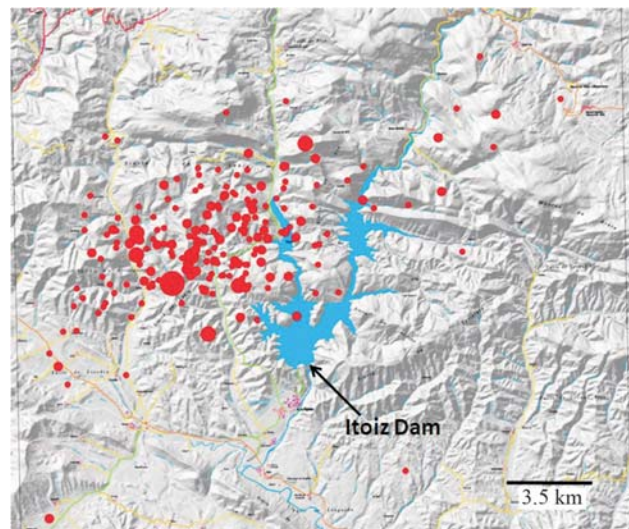


**Figure 3** - Epicentres of earthquakes recorded during the first reservoir filling.

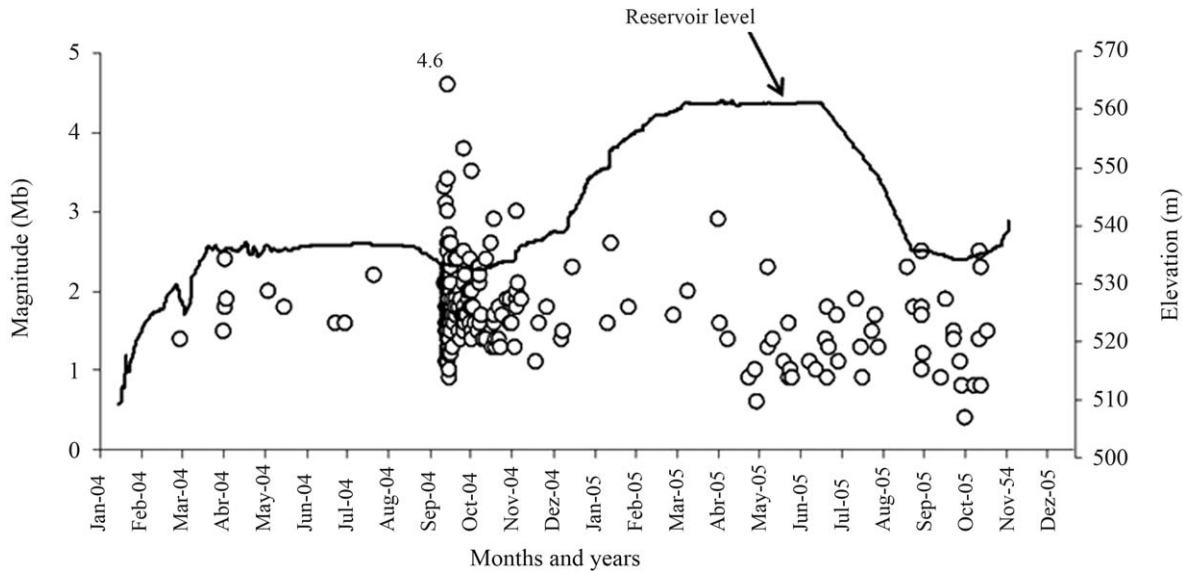


**Figure 4** - Earthquake magnitudes during the first reservoir filling.

**Table 6** - Triggering seismicity criteria in Itoiz dam (González de Vallejo *et al.*, 2005).

Triggering criteria	Itoiz dam				Triggering seismicity	
					Yes	No
Coincidence in time (< several years)	9 months after initiation reservoir filling; 5 months after reached maximum elevation				X	
Spatial distribution						
Epcentres (< 20 km)	4-7 km				X	
Hypocentres (< 30 km)	3-8 km				X	
Reservoir located in low/moderate seismic zone	Moderate / Low seismicity				X	
Normal or strike-slip faults	Normal faults				X	
Seismic parameters						
Parameter $b$ :						
$b_{pre} > b_{after}$	$b_{pre} = 0.42$ $b_{after} = 1.12$					X
$b_{trig} > b_{nat}$	Itoiz	$b_{pre} = 0.42$ $b_{after} = 1.12$	Nat	$b_{pre} = ?$ $b_{after} = ?$	-	-
$b_{trig} > b_{rec}$	Itoiz	$b_{pre} = 0.42$ $b_{after} = 1.12$	$b_{reg} = 0.62$		-	-
Magnitude relationships						
$M_{max}/M_0$ (near 1)	$M_{max} = 3.8 m_b Lg$	$M_{max}/M_0 = 0.82$			X	
$M_0 - M_{max}$ low (< 1)	$M_0 = 4.6 m_b Lg$	$M_0 - M_{max} = 0.8$			X	
Low decrease of the number of aftershocks with time ( $h = 1$ )	Itoiz	$h = 0.67$	Nat	$h = ?$	X	-
Mogi (1963) model distribution of aftershocks and premonitory seismicity	Type II				X	

$b$  - Gutenberg-Richter parameter (see Table 10). Nat = "natural" seismicity to differentiate with "triggering" seismicity.  $M_0$  = the largest magnitude event.  $M_{max}$  = the maximum magnitude of the aftershocks events.  $h$  = rate decrease of the number of aftershocks with time.

period it was 0.13 g; and for a 5,000 year return period it was 0.30 g. These PGA values are considerably higher than those calculated in the construction project for the dam and than those recommended in the Spanish earthquake resistant building standards (NCSE-02).

The most probable earthquake for a 1,000 years return period could reach a moment magnitude ( $M_w$ ) of between 4.7 and 5.1, according to the possible seismogenetic sources and would take place in the immediate area of the dam (epicentral distance  $\leq 5$  km). For a 5,000 year return period the earthquake could reach a moment magnitude ( $M_w$ ) of between 6.4 and 6.6, and would take place at an epicentral distance of 15-20 km.

### 5.3. Landslides stability analysis

The left slope of the dam is composed of the following materials (Figs. 5 and 6):

- Colluvial. Most superficial level, composed of gravel and cobbles in a sand-silt matrix with clays of up to 12 m thick. Presents high electrical resistivity values and low seismic wave propagation velocity. Highly permeable.
- Upper calcareous breccia (UCB). Composed of boulders and sub-angular gravel, with heterometric calcareous material contained in a low consistency sand-clay matrix. The matrix content is 45%. Presents areas with karstification. Very varied thickness, of up to 31 m. The permeability of these materials is very high.
- Lower calcareous breccia (LCB). This is composed of the same materials as the UCB. The matrix content is 55%. Variable thickness of up to 28 m. Presents slickenside surfaces. Higher seismic wave propagation velocity and lower electrical resistivity than the UCB. High permeability.
- Bedrock. Formed by stratified marls, limestones and calcarenites with 20°-25° dip. This is slightly weathered medium quality rock (Class III). High seismic wave velocity and electrical resistivity.



**Figure 6** - Borehole cores of the calcareous breccias of the slided material.

The geomechanical properties of these materials are summarized in Table 7. The UCB and LCB deposits both correspond to landslide materials. Figure 7 shows their extension and situation in relation to the dam. The landslides occurred along stratification planes in the bedrock, with 20° -25° dip in the direction of the slope. The slickenside surfaces of the LCB layer correspond to failure planes.

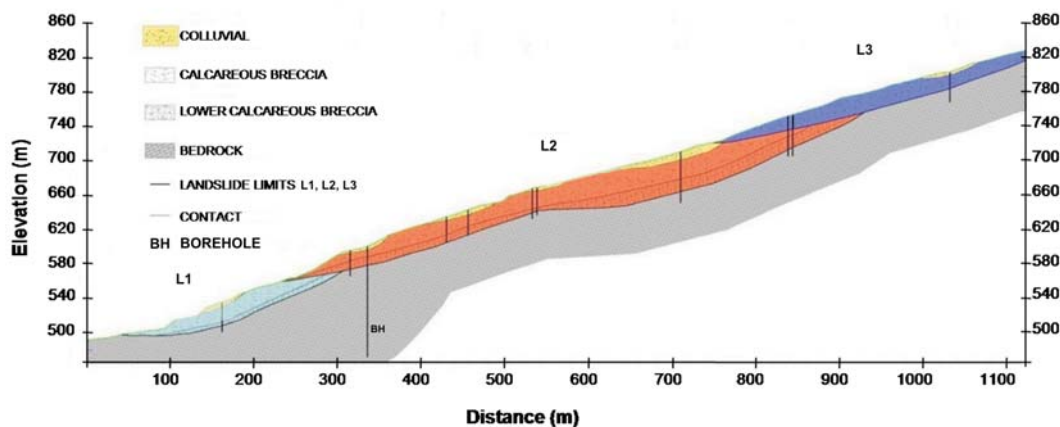
Three landslides were identified on the left slope (L1, L2 and L3) which correspond to different episodes of successive landslides (Figs. 5 and 7). Their total volume is of the order of  $3 \times 10^6 \text{ m}^3$ .

Figure 8 shows a detail of the slip materials observed in a trench (Gutierrez *et al.*, 2007). The absolute dating gives an age of 12 ka for the most recent landslide and 38 ka for the oldest one. These results indicate different reactiva-

**Table 7** - Geomechanical mean properties of the materials of the left slope of Itoiz dam.

Material	Cohesion (kPa)	Angle of internal friction (°)	Young modulus (GPa)
Colluvial	10	30	2.6
UCB	50	32	5.0
LCB	70	30	6.6
Bedrock	-	-	25.2

UCB: Upper calcareous breccia. LCB: Lower calcareous breccia.



**Figure 5** - Geological profile of the left slope of the reservoir near the dam site. L1, L2 and L3 correspond to 3 different landslides.



**Figure 7** - Paleo-landslides area near the Itoiz dam.

tion periods of these movements, although no movements more recent than 12 ka were observed.

The failure surface strength, the slope saturation degree and the seismicity were evaluated. With regard to the strength properties of the materials, in particular the lower breccia (LCB), the values taken were  $c = 70 \pm 50$  kPa and  $\phi = 30 \pm 5^\circ$ , from the results of the laboratory tests. Different slope saturation degrees were assumed equivalent to a 23% saturation degree and to a 46% saturation degree, according to the hydrogeological data. However, full saturated slope hypothesis was also considered.

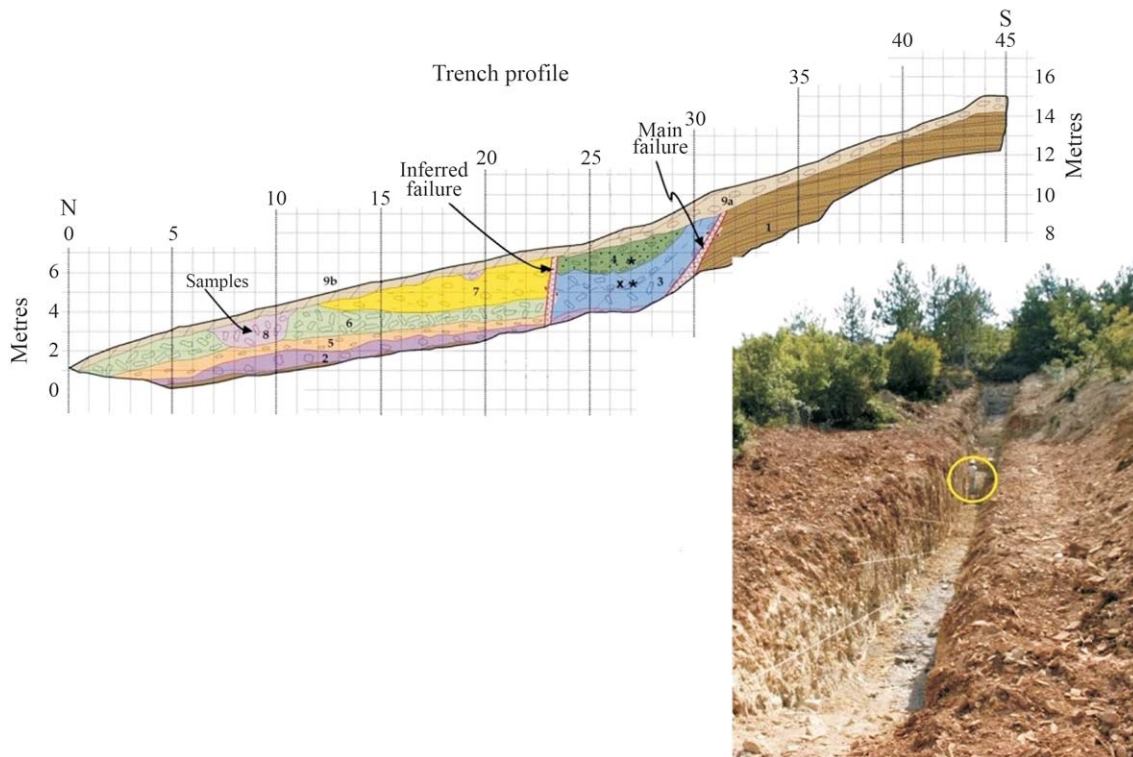
Different PGA values and accelerograms were considered depending on whether a pseudostatic or dynamic analysis, respectively, was applied. Slope stability was analysed using limit equilibrium and stress-strain methods for different scenarios. The results obtained are shown in Table 8 and in Figs. 9 and 10.

#### 5.4. Slope instrumentation and monitoring

The left slope has been instrumented for over 10 years with numerous piezometers, inclinometers, extensometers and surface measurements with GPS. Most of the piezometers installed on the slope are dry and are not affected by the variations in the reservoir level or by the rainy periods in the area. Only the piezometers nearest the dam reproduce the variations in it. These results reflect the high permeability of the medium, its high hydraulic transmissivity and transversal drainage.

The manual inclinometers display extremely low displacements, which are mostly negligible or are within instrumental error limits. The greatest displacement, 17 mm, was obtained in an inclinometer near the dam. In the other inclinometers the maximum displacements were lower than 11 mm. The displacements recorded by the automatic inclinometers were very low, below the instrumental error limit.

The measurements taken on the surface with GPS show displacements lower than 15 mm. The results ob-

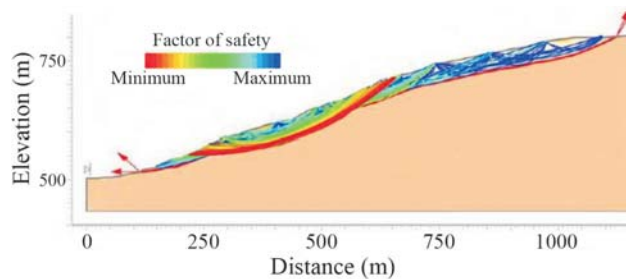
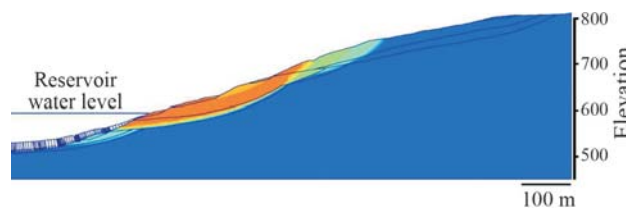


**Figure 8** - Geological profile along a trench where detail sedimentological, geomorphological and geotechnical observations were carried out (modified from Gutierrez *et al.*, 2007).

**Table 8** - Stability analysis results for the left slope of Itoiz dam.

Hazard scenarios	Design condition for 500 years RP	Design condition for 1,000 years RP	Extreme conditions for 5,000 years RP
<i>DS</i> (%)	5	23	46
PGA ( <i>g</i> )	0.08	0.13	0.30
<i>FS</i> calculated	> 1.6	> 1.5	> 1.15
<i>FS</i> required by dam codes	> 1.3	> 1.15	> 1.0

*DS*: degree of saturation of the slope materials. RP: return period. PGA: peak ground acceleration.

**Figure 9** - Slope stability analysis by limit equilibrium methods showing critical failure surfaces for PGA = 0.13 *g*.**Figure 10** - Slope stability analysis by stress-strain analysis showing maximum displacements.

tained do not reflect any existing trend in the movements, since the displacements are erratic and do not occur in the same direction. An automatic topographical control system has been installed on the slope, which triggers alarms at different levels if the displacement thresholds established are exceeded. Since the system was installed no displacements higher than the instrumental errors have been recorded. The numerous monitoring systems installed on the slope have not detected movements of the ground or high piezometric levels.

## 5.5. Conclusions

The seismicity recorded during the first reservoir filling corresponds to the concept of triggered seismicity. That means that the reservoir filling itself will not generate seismicity, but it anticipates a natural seismic phenomena. The reservoir filling will not affect the seismic potential of the area, nor will it induce an earthquake higher than those considered or expected from slope and dam stability analysis.

The results obtained demonstrate that the left slope is currently stable, and also that it will continue to be stable even in extreme seismic and hydrogeological conditions.

## 6. Seismic Hazard Assessment in Regions with Insufficient Information: The Canary Islands Case Study

### 6.1. Introduction

Insufficient or incomplete seismic data can lead to great uncertainties and unreliable seismic hazard results even when the tectonic sources are unknown or not well identified. In many regions of the world the instrumental period of seismic records is too short and the historical seismic catalogue is incomplete. This is the case of the Canary Islands.

Few investigations have been carried out so far on seismicity and none on seismic hazard in this region. The Spanish Seismic Code (NCSE-02) is currently the only reference related to seismic hazard in the Canarian archipelago. This Code provides an updated version of the 1994 seismic-hazard map of Spain (NCSE-94). Both maps were derived in terms of macroseismic intensity, and then converted to a characteristic ground acceleration, which in practice is taken as peak ground acceleration (PGA), related to a 500 years return period. However, the probabilistic assessment was not performed for the Canary Islands either in the 1994 nor the 2002 version, and a 0.04 *g* PGA was arbitrarily adopted for the whole archipelago.

Conducting a seismic-hazard analysis of the Canarian Archipelago is plagued by important shortcomings. Very few tectonic structures have been described so far and seismic instrumental recording dates only since 1975. Historical seismic catalogue dates from the 14<sup>th</sup> Century and only the largest earthquakes have been recorded, including earthquakes with intensities of VIII and X, all related with volcanic eruptions. Nevertheless, assessing the seismic hazard is currently of prime importance for the near-future development of industrial facilities and urban expansion on the islands.

Tenerife, the most populated island, holds a density of population 5 times of Spain and 4 times of Europe. Even

low magnitude earthquakes can cause a great social alarm and seismic resistant design is not required in practice for building construction.

## 6.2. Geological and tectonic setting

The Canary Islands form a volcanic archipelago located on the passive margin of the African plate, 100 km off west Africa. Active volcanism has taken place on the islands in historical times, commonly together with the occurrence of volcanic-related seismic sequences, some of them felt as high as  $I_{MSK} = X$ . In the past 500 years several volcanic eruptions have taken place in Tenerife, La Palma, Lanzarote and El Hierro. The last eruptions occurred in 1971 on La Palma (Teneguía volcano). A new submarine eruption occurred in 2011 near the south coast of El Hierro.

Very few tectonovolcanic structures have been described yet in the Canarian Archipelago (Fig. 11). One of the first structures described were triple rift junction located in relation to the main volcanic centres on Tenerife and El Hierro (Navarro, 1974). Seismic exploration and marine geophysics have revealed the different crustal structure of the eastern islands to the western islands (Banda *et al.*, 1981; Carbó *et al.*, 2003). The eastern islands lie on a crust 15 km thick and form a very conspicuous north-northeast-south-southwest structure, the so-called East Canary Ridge. In contrast, the crust in the western islands is 11 km thick and structures show a general north-south trend.

The most important seismo-tectonic feature known in the archipelago is located between the islands of Tenerife and Gran Canaria (Fig. 12). In this area, a north-east-southwest-trending fault was first described by Bosshard & McFarlane (1970), and later, Mezcua *et al.* (1992).

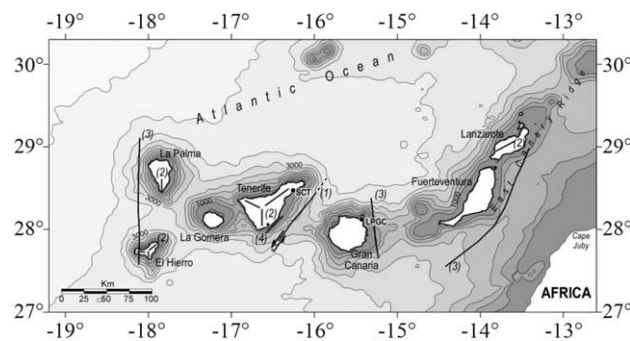


**Figure 11** - Main tectonovolcanic features and lineations of the Canary Islands (González de Vallejo *et al.*, 2006). Numbers refer to the main works describing the structures shown in the figure: (1) Bosshard & McFarlane, 1970; Mezcua *et al.*, 1992; (2) Navarro, 1974; (3) Carbó *et al.*, 2003; (4) González de Vallejo *et al.*, 2003. Isolines show the bathymetry. The capital cities of the archipelago are displayed: Santa Cruz de Tenerife (SCT) and Las Palmas de Gran Canaria (LPGC). The star marks the location of the paleoliquefaction features.

## 6.3. Seismic data

The beginning of the historical period in the islands dates from the fourteenth century. Since then, a noticeable number of earthquakes have been registered, mainly related to volcanic eruptions (Fig. 12). The first great seismic event was registered on La Palma in 1677 ( $I_{MSK} = VII-VIII$ ). However, the most intense earthquake in the archipelago took place near Yaiza (Lanzarote) in 1730 ( $I_{MSK} = X$ ) related to the Lanzarote eruption (1730-1736) of the Timanfaya volcano. The so-called Yaiza earthquake took place on 1 September 1730 reaching an MSK intensity of X, however the intensity assigned to the Yaiza earthquake is very likely to be overestimated.

Other noticeable earthquakes were registered in 1920 and 1949 in Cumbre Vieja (La Palma) ( $I_{MSK} = VII$ ), in Ingenio (Gran Canaria) in 1913 ( $I_{MSK} = VII$ ), and in Fuerteventura in 1915 and 1917 (both  $I_{MSK} = VII$ ). Many other events with intensity VI and V have been registered in the archipelago. The first seismic network in the region started operating in 1975. Since then most of the stations have been updated by digital recording broadband instruments (IGN, 2004).

The instrumental catalogue is mostly composed of small events distributed preferentially around Gran Canaria and Tenerife, in particular, between the two islands (Fig. 12). The largest instrumental earthquakes in the archipelago were recorded on 22 January 1991 and 9 May 1989. The 1991 event ( $m_b Lg = 5.1$ ) was located 60 km southwest of La Palma and no aftershocks were recorded, probably because of the long distance to the seismic network. In contrast, the 1989 event ( $m_b Lg = 5.2$ ) was located between Gran Canaria and Tenerife, permitting the record of a noticeable number of aftershocks. The hypocenter of the main shock was located by Dziewonski *et al.* (1990) at a depth of 15 km, whereas the IGN located it at a depth of 36 km, with an uncertainty in the focal depth of  $\pm 12$  km. The fault lo-

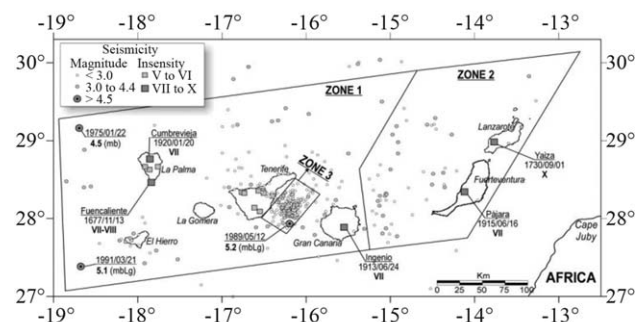


**Figure 12** - Seismicity of the Canary Islands. Only historical events with intensity greater than V (MSK) are displayed. Only main events are labelled: name of the town, date and intensity for the historical events, and date and magnitude for the instrumental records. The seismogenic zones considered in the hazard calculations are shown. See text for details. (Gonzalez de Vallejo *et al.*, 2006).

cated between Gran Canaria and Tenerife was pointed out as the source of the 1989 event (Mezcua *et al.*, 1992). The focal mechanism of the main shock shows strike-slip movement with two nodal planes oriented north-northeast-south-southwest and northwest-southeast. The former agrees very well with the strike of the submarine fault and aftershock distribution. The length of the fault was estimated as 30 km.

#### 6.4. Paleoseismic investigations

Paleoseismic investigations can provide very important seismic and tectonic information, especially in areas with few seismic records. One of its main contributions to seismic hazard is to identify possible earthquakes linked with active faults, although if liquefaction structures are identified in these studies, the acceleration due to the earthquake can also be estimated. Where possible, the age of the palaeo-earthquake can also be estimated.

Several structures attributed to liquefaction phenomena of seismic origin have been identified in exposed sand deposits near El Médano, on the south coast of Tenerife. Tectonic and geophysical investigations, geotechnical characterization, geochronological analysis, seismicity, and neotectonic data were carried out, as well as soil dynamic analysis (González de Vallejo *et al.*, 2003).

The liquefaction structures consist on clastic dikes and tubular vents. Their origin has being attributed to the liquefaction of sands by an earthquake of high intensity. The mechanisms that gave rise to the clastic dikes were hydraulic fracturing and lateral spreading of a layer of compact sands in response to high pore pressures of seismic origin (Fig. 13). These pressures, in turn, led to the movement and injection of sands across the compact sands level. The vents are the result of high upward hydraulic pressures causing the ejection of water and sand through these conduits to the surface, possibly forming sand blows and explosion craters (Fig. 14).



**Figure 13** - Clastic dikes due to hydrofracturing by seismic shaking.



**Figure 14** - Dikes showing a central aperture and a tabular vent.

The peak ground acceleration needed to produce liquefaction and the sand dikes was estimated at 0.22 to 0.35 *g* applying the Ishihara (1985), Obermeier (1996) and Obermeier *et al.* (2001) methods. An acceleration of 0.30 *g*, considered to be the most characteristic, would correspond to an intensity of VIII to IX at the site of liquefaction. The magnitude of the earthquake causing liquefaction was calculated to be in the range 6.4 to 7.2 with a value of  $M = 6.8$  taken to be representative. This result was obtained assuming that a submarine fault (Figs. 11 and 12) was the seismic source.

The liquefaction structures developed over a tectonically uplifted beach of sand deposits dated as  $10.081 \pm 933$  years BP. Over these sands and liquefaction structures, fine calcareous crust levels dated as  $3490 \pm 473$  years BP were observed. The paleoearthquake responsible for liquefaction occurred during the Holocene; its age lying between these two dates. Nevertheless, tectonic and geomorphological data from field observations suggest an age closer to the younger constraint.

Possible seismic sources near the site of liquefaction were considered. The main source is inferred to have been a submarine NNE-SSW trending fault some 35 km from the site between the islands of Tenerife and Gran Canaria. Its movement takes the form of a sinistral thrust. This fault shows associated seismicity.

#### 6.5. Seismogenic sources

Based on the main regional tectonic features and the distribution of seismicity, three seismogenic zones have been defined to be used in the hazard calculations: zones 1, 2 and 3 (Fig. 12). The area consisting of zones 1 and 2 accounts for the occurrence of low-to-moderate magnitude events, independent of their tectonic or volcanic origin. The boundaries of the zones have been drawn coinciding with the decrease in seismicity that occurs either toward the open Atlantic Ocean or toward the African continent, respectively (Fig. 12). The northern and southern limits of

these zones also follow the offshore extension of the Atlas structure (Figs. 11 and 12). The boundary between both zones represents the abrupt change in crustal thickness that takes place moving away from the eastern islands toward the western islands. The orientation of this boundary coincides approximately with the apparent north-northwest-south-southeast orientation displayed by the East Canary Ridge (Fig. 12).

Zone 3 has been defined to outline a specific area inside zone 1, between Gran Canaria and Tenerife, where moderate-to-large ( $M_w > 6.0$ ) tectonic earthquakes are likely to occur due to the presence of the fault responsible for the 1989 sequence, and in accordance with the size of estimated earthquake magnitudes ( $M_w = 6.8$ ) from paleoliquefaction analysis on the south Tenerife coast.

### 6.6. Seismic parameters for hazard calculations

Analyzing the temporal completeness of the database is of prime importance for estimating earthquake recurrence parameters in each seismogenic zone (Table 9).

Seismic hazard was calculated following the well-known method of Cornell (1968). This method assumes that earthquake occurrence follows a Poisson process and is distributed uniformly within several specific areas delimited by the analyst (source zones). In each of these zones, earthquake magnitudes fit an exponential distribution, so the mean annual exceedance rate of magnitude  $m(\lambda_m)$  is given by (Cornell & Vanmarcke, 1969):

$$\lambda_m = \lambda_{m_0} \frac{\exp(-\beta m) - \exp(-\beta m_1)}{\exp(-\beta m_0) - \exp(-\beta m_1)}, m_0 \leq m \leq m_1 \quad (6)$$

where  $\lambda_{m_0}$  is the mean annual exceedance rate of magnitudes above  $m_0$ , and  $m_1$  and  $m_0$  are the upper and lower bounds of the distribution, respectively, and ( $\beta$ ) is the exponential parameter of the distribution. The  $\lambda_{m_0}$  parameter is given by:

$$\lambda_{m_0} = \exp(\alpha - \beta m_0) \quad (7)$$

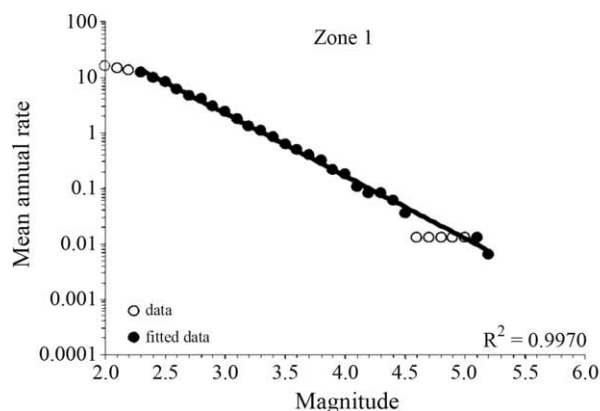


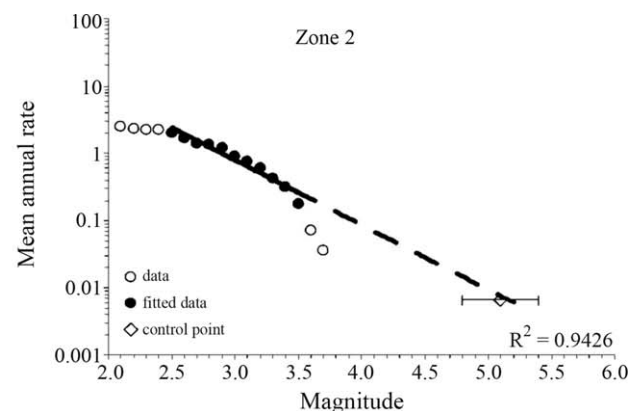
**Table 9** - Estimated starting year of completeness for specific magnitude ranges.

Magnitude range ( $M_w$ )	Starting year	Temporal length (yr)
5.1-5.2	1850	153
4.1-5.0	1960	43
3.1-4.0	1975	28
2.6-3.0	1980 (zones 1 and 3) 1985 (zone 2)	23 18
2.0-2.5	1990	13

Temporal length extends from starting year to 2002.

where  $\alpha = a \ln(10)$  and  $\beta = b \ln(10)$ , and  $a$  and  $b$  are the Gutenberg-Richter parameters. The Gutenberg-Richter parameters estimated in each zone after regression analysis are shown in Table 10. Zones 1 and 2 have shown a very different  $a$  value, which could be related to distinctive seismogenic characteristics. Nevertheless, this observation has to be taken with caution because of significant statistical uncertainty affecting zone 2 parameters (Fig. 15).

Zone 3 represents a specific area inside zone 1 where earthquake occurrence is extended to larger magnitudes ( $M_w \geq 6.0$ ) due to the presence of the Gran Canaria-Tenerife submarine fault. Hence, the maximum earthquake potential of zone 3 has been assessed based on the surface length of the Gran Canaria-Tenerife fault and paleoliquefaction evidence on the south coast of Tenerife. Making use of the surface rupture length versus moment magnitude relationship of Wells & Coppersmith (1994) and considering the 30 km length of the fault, an expected  $M_w = 6.8 \pm 0.28$  event can be derived, which is very similar to the  $M_w = 6.8$  estimated on the paleoliquefaction study of González de Vallejo *et al.* (2003). These authors estimated that such a seismic event occurred between 3,500 and 10,000 years ago, which is consistent with the mean recurrence period derived from extrapolating instrumental data to the large magnitude range (see Table 10).



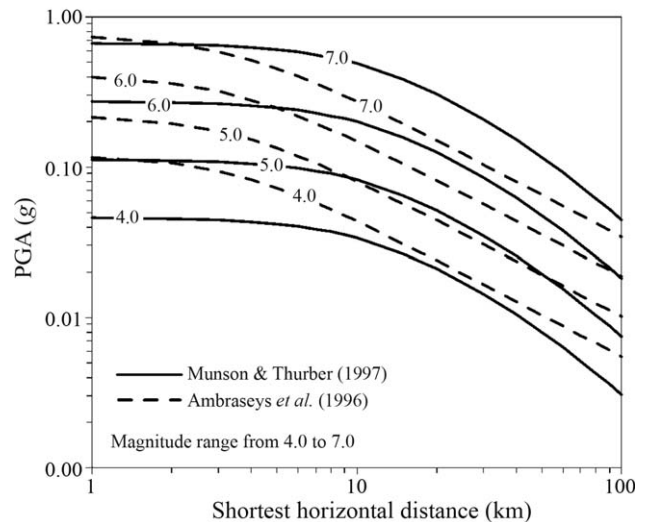
**Figure 15** - Cumulative earthquake occurrence rates versus magnitude in zones 1 and 2, and exponential ts (González de Vallejo *et al.*, 2006).

Table 10 also shows the lower ( $m_0$ ) and upper ( $m_1$ ) magnitude thresholds adopted in zones 1 and 2. Minimum magnitude was set to  $M_w = 4.0$  in zones 1 and 2. Standard practice in seismic-hazard assessment usually sets the minimum magnitude to  $M_w = 5.0$ , which is thought to be the smallest earthquake of engineering interest. Nevertheless, adopting such a value in a low-to-moderate seismic area like the Canary Islands, could lead to underestimating the hazard for relatively high exceedance probabilities (e.g. 10% in 50 yr or 475-yr return period). Besides, seismic events with magnitudes smaller than  $M_w = 5.0$  have actually produced significant damage in other parts of Spain.

To assess the maximum magnitude in zones 1 and 2, it was adopted a deterministic procedure of increasing the intensity of the maximum historical earthquake (MHE) by half a unit, and transforming it to the moment magnitude scale. MHEs in zones 1 and 2 are  $I_{MSK} = VIII$  and  $I_{MSK} = X$ , respectively. The former value suggests an average  $M_w = 6.0$  with the relationships of IGN (1982) and Benito *et al.* (1999). In fact, adopting such intensity would indicate an average  $M_w = 6.8$ , which is no realistic if considering the maximum size of instrumentally recorded earthquakes related to major eruptions (Miyake-jima, 1983,  $M_s = 6.2$ ; Oshima, 1986,  $M_w = 6.0$ ; Benoit & McNutt, 1996). A maximum  $M_w = 6.0$  was finally adopted for zone 2.

### 6.7. Ground-motion attenuation relationships

There is no ground-motion relationship specifically developed for the Canary Islands. The only attenuation relationships derived for a similar volcanic archipelago to date are those developed by Munson & Thurber (1997) and Atkinson (2010) from Hawaiian strong-motion data. The Munson and Thurber equation was selected for the calculations. However, it is interesting to compare that relationship with the one of Ambraseys *et al.* (1996), which is one of the most used in Europe. Ambraseys *et al.* predicts higher PGA values for small-to-large magnitudes ( $M_s = 5.0-7.0$ ) and at short distances (10 km approximately), Fig. 16. On the other hand, Munson and Thurber predict higher PGA in the medium distance range (10-100 km), although it attenuates much faster. These significant differences between attenuation models suggest that the distinctive characteristics of active volcanic crust (e.g. fracturation, temperature, and fluids) may produce a



**Figure 16** - Munson & Thurber (1997) PGA attenuation curves for  $M_w = 4.0$  to 7.0 for rock conditions. The Ambraseys *et al.* (1996) curve is also shown for comparison purposes (González de Vallejo *et al.*, 2006).

damping effect on high frequency ground motion, in particular, at short distances.

### 6.8. Seismic-hazard results

Seismic hazard has been calculated for a grid spacing of  $0.1^\circ$ , as well as for the two capital cities (Las Palmas de Gran Canaria and Santa Cruz de Tenerife), (Gonzalez de Vallejo *et al.*, 2006). Computation was performed using the program CRISIS (Ordaz *et al.*, 1999). Figure 17 shows the seismic-hazard curve for the capital cities, and Fig. 18 (A and B) shows the resulting seismic-hazard maps in terms of PGA levels related to 475- and 950-yr return periods, respectively. PGA is for rock conditions, which are the most common site conditions on the islands. It is clear from both maps that zone 3 controls the distribution of the highest acceleration levels.

### 6.9. Conclusions

The east coast of Tenerife has been identified as the on-shore area with highest seismic hazard in the archipelago because of the existence offshore east of Tenerife of a seismogenic source capable of generating moderate-to-

**Table 10** - Seismic parameters of the seismogenic zones.

Sources	$b$	$a$	$m_0$	$\lambda m_0$	$m_1$	MRP (yr)
Zone 1	1.12 ( $\pm 0.01$ )	3.72 ( $\pm 0.05$ )	4.0	0.1676	6.0	1,050 $\pm$ 120
Zone 2	0.95 ( $\pm 0.08$ )	2.75 ( $\pm 0.23$ )	4.0	0.0909	6.5	870 $\pm$ 160
Zone 3	1.12 ( $\pm 0.01$ )	3.72 ( $\pm 0.05$ )	6.0	0.00095	6.8	8,350 $\pm$ 950

$a$  and  $b$ , Gutenberg-Richter parameters with indication of the standard error;  $m_0$  and  $m_1$ , lower and upper bounds of magnitude ( $M_w$ ) distribution;  $\lambda m_0$  mean annual cumulative rate of magnitude  $\geq m_0$ ; MRP, mean recurrence period of  $m_1$  in each of the zones.

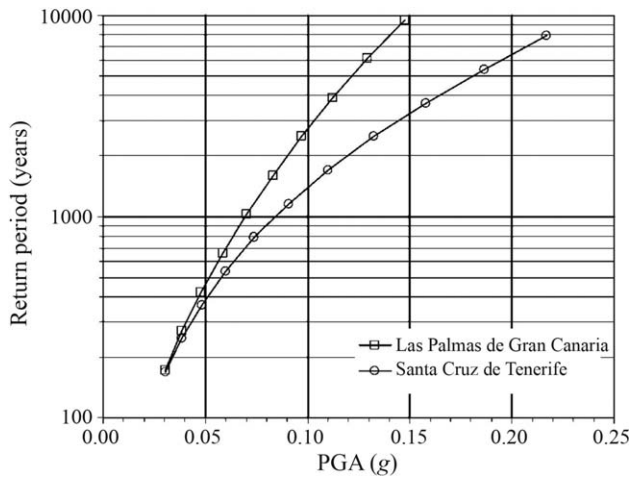


**Figure 17** - Seismic-hazard curves for the two capital Canarian cities. PGA values are for rock conditions, (González de Vallejo *et al.*, 2006).

large magnitude ( $M_w > 6.0$ ) tectonic earthquakes, that is, the Gran Canaria-Tenerife fault.

The eastern and south-eastern part of Tenerife show PGA values of 0.06 g and 0.08 to 0.09 g for the 475- and 950-yr return periods, respectively. The rest of the Canary Islands show a uniform PGA of 0.05 g for the 475-yr return period and 0.06 to 0.07 g for the 950-yr return period. PGA in the capital cities of Santa Cruz de Tenerife and Las Palmas de Gran Canaria are 0.06 and 0.05 g, respectively for the 475-yr return period, and 0.08 and 0.07 g for the 950-yr return period. These results on Tenerife and the rest of the Canary Islands are 50% and 25% higher than those stated in the Spanish Seismic Code (NCSE-02) for the 475-yr return period, respectively. Seismic Codes for building construction in the Canaries should be revised.

The presence of active faults affecting materials of very recent age and their association with a paleoearth-

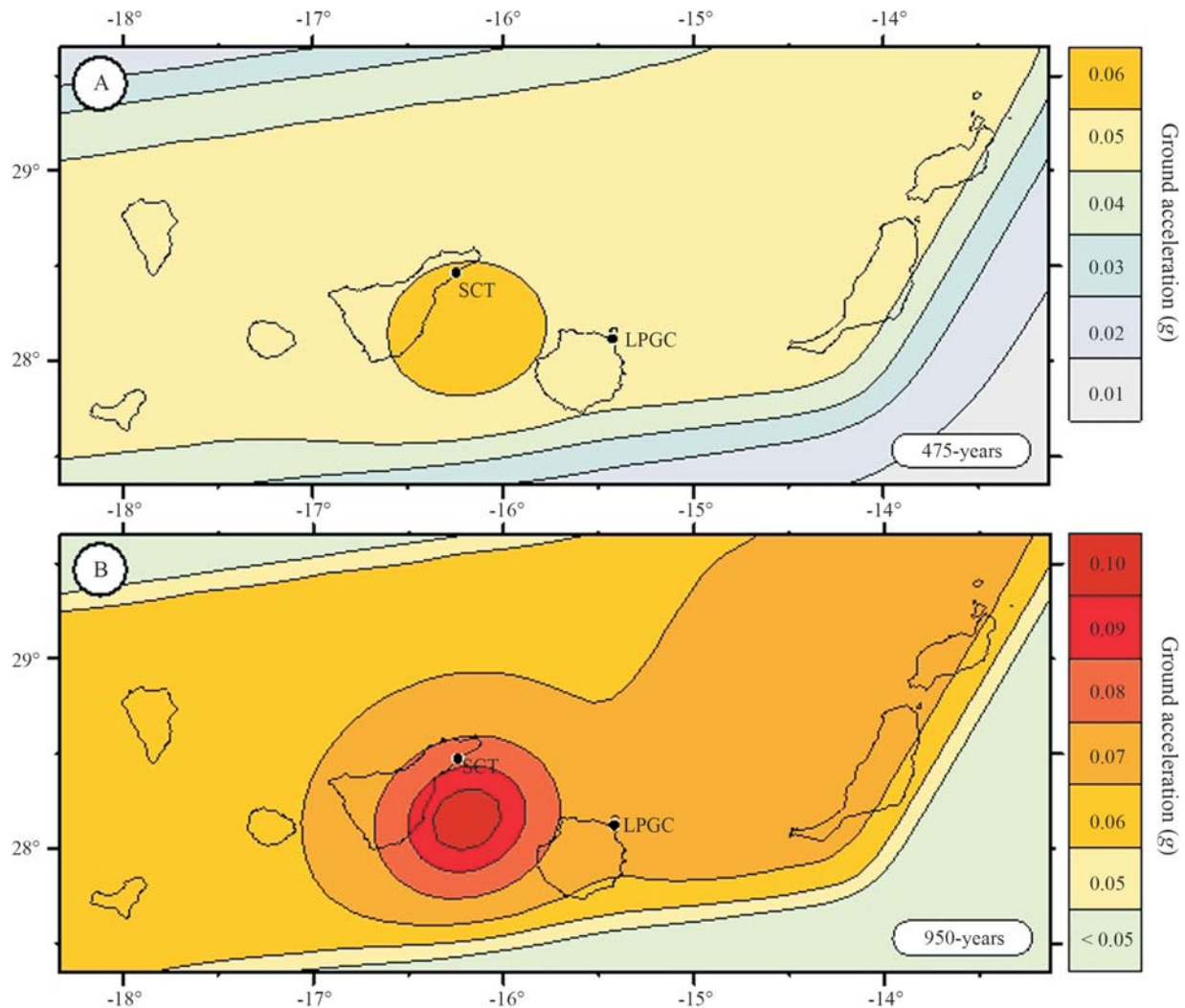


**Figure 18** - Seismic-hazard maps of the Canary Islands in terms of PGA on rock for the 475 (A) and 950-yr (B) return period. Acceleration values are in g units (González de Vallejo *et al.*, 2006).

quake of high intensity in the south of Tenerife are key factors that need to be borne in mind when evaluating seismic hazards on the Canaries, a region which, up until now, had been considered to be of low tectonic seismic activity.

## 7. Large Landslides and Associated Tsunami Hazards: The Instability of the Volcanic Island Flanks of the Canary Islands Case Study

### 7.1. Introduction

The large landslides in the Canary Islands, have been the subject of many research studies although there was most scientific and social interest in them when alarming news was published on the possibility that the collapse of the island of La Palma could cause a catastrophic tsunami on the east coast of the US (Ward & Day, 2001). The resulting social alarm led to the start of an investigation into the causes of volcanic island flank instability in the Canaries, their failure mechanisms, and the possible associated hazards, particularly tsunamis. This investigation focused on two of the world's largest known landslides: the Güímar and La Orotava landslides in Tenerife (Ferrer *et al.*, 2008 and 2011, and Seisededos, 2008).

Although more than 20 mega-landslides have been described in the Canary Islands affecting the flanks of the volcanic edifices, the Güímar and La Orotava landslides, (Fig. 19), originating 1 Ma and 0.6 Ma respectively, are two exceptional cases due to their huge dimensions and outstanding geomorphological features. Tsunami deposits have been also identified in some of the Canary Islands, probably associated with the landslide of the island flanks.

The presence of large masses of rocks and debris avalanche deposits lying on the sea bed surrounding the island of Tenerife is the main evidence of the Güímar and La Orotava landslides. According to Acosta *et al.* (2003) La Orotava submarine debris avalanche deposits cover an area of 2,200 km<sup>2</sup> reaching up to 75 km from the coast, and the submarine deposits from the Güímar landslide occupy an

area of 2,600 km<sup>2</sup> up to a distance of 85 km from the coast. The volume of these debris avalanches on the ocean floor has been estimated at around 120 km<sup>3</sup> in the case of the Güímar landslide and less than 500 km<sup>3</sup> in La Orotava (Masson *et al.*, 2002).

The morphological characteristics of the valleys are extraordinary, with their outstanding symmetry and the important height of the lateral scarps (more than 500 m in some areas; Fig. 20), cut in pre-landslide volcanic materials with slope angles higher than 35°. The depressions formed by the landslides were filled with post-landslide volcanic materials, mainly lava flows from new volcanoes in the upper part of the valleys, with slope angles currently lower than 15°. The estimated volume of the landslide rocks from the volcanic flanks, calculated roughly from the depressions created by the rockslides, is of the order of 70-100 km<sup>3</sup> each.

### 7.2. Geological and geomechanical model

Geological and geotechnical data were recorded from field surveys and in the extensive network of small diameter galleries, with a total length of over 1,000 km, excavated for groundwater supply purposes. The geotechnical properties of the volcanic materials of the emerged edifice have been also obtained from in-situ and laboratory tests (González de Vallejo *et al.*, 2008; Seisededos, 2008).

With regard to the geological and geomechanical data of the submarine edifice, only morphological and tectonic data are available from marine geological and bathymetric surveys. In the north-eastern corner of the island site investigations have been carried out where the submarine rock outcrops (Fig. 19). Three boreholes have been drilled in hyaloclastites with one of them reaching a depth of 200 m.

Nine lithological units have been described as representative of the island flanks and the structural axis of the pre-rockslide edifice as shown in Fig. 21. These units have been differentiated following engineering geological criteria:

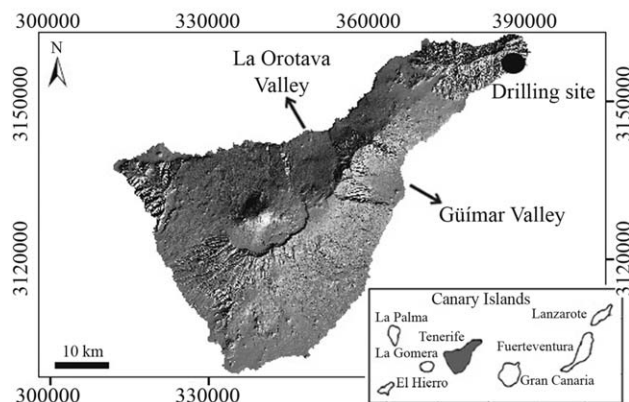


**Figure 19** - Location of Güímar and La Orotava valleys and drilling site, Tenerife.



**Figure 20** - View of La Orotava valley, 12 km wide, bordered by 500 m high lateral scarps. In the background El Teide volcano (3,718 m).

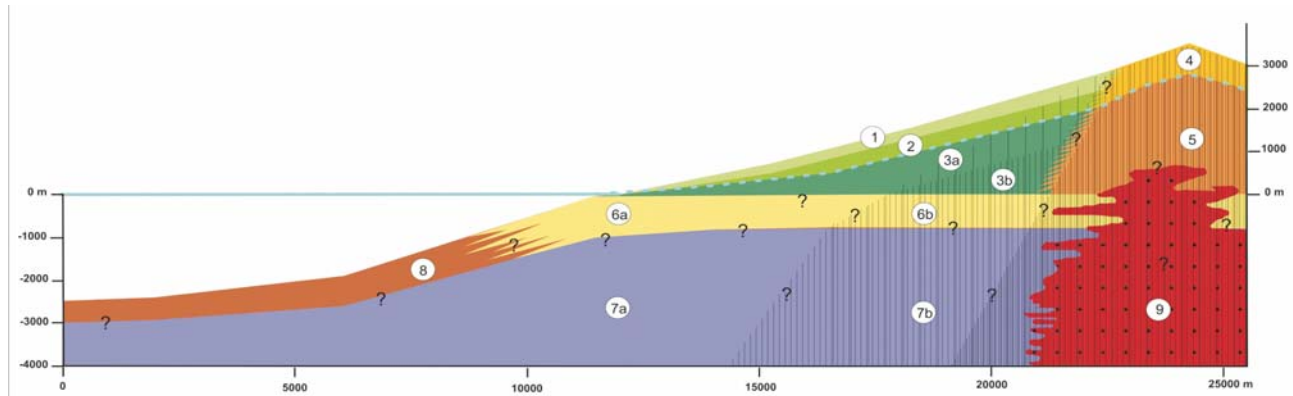


**Figure 21** - Geological and geomechanical model representative of the pre-landslide volcanic edifice of Gúimar and La Orotava landslides (Ferrer *et al.*, 2008). Dashed blue line: water level; question marks: uncertainties.

- Unit 1: Recent lava flows with scoria layers, with a low degree of alteration, interbedded lenses of loose scoria and cavities.
- Unit 2: Slightly altered lava flows with scoria layers; lower presence of cavities than Unit 1.
- Unit 3: Altered lava flows and highly compacted pyroclastic layers with intense dike intrusion.
- Unit 4: Pyroclasts and lava flows with scoria, low alteration, high compaction and intense dike intrusion.
- Unit 5: Pyroclasts and altered lava flows, with very intense dike intrusion, highly compacted and fractured.
- Unit 6: Hyaloclastite rocks from subaerial flows as well as from submarine eruptions.
- Unit 7: Pillow-lavas from submarine eruptions representing the main phase of submarine growth of the island.
- Unit 8: Deposits from gravitational slides on the submarine island flanks.
- Unit 9: Dikes and plutonic complex.

A summary of geomechanical properties corresponding to the rock units is shown in Table 11.

From these 9 units, hyaloclastite rocks (unit 6) are a rare rock type not only from the mineralogical and fabric

point of view but also because of their unusual geomechanical properties. However, very few geotechnical studies have been carried out on this type of rock.

Hyaloclastites are composed of clastic particles of irregular shape with sizes ranging from 0.5 to 3 cm, forming a green, grey or brown coloured breccia (Fig. 22). This material is poorly consolidated and weakly cemented. Voids and vacuoles with sizes from 0.5 to 3 cm are occasionally present. Secondary minerals are observed inside them. Fracture zones and slickenside surfaces have been identified.

The deformational properties of the hyaloclastite rock mass were obtained from 16 pressuremeter tests carried out at different depths in boreholes. Pressuremeter module values ranged from 50 MPa to 3,200 MPa, with mean representative values of 560 MPa. Table 12 shows some mechanical properties of the hyaloclastites obtained from laboratory tests.

### 7.3. Stability conditions of the pre-failure edifice

Stability analysis was carried out on the pre-failure edifices of the Gúimar and La Orotava valleys applying limit equilibrium and stress-strain methods (Ferrer *et al.*, 2011). A first analysis was developed using rock mass pa-

**Table 11** - Geomechanical indexes and properties of volcanic rocks.

Material	RMR*	GSI*	$\sigma_{ci}$ (MPa)	$\gamma_{dry}$ (kN/m <sup>3</sup> )	$\gamma_{sat}$ (kN/m <sup>3</sup> )
Lava flows in massive layers	57-68	52-63	98	24	25
Lava flows and scoria layers	-	14-25	34	15	16
Altered lava flows	44-55	39-50	46	17	18
Pyroclasts	-	9-20	2	12	14
Dikes	55-70	50-65	175	27	28
Hyaloclastite rocks	-	10-21	6	21	24
Pillow-lavas	63-68	58-63	150	27	28

\*The lower values of intervals correspond to materials below water table.

RMR = rockmass rating, GSI = Geological strength index,  $\sigma_{ci}$  = uniaxial compressive strength,  $\gamma_{dry}$  = dry unit weight,  $\gamma_{sat}$  = saturated unit weight.



**Figure 22** - Hyaloclastite rock cores.

**Table 12** - Hyaloclastite intact rock properties.

Property	Mean values
Unit weigh	23-29 kN/m <sup>3</sup>
Uniaxial strength	16 MPa
Tensile strength	1.5-1.8 MPa
Young modulus	4,300 MPa
Poisson coefficient	0.27-0.31
Strength parameters $c, \phi$	3-5 MPa; 43-50°

rameters obtained from the application of Hoek-Brown failure criterion (Table 13). Figure 23 gives the results of the analysis showing a deformational pattern affecting the whole edifice. In this case the factor of safety is higher than 1.3. A second stability analysis was carried out to obtain the strength values for the hyaloclastites for limit equilibrium conditions. Figure 24 shows the results obtained. In this

**Table 13** - Strength and deformation properties obtained for the units of the pre-failure edifice using Hoek and Brown criterion.

Unit	$c$ (MPa)	$\phi$ (°)	$E$ (MPa)
1	0.9	51	6,750
2	1.7	47	8,920
3a	2.3	34	4,200
3b	3.1	25	2,780
4	0.9	33	2,300
5	2.8	22	2,050
6a	1.5	30	1,010
6b	2.5	35	1,170
7a	8.0	36	12,020
7b	11.4	34	13,180
8	1.0	20	1,000
9	13.2	33	10,230

case, the strain distribution shows larger deformations affecting the hyaloclastites and defining a complex failure surface. Values of 0.1 MPa for cohesion and 16° for angle of friction were obtained to reach limit equilibrium conditions.

A multiple successive failure mechanism was also analysed. The results are shown in Fig. 25. A critical factor of safety (near or lower than 1.00) is obtained for this type of failure mechanism. Potential failure surfaces are obtained from these results that are in accordance with the geomorphological and geological features observed in the Güímar and La Orotava valleys, as well as with the geomechanical properties of the materials involved (Ferrer *et al.*, 2010).

#### 7.4. Uncertainty analysis

The uncertainties in the stability model of the island edifices were analysed by logic tree methods. To identify sources or larger uncertainties a preliminary analysis was carried out at the early stages of the project, before site investigations. The results showed that the geomechanical properties of the hyaloclastite submarine rocks rated the highest uncertainty values (63%). A second uncertainty analysis was carried out after site investigation on the submarine rocks. The uncertainties were reduced to 21%. Several logic trees were developed for each factor contributing to flank stability. Figure 26 gives an example, showing the uncertainty value of 39% for flank stability before site investigation. After site investigation this value was reduced to 26%.

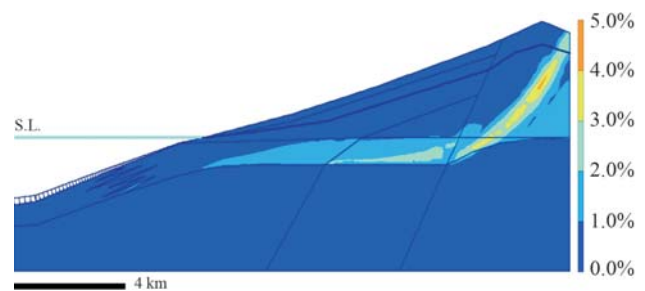


**Figure 23** - Deformational model from the stability analysis using Table 13 data. Horizontal scale = vertical scale.

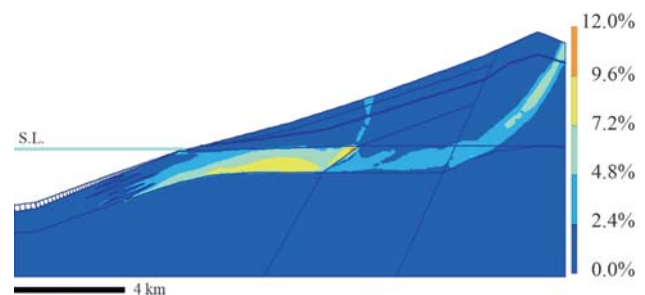


**Figure 24** - Deformational model for the initiation of failure ( $FS = 1.0$ ) and strength values for hyaloclastite rocks:  $c = 0.1$  MPa and  $\phi = 19^\circ$ . Horizontal scale = vertical scale.

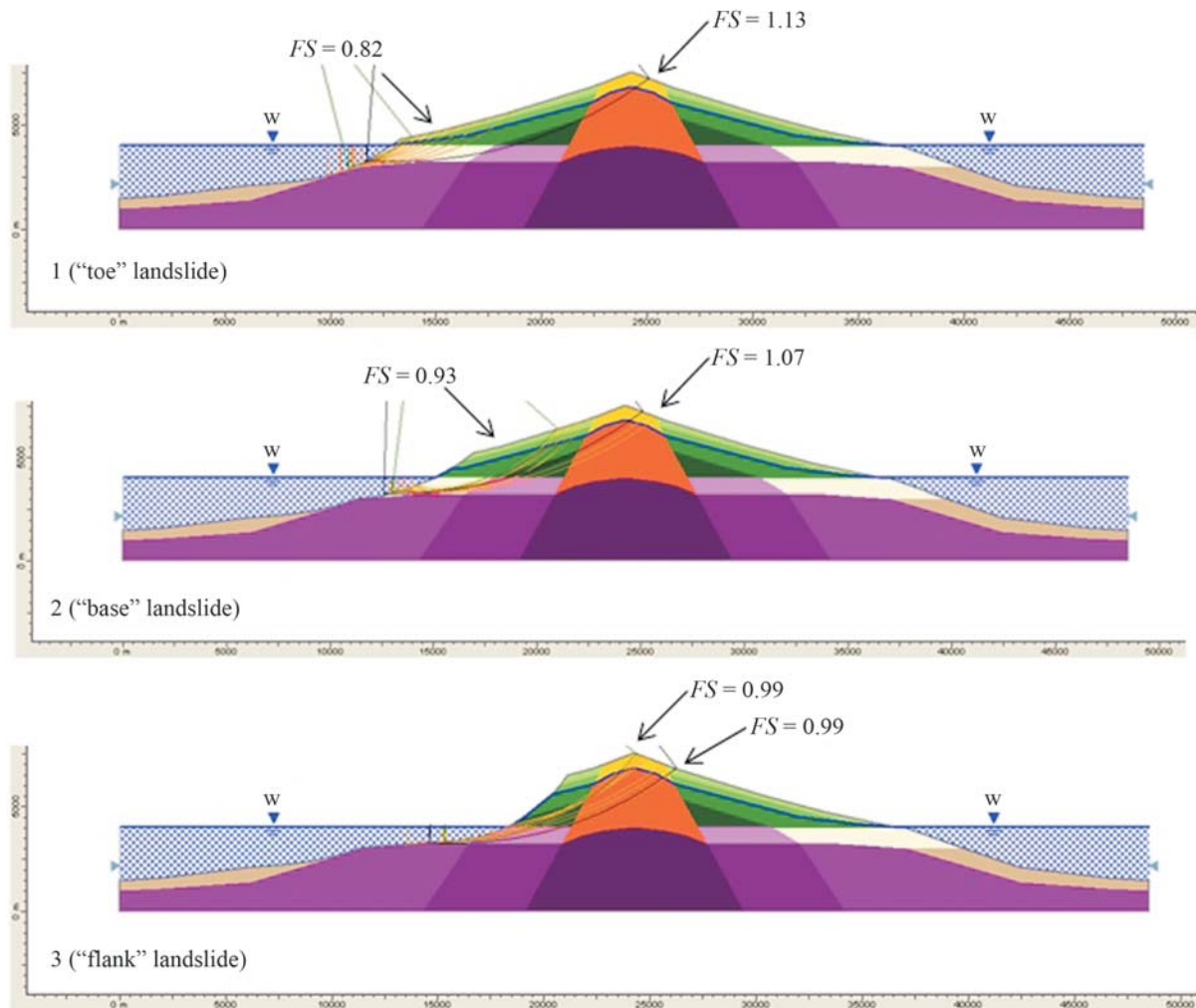


**Figure 25** - Successive failure mechanism analysis for the volcanic flanks of Tenerife.

### 7.5. Tsunami deposits

Tsunami deposits have been identified in Teno (Tenerife), Piedra Alta (Lanzarote) and Agaete (Gran Canaria) (Fig. 27). The Agaete deposits have been described by Pérez Torrado *et al.* (2002) and Madeira *et al.* (2011). At least 3 different tsunami events have been identified over the last 2 Ma. Some sedimentological features of these deposits are shown in Fig. 28. Paleontological and paleoclimatic investigations indicate an age between 1.8 to 2.0 Ma (Meco *et al.*, 2008).

The Teno tsunami deposits, in Tenerife (Fig. 29), are probably associated with the flank collapse of El Teide volcanic pre-edifice or Cañadas Edifice, c. 150-180 ka. The Piedra Alta tsunami deposits, on the island of Lanzarote (Fig. 30), contain many specimens of marine fauna. An age of c. 330 ka has been attributed, based on paleoclimatic and paleontological criteria (Meco *et al.*, 2008).

The sedimentological characteristics of all these deposits indicate a high energy source and a high speed mechanism of the landslide materials entering the sea. Although

the tsunami sources are still being investigated, a relationship with the large landslides occurring in the Canary Islands during the Pleistocene is the most probable origin.

The possible run-up of the largest waves of these tsunamis may have exceeded a height of 50 m at the Agaete and Teno sites, and of at least 25 m at the Piedra Alta site, as deduced from the location of the deposits today and sea level changes during the last 2 Ma.

Figure 27 shows the location of tsunami deposits and potential landslide source areas. More absolute dating measurements are needed to establish direct relationships between specific landslides and tsunami deposits.

### 7.6. Conclusions

The instability of the pre-failure edifices of the island flanks of Güimar and La Orotava, originated when a critical height of the island and a critical slope angle were reached. Flank instability was initiated under the sea where hyaloclastite rocks are present with low strength and high deformability properties, playing a fundamental role in sta-

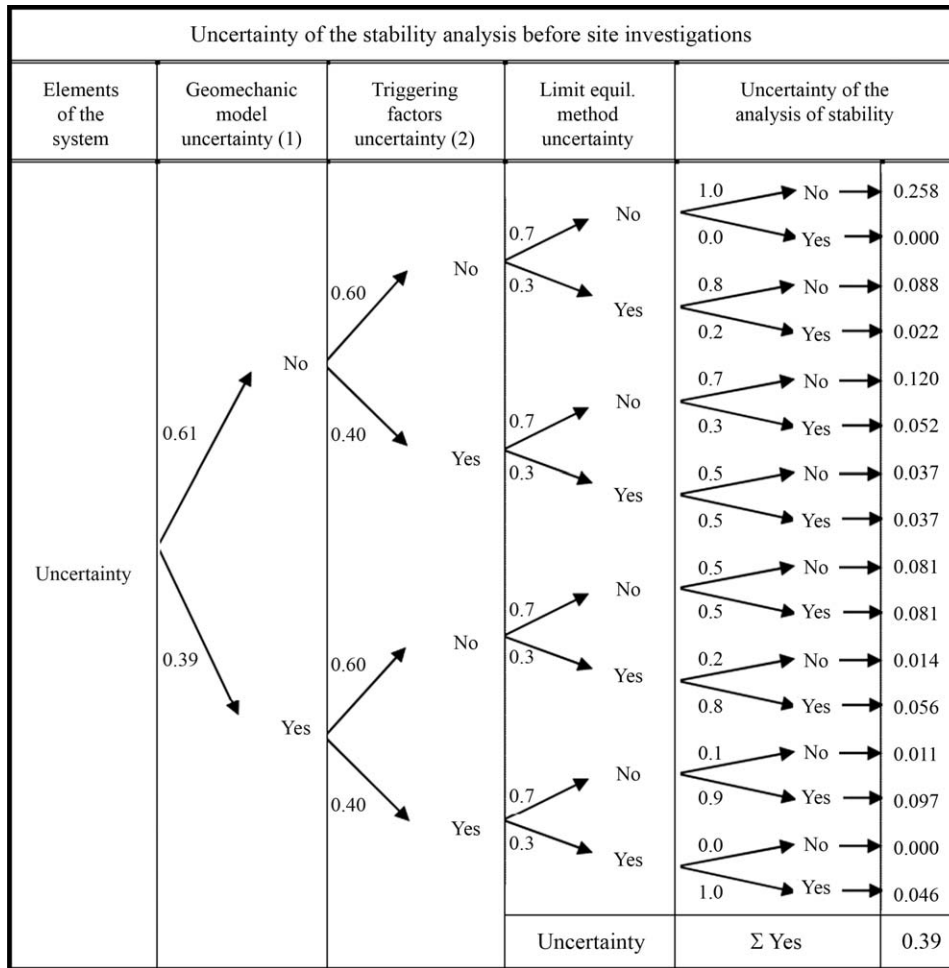


**Figure 26** - Uncertainties of the stability analysis before site investigations were carried out by logic tree methods (Seisdedos, 2008). 1 and 2: uncertainties of the geomechanical model and the triggering factors, respectively, using additional logic trees results.

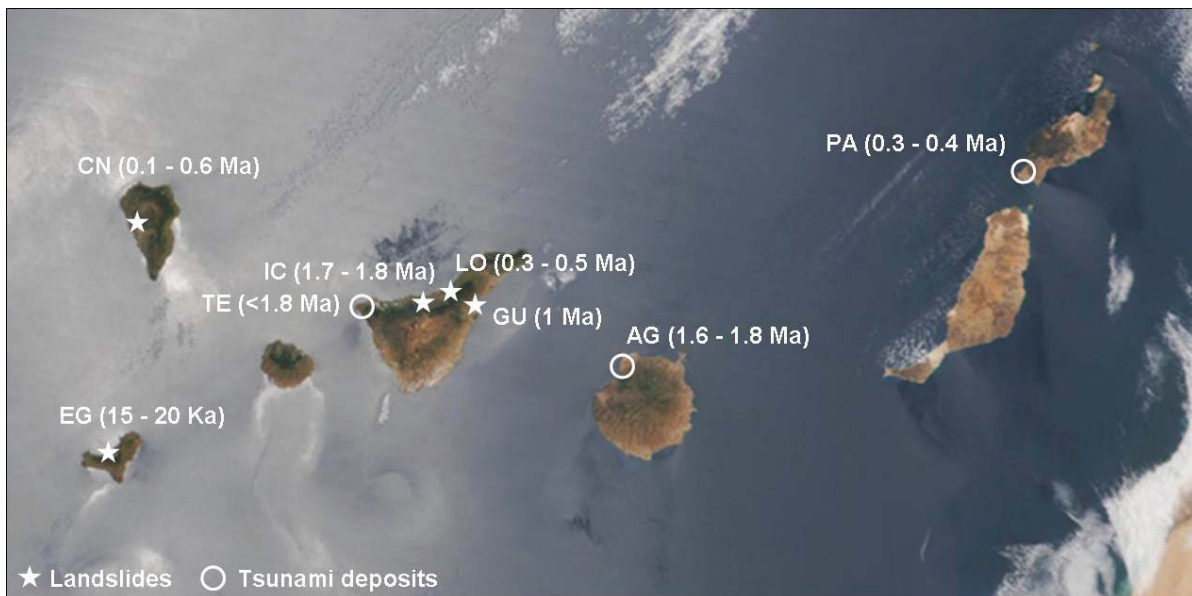


**Figure 27** - Large paleo-landslides and tsunami deposits in the Canary Islands. Landslides: CN- Cumbre Nueva (La Palma), EG- El Golfo (El Hierro), IC: Icod, LO: La Orotava (Tenerife), GU: Guímar (Tenerife). Tsunamis: TE- Teno (Tenerife), AG- Agaete (Gran Canaria), PA- Piedra Alta (Lanzarote).

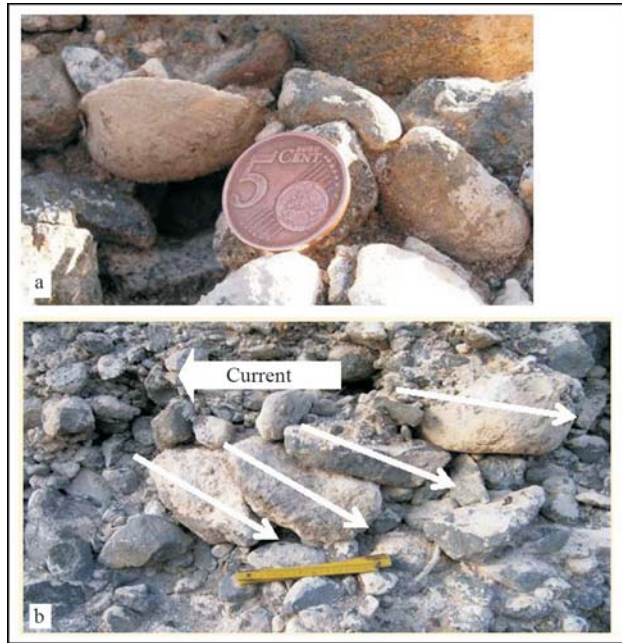


**Figure 28** - Agaete tsunami deposits with *glycimeris* shells fossils and imbricated flat boulders showing paleo-current direction (photos from J. Madeira).



**Figure 29** - Tsunami deposits in Teno, northwest coast of Tenerife (area shown 2 m height).

bility. Other contributing factors to flank instability include volcanic activity and seismic shaking. The instability process may have generated several large landslides and associated tsunamis. The tsunami deposits identified on several islands suggest a very rapid mass movement of rocks and debris falling into the sea with a high energy impact. Tsunami waves may have reached a height of over 50 m and may have been propagated to neighbouring islands many km away from the tsunami sources. Landslides are natural building and dismantling processes on volcanic islands, and are present not only in the Canary Islands but in many other islands worldwide, e.g. Hawaii, Fogo in Cabo Verde and Reunion.



**Figure 30** - Piedra Alta tsunami deposits located in the southwest coast of Lanzarote (area shown 2.5 m height).

At least 3 mega-landslides have occurred in Tenerife in the last 1 Ma being the recurrent time of tsunamis generated by these large landslides of some hundreds of thousands of years. On the other hand, Eff-Darwich *et al.* (2010), estimate a recurrent time from El Teide (Tenerife) and Cumbre Vieja (La Palma) flank collapses over 130,000 years.

## 8. Concluding Remarks

In the previous sections 3 case studies have been analysed as examples of the Engineering Geological Method (EGM) applied to geo-hazard assessment for engineering and territorial planning purposes. Different types of geo-hazards, including landslides on geotechnical and geological scales, earthquakes, tsunamis and induced seismicity, have been considered. The most significant results are summarised in Tables 14, 15 and 16.

Fifteen different types of methodologies have been used in the 3 cases (Table 14), 6 of these common to all cases:

- Geological surveys
- Geomorphologic and remote sensing studies
- Tectonic and active faulting investigations
- Geochronology and absolute dating
- Geotechnical site investigations
- Statistical and probabilistic analysis.

Table 15 shows the most relevant results: in case 1 and case 3, the extremely low probability of the geo-hazards analysed practically rules out any risk; however, in case 2, the earthquake resistant building standards for the region underestimate the seismic hazard.

Social acceptability has been compared before and after hazard assessment results (Table 16). These results point out the importance of the EGM approach to social acceptability. According with the criteria shown in Table 5, social acceptability to risks in the cases analysed can be

classified as follow: acceptable (I) for case 1 and case 3, and acceptable with restrictions (II) for case 2.

To conclude, the following aspects can be highlighted:

- Engineering Geological Methodology (EGM) is a practical tool for geo-hazard and risk assessment when engineering or planning design decisions have to be considered. This approach integrates different methodologies and procedures from geological, geo-engineering, statistic and probabilistic and engineering sciences.
- Applying EGM to the case studies analysed has resulted in the following engineering decisions and social implications:
  - Itoiz dam is safe for the geo-hazards considered. Social alarm has subsided and legal and political actions have been cancelled.
  - The extremely low probability of mega-landslides and tsunamis rules out any practical consideration of these for engineering and urban planning purposes in the Canary Islands.
  - Earthquake resistant standards for building construction in the Canary Islands underestimate the seismic hazard and should be revised.

**Table 14** - Engineering geological methods used in the case studies analysed for hazard assessment.

Type of studies, surveys and methods	Case 1	Case 2	Case 3
Geological surveys	X	X	X
Geomorphological and remote sensing	X	X	X
Sedimentological, petrological and mineralogical investigations	-	X	X
Tectonic and active faulting studies	X	X	X
Geochronology and absolute dating	X	X	X
Paleontological studies	-	-	X
Geotechnical site investigation	X	X	X
Land geophysics	X	-	-
Marine geophysics	-	X	X
Geotechnical instrumentation	X	-	-
Geotechnical modelling and analysis	X	-	X
Seismicity studies	X	X	-
Paleo-seismological investigation	-	X	-
Historical records	-	X	-
Statistical and probabilistic analysis	X	X	X

Case 1: Itoiz dam. Case 2: regional seismic hazards. Case 3: landslides and tsunamis.

**Table 15** - Results of the application of engineering geological methods to geo-hazard assessment.

Case study	Case 1		Case 2		Case 3	
	Itoiz dam safety	Regional seismic hazards	Regional seismic hazards	Landslides and tsunamis hazards	Landslides	Tsunamis
Type of hazard	Slope instability	Earthquake hazard	Seismic hazard	Large landslides	Large landslides	Large tsunamis affecting the Canary Islands coasts
Size	3x10 <sup>6</sup> m <sup>3</sup> landslide volume	Max. event during reservoir filling <i>M</i> = 4.6	Max. historic event <i>I</i> = IX Max. instrumental event <i>M</i> = 5.2	Some of the largest in the world by volume	Some of the largest in the world by volume	Large tsunamis affecting the Canary Islands coasts
Frequency	3 landslides from 38 ka to 12 ka ago	Probable EQ <i>M</i> = 5.1	Moderate to low magnitude EQ for 500 to 1,000 years RP	Over 20 landslides during last 2 Ma	Over 20 landslides during last 2 Ma	Tsunamis associated to large landslides
Maximum potential events	Non active for the last 12 ka	EQ from potential active fault <i>M</i> ≈ 6.5	EQ from potential active fault <i>M</i> = 6.8	> 100 km <sup>3</sup> volume	> 100 km <sup>3</sup> volume	Tsunamis run up waves 50 m height
Hazard assessment	<i>FS</i> > 1.6-500 yr RP <i>FS</i> > 1.5-1,000 yr RP <i>FS</i> > 1.1-5,000 yr RP	PGA 0.08 <i>g</i> - 500 yr RP PGA 0.12 <i>g</i> - 1,000 yr RP PGA 0.30 <i>g</i> - 5,000 yr RP	EQ from paleoseismic data PGA ≈ 0.22-0.35	<i>p</i> < 10 <sup>-5</sup>	<i>p</i> < 10 <sup>-5</sup>	<i>p</i> < 10 <sup>-5</sup>
Engineering implications	No risk even for extreme events	Conventional buildings at risk in zones with PGA values ≥ 0.05 <i>g</i> . Seismic codes should be revised	No risk for either infrastructures nor territorial planning			

*M* = magnitude; *I* = intensity; EQ = earthquake; RP = return period; PGA = peak ground acceleration; *FS* = factor of safety; *p* = probability of occurrence.

**Table 16** - Social acceptability and economical impact of the case studies analysed.

Case study	Before hazard assessment	After hazard assessment
Case 1 Itoiz dam safety	Social opposition to dam construction. Negative economic impact.	No social opposition. Dam operating normally. Positive economic impact.
Case 2 Regional seismic hazard	Social concern even with low magnitude earthquakes.	Social and professional demands on revision building seismic codes.
Case 3 Landslides and tsunamis	Social alarm. High impact on media. Increase if insurance costs. Negative tourism impact.	No social alarm. No tourist concern.

- Although codes and regulations can state design criteria for different hazard scenarios, the society will not accept the risk of failure or its environmental consequences in the short, medium or long term, therefore engineering projects should provide not only design parameters, but also include scientific criteria that prove that the project solutions are socially acceptable.

## Acknowledgments

The author is very grateful to the Portuguese Geotechnical Society and Association of Geotécnicos Antigos Alunos da Universidade Nova de Lisboa to be invited to present the XXVII Manuel Rocha Lecture. He is indebted to his colleagues who have contributed to the results presented in this paper, in particular to Dra. Mercedes Ferrer, Dra. Julia Seisdodos, Angel Rodriguez Franco, Dr. Juan Miguel Insua, Dr. Julian Garcia Mayordomo, Juan Jesus Coello, Jose Manuel Navarro, Dr. Jose Antonio Rodriguez Losada, Juan Carlos Garcia Davalillo, Luis Enrique Hernandez, Prof. Cesar Andrade, Dr. Jose Madeira, Dra. Conceição Freitas, Prof. Ramón Capote and Luis Cabrera. The author gratefully acknowledges the cooperation of Rene Gomez and Raimundo Lafuente and the assistance of Beatriz Blanco in the preparation of this paper.

## References

- Acosta, J.; Uchupi, E.; Muñoz, A.; Herranz, P.; Palomo, C. & Ballesteros, M. (2003) Geologic evolution of the Canary Islands of Lanzarote, Fuerteventura, Gran Canaria and La Gomera and comparison of landslides at these island with those at Tenerife, La Palma and El Hierro. *Mar. Geophys. Res.*, 24:1-40.
- Ambraseys, N.N.; Simpson, K.A. & Bommer, J.J. (1996) Prediction of horizontal response spectra in Europe. *Earthquake Eng. Struct. Dynamics*, 25:371-400.
- Atkinson, G.M. (2010) Ground motion prediction equations for Hawaii from a referenced empirical approach. *Bull. Seism. Soc. Am.*, 100:751-761.
- Banda, E.; Danobeitia, J.J.; Suriñach, E. & Ansorge, J. (1981) Features of crustal structure under the Canary Islands. *Earth Planet. Sci. Lett.*, 55:11-24.

- Benito, B.; Cabañas, L.; Jiménez Peña, M.E.; Cabañas, C.; Álvarez Rubio, S.; López Arroyo, L.; Ramírez, M.S. & Nuche, R. (1999) Caracterización Sísmica de Emplazamientos de la Península Ibérica y Evaluación del Daño Potencial en Estructuras. Proyecto Daños. Consejo de Seguridad Nuclear, Madrid, 240 pp.
- Benoit, J.P. & McNutt, S.R. (1996) Global volcanic earthquake swarm database 1979-1989. *U.S. Geol. Surv. Open-File Rep.*, 96-69, 32 pp.
- Bommer, J.J.; Scherbaum, F.; Bungum, H.; Cotton, F.; Sabetta, F. & Abrahamson, N.A. (2005) On the use of logic trees for ground-motion prediction equations in seismic hazard analysis. *Bull. Seism. Soc. Am.*, 95:377-389.
- Bosshard, E. & MacFarlane, D.J. (1970) Crustal structure of the western Canary Islands from seismic refraction and gravity data. *J. Geophys. Res.*, 75:4901-4918.
- Carbó, A.; Muñoz-Martín, A.; Llanes, P.; Álvarez, J. & ZEE Working Group (2003) Gravity analysis offshore the Canary Islands from a systematic survey. *Mar. Geophys. Res.*, 24:113-127.
- CETS (Commission on Engineering and Technical System) (1995) Probabilistic Methods in Geotechnical Engineering. National Research Council, Washington, D.C., 95 pp.
- Cornell, C.A. (1968) Engineering seismic risk analysis. *Bull. Seism. Soc. Am.*, 58:1583-1606.
- Cornell, C.A. & Vanmarcke, E.H. (1969) The major influences on seismic risk. *Proc. Fourth World Conference on Earthquake Engineering*, Santiago, v. 1, pp. 69-83.
- Dziewonski, A.M.; Ekström, G.; Woodhouse, J.H. & Zwart, G. (1990) Centroid-moment tensor solutions for April-June 1989. *Phys. Earth Planet. Int.*, 60:243-253.
- Eff-Darwich, A.; García-Lorenzo, B.; Rodríguez-Losada, A.; de la Nuez, J.; Hernandez-Gutierrez, L.E. & Romero-Ruiz, M.C. (2010) Comparative analysis of the impact of geological activity on the structural design of the telescope facilities in the Canary Islands, Hawaii and Chile. *Mon. Not. R. Astron. Soc.*, 407:1361-1375.
- Fenton, G.A. & Griffiths, D.V. (2008) Risk Assessment in Geotechnical Engineering. John Wiley & Sons, New York, 461 pp.

- Ferrer, M.; González de Vallejo, L.; Seisdedos, J.; Coello, J.J.; García, J.C.; Hernandez, L.E.; Casillas, R.; Martín, C.; Rodríguez, J.A.; Madeira, J.; Andrade, C.; Freitas, C.; Lomoschitz, A.; Yepes, J.; Meco, J. & Betancort, J.F. (2011) Güimar and La Orotava landslides (Tenerife) and tsunami deposits in Canary Islands. Proc. 2nd World Landslide Forum, Roma, Springer. (In press).
- Ferrer, M.; Seisdedos, J. & González de Vallejo, L.I. (2010) The role of hyaloclastite rocks in the stability of the volcanic island flank of Tenerife. Olalla, C.; Hernández, L.E.; Rodríguez-Losada, J.A.; Perucho, A. & González-Gallego, J. (eds), Volcanic Rock Mechanics. Taylor and Francis Group, London, v. 1, pp. 167-170.
- Ferrer, M.; González de Vallejo, L.I.; Seisdedos, J.; García, J.C.; Coello Bravo, J.J.; Casillas, R.; Martín, C. & Hernández, L.E. (2008) Large rockslides hazards in Tenerife island. Geological analysis and geomechanical modeling of instability mechanism. Proyecto CGL2004-00899, Instituto Geológico y Minero de España, Madrid, 340 pp.
- Gomes Coelho, A. (2005) O problema das falhas activas na engenharia civil. Número especial XXII Lição Manuel Rocha. Geotecnia, 105:13-67.
- González de Vallejo, L. & Ferrer, M. (2011) Geological Engineering. CRC Press / Balkema, 678 pp.
- González de Vallejo, L.; Rodriguez Franco, J.A.; Seisdedos, J.; Insua, J.M., García-Mayordomo, J.; Blazquez, R. & López Queiro, S. (2009) Análisis y Seguimiento del Embalse de Itoiz: Estabilidad de Laderas, Sismicidad y Condiciones Geotécnicas. Plan Nacional de Investigación Científica, Ministerio de Medio Ambiente, Madrid, 1056 pp.
- González de Vallejo, L.I.; Hijazo, T. & Ferrer, M. (2008) Engineering geological properties of the volcanic rocks and soils of the Canary Islands. Soils and Rocks, 31:3-13.
- González de Vallejo, L.I.; García-Mayordomo, J. & Insua, J.M. (2006) Probabilistic seismic hazard assessment of the Canary Islands. Bull. Seism. Soc. Am., 96:2040-2049.
- González de Vallejo, L.; Rodriguez Franco, J.A.; Insua, J.M. & García-Mayordomo, J. (2005) Informe de supervisión de los estudios y análisis disponibles sobre la seguridad de la Presa de Itoiz. Ministerio de Medio Ambiente, Colegio Oficial de Geólogos de España, Madrid, 110 p. www.icog.es and downloader on January 1st 2012.
- González de Vallejo, L.I.; Capote, R.; Cabrera, L.; Insua, J.M. & Acosta J. (2003) Paleoliquefaction evidence in Tenerife (Canary Islands) and possible seismotectonic sources. Mar. Geophys. Res., 24:149-160.
- González de Vallejo, L. (1994) Seismotectonic hazard for engineering projects in moderate seismicity regions. Proc. 7th. Int. Congress of Eng. Geology, Lisbon, Key-note Lecture Volume, pp. XIX-XXXVIII.
- Gupta, H.K. (2002) A review of recent studies of triggered earthquakes by artificial water reservoirs with special emphasis on earthquakes in Koyna, India. Earth-Sciences Reviews, 58:279-310.
- Gutierrez, F.; Lucha, P. & Galve, J.P. (2007) Cartografía geomorfológica del entorno del embalse de Yesa. Confederación Hidrográfica del Ebro, Zaragoza, 35 pp.
- Hoek, E. (1991) When is a design in rock engineering acceptable? Proc. 7th Int. Conf. on Rock Mechanics. ISRM. Aachen, Germany, v. 3, pp. 1485-1497.
- Instituto Geográfico Nacional (IGN) (1982) Catálogo General de Isostas de la Península Ibérica. Publicación 202. Instituto Geográfico Nacional, Madrid, 323 pp.
- Instituto Geográfico Nacional (IGN) (2004) Seismic Network and Stations. Instituto Geográfico Nacional, Madrid, www.geo.ign.es on January 1st 2012.
- Ishihara, K. (1985) Stability of material deposit during earthquakes. Proc. 11 th. Int. Conf. Soil. Mech. and Found. Eng. San Francisco. A.A. Balkema, Rotterdam, v. 1, pp. 321-376.
- Madeira, J.; Ferrer, M.; González de Vallejo, L.I.; Andrade, C.; Freitas, M.C.; Lomoschitz, A. & Hoffman, D. (2011) Agaete revisited: new data on the Gran Canaria tsunamites. Geophysical Research Abstracts. European Geosciences Union (EGU). General Assambly, 13:2292-2294.
- Masson, D.G.; Watts, A.B.; Gee, M.J.R.; Urgeles, R.; Mitchell, N.C.; Le Bas, T.P. & Canals, M. (2002) Slope failures on the flanks of the western Canary Islands. Earth Sci. Rev., 57:1-35.
- McGarr, A.; Simpson, D. & Seeber, L. (2002) Case histories of induced and triggered seismicity. Lee, W.H.K.; Kanamori, H.; Jennings, P.C. & Kisslinger, C. (eds) International Handbook of Earthquake and Engineering Seismology, Part A. Academic Press, New York; pp. 647-661.
- McHarg, I.L. (1969) Design with Nature. The American Museum of Natural History, New York, 198 pp.
- Meco, J. (2008) Paleoclimatología del Neógeno en las Islas Canarias - Pleistoceno y Holoceno. Ministerio de Medio Ambiente, Madrid, 204 pp.
- Mezcua, J.; Burford, E.; Udías, A. & Rueda, J. (1992) Seismotectonic of the Canary Islands. Tectonophysics, 208:447-452.
- Mogi, K. (1963) Some discussion on aftershock, foreshocks and earthquake swarms. The fracture of a semi-infinite body caused by an inner stress origin and its relation to the earthquake phenomena. Bull. Earth. Res. Inst., 41:615-658.
- Morgenstern, N.R. (1991) Limitations of stability analysis geotechnical practice. Geotecnia, 61:5-19.

- Munson, C.G. & Thurber, C.H. (1997) Analysis of the attenuation of strong ground motion on the Island of Hawaii. *Bull. Seism. Soc. Am.*, 87:945-960.
- Nadim, F. (2007) Tools and strategies for dealing with uncertainty in Geotechnics. Griffiths, D.V. & Fenton, G.A. (eds) *Probabilistic Methods in Geotechnical Engineering*, Springer, New York, pp. 71-96.
- Navarro, J.M. (1974) Estructura geológica de la isla de Tenerife y su influencia sobre la hidrogeología. *Actas del I Congreso Internacional sobre Hidrología en Islas Volcánicas*, Lanzarote, v. 1, pp. 37-57.
- NCSE-94 (1994) Norma de Construcción Sismorresistente: Parte General y Edificación, Real Decreto 2543/1994 de 29 de Diciembre, Boletín Oficial del Estado núm. 33 de 8 de Febrero de 1995, Madrid, pp. 3935-3980.
- NCSE-02 (2002) Norma de Construcción Sismorresistente Parte General y Edificación, Real Decreto 997/2002 de 27 de septiembre, Boletín Oficial del Estado núm. 244 del viernes 11 de octubre de 2002, Madrid, pp. 35898-35967.
- Obermeier, S.F.; Pond, E.C. & Olson, S.C. (2001) Paleoliquefaction studies in continental settings: geological and geotechnical features in interpretations and back-analysis. U.S. Geol. Survey. Openfile Report, 01-29, 75 pp.
- Obermeier, S.F. (1996) Use of liquefaction induced features for paleoseismic analysis. *Eng. Geol.*, 44:1-76.
- Ordaz, M.; Aguilar, A. & Arboleda, J. (1999) Program for Computing Seismic Risk. Instituto de Ingeniería, Universidad Nacional Autónoma de México, México City.
- Pérez Torrado, F.; Paris, R.; Cabrera, M.C.; Carracedo, J.C.; Schneider, J.L.; Wassmer, P.; Guillou, H. & Gimeno, D. (2002) Depósitos de tsunami en el valle de Agaete, Gran Canaria (Islas Canarias). *Geogaceta* 32:75-78.
- Seisdedos, J. (2008) Large Paleo-Rokslides of Güimar and La Orotava (Tenerife): Geological Analysis, Instability Mechanisms and Geomechanical Modeling. PhD Thesis, Universidad Complutense de Madrid. E-prints Complutense, Madrid, 512 p.
- Simpson, D.W. (1986) Triggered earthquakes. *Ann. Rev. Earth Planet. Sci.*, 14:21-42.
- Smith, K. (2001) *Environmental Hazards. Assessing Risk and Reducing Disaster*. 3rd ed. Routledge, London, 392 pp.
- Varnes, D.J. (1984) *Landslide Hazard Zonation: A Review of Principles and Practice*. UNESCO, Paris, 64 pp.
- Ward, S.N. & Day, S. (2001) Cumbre Vieja volcano potential collapse and tsunami at La Palma, Canary Islands. *Geophys. Res. Lett.*, 28(17):3397-3400.
- Wells, D.L. & Coppersmith, K.J. (1994) New empirical relationships among magnitude, rupture length, rupture area, and surface displacement. *B. Seismol. Soc. Am.*, 84:974-1002.
- Whitman, R.V. (1984) Evaluating calculated risk in geotechnical engineering. *Proceed. Geotech. Div. JI. of the American Soc. of Civil Engineers*, 110(2):143-188.

## ***Articles***

***Soils and Rocks***  
**v. 35, n. 1**



# Considerations on the Probability of Failure of Mine Slopes

A.S.F.J. Sayão, S.S. Sandroni, S.A.B. Fontoura, R.C.H. Ribeiro

**Abstract.** Probabilistic and deterministic stability analyses of the progress of a large mine pit excavation in Brazil are presented herein. A simple method of reliability analysis for quantifying the probability of failure of slopes has been considered and its advantages and limitations are briefly discussed. The variance of the factor of safety is computed for several stages of the mine excavation. It is shown that, depending on the slope height, either the friction angle or the effective cohesion may be the most important variable controlling stability. In the case of mine pit excavations ranging from 50 to 400 m in height, pore pressures are of lesser relative importance. Consequently, increasing the capacity of the horizontal drainage system may be of limited efficiency in stabilizing potentially unsafe mine slopes. In addition, variables with no significant effect on the stability, such as the apparent specific gravity of the slope material, may be simply considered as deterministic parameters.

**Keywords:** probability of failure, reliability analysis, slope stability, factor of safety.

## 1. Introduction

In open pit mine slopes, adequate safety and serviceability must be ensured with maximum economy. Deterministic stability analysis for a specific slope configuration involves assigning an average value to each variable considered in calculating the Factor of Safety ( $FS$ ), which is usually defined as the ratio between strength  $R$  and solicitation  $S$ . The minimum acceptable value of  $FS$  in slope studies is usually defined on the basis of the designer's previous experience and on the predicted consequences of a potential failure. Uncertainties present in the definition of geomaterial parameters are not taken into consideration in deterministic computations.

However, each variable has a distribution of probable values, from which a mean value and a standard deviation can be defined. A probabilistic analysis considers the distributions of random variables in  $R$  and  $S$  for obtaining the distribution of  $FS$  values. Acceptable risk in mine pit slope design varies from one situation to another. It is not rare to consider a high probability of failure to be tolerable in situations where the cost of slope stabilization is higher than the costs of cleaning up or mining to flatter angles (Barnett *et al.*, 2001).

Different designers will usually accept or assume different safety degrees for a given slope situation. As a consequence, diverse values of calculated risk will be inherently adopted (Sandroni & Sayão, 1992). Hence, two questions may be raised: (1) How reliable is the adopted slope design? (2) How to compute the calculated risk of a slope failure in a simple, practical method?

In trying to answer these questions, probabilistic and statistic tools should be used in a rational reliability procedure, thus providing a means for evaluating the combined effects of uncertainties (Duncan, 2000). Two types of reliability analysis may be considered. The first, denoted as Relative Reliability, consists on the evaluation of the slope safety by a reliability index ( $\beta$ ). Its use has become progressively common in geotechnical practice. The second type of analysis, defined as Global Reliability, describes the slope risk by taking into consideration all random variables involved. Although this global risk analysis may be considered as more accurate, it is very difficult to be implemented in practice (Mostyn & Li, 1993).

This paper presents a simplified procedure for quantifying the relative reliability of mine slopes, with comments on the advantages and limitations of the probabilistic approach. The examples herein reported are based on the First Order Second Moment (FOSM) method (Christian *et al.*, 1992).

Other probabilistic techniques, like the Monte Carlo and the Point Estimate methods, have also been used in Geotechnical Engineering. Details on these methods are provided by El-Ramly *et al.* (2002) and Baecher & Christian (2003). More innovative probabilistic analysis procedures, like the random finite-element method (RFEM), are also becoming available. This method employs elastoplastic relations in a finite-element model combined with a random field theory in a Monte Carlo or a Point Estimate framework (Hammah *et al.*, 2009; Griffiths *et al.*, 2009). The RFEM was shown to correctly search for the weakest

A.S.F.J. Sayão, Associate Professor, Departamento de Engenharia Civil, Pontifícia Universidade Católica do Rio de Janeiro, Rio de Janeiro, RJ, Brazil. E-mail: sayao@puc-rio.br.

S.S. Sandroni, Principal, Geoprojetos Eng. Ltd, and Visiting Professor at Pontifícia Universidade Católica do Rio de Janeiro, Rio de Janeiro, RJ, Brazil. E-mail: sandro@geoprojetos.com.br.

S.A.B. Fontoura, Associate Professor, Departamento de Engenharia Civil, Pontifícia Universidade Católica do Rio de Janeiro, Rio de Janeiro, RJ, Brazil. E-mail: fontoura@puc-rio.br.

R.C.H. Ribeiro, Associate Professor, Departamento de Engenharia Civil, Universidade Federal do Espírito Santo, Vitória, ES, Brazil. E-mail: romulocastello@yahoo.com.br.

Submitted on December 15, 2009; Final Acceptance on April 3, 2012; Discussion open until September 30, 2012.

failure path through heterogeneous materials, leading to probabilities of failure higher than would be predicted by disregarding spatial variations. Although promising, this advanced numerical technique is not yet readily available to geotechnical practice.

## 2. Reliability Index

The reliability index concept comprises the behaviour of a performance function defined by  $G = R - S$ , which describes the safety condition of a slope and may be denoted by  $G(X)$ . In this function,  $X$  is an array of the random input parameters or variables. A safe condition is defined by  $G(X) > 0$ . An unstable domain is defined by  $G(X) < 0$ , characterizing the slope failure. The boundary value,  $G(X) = 0$ , is generally referred as the limit state boundary.

In a slope stability problem, considering that the random variables have a normal (Gaussian) distribution, the margin of safety may be expressed by the reliability index  $\beta$ , as proposed by Hasofer & Lind (1974):

$$\beta = \frac{\overline{FS} - 1.0}{\sigma[FS]} \quad (1)$$

In Eq. 1,  $\overline{FS}$  denotes the mean value of the factor of safety distribution and 1.0 is the value corresponding to failure, while  $\sigma[FS]$  is the standard deviation of  $FS$ . The index  $\beta$  is therefore equivalent to the number of standard deviations that separates the computed safety factor from the failure value. It is important to note that the use of non-Gaussian distributions in Eq. 1 may yield to inaccurate results. Similar considerations in slope safety applications have been reported by Chowdhury *et al.* (1987) and Christian *et al.* (1994). Probabilistic approaches for various design applications have been presented: Fenton *et al.* (2005) and Ribeiro *et al.* (2008) reported on slope stabilization walls while Aoki & Tsuha (2010) described the use of reliability on pile design.

## 3. Probability of Failure

The risk associated to the collapse of a slope is directly related to its relative probability of failure  $P_f$ , which is the probability of  $G(X)$  being smaller than zero. The relationship between the reliability index  $\beta$  and the probability of failure  $P_f$  is given by the following expression (Catalán & Cornell, 1976):

$$P_f = \Phi(-\beta) = 1 - \Phi(\beta) \quad (2)$$

In this equation,  $\Phi(\beta)$  is the cumulative distribution function of normalized  $G(X)$  with reference to  $\beta$ . Equation 2 is applicable to any distribution of  $FS$ , depending on the value of the reliability index  $\beta$ . Lee *et al.* (1983) and Whitman (1984) present typical values of the reliability index for non-Gaussian distributions.

Dell Avanzi (1995) proposed an indirect relation between Eq. 1 and other non-Gaussian distributions. In this case, the relationship between  $\beta$  and  $P_f$  is not unique and depends on the standard deviation  $\sigma[FS]$ .

Figure 1 compares the  $\beta \times P_f$  relations for normal and lognormal densities. For any given  $FS$  distribution, it is seen that an increasing reliability index  $\beta$  corresponds to a decreasing probability of failure  $P_f$ . For  $\beta < 0.8$ , the value of  $P_f$  is nearly independent of the assumed distribution of  $FS$  function. For  $\beta > 0.8$ , the normal (Gaussian) distribution gives the highest value of  $P_f$ . Hence, it may be considered as a conservative assumption.

The value of maximum  $P_f$  (or minimum  $\beta$ ) to be recommended for a slope condition will depend on the consequences of a potential failure and on the uncertainties related to the project. Whitman (1984) and Harr (1987) recommended typical values of relative probability of failure for various geotechnical design situations in practice. Table 1 presents a summary of these recommendations. It may be noted that the reliability of open pit mine slopes is usually the lowest within geotechnical problems. This suggests that mining engineers usually work with lower margins of safety, or higher values of relative probability of failure. This may be explained by the need to minimize volumes of

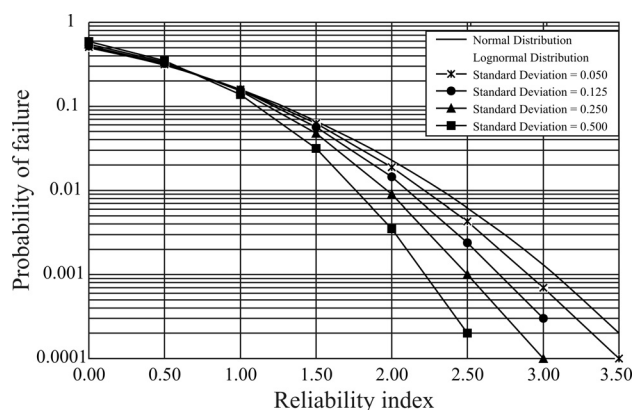


**Figure 1** - Comparison of  $\beta$  vs.  $P_f$  relationships for normal and lognormal distributions of  $FS$ .

**Table 1** - Typical values of reliability index and relative probability of failure in geotechnical practice.

Application	Reliability index $\beta$	Probability of failure $P_f$
Mine pit slopes	1.0 to 2.3	$2 \times 10^{-1}$ to $10^{-2}$
Foundations and retaining structures	2.0 to 3.0	$2 \times 10^{-2}$ to $10^{-3}$
Earth dams	3.5 to 5.0	$2 \times 10^{-3}$ to $10^{-5}$

waste excavation. Moreover, an eventual slope failure may have only limited consequences.

#### 4. Procedure for Reliability Analysis

The technique considered for reliability analyses is called FOSM – First Order Second Moment method (Christian *et al.*, 1992) and may be summarized in five simple steps:

##### Step 1 - Evaluation of the mean and standard deviation values for all variables

Geotechnical parameters (friction angle, cohesion, unit weight, and pore pressure) and geometrical factors (slope height, and inclination) may be defined as random variables. The cost for obtaining meaningful experimental data is an important consideration in this step. Lee *et al.* (1983) and Ribeiro (2008) listed typical values of coefficient of variation ( $CV = \sigma[FS] / \overline{FS}$ ) for different soil parameters. These typical values are summarised in Table 2 and may be helpful in preliminary reliability estimates.

##### Step 2 - Search for the critical slip surface and $\overline{FS}$

In this step, deterministic stability analyses are accomplished with one of the well known limit equilibrium methods (*i.e.*, Bishop, 1955; Janbu, 1957; Morgenstern & Price, 1965). The mean values of the random variables are used in these analyses. Two assumptions are implicitly related to the critical slip surface (Sandroni & Sayão, 1992): the computed factor of safety is the mean value of the  $FS$  distribution, and the corresponding  $\beta$  is the lowest value of the reliability index. The errors associated to these assumptions were reported to be negligible for earth dam and mine slopes (Dell Avanzi, 1995, and Guedes, 1997, respectively). However, Li & Lumb (1987) and Assis *et al.* (1997) suggested that critical surfaces for minimum  $FS$  and minimum  $\beta$  should be always investigated.

##### Step 3 - Evaluation of the partial derivatives of the $FS$ function

These derivatives are estimated by divided differences. A small increment is separately imposed to each variable  $x_i$ , yielding the corresponding variation of the factor of safety ( $dFS$ ). The ratio  $dFS/dx_i$  may be approximated to the partial derivative of the performance function for the variable  $x_i$  (Christian *et al.*, 1992). The magnitude of  $dx_i$  needs to be small enough to validate the partial derivative approximation, but large enough to yield a meaningful value of  $dFS$ . Dell Avanzi (1995) reported that increments of 10% of the mean value of the selected variable may be acceptable for slope safety calculations. However, in other practical situations, like shallow or deep foundations, the increments  $dx_i$  may need to be smaller (Ribeiro, 2008).

##### Step 4 - Evaluation of the standard deviation of $FS$ distribution

The variance of the  $FS$  function has been defined by (Harr, 1987):

$$V[FS] = \sum_{i=1}^n \left( \frac{\partial FS}{\partial x_i} \right)^2 \cdot V[x_i] \quad (3)$$

where  $V[x_i]$  is the variance of variable  $x_i$ . By definition, the variance of  $x_i$  is the square of its standard deviation ( $\sigma[x_i]$ ). Likewise, the standard deviation  $\sigma[FS]$  is obtained by computing the square root of the variance  $V[FS]$ . The use of Eq. 3 is appropriate only to statistically independent random variables. Its application to dependent variables may induce significant errors, depending on the covariance of each pair of variables considered in the analysis. In the applications herein described, the assumption of statistical independence is adequate.

**Table 2** - Typical values of the coefficient of variation from geotechnical literature.

Geotechnical parameter	Coefficient of variation (%)	
	Minimum	Maximum
Unit weight of saturated soils ( $\gamma_{sat}$ )	3	7
Coefficient of permeability of saturated clays ( $k$ )	68	90
Coefficient of consolidation of saturated clays ( $c_v$ )	33	68
Compression index of saturated clays ( $c_c$ )	10	37
Undrained strength of saturated clays ( $S_u$ )	13	40
Effective friction angle of saturated clays ( $\phi'$ )	2	13
Tangent of effective friction angle of gneissic residual soils ( $\tan \phi'$ )	2,4	16,1
Effective cohesion of gneissic residual soils ( $c'$ )	13,4	18,4
Standard penetration number ( $N_{SPT}$ )	15	45
Piezicone tip resistance ( $q_c$ )	5	15

### Step 5 - Evaluation of the probability of failure

After computing the reliability index  $\beta$  from Eq. 1, the value of  $P_f$  may be obtained from Fig. 1, considering the assumed distribution of  $FS$ .

## 5. Example of Probabilistic Analysis of a Mine Slope

The FOSM method described in the previous section allows identifying the relative contributions of each random variable in the uncertainty associated to the factor of safety. This may be very useful for the designer, when deciding upon the most adequate method for stabilising a potentially unstable slope (Sandroni & Sayão, 1992; Dell Avanzi & Sayão, 1998).

An example illustrating this aspect is the following analysis of relative probability of failure for a large open pit mine in Brazil. The slope consists predominantly of residual soil from a schist rock, with high content of quartz and mica, remaining from exploration of iron ore. Fig. 2 shows a schematic cross section of the slope. Average inclination was  $34^\circ$  and the height ranged from  $H = 30$  to  $400$  m, as mining operations progressed.

Piezometric conditions were defined from comprehensive long-term field instrumentation and may be reasonably represented by two linear phreatic segments. At the top portion of the slope, the water table was horizontal and  $80$  m deep. As the mine pit was deepened, horizontal drainage holes were progressively installed to avoid the pit bottom area to becoming submerged. Therefore, the phreatic line could be taken as an inclined line ending at the foot of the slope.

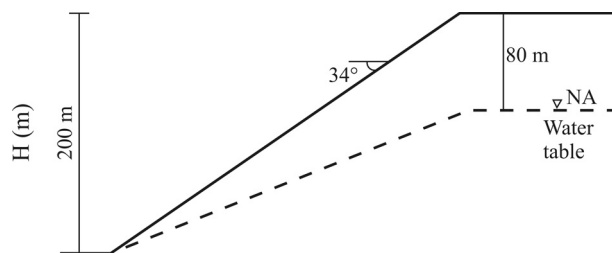


Figure 2 - Cross-section of a large mine slope in Brazil.

Average and standard deviation values of geotechnical and piezometric parameters, which were considered as variables, are presented in Table 3. Geotechnical data was obtained from about 50 direct shear tests on undisturbed specimens of the residual soil. For convenience,  $\tan \phi'$  was considered as the friction random variable, instead of  $\phi'$ . Farias & Assis (1998) reported that either  $\phi'$  or  $\tan \phi'$  may be used, with no differences in the computed value of  $P_f$ . In this case, geometric factors (slope height and inclination) have been considered as deterministic variables.

Conventional limit equilibrium slope stability analyses, with Janbu's method and average values from Table 3, indicated a safety factor  $\overline{FS} = 1.34$  for a  $200$  m high slope. Computation of the variance of the safety factor for this case is detailed in Table 4, which summarizes steps 3 and 4 of the procedure for reliability analysis. The computed variance of the safety factor is  $V[FS] = 0.0259$ , which corresponds to a standard deviation  $\sigma[FS] = 0.161$ .

From Eq. 1, the reliability index  $\beta = 2.12$  is computed. For estimating the relative probability of failure (step 5), an assumption is required on the  $FS$  distribution. From Fig. 1,

Table 3 - Variable parameters for the iron ore mine slope analysis.

Variable $x_i$	Symbol	Average $\bar{x}_i$	Standard deviation $\sigma [x_i]$	Variance $V[x_i]$
Effective friction	$\tan \phi'$	0.781	0.085	0.0072
Effective cohesion	$c'$ (kPa)	25.0	24.3	590.0
Unit weight (natural)	$\gamma_{nat}$ (kN/m <sup>3</sup> )	28.3	1.4	1.96
Unit weight (saturated)	$\gamma_{sat}$ (kN/m <sup>3</sup> )	29.0	1.4	1.96

Table 4 - FOSM method: probabilistic analysis of a mine slope with  $\overline{FS} = 1.34$ .

Variable $\bar{x}_i$	$V[x_i]$	$dx_i$	$dFS_i$	$dFS_i/dx_i$	$(dFS_i/dx_i)^2 \cdot V[x_i]$
$\tan \phi' = 0.781$	0.0072	0.11	+0.188	+1.6682	0.020037 (77.1%)
$c' = 25.0$ kPa	590.0	2.50	+0.004	+0.0016	0.001510 (5.8%)
$\gamma_{nat} = 28.3$ kN/m <sup>3</sup>	1.96	2.83	-0.004	-0.0014	0.000004 (0.0%)
$\gamma_{sat} = 29.0$ kN/m <sup>3</sup>	1.96	2.90	+0.022	+0.0078	0.000119 (0.4%)
$z_p = 80$ m	400.0	10.0	-0.033	-0.0033	0.004356 (16.7%)
Total $V[FS] = 0.026026$ (100%)					

$\overline{FS} = 1.34$ ,  $\sigma[FS] = 0.161$ ,  $\beta = 2.12$ ,  $P_f = 0.017$ .

and assuming a normal distribution of  $FS$ , the value  $P_f = 0.017$  (or  $P_f = 1:60$ ) may be obtained for the 200 m high slope.

An important aspect to be noted in Table 4 refers to the relative significance of each variable in the stability calculations. Friction angle is by far the most relevant variable in this case, contributing to about 77% of the computed variance of  $FS$ . On the other hand, uncertainty in cohesion has little effect, contributing to less than 6% of  $V[FS]$ . The piezometric head, given by the phreatic surface, is of limited importance (about 17% of  $V[FS]$ ). This implies that a more intense drainage system could be of limited efficiency for increasing the safety in this 200 m high mine slope.

For the same 200 m high mine slope, an attempt was made for obtaining the value of  $P_f$  from Monte Carlo technique. Computations with  $10^5$  iterations made use of GeoSlope software adopting Janbu method. The random field piezometric conditions could not be correctly simulated in this procedure, because the inclined phreatic segment would not end at the slope's base when the standard deviation was automatically taken into account. Hence, deterministic piezometric conditions were considered, with the top horizontal phreatic level at the minimum ( $z_p = 60$  m), intermediate ( $z_p = 80$  m) or maximum ( $z_p = 100$  m) depths and the inclined phreatic line passing through the foot of the slope. Strength parameters and unit weights were the only random variables, with average and deviation values listed in Table 3. The results of Monte Carlo simulations are shown in Table 5.

The worst scenario in Monte Carlo analyses (60 m deep deterministic phreatic level) leads to a  $P_f$  value similar to the one given by FOSM method ( $P_f = 0.017$ ). Disregarding the field variation of the phreatic level about its average 80 m depth was highly non-conservative, for it resulted in a much lower probability of failure. Considering this limitation of the Monte Carlo method in simulating the field phreatic variations in this case, further probabilistic analyses were carried out with the FOSM technique.

### 6. Probabilistic Analyses of a Progressing Excavation

Several configurations of the same iron ore mine slope have then been analyzed, with heights ranging from 30 to 400 m. Geotechnical variables were presented in Table 3. Figure 3 shows schematically the slope cross-sections, with the water level being considered to pass through

**Table 5** - Monte Carlo method: probabilistic analysis of a mine slope with  $FS = 1.34$ .

$z_p$ (m)	$FS$	$\sigma [FS]$	$\beta$	$P_f$
60	1.28	0.14	1.98	0.0166
80	1.37	0.15	2.47	0.0037
100	1.45	0.16	2.85	0.0017

the slope foot, in slopes with  $H > 80$  m. For smaller slopes, pore pressures were considered to be insignificant.

Figure 4 presents a summary of the stability studies, with both  $FS$  and  $P_f$  plotted as a function of slope height. In these analyses, safety factors were computed by the Simplified Bishop procedure (Bishop, 1955).

It may be noted that the magnitude of the mean factor of safety ( $FS$ ) is continuously reduced with the progress of mine excavation (or with increasing slope height). As a consequence, a continuous increase in the probability of failure with increasing height could be expected. However, for  $H$  values up to 150 m,  $P_f$  exhibits no increase with increasing slope height. On the contrary, an initial slight reduction of  $P_f$  may be observed. This may be explained by a stronger contribution of cohesion to the variance of  $FS$ , when slope height is still less than 150 m. A high variability of  $c'$ , as represented by its high value of standard deviation, has been commonly reported for unsaturated residual soils.

An investigation of the relative contributions of all variables to the computed values of  $V[FS]$  is summarized in Table 6. The relevance of  $c'$  is noted to decrease significantly with increasing height. Cohesion is shown to be the most important variable only for mine slope heights inferior to 100 m. For higher values of  $H$ , normal stresses at the potential slip surface become large enough to cause friction

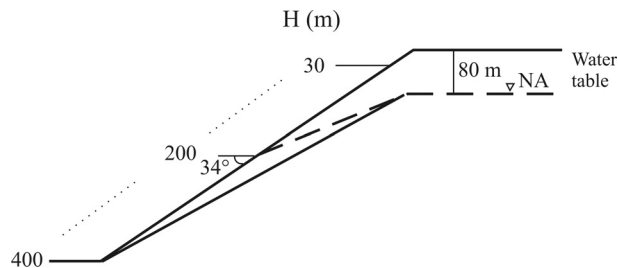


**Figure 3** - Geometry of mine slopes considered in the reliability studies of stability.

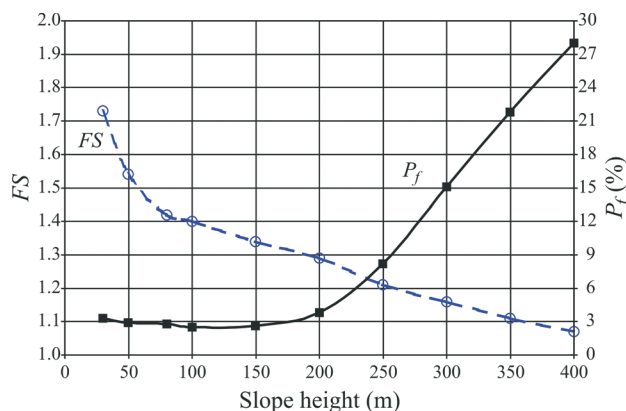


**Figure 4** - Effect of height in the stability studies of the iron ore mine slope.

**Table 6** - Relative contribution of random variables to  $V[FS]$  for various slope heights.

Height (m)	Relative contribution (%)				
	$c'$	$\tan\phi'$	$\gamma_{nat}$	$\gamma_{sat}$	Piezometric head (m)
30	86.3	13.4	0.18	0.00	0.00
50	76.8	22.9	0.20	0.00	0.00
80	66.0	33.8	0.15	0.00	0.00
100	58.4	41.2	0.15	0.00	0.15
150	43.9	55.1	0.76	0.01	0.12
200	9.2	69.2	0.02	0.07	21.4
250	10.1	68.5	0.00	0.20	21.1
300	7.4	72.0	0.00	0.29	20.1
350	7.9	72.8	0.02	0.35	18.8
400	2.2	76.9	0.02	0.36	20.4

to be the most significant variable in the stability of this mine slope.

Table 6 also shows that natural or saturated unit weights always have a very small contribution to the uncertainty of  $FS$ . Therefore,  $\gamma_{nat}$  or  $\gamma_{sat}$  could have been taken as deterministic variables in this case, with very little effect in the computed values of  $\beta$  and  $P_f$ .

A relevant practical conclusion may also be taken from Table 6, regarding the role of pore pressures in the stability of these mine slopes. For all excavation depths ranging from 80 to 400 m, the relative contribution of the piezometric head ranges from 15 to 20% of  $V[FS]$ . This suggests that the drainage system was well dimensioned and further drainage would be of limited consequence to the stability of this mine slope.

An additional aspect to be noted is the marked influence of the limit equilibrium stability method on the relative probability of failure. For  $H = 200$  m, a value of  $P_f = 0.038$  (or  $P_f = 1:26$ ), based on the Simplified Bishop's method, is obtained from Fig. 4. With Janbu's method, however, a lower probability of failure value of  $P_f = 0.017$  (or  $P_f = 1:60$ ) has been computed, as reported in section 5.

Similar conclusions have also been warned by Dell Avanzi & Sayão (1998) and Farias & Assis (1998). It is therefore essential to always consider the same limit equilibrium method when comparisons are to be made in probabilistic analyses of slope safety.

## 7. Conclusions

A comprehensive investigation on the reliability of a mine slope has been reported. Several situations of the same mine, as excavation proceeded with slope heights from 30 to 400 m, have then been analysed. Practical conclusions on the advantages and limitations of the probabilistic approach in assessing the stability of the slope mine

have been presented. Reliability analyses based on the FOSM (First Order Second Moment) method proved to be very simple and practical.

The value of mean factor of safety ( $\overline{FS}$ ) was shown to decrease continuously with the progress of mine excavations. However, the relative probability of failure ( $P_f$ ) was noted to increase only for slope heights  $H$  greater than 150 m.

The relative importance of each variable in the stability of the mine slope is a relevant information resulting from FOSM computations. The contributions of natural and saturated unit weights to the uncertainty of  $FS$  were negligible. Therefore,  $\gamma_{nat}$  or  $\gamma_{sat}$  could be taken as deterministic variables in this stability assessment. As the mine excavation progressed, the most important parameter was gradually changed from effective cohesion to friction angle. Moreover, for excavation heights smaller than 150 m, pore pressures were shown to be insignificant to these reliability analyses. For higher slopes, pore pressure was still of secondary relevance in comparison to the friction angle. As a consequence, further drainage of the mine slope would have a limited impact on the stability of the excavation.

For the mine slope herein described, the use of Monte Carlo method was not suitable for incorporating the field random variation of the piezometric head (or pore pressure). Horizontal drains ensured the phreatic line was fixed at the foot of the excavation, but it was variable at the top. This condition has been easily incorporated in the FOSM analyses, but is difficult to be duplicated in the Geo-Slope program. Yet, for comparison, Monte Carlo computations were carried out considering the pore pressure as a deterministic variable. For a 200 m high excavation, the value of  $P_f$  obtained from FOSM was close to  $P_f$  from Monte Carlo with the top phreatic line at its maximum level (worst condition).

The marked influence of the limit equilibrium stability method on the relative value of  $P_f$  was demonstrated. It is thus essential to always consider a single limit equilibrium method in probabilistic analyses of slope safety.

## Acknowledgments

The authors thank the Brazilian research agencies CNPq and CAPES for the financial support. Contributions from Dr. E. Dell Avanzi and Ms. M.C. Guedes in earlier studies on reliability analyses at PUC-Rio are also appreciated.

## References

- Aoki, N. & Tsuha, C.H.C (2010) Use of Characteristic Value in the analysis of safety and confiability of structures and foundations (in Portuguese). Proc. 15<sup>o</sup> Brazilian Conference on Soil Mechanics and Foundation Engineering, COBRAMSEG, Gramado, v. 1, ID467.
- Assis, A.P.; Espósito, T. & Almeida, M. (1997) Comparison between two probabilistic methods in the stability

- analysis of a mine slope (in Portuguese). Proc. 2nd Pan-American Symposium on Landslides, PSL, Rio de Janeiro, v. 1, p. 347-352.
- Baecher, G. & Christian, J.T. (2003) Reliability and Statistics in Geotechnical Engineering. John Wiley and Sons Ltd, 618 pp.
- Barnett, W.; Guest, A.; Terbrugge, P. & Walker, D. (2001) Probabilistic pit slope design in the Limpopo metamorphic rocks at Venetia Mine. The Journal of the South African Institute of Mining and Metallurgy, v. 101:8, p. 381-392.
- Bishop, A.W. (1955) The use of the slip circle in the stability analysis of slope. Géotechnique, v. 5:1, p. 7-17.
- Catalán, J.M. & Cornell, C.A. (1976) Earth slope reliability by a level crossing method. Journal of Geotechnical Engineering Division, ASCE, v. 102:GT6, p. 591-604.
- Chowdhury, R.N.; Tang, W. & Sidi, I. (1987) Reliability model of progressive slope failure. Géotechnique, v. 37:4, p. 467-481.
- Christian, J.T.; Ladd, C.C. & Baecher, G. (1992) Reliability and probability in stability analysis. Journal of Geotechnical Engineering Division, ASCE, v. 120:2, p. 1071-111.
- Christian, J.T.; Ladd, C.C. & Baecher, G. (1994) Reliability applied to slope stability analysis. Journal of Geotechnical Engineering Division, ASCE, v. 120:12, p. 2180-2207.
- Dell Avanzi, E. (1995) Confiability and Probability in Slope Stability Analyses (in Portuguese). M.Sc. Thesis, Civil Engineering Department, Pontifical Catholic University of Rio de Janeiro, 125 pp.
- Dell Avanzi, E. & Sayão, A.S.F.J. (1998) Evaluation of the probability of failure of slopes (in Portuguese). Proc. 11th Brazilian Conference on Soil Mechanics and Geotechnical Engineering, COBRAMSEG, Brasília, v. 2, p. 1289-1296.
- Duncan, J.M. (2000) Factors of safety and reliability in geotechnical engineering. Journal of Geotechnical and GeoEnvironmental Engineering, ASCE, v. 126:4, p. 307-316.
- El-Ramly, H.; Morgenstern, N.R. & Cruden D.M. (2002) Probabilistic slope stability analysis for practice. Canadian Geotechnical Journal, v. 39:3, p. 665-683.
- Farias, M.M. & Assis, A.P. (1998) A Comparison of Probabilistic Methods Applied to the Stability of Slopes (in Portuguese). Proc. 11th Brazilian Conference on Soil Mechanics and Geotechnical Engineering, COBRAMSEG, Brasília, v. 2, pp. 9.
- Fenton, G. A.; Griffiths, D.V. & Williams, M.B. (2005) Reliability of traditional retaining wall design. Géotechnique, v. 55:1, p. 55-62.
- Griffiths, D.V.; Huang, J. & Fenton, G. A. (2009) Reliability influence of spatial variability on slope reliability using 2-D random fields. Journal of Geotechnical and Geo-Environmental Engineering, ASCE, v. 135:10, p. 1367-1378.
- Guedes, M.C.S. (1997) Considerations on Probabilistic Analyses of Slope Stability (in Portuguese). M.Sc. Thesis, Civil Engineering Department, Pontifical Catholic University of Rio de Janeiro, 146 pp.
- Hammah, R.E.; Yacoub, T.E. & Curran, J.H. (2009) Probabilistic slope analysis with the finite element method. Proc. 43rd US Rock Mechanics Symposium and 4th US-Canada Rock Mechanics Symposium, Asheville, v. 1, pp. 8.
- Harr, M.E. (1987) Reliability Based Design in Civil Engineering. McGraw Hill Book Co., New York, 291 pp.
- Hasofer, A.M. & Lind, N.C. (1974) Exact and invariant second-moment code format. Journal of the Engineering Mechanics Division, ASCE, v. 100:1, p. 111-121.
- Janbu, N. (1957) Earth pressure and bearing capacity calculations by generalised procedure of slices. Proc. 4th International Conference on Soil Mechanics and Foundation Engineering, London, v. 2, pp. 207-212.
- Lee, I.K.; Weeks, W. & Ingles, O. (1983) Geotechnical Engineering. Pitman Pub. Co., Marshfield, 508 pp.
- Li, K.S. & Lumb, P. (1987) Probabilistic design of slopes. Canadian Geotechnical Journal, v. 24:4, p. 520-535.
- Morgenstern, G.G. & Price, V.E. (1965) The analysis of the stability of general slip surfaces. Géotechnique, v. 15:1, p. 79-93.
- Mostyn, G.R. & Li, K.S. (1993) Probabilistic Slope Analysis – State of Play. Li, K.S. & Lo, S-C.R. (eds) Probabilistic Methods in Geotechnical Engineering, A.A. Balkeema, The Netherlands, pp. 89-110.
- Ribeiro, R.C.H.; Sayão, A.S.F.J. & Castello, R.R. (2008) Application of probabilistic methods to the design of retaining walls (in Portuguese). Proc. 11th National Geotechnical Congress, Portuguese Geotechnical Society, Coimbra, v. 2, pp. 283-288.
- Ribeiro, R.C.H. (2008) Applications of Probability and Statistics in Geotechnical Analyses (in Portuguese). Doctoral Thesis, Civil Engineering Department, Pontifical Catholic University of Rio de Janeiro, 161 pp.
- Sandroni, S.S.; Santana, F.C.; Ramos, J.M. & Sayão, A.S.F.J. (1992) Failed slope in mica-schist saprolitic soil in Cauê Mine (in Portuguese). Proc. 1st Brazilian Conference on Slopes, COBRAE, Rio de Janeiro, v. 1, pp. 285-292.
- Sandroni, S.S. & Sayão, A.S.F.J. (1992) Statistical evaluation of the factor of safety of slopes (in Portuguese). Proc. 1st Brazilian Conference on Slopes, COBRAE, Rio de Janeiro, v. 2, pp. 523-535.
- Whitman, R.V. (1984). Evaluating calculated risk in geotechnical engineering. Journal of Geotechnical Engineering Division, ASCE, v. 110:2, p. 145-188.



# Electroosmosis in the Remediation of Tropical Soils Contaminated with Cadmium: Effect of the Incubation Time

R.Z. Velten, D.C. Lima, M.P.F. Fontes, C.A.B. Carvalho

**Abstract.** This paper addresses the effect of cadmium incubation time on the electroosmotic decontamination of three residual soils from the *Zona da Mata Norte*, Minas Gerais State, Brazil. The laboratory testing program included the following: (i) materials, encompassing a lateritic clayey silty sand (soil 1), a non-lateritic clayey silty sand (soil 2), and a non-lateritic sandy silty clay (soil 3) impregnated with an aqueous solution of cadmium nitrate in the concentration of  $100 \text{ mg.L}^{-1}$ ; (ii) soils and mixtures specimens compaction at the Standard AASHTO compaction effort; (iii) mixtures contaminant incubation times of 1, 10 and 20 days before performing the electroosmotic decontamination tests; (iv) sequential extraction analysis in order to identify the different contaminant chemical forms in the mixtures specimens. The results support that incubation time and soils chemistry and mineralogy were significant and influential factors in the decontamination process, as well as the 20 days incubation period was the optimum among the tested times.

**Keywords:** soils contaminated with Cadmium, electroosmotic remediation, incubation time, sequential extraction.

## 1. Introduction

Soils may be contaminated by heavy metals from several sources, including disposal of mining residues, inadequate treatment of industrial hazardous wastes, improper disposal of used batteries, accidental leaks and military activities (Adriano, 1986).

Even though several soil decontamination techniques have been developed in the past decades, many of them proved to be unsatisfactory and, in some cases, too expensive for *in situ* remediation. However, the use of electroosmosis and, consequently, of electrokinetic phenomena has been a technical and economical solution for the remediation of clayey soils contaminated by heavy metals, once these materials generally present low hydraulic conductivity, high specific surface, and also because many reactions that happen during the soil remediation process are dynamic, pH dependent, reversible and currently not yet well understood, as emphasized by Alshawabkeh *et al.* (1999).

According to Chang & Liao (2006), electrokinetic phenomena have been a better way to the remediation of contaminated areas by different pollutants, such as: heavy metals, organic compounds and tailings from radionuclides and mining. According to these authors, the main practical aspects of interest to the application of decontamination of soils by electrokinetic phenomena are: (i) it is a technique that can be used *in-situ* or in laboratory; (ii) it has high effi-

ciency in the decontamination of different contaminants; (iii) there is electro-osmotic flux in any kind of soil, including heterogeneous soils; (iv) it has applicability in contaminated soils with low hydraulic conductivity; (v) it has high economic efficiency; and (vi) it can be used interacted or integrated with other chemical or biological remediation technique. These authors mention that electrokinetic remediation technique presents some advantages, and the main one is the generation of an acid front in the anode, which can be beneficial because it releases the metals in the soil, but it can be also responsible for the destruction of minerals presents in the soil.

The electrokinetic phenomena in soils involve relative movements of electricity, charged surfaces, and liquid phases, basically, represented by four conduction mechanisms known as electroosmosis, streaming potential, electrophoresis and migration or sedimentation potential, as reported by Mitchell (1993). However, it should be emphasized that the most important mechanisms for the removal of soil contaminants through electrokinetic processes are the electroosmosis and the electrophoresis.

The electroosmosis remediation technique uses a direct and low density electric current of order of mA by  $\text{cm}^2$  of the transversal section area between the electrodes or a difference of electric potential of few volts per centimeter through distant electrodes in soil with open-flow arrangement (Shapiro & Probstein, 1993; Acar & Alshawabkeh, 1993, 1996).

R.Z. Velten, MSc, Universidade Federal de Viçosa, Av. P.H. Rolfs s/n, 36570-000 Viçosa, MG, Brazil. e-mail: rodrigozorral@hotmail.com.

D.C. Lima, Professor, Universidade Federal de Viçosa, Departamento de Engenharia Civil, Av. P.H. Rolfs s/n, 36570-000 Viçosa, MG, Brazil. e-mail: declima@ufv.br.

M.P.F. Fontes, Professor, Universidade Federal de Viçosa, Departamento de Solos, Av. P.H. Rolfs s/n, 36570-000 Viçosa, MG, Brazil. e-mail: mpfontes@ufv.br.

C.A.B. Carvalho, Associate Professor, Universidade Federal de Viçosa, Departamento de Engenharia Civil, Av. P.H. Rolfs s/n, 36570-000 Viçosa, MG, Brazil. e-mail: cabraz@ufv.br.

Submitted on December 23, 2009; Final Acceptance on April 3, 2012; Discussion open until September 30, 2012.

According to Darmawan & Wada (1999), the heavy metals in soils take up different chemical forms, especially: (i) ionic and dissolved; (ii) electrostatically adsorbed; and (iii) complexation to the mineral surface. In other study, Gu & Yeung (2010) analyzed the effect of citric acid industrial wastewater as an enhanced agent to electrokinetic extraction of cadmium from natural clay using sequential extraction in the chemical analysis to quantify the proportions of cadmium of different states in the soil. In this study were analyzed five different chemical forms of cadmium in the soil, which was also used by Reddy *et al.* (2001): (i) exchangeable; (ii) carbonated bound; (iii) Fe-Mn oxides bound; (iv) organic bound; and (v) residual form. Therefore, it seems that viability of the electrokinetic remediation strongly depends on the soil mineralogical composition, especially on the clay fraction that reflects its active and colloidal part, and on the quantity of organic matter. Previous studies by Puppala *et al.* (1997), Grundl & Reese (1997), as well as by Reddy *et al.* (2001) suggest that the electrokinetic methods are not always effective for the decontamination of soils with high specific capacity of adsorption, and also for those containing calcium carbonate. However, Schmidt *et al.* (2007) obtained good results in the decontamination of an organic tropical clayey soil with high cationic exchange capacity contaminated with crude oil and saline water, when introduced nitrogen compounds, mainly ammonium nitrate, in the initial solution of distilled water in the anolyte compartment. Accordingly, sequential extraction techniques have been applied before and after application of electrokinetic phenomena for soils remediation, in order to gather information about the different forms that contaminants assume when integrated to fine grained soils, as referred by Reddy *et al.* (2001) and Darmawan & Wada (2002).

Regarding the referred sequential extraction techniques, the one depicted by Reddy *et al.* (2001), and originally developed by Tessier *et al.* (1979), is not, generally speaking, applicable to tropical soils. Darmawan & Wada (2002) understand that this technique does not separate the strongly adsorbed metals from the residual fraction. On the other hand, in published works about soil remediation, independently of the process used, and generally speaking, there is no conclusive information about the contaminant incubation time that should be used, although it is common to refer to 7 days. Obviously, comparative studies about the influence of this parameter in the process of remediation are significantly important for the adequate use of the decontamination electrokinetic techniques.

This paper addresses the effect of the incubation time on the electroosmotic remediation of residual soils from the *Zona da Mata Norte*, Minas Gerais State, Brazil, contaminated with Cadmium in order to reach a better understanding of the development of reactions between contaminant and soils minerals.

## 2. Materials Characterization

### 2.1. The soil type

All soil samples were collected in the campus of the Universidade Federal de Viçosa (UFV), located in the Zona da Mata Norte, Minas Gerais state, Brazil, as follows: (i) sample 1, from a mature gneiss residual clayey silty sand, and pedologically classified as Red-Yellow Latosol (B horizon). The sample was collected from a cut slope, at the point of geographic position coordinates 20° 45' 11.1" of South latitude and 42° 51' 31.2" of West longitude; (ii) sample 2, from a young gneiss residual clayey silty sand (saprolite). The sample was collected from a cut slope situated on the road that connects the cities of Viçosa and Paula Cândido, on the place of geographic position coordinates 20° 46' 48.2" of South latitude and 42° 52' 52" of West longitude; (iii) sample 3, from a mature gneiss residual sandy silty clay, and pedologically classified as Red-Yellow Argisol. The sample was collected from a cut slope located at the UFV Alcohol Plant, on the left side of route MG-60, on the place of geographic position coordinates 20° 45' 23.5" of South latitude and 42° 50' 22.4" of West longitude.

Tables 1 and 2 show, respectively, geotechnical parameters and classifications of the soils samples following the Transportation Research Board (TRB) and Unified Soil Classification (USC) Systems (DNIT, 2006), as well as according to the Miniature Compacted Tropical (MTC) Methodology (Nogami & Vilibor, 1995).

The sand fraction of soils 1, 2 and 3 showed quartz as the dominant mineral, even though peaks of kaolinite, mica and hydroxy-interlayer-vermiculite (HIV) were identified in soils 2 and 3; the kaolinite peaks in the sand fraction of these soils were classified as pseudomorphic mica. The clay fraction of the three soils showed kaolinite as the dominant mineral, as well as gibbsite, goethite, hematite and hydroxy-interlayer-vermiculite (HIV) peaks. Table 3 shows the dominant minerals identified in the sand and clay fractions of the tested soils by X-ray diffractometry.

Table 4 presents the chemical characterization of soils 1, 2 and 3 following the standard procedures proposed by EMBRAPA (1997). Soils 1, 2 and 3 presented pH higher than 5, low organic matter content and little amount of exchangeable bases. Regarding the PZC, defined as the soils pH at the point of zero charge, soils 1 and 3 presented PZC higher than its pH, while soil 2 showed PZC lower than their respective pH.

### 2.2. The contaminant

The heavy metal cadmium was selected to be used throughout the study based on the fact that it is commonly found in contaminated areas as a waste from electronic products, among others, and also because it exhibits intermediate specific adsorption by fine-grained soil clay minerals.

The amount of contaminant added to the soil samples was based on the CETESB-SP (2001) minimum guiding

**Table 1** - Geotechnical parameters of soils.

Geotechnical parameters	Units	Soil 1	Soil 2	Soil 3
Sand ( $2 \text{ mm} < \phi \leq 0.06 \text{ mm}$ )	%	38	58	8
Silt ( $0.06 \text{ mm} < \phi \leq 0.002 \text{ mm}$ )	%	37	30	40
Clay ( $\phi \leq 0.002 \text{ mm}$ )	%	25	13	52
Liquid limit ( $w_L$ )	%	79	31	81
Plastic limit ( $w_p$ )	%	41	19	58
Plastic index ( $I_p$ )	%	38	12	22
$A_c$	$[I_p / (\% \phi \leq 2 \mu\text{m})]$	1.52	0.92	0.42
$\gamma_s$	$\text{kN/m}^3$	27.33	26.29	27.59
$w_{ot}$	%	30.50	20.23	33.68
$\gamma_{d \text{ max}}$	$\text{kN/m}^3$	13.90	15.57	12.87

**Table 2** - Geotechnical classifications of soils according to the TRB and USC Systems, and the MCT Methodology.

Soil	Geotechnical classifications		
	TRB	USC	MCT
1	A-7-5 (18)	MH	LG
2	A-6 (2)	SC-SM	NS
3	A-7-5 (17)	MH	NG

values that require intervention in agricultural or residential contaminated areas, which are in the range of 10 to 12 mg/kg of dry soil mass.

A cadmium mono-species solution with concentration of 100 mg/L of salt was added to the soil samples in different volumes, according to their original moisture contents and considering the water amounts required to make them reach the cadmium concentration of 10 to 12 mg/kg of dry soil mass. The cadmium salt used was cadmium nitrate tetra hydrated  $[\text{Cd}(\text{NO}_3)_2 \cdot 4\text{H}_2\text{O}]$  99% from Riedel-de Haën with molecular weight of 308.48 g.

### 3. Methodology

#### 3.1. Electroosmotic cell

The electroosmotic cell used in this study, Figs. 1 and 2, was originally projected and built by Damasceno (2003). Currently, this cell has been modified in order to include graphite in substitution to copper electrodes which usually suffer oxi-reduction reactions. A description of the cell parts can be found in Damasceno (2003).

#### 3.2. Decontamination tests

##### 3.2.1. Samples preparation

The following sequence was adopted during soil samples preparation:

- Soil samples were air dried and passed in the #2 mm;

**Table 3** - Mineralogy of soils 1, 2 and 3.

Soils fractions	Soil 1	Soil 2	Soil 3
Sand	Quartz	Quartz Kaolinite Mica HIV	Quartz Kaolinite Mica
	Clay	Kaolinite Gibbsite Goethite Hematite HIV	Kaolinite Goethite Hematite HIV

- Compaction tests carried out at the AASHTO Standard compaction effort according to ABNT (1986), in order to determine the soils optimum water content ( $w_{ot}$ ) and maximum dry density ( $\gamma_{d \text{ max}}$ );
- Addition of water and 100 mg.L<sup>-1</sup> cadmium nitrate solution to the air dried soil samples, in order to reach the optimum moisture content previously determined in the compaction tests, and the cadmium concentration of 10 to 12 mg/kg of dry soil;
- Incubation of the contaminated soil samples during 1, 10 and 20 days in a temperature controlled chamber ( $20 \text{ }^\circ\text{C} \pm 1 \text{ }^\circ\text{C}$ ).

##### 3.2.2. Test procedure

The following sequence was adopted when performing the electroosmotic decontamination tests:

- After soils sample incubation times, it was taken a small fraction of each of the contaminated soil to the UFV's Laboratory of Mineralogy of the Department of Soils in order to perform sequential extraction test and pH determination;

**Table 4** - Chemical characterization of soils 1, 2 and 3 - EMBRAPA (1997).

Soil	pH in H <sub>2</sub> O	PZC	P (mg.dm <sup>-3</sup> )	K (mg.dm <sup>-3</sup> )	Na (mg.dm <sup>-3</sup> )	Ca <sup>2+</sup> (cmol <sub>c</sub> .dm <sup>-3</sup> )	Mg <sup>2+</sup> (cmol <sub>c</sub> .dm <sup>-3</sup> )	Al <sup>3+</sup> (cmol <sub>c</sub> .dm <sup>-3</sup> )	H + Al (cmol <sub>c</sub> .dm <sup>-3</sup> )	SB (cmol <sub>c</sub> .dm <sup>-3</sup> )	(t)	(T)
Soil	V (%)	m (%)	SSI (%)	OMC (dag.kg <sup>-1</sup> )	P-rem (mg.L <sup>-1</sup> )	Zn (mg.dm <sup>-3</sup> )	Fe (mg.dm <sup>-3</sup> )	Mn (mg.dm <sup>-3</sup> )	Cu (mg.dm <sup>-3</sup> )	B (mg.dm <sup>-3</sup> )	S (mg.dm <sup>-3</sup> )	
1	5.00	5.04	0.6	1	0.0	0.00	0.07	0.00	1.0	0.07	0.07	1.07
2	5.75	3.73	0.9	2	0.0	0.00	0.05	0.45	1.9	0.06	0.51	1.96
3	5.81	6.00	2.2	8	0.0	0.00	1.11	0.00	0.6	1.13	1.13	1.73

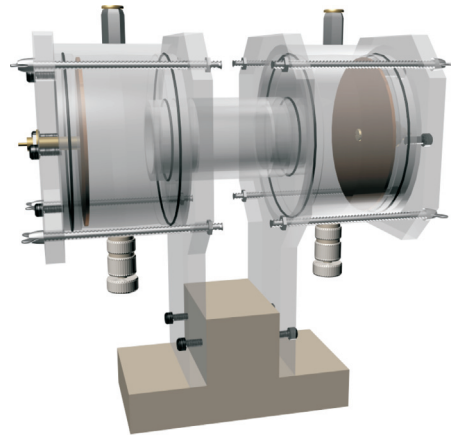


**Figure 1** - Tridimensional view of the electroosmotic cell.

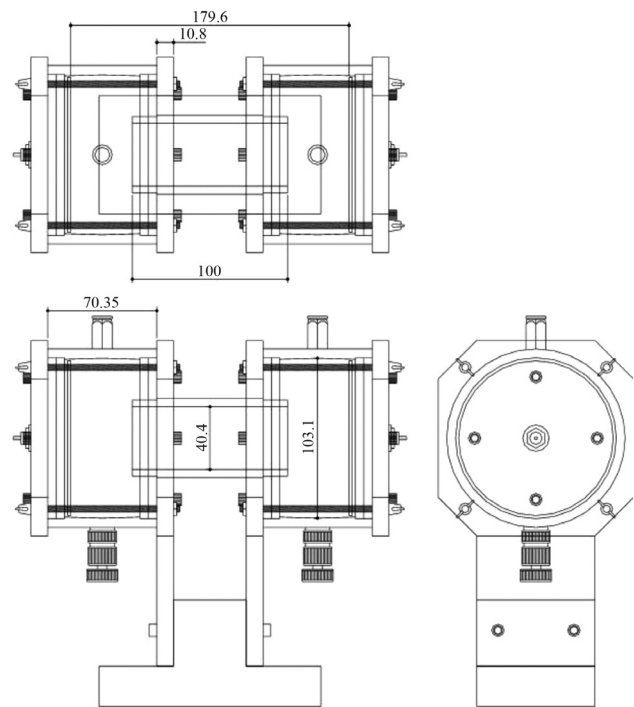


**Figure 2** - Layout, views and dimensions of parts of the electroosmotic cell (dimensions in mm).

- From each remaining contaminated soil sample were molded 5 cm internal diameter and 10 cm long specimens using Plexiglas cylinders at the AASHTO Standard optimum compaction parameters ( $w_{ot}$  and  $\gamma_{d \max}$ ) to be tested in the electroosmotic cell;
- After placing each specimen in the electroosmotic cell, its anode and cathode were filled with distilled water up to the desired level. The cell was then left to rest for 24 h in order to prevent operational and leaking problems;
- A decontamination test was carried out under controlled temperature ( $20 \text{ }^\circ\text{C} \pm 1 \text{ }^\circ\text{C}$ ) for a period of time of approximately 216 h (9 days), using an electric potential difference of 30 V allowing the electric current to vary throughout the test. Considering that the electrodes of the

electroosmotic cell were 180 mm apart, it was generated an electric gradient of 1.67 V/cm;

- During decontamination test, the solutions presented in the anode and cathode reservoirs were collected each 3 days to analyze cadmium concentration and cadmium amount that was removed with the process;
- At the end of the decontamination test, the specimen was taken from the cell in order to determine its moisture content. It was subdivided in five equally apart layers in order to determine their cadmium concentrations, taking samples from the anode e cathode cells solutions.

Determination of cadmium concentrations in all the specimen layers and in the anode and cathode cell solutions were carried out using the Flame Atomic Absorption Spectrophotometry technique (FAAS).

### 3.3. Sequential extraction technique – Chemical analyses

After the decontamination tests, each specimen was divided into five parts approximately equal which were identified and submitted to chemical analyses of sequential

extraction (Egreja Filho, 2000), in order to determine the different chemical forms of the contaminant.

In the sequential extraction technique, the soil samples were submitted to continuous extractions with different extractors in each step, and using higher extraction power as the process advanced. In this test, the extractor acted by changing the interaction between the heavy metal and the solid phase, promoting solubilization to be dosed by a convenient analytic method. The sequential extraction was carried out in four steps, as illustrated in Table 5 and in Fig. 3.

## 4. Results

### 4.1. Electroosmotic parameters

Table 6 presents the geotechnical parameters of the tested soils before and after performing the electroosmotic decontamination tests.

During the electro-osmotic decontamination tests performed in specimens of the tested soils, the geotechnical parameters called electroosmotic conductivity coefficient ( $k_{e\ stable}$ ) were determined. Besides, it was observed that the behavior of the test parameters, generally speaking, was similar, noting that the electric current decreased with time

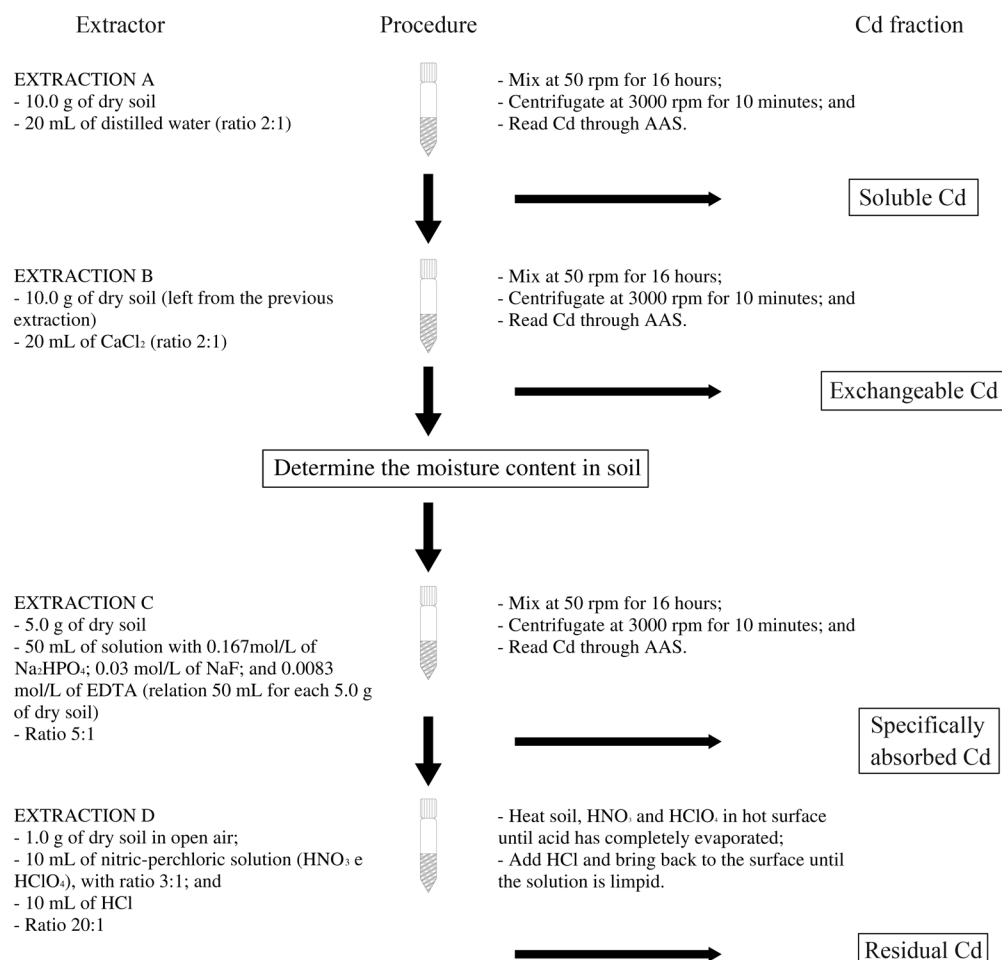


Figure 3 - Fluxogram of the sequential extraction technique developed by Egreja Filho (2000).

**Table 5** - Steps of the sequential extraction technique referring to the used extractor and to the determined chemical form.

Steps	Extractor	Determination
A	Distilled water	Soluble metals in the soil solution
B	0.1 mol L <sup>-1</sup> de CaCl <sub>2</sub>	Exchangeable metals (weakly absorbed)
C	Solution composed by 0.167 mol L <sup>-1</sup> of Na <sub>2</sub> HPO <sub>4</sub> , 0.03 mol L <sup>-1</sup> of NaF and 0.0083 mol L <sup>-1</sup> of EDTA	Specifically absorbed metals (strongly adsorbed)
D	Nitric-perchloric digestion	Metals in the residual fraction

**Table 6** - Geotechnical parameters of specimens submitted to the electro-osmotic decontamination tests, which were obtained before and after tests.

Soil	Contaminant incubation time (day)	Electroosmotic test duration (h)	$w_o$ (%)	$w_f$ (%)	$Sr_o$ (%)	$Sr_f$ (%)	$k_{e\ stable}$ [cm <sup>2</sup> /s*V]
1	1	215.20	29.95	34.33	86.89	98.63	0.740 x 10 <sup>-6</sup>
	10	219.75	29.95	32.86	87.19	97.16	1.204 x 10 <sup>-6</sup>
	20	217.12	29.95	36.31	86.97	100.00	1.092 x 10 <sup>-6</sup>
2	1	217.17	21.21	24.35	78.75	93.68	5.009 x 10 <sup>-6</sup>
	10	218.93	21.21	25.17	80.89	96.04	3.815 x 10 <sup>-6</sup>
	20	220.48	21.21	24.35	78.67	94.32	4.443 x 10 <sup>-6</sup>
3	1	217.32	37.19	42.22	86.99	97.74	2.127 x 10 <sup>-6</sup>
	10	217.54	37.19	43.34	86.84	98.61	4.071 x 10 <sup>-6</sup>
	20	216.78	36.51	41.39	86.43	95.39	2.992 x 10 <sup>-6</sup>

and the electroosmotic flow increased in the beginning of each test, tending to stabilize with time.

Researches performed in some Brazilian soils showed that the electroosmotic conductivity coefficient is in the order of 10<sup>-7</sup> cm<sup>2</sup>\*s<sup>-1</sup>\*V<sup>-1</sup> (Araruna *et al.*, 2002; Damasceno, 2003).

#### 4.2. Decontamination by electrokinetic phenomena

During decontamination tests the solutions at the anode and cathode compartments were collected each three days in order to perform chemical analysis. Besides, it was measured the pH of soils before tests and in each section of the specimens after tests. Figures 4 to 6 show these data.

It should be emphasized that soils 1 and 3 showed reverse electroosmotic flow, *i.e.*, in a cathode-anode direction. The main explanation for this fact is based on the behavior of its electrochemical parameter called Point of Zero Charge (PZC), observing that this value was higher than their pH, which caused the inversion of the electroosmotic flow in accordance with the observations of Yang & Lin (1998). According to these authors, when soil pH is higher than its PZC, the soil presents more negative charges in its clayey mineral surfaces than positive charges, which favors cationic exchangeable and, as a result, the electroosmotic flow is normal (anode-cathode direction). On the other hand, when the soil pH is lower than the soil PZC, it presents more positive than negative charges in the clayey

mineral surfaces, which favors anionic absorption and, as a result, occurrence of electroosmotic reversal flow (cathode-anode direction).

The results illustrated in Figs. 4 to 6 showed that in soils 1 and 3, which present clayey texture and pH below PZC, the cadmium concentration decreased with time in both compartments. Regarding soil 2, which presents sandy texture and pH higher than its PZC, the cadmium concentration decreased with time in the anode compartment, but increased in the cathode compartment. Besides, these figures showed that soils pH increased from anode to cathode, which confirms data presented in the technical literature (Yang *et al.* 1998); also, in general, it was observed that soil pH increased after application of the electrokinetic process.

#### 4.3. Sequential extraction data analysis

Figures 7 to 9 show the results of the sequential extraction analyses performed on contaminated specimens from soils 1, 2 and 3 before (named *initial*) and after performing the electroosmotic decontamination tests, considering the incubation times of 1, 10 and 20 days, and the respective distances of the five specimen layers from the cathode to the anode, which were labeled 1, 2, 3, 4 and 5.

Regarding the behavior of the tested soils and considering all cadmium extracted forms, Figs. 7 to 9 shows that the behavior of the cadmium ion before electroosmotic de-

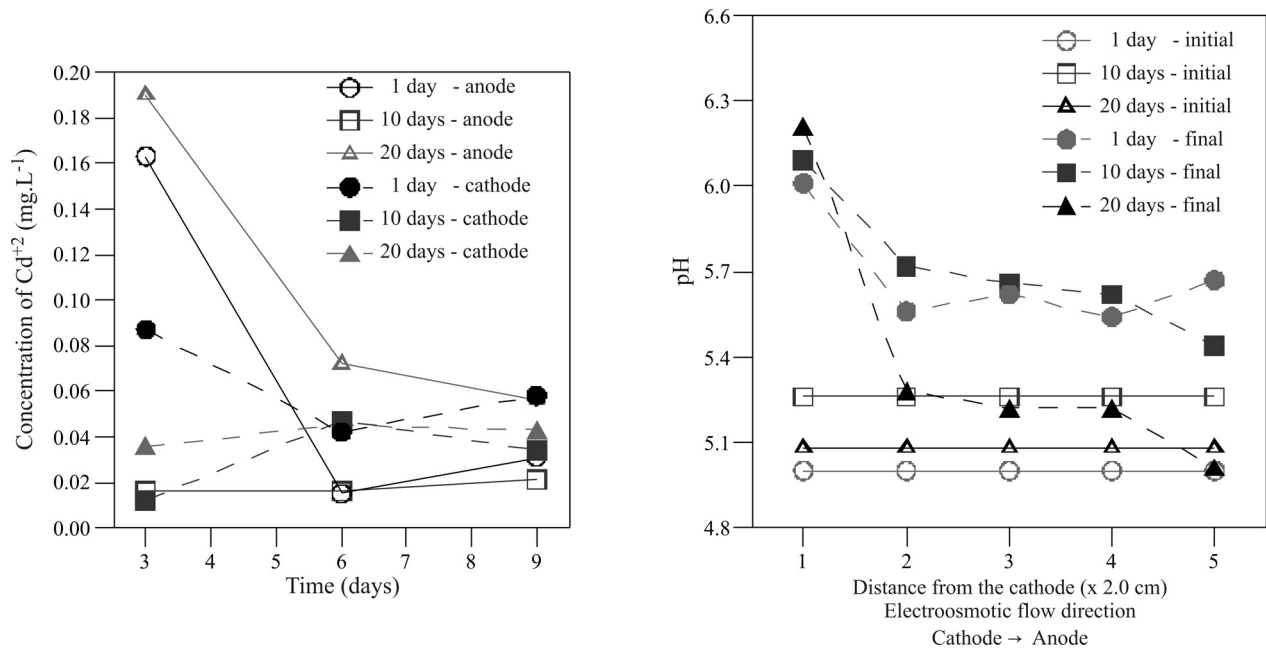
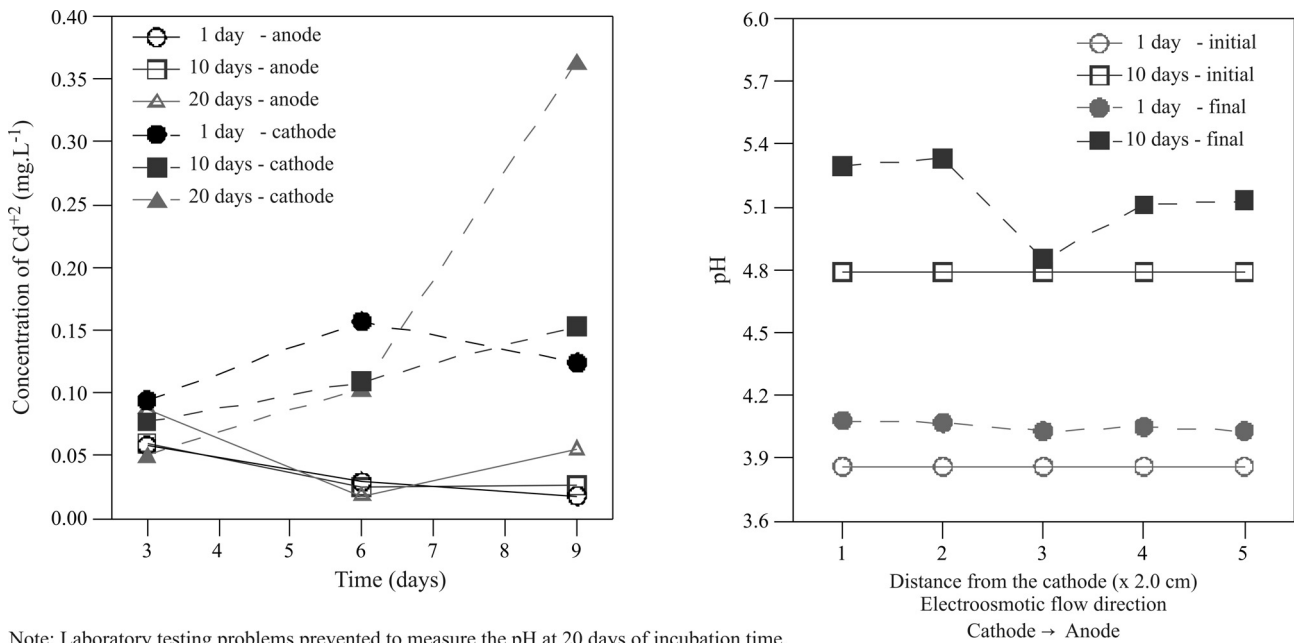


**Figure 4** - Cadmium concentration in the anode and cathode compartments during decontamination tests, and pH values determined in the specimens before and after decontamination tests: soil 1.



Note: Laboratory testing problems prevented to measure the pH at 20 days of incubation time.

**Figure 5** - Cadmium concentration in the anode and cathode compartments during decontamination tests, and pH values determined in the in the specimens before and after decontamination tests: soil 2.

contamination (initial stage) varied with the incubation time.

As illustrated in Fig. 7, when the incubation time was increased, more contaminant was taken from soil 1, especially in the soluble, specifically absorbed, and residual fractions. However, considering the exchangeable form, which is the fraction electrostatically attracted by the soil

colloidal phase, the opposite happened; in other words, the quantity extracted decreased with the increase of the incubation time. Arguably, an explanation for this behavior is that with the increase of incubation time, the strongly absorbable fraction became attracted to the soil colloids with less strength; therefore, the metals were more dissolved with the application of electric potential, settling in

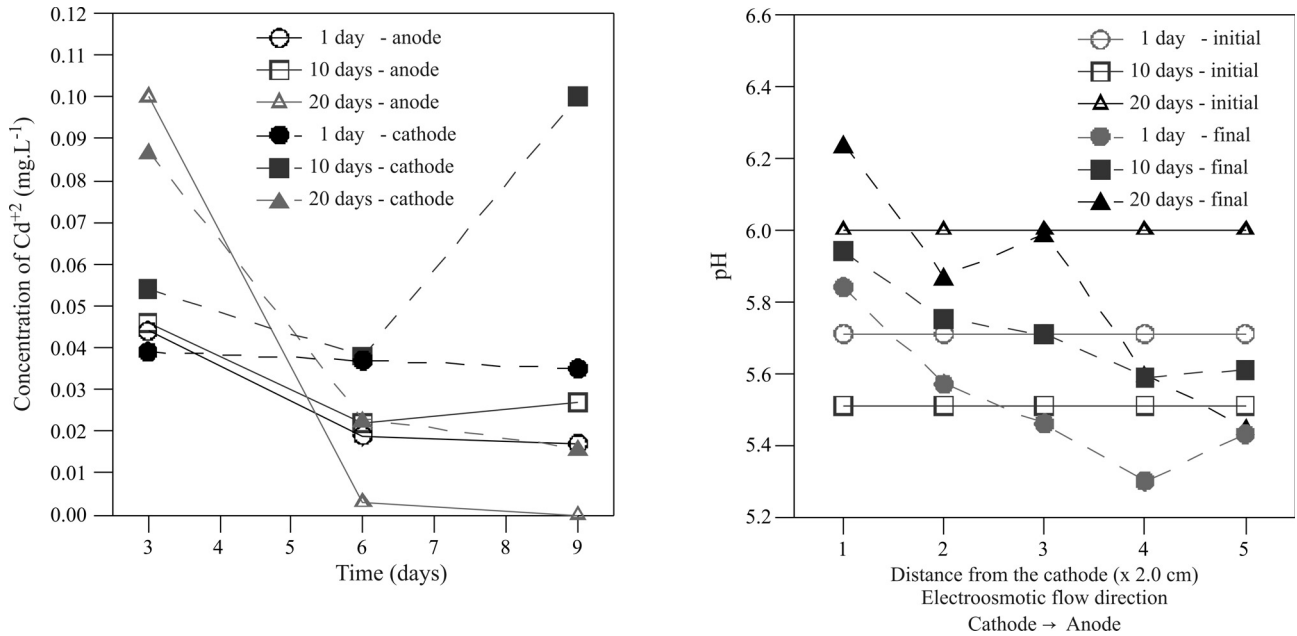


**Figure 6** - Cadmium concentration in the anode and cathode compartments during decontamination tests, and pH values determined in the in the specimens before and after decontamination tests: soil 3.

electrostatic form. Thus, the electrostatic fraction quantitatively increased and reached such amount that could not be taken away in the adopted periods of time. Also, increasing the incubation time, reactions which occurred in soil 1 and application of the electric potential difference made the ions less strongly absorbed and more electrostatically attracted to soil colloids.

As shown in Fig. 8, the efficiency of the decontamination process increased with the incubation time, in all sequential extraction fractions, which may be associated with the fact that soil 2 has low quantity of iron and aluminum oxides, which are the most important minerals in the cation absorption

process. However, when the incubation period changed from 10 to 20 days, the differences were not significant. Thus, the results indicated that chemical and mineralogical factors of soil 2, as well as incubation time had significant influence in the electroosmotic decontamination process.

Concerning soil 3, based on the results presented in Fig. 9, it was observed that the increase of the incubation time led to an increase on the amount of extracted cadmium, in all sequential extraction fractions, inferring that there was decrease of the electrostatically attracted fraction and increase of the strongly absorbed fraction with the incubation time, before and after the remediation process.

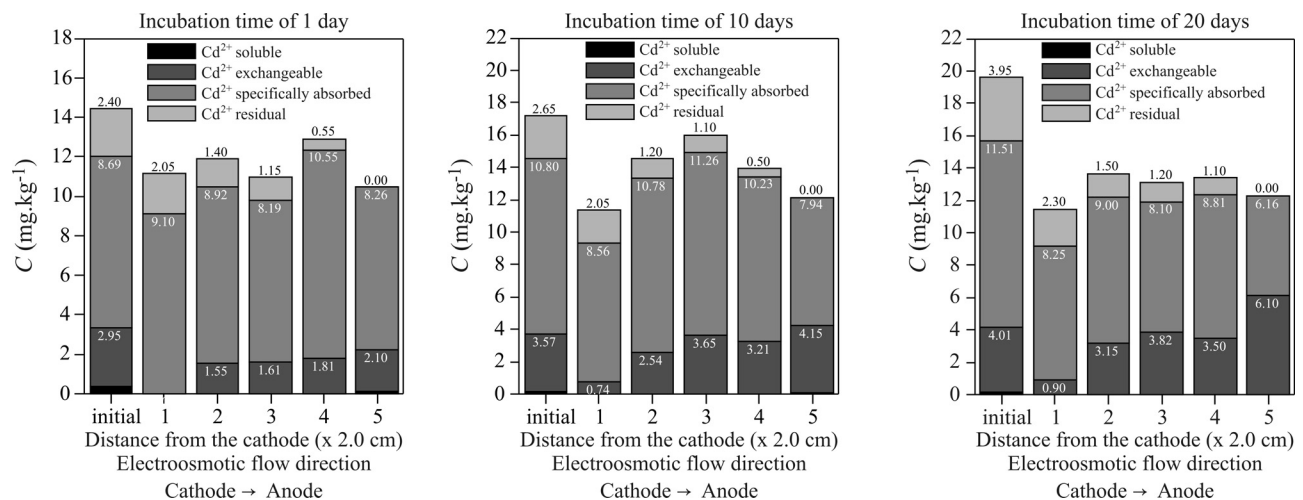


**Figure 7** - Results from the sequential extraction performed in the contaminated specimen from soil 1 before and after the electroosmotic decontamination test, considering the incubation times of 1, 10 and 20 days, and the distances of the specimen layers to the cathode.

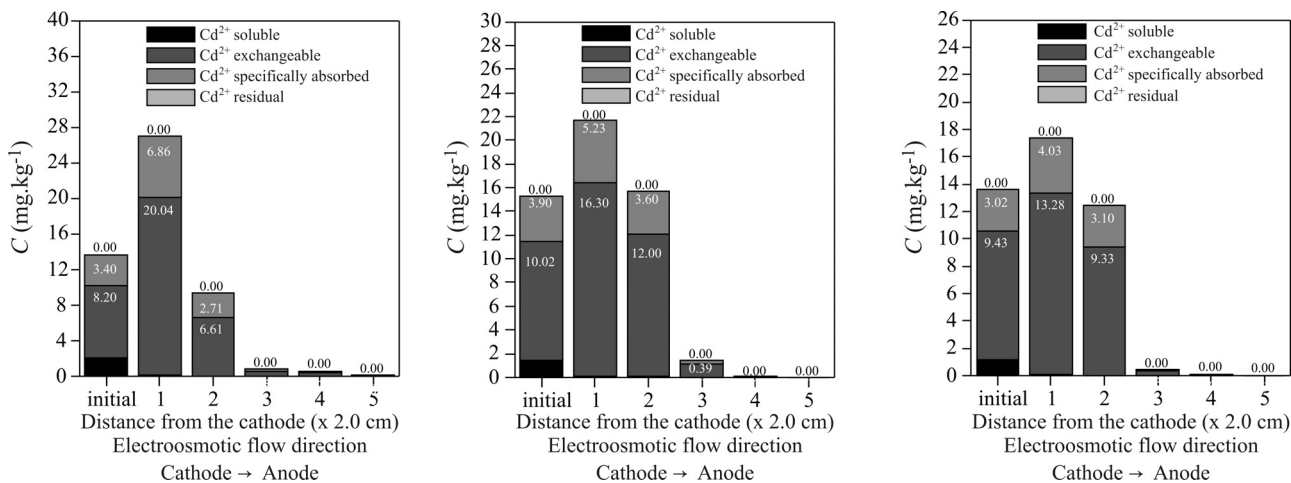


**Figure 8** - Results from the sequential extraction performed in the contaminated specimen from soil 2 before and after the electroosmotic decontamination test, considering the incubation times of 1, 10 and 20 days, and the distances of the specimen layers to the cathode.

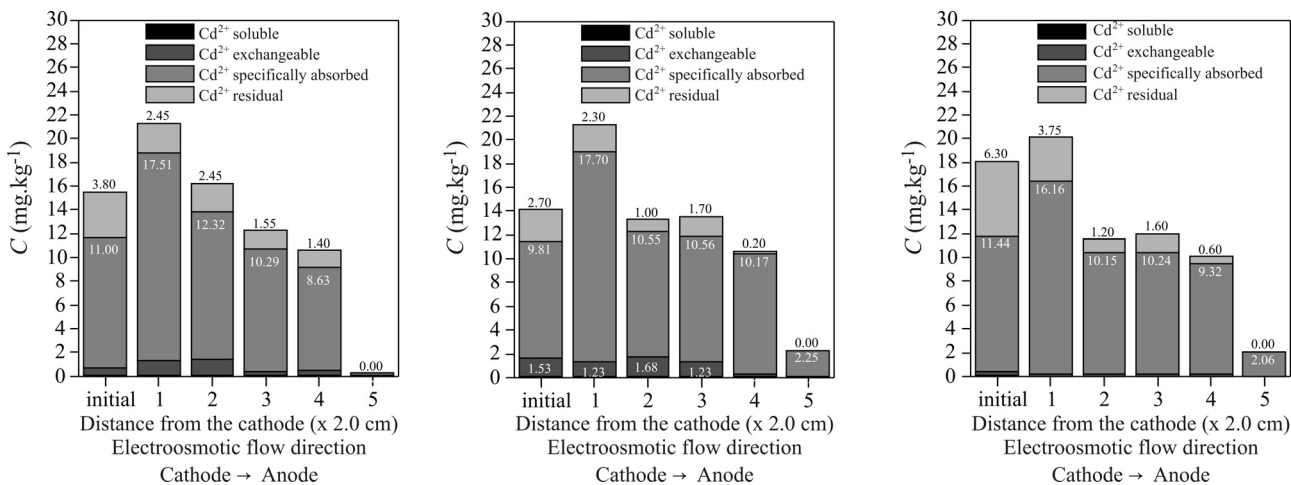


**Figure 9** - Results from the sequential extraction performed in the contaminated specimen from soil 3 before and after the electroosmotic decontamination test, considering the incubation times of 1, 10 and 20 days, and the distances of the specimen layers to the cathode.

The contaminant behavior observed in soils 1 and 3 after the electrokinetic process was similar to that reported by Gu & Yeung (2010). Certainly, the measurement of the quantity of cadmium before and after each step of the sequential extraction could provide a basis to explain the behaviors previously reported.

Table 7 shows the final quantities of cadmium taken in each extraction in comparison with its initial quantity, in percentage. It should be emphasized that at the beginning of the decontamination process, each slice of the specimen had the same cadmium concentration that can be represented by a constant line in a figure that shows cadmium concentration in the Y axis versus distance from cathode in the X axis. At the end of the process, it was possible to obtain a curve of cadmium concentration using the cadmium concentrations determined from each slice of the specimen in each step of the sequential extraction procedure. Therefore, from comparison of the areas under these curves, the

amount of cadmium extracted from the specimen in each step of the sequential extraction could be inferred by the ratio of the difference between the area determined after the electrokinetic remediation and the area determined before electrokinetic remediation by the area determined before electrokinetic remediation.

From Table 7 data, the values of the negative percentages found in soils 1 and 3 were unexpected. One possible explanation for this behavior can be related to the fact that more contaminant remained in that fraction at the end of the test, although it does not necessarily mean that decontamination was effective, once the other fractions presented high positive percentages, overcoming the observed negative fraction. On the other hand, it could be noticed that soil 1 (clayey) presented a great amount of retained cadmium in the specifically absorbed fraction, while soil 2 (sandy soil with lower iron and aluminum oxide contents) presented the best global decontamination results.

**Table 7** - Percentage of cadmium removed from the analyzed soils by the electroosmotic process in each step of the sequential extraction.

Soil	Contaminant incubation time (day)	% of cadmium removed			
		Soluble	Exchangeable	Specifically absorbed	Residual
1	1	93.89	52.13	-3.57	57.08
	10	92.59	19.92	9.70	63.40
	20	96.98	12.91	29.94	69.11
2	1	98.76	32.77	40.68	100.00
	10	96.57	41.37	52.39	100.00
	20	96.59	51.32	52.28	100.00
3	1	31.96	-15.12	10.98	58.68
	10	38.16	42.75	-4.46	61.48
	20	100.00	40.37	16.18	77.30

To sum up and based on the results shown on Figs. 7 to 9 and on Table 7, among the tested incubation times, it was observed that 20 days ended up being the most satisfactory period for soils 1 and 3, and 10 days ended up being satisfactory for soil 2; however, further research is required to confirm this behavior. On the other hand, soil surface chemistry and mineralogy influenced the results obtained in the decontamination tests. All soils analyzed presented Kaolinite, Goethite, Gibbsite, HIV and/or Hematite minerals in their clayey fractions; however, soils 1 and 3 presented higher percentages of clay fraction than soil 2 and, consequently, higher adsorption capacity.

## 5. Conclusions

Regarding the tested soils, applied ddp and incubation times, the analysis of the results obtained supports the following conclusions:

- The PZC of soils influenced the cadmium migration under application of the electric potential difference; specifically, soils 1 and 3 presented reversal electroosmotic water flow, *i.e.*, in the cathode-anode direction;
- In soils 1 and 2, application of the electric potential difference generated cadmium migration in the electroosmotic flow direction. However, in soil 3 the contaminant migrated in the anode-cathode direction, bringing up to attention the importance of the parameter of soil PZC in the electroosmotic decontamination process;
- In general, the values of pH of all tested soils determined after decontamination tests were higher than those determined before, increasing from the anode to the cathode direction;
- It was observed that changing the incubation time, the results obtained from the sequential extraction performed before and after application of the electrokinetic remediation process showed that chemical and mineral-

ogical characteristics of the tested soils influenced their cadmium adsorption;

- 20 days and 10 days were, respectively the optimum tested incubation times for soils 1 and 3, and for soil 2.

## Acknowledgments

The authors would like to express their thanks to CAPES for granting a scholarship to the first author, to the Departments of Civil Engineering and of Soils from UFV for all the support required for the development of this research, as well as to FAPEMIG for his support through the grant TEC-PPM-00081-10.

## References

- ABNT (1986) Soil: Compaction Test - NBR 7182. Rio de Janeiro, Brazil, 10 pp.
- Acar, Y.B. & Alshawabkeh, A.N. (1993) Principles of electrokinetic remediation. *Environmental Science and Technology*, v. 27:13, p. 2638-2647.
- Acar, Y.B. & Alshawabkeh, A.N. (1996) Electrokinetic remediation I: Pilot-scale tests with lead-spiked kaolinite. *ASCE Journal of Geotechnical Engineering*, v. 122, p. 173-185.
- Adriano, D.C. (1986) Trace Elements in the Terrestrial Environment. Springer-Verlag, New York, 533 p.
- Alshawabkeh, A.N.; Yeung, A.T. & Bricka, M. (1999) Practical aspects of in-situ electrokinetic extraction. *Journal of Environmental Engineering*, v. 125:1, p. 27-35.
- Araruna, J.T.; Rivas, B.M.M.; Mergulhão, A.J.P.P.; Souza, M.V. & Antunes, F.S. (2002) Laboratory investigation of electroosmosis flow efficiency in a residual soil from gneiss. *Proc. 4th ICEG Environmental Geotechnics, Rio de Janeiro*, v. 2, pp. 881-886.
- CETESB-SP (2001) São Paulo State Orientation Values for Soils and Subterranean Waters Report (in Portuguese). Technology and Environmental Sanitary Company, São Paulo, Brazil, 232 p..

- Chang, J-H. & Liao, Y-C. (2006) The effect of critical operational parameters on the circulation-enhanced electrokinetics. *Journal of Hazardous Materials*, v. 129:1-3, p. 186-193.
- Damasceno, V.M. (2003) Electroosmotic Conductivity and Remediation of a Lateritic Soil from the Zona da Mata Norte, Minas Gerais, via Electrokinetic Phenomena (in Portuguese). MSc Thesis, Graduate Program in Civil Engineering, Federal University of Viçosa, Viçosa, 81 pp.
- Darmawan, S. & Wada, S.I. (1999) Kinetics of speciation of Cu, Pb and Zn loaded to soils that differ in cation exchanger composition at low moisture content. *Commun. Soil Science Plant Anal.*, v. 30:17-18, p. 2362-2375.
- Darmawan, S. & Wada, S.I. (2002) Effect of clay mineralogy on the feasibility of electrokinetic soil decontamination technology. *Elsevier Applied Clay Science*, v. 20:6, p. 283-293.
- DNIT (2006) Pavement Design Manual (in Portuguese). 3rd ed. Highway Research Institute Publication No. 719, Rio de Janeiro, 320 pp.
- Egreja Filho, F.B. (2000) Heavy Metal Sequential Extraction in Highly Altered Soils: Components Utilization - Model and Planning of Method Optimization with Ternary Mixtures (in Portuguese). DSc Dissertation, Soils Graduate Program, Federal University of Viçosa, Viçosa, 287 pp.
- EMBRAPA (1997) Manual of Methods and Analysis of Soils (in Portuguese). National Service of Soils Researches and Conservation, Rio de Janeiro, 212 pp.
- Grundl, T. & Reese, C. (1997) Laboratory study of electrokinetic effects in complex natural sediments. *Journal of Hazardous Materials*, v. 55:1-3, p. 187-201.
- Gu, Y.Y. & Yeung, A.T. (2010) Enhanced electrokinetic extraction of cadmium from Natural clay by citric acid industrial wastewater. *Proc. 9th Symposium on Electrokinetic Remediation, EREM-2010, Kaohsiung, Taiwan*, pp. 29-30.
- Mitchell, J.K. (1993) *Fundamentals of Soil Behavior*, 2nd ed. John Wiley & Sons, Inc., New York, 437 pp.
- Nogami, J.S. & Vilibor, D.F. (1995) Low Cost Pavement with Lateritic Soils (in Portuguese). Vilibor, São Paulo, 213 pp.
- Puppala, S.K.; Alshawabkeh, A.N.; Acar, Y.B.; Gale, R.J. & Bricka, M. (1997) Enhanced electrokinetic remediation of high sorption capacity soils. *Journal of Hazardous Materials*, v. 55:1-3, p. 203-220.
- Reddy, K.R.; Xu, C.Y. & Chinthamreddy, S. (2001) Assessment of electrokinetic removal of heavy metals from soils by sequential extraction analysis. *Journal of Hazardous Materials*, v. 84:2-3, p. 279-296.
- Shapiro, A.P. & Probstein, R.F. (1993) Removal of contaminants from saturated clays by electroosmosis. *Environmental Science and Technology*, v. 27:2, p. 283-291
- Schmidt, C.A.B.; Barbosa, M.C. & Almeida, M.S.S (2007) A laboratory feasibility study on electrokinetic injection of nutrients on an organic, tropical, clayey soil. *Journal of Hazardous Materials*, v. 143:3, p. 655-661.
- Tessier, A.; Campbell, P.G.C. & Bisson, M. (1979) Sequential extraction procedure for the speciation of particulate trace metals. *Anal. Chem.*, v. 51:7, p. 844-851.
- Yang, G.C. & Lin, S-L. (1998) Removal of lead from a silt loam soil by electrokinetic remediation. *Journal of Hazardous Materials*, v. 58:1, p. 285-299.

## List of Symbols

- $w_L$ : liquid limit  
 $w_p$ : plastic limit  
 $I_p$ : plasticity index  
 $A_c$ : Skempton's activity index ( $I_p/(\% \phi \leq 2 \mu\text{m})$ )  
 $\gamma_s$ : Specific gravity of soil solids  
 $w_{ot}$ : optimum water content  
 $\gamma_{d \max}$ : maximum dry density  
 $w_o$ : initial moisture content  
 $w_f$ : final moisture content  
 $Sr_o$ : initial degree of saturation  
 $Sr_f$ : final degree of saturation  
 $k_{e \text{ stable}}$ : electroosmotic conductivity coefficient after water flow stabilization  
SB: Sum Exchangeable Bases  
CEC (t): Cationic Exchange Capacity  
CEC (T): Cationic Exchange Capacity in pH 7.0  
V: Base Saturation Index  
m: Aluminum Saturation Index  
SSI: Sodium Saturation Index  
OMC: Organic Carbon x 1.724 - Walkley-Black  
P-rem: Remanescant Phosphorus



# Modification of a Lateritic Soil with Lime and Cement: An Economical Alternative for Flexible Pavement Layers

F.H.M. Portelinha, D.C. Lima, M.P.F. Fontes, C.A.B. Carvalho

**Abstract.** Lateritic soils are widely spread in the Brazilian territory and they have been used as subgrade of pavement layers. Specifically, the Red-yellow latosols are usually clayey soils and are characterized as low bearing capacity materials for flexible pavement layers. As a conventional solution, soil stabilization with hydrated lime or Portland cement has been used as pavement layers reinforcement. However, the addition of low contents of stabilizers, referring to the soil modification, has not been applied on regular basis in highway designs. The purpose of this paper is to evaluate the use of low contents of lime and cement in the modification of a lateritic soil properties concerning the behavior of mixtures since the beginning of construction to the resulting final product. At this point, the workability, chemical properties, mechanical behavior and mineralogical composition were evaluated. Mechanistic analyses were performed in order to verify fatigue failures on asphalt layers in roadways structural layers. Experimental results showed that addition of 2% and 3% of lime or cement was enough to change the soil workability and mechanical strength. Additionally, mechanistic analyses supported the soil modification technique as valuable practice with low elastic strains in the asphalt layer when applied in pavement base layers.

**Keywords:** soil modification, hydrated lime and Portland cement, lateritic soil, flexible pavement layers; mechanistic analysis.

## 1. Introduction

Pavement designers have always been searching for technical and economical solutions for roadway applications. Soil stabilization technique, which is normally used for the improvement of local soils, is considered an economical solution in places where granular materials are not available. Hydrated lime and Portland cement have been considered excellent stabilizers for the improvement of different soils and have been extensively used in the past decades. Beneficial effects of compacted soil-lime and soil-cement mixtures on geotechnical properties have been discussed in the technical literature (Herrin & Mitchell, 1961; Moh, 1965; Kennedy *et al.*, 1987; Bhattacharja *et al.*, 2003; Felt & Abrams, 2004; Galvão *et al.*, 2004; Koliass *et al.*, 2005; Osinubi & Nwaiwu, 2006; Consoli *et al.*, 2009; Sariosseri & Muhunthan, 2009; Cristelo *et al.* 2009). Ordinarily, these stabilizers can promote plasticity reduction, grain size distribution alterations caused by flocculation reactions, and expressive mechanical strength increase. Thereby, benefits of the soil stabilization for pavement applications can be available since the construction phase until to the final product.

The geotechnical behavior of lime or cement treated soils depends on physical and chemical properties of soils, in which are directly related with soil formation conditions

and mineralogical composition of the matrix rock (Kennedy *et al.*, 1987; Consoli *et al.*, 2009). In general, temperate soils, usually composed of active clayey soils (montmorillonites and smectites minerals) can respond better than tropical soils (kaolinitic soils) after lime stabilization. However, Brazilian experiences have shown excellent mechanical improvement in lateritic soils treated with lime or cement in roadways applications.

Regarding lateritic soils, they are widely spread in the Brazilian territory and appear in almost all regions in different climatic conditions, topography and matrix rock (Fig. 1a). Lateritic soils have been extensively used in roadways, embankments and retaining walls due to the excellent improvement after compaction. However, Red yellow latosols normally appear as clayey soils with relatively low bearing capacity for flexible pavement structural layers. Considering that these soils cover almost a third of the Brazilian territory (Fig. 1b), soil modification technique come up as an economical solution in these situations.

In this study, the term “soil stabilization” refers to a substantial improvement of the mechanical behavior, whereas the term “soil modification” applies to a significant improvement of the soil workability and compaction characteristics, and to a minor improvement of the soil mechanical strength using low contents of stabilizers, as visu-

F.H.M. Portelinha, MSc, Setor de Geotecnia, Departamento de Engenharia Civil, Universidade Federal de Viçosa, 36570-000 Viçosa, MG, Brazil. e-mail: fernando@sc.usp.br.

D.C. Lima, Professor, Departamento de Engenharia Civil, Universidade Federal de Viçosa, 36570-000 Viçosa, MG, Brazil. e-mail: declima@ufv.br.

M.P.F. Fontes, Professor, Departamento de Solos, Universidade Federal de Viçosa, 36570-000 Viçosa, MG, Brazil. e-mail: mpfontes@ufv.br.

C.A.B. Carvalho, Associate Professor, Departamento de Engenharia Civil, Universidade Federal de Viçosa, 36570-000 Viçosa, MG, Brazil. e-mail: cabraz@ufv.br.

Submitted on August 30, 2010; Final Acceptance on March 7, 2012; Discussion open until September 30, 2012.

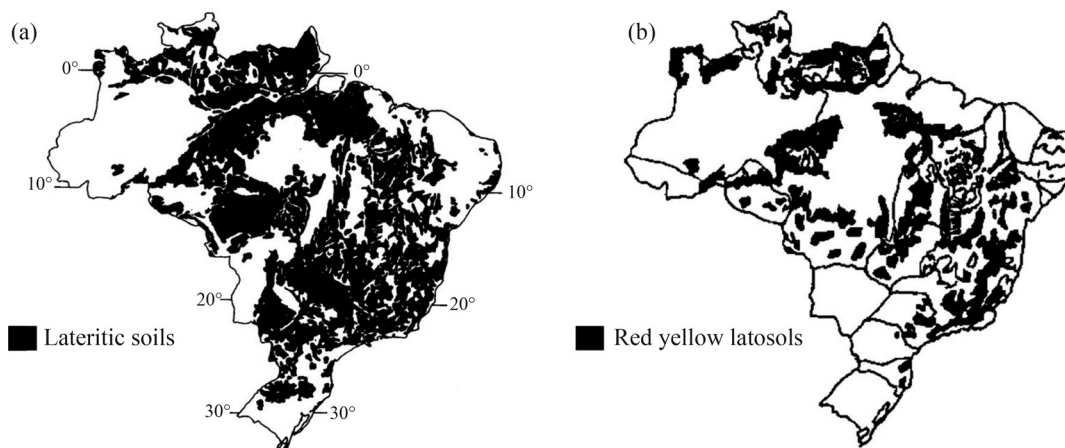


**Figure 1** - Distribution of lateritic soils in Brazil: (a) Lateritic soils; (b) Red Yellow latosol (Ker, 1998).

alized by Osula (1996) and Sariosseri & Muhunthan (2009). From this point, it must be emphasized that the use of mixtures with high contents of lime or Portland cement (as stabilized soils) generally produces materials with excellent mechanical behavior, as well as the application of mixtures with low contents of these stabilizers (as modified soils) can represent an economical and efficient solution for flexible pavement design, as reported by Sariosseiri & Muhunthan (2009) and Solanki *et al.* (2009).

This paper presents the evaluation of the workability, mineralogical composition and mechanical behavior of a lateritic soil (Red-yellow latosol) modified with hydrated lime and with Portland cement (percentages of 1%, 2% and 3%), for highway engineering applications. The experimental program was directed to the evaluation of the soil and its mixtures index properties, unconfined compressive strength (UCS), initial tangent modulus at strain levels up to 0.1%, California bearing ratio (CBR), and mineralogical composition. The behavior of the mixtures in flexible pavement design was evaluated through mechanistic analysis of two different pavement configurations using, respectively, the modified soil as subbase or base layer.

## 2. Experimental Program

The experimental program was conducted in three steps. The first addressed the application of low contents of hydrated lime (HL) and of Portland cement (PC) in order to promote soil workability modification. The following parameters were used in these analyses: plastic and liquid limits, grains size distribution and compaction parameters (Proctor tests). In the second step, UCS tests were conducted in order to access the improvement in strength and initial tangent modulus (at strain levels up to 0.1%); additionally, CBR and cyclic triaxial tests were implemented to verify the potential applications of materials in roadways. In the third step, X-ray diffraction analyses were carried out to study the mineralogical modification in the lateritic soil after treatment. Thereafter, mechanistic analyses of modi-

fied soil layers were performed using the finite difference computational program ELSYM5.

### 2.1. Materials

A lateritic fine-grained soil from Viçosa city, located in the Minas Gerais state, Brazil, was used in this study. Table 1 summarizes the geotechnical properties of the soil, whereas Table 2 introduces chemical soil properties. The material is a residual gneiss soil, pedologically classified as Red-yellow latosol, which commonly appears in B horizons of soft slopes and classified as silty sand clay. Follow-

**Table 1** - Geotechnical properties of soil.

Properties		Standard method
Clay (%)	66	
Silt (%)	6	
Fine sand (%)	13	NBR 7181/84
Medium sand (%)	13	
Gravel sand (%)	2	
Liquid limit (%)	69.5	NBR 6459/84
Plasticity limit (%)	40.9	NBR 7180/84
Plasticity index (%)	28.6	
Specific gravity	2.725	NBR 6508/84
Maximum dry unit weight (kN/m <sup>3</sup> )	14.9	NBR 7182/86
Optimum water content (%)	27.9	

**Table 2** - Chemical properties of soil.

Properties	
pH	6.76
ZPC	6.02
CEC (cmol/dm <sup>3</sup> )	1.25
BS (%)	80

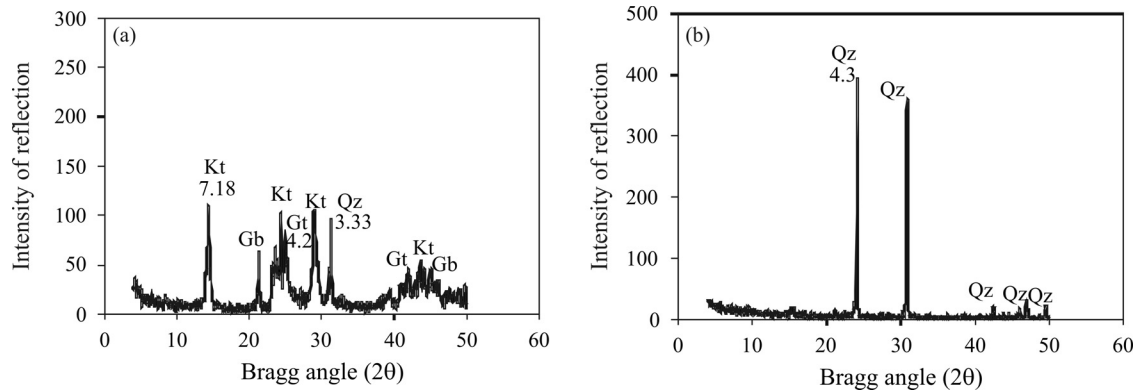


**Figure 2** - XRD of untreated soil samples: (a) clay-silt and (b) sand fractions.

ing the USC and the TRB soil classifications systems, the soil is classified as a CL and A-7-5 soil, respectively. According to MCT soil classification system (*Miniature, Compacted, and Tropical*), the soil is a lateritic sandy clay. (LG'). Figure 2 presents X-ray diffraction data, in which kaolinite, goethite and gibbsite were identified as the main minerals.

A commercial chemically pure powdered hydrated lime (CH-III), and Portland cement (PC II-E-32) were used throughout the study.

## 2.2. Methods

Contents of 1%, 2% and 3% in weight of hydrated lime and Portland cement were mixed to dry soil samples. Thereafter, water contents were added to each mixture in order to reach its optimum water content (Standard Proctor compaction effort). Samples of homogeneous mixtures were put into plastic bags and rested during one hour before running chemical analysis, particle size distribution, Atterberg limits and compaction tests. Specimens for UCS, CBR and cyclic triaxial tests were molded at the optimum water content and maximum dry unit weight of each mix, and subsequently cured during 7 days and 28 days. In addition, stabilizers contents of 0.5%, 1%, 2%, 4%, 8% and 12% were used in the determination of plastic ( $w_p$ ) and liquid limits ( $w_l$ ) of mixtures, in order to compare the plasticity index changes provided by soil modification and soil stabiliza-

tion techniques, as well as in the classification of mixtures following the Unified Soil Classification (UCS) and the Transportation Research Board (TRB) systems. XRD analyses were performed in post-failure specimens from UCS tests; on the other hand, specimens for CBR tests were prepared using 2% and 4% of stabilizers, and for cyclic triaxial tests using only 2% of stabilizers.

### 2.2.1. Workability properties

The workability improvement of soils in field applications is related to its plasticity, finer fraction, optimum water content reductions and maximum dry density increases (Osula, 1996; Sariosseri & Muhunthan, 2009). Therefore, workability modifications assessed through particle size distribution, plasticity index, and compaction tests parameters. Particle size distribution was carried out by sieve analyses and sedimentation test using sodium hexametaphosphate as dispersant solution.

Compaction test was performed at the Standard Proctor compaction effort (NBR7182, 1986) in order to determine compaction curves, and, consequently the optimum water content and maximum dry unit weight of soil and mixtures.

### 2.2.2. Chemical parameters

The chemical analyses of soil and mixtures were conducted according to EMBRAPA (1997). Samples from

**Table 3** - TRB classification of mixtures.

Materials	Passing #200 (%)	LL (%)	PI (%)	GI (%)	TRB classification	OBS
Soil	66	73.4	32.6	17	A-7-5	
Soil + 1% HL	59	65.1	28.1	18	A-7-5	
Soil + 2% HL	59	67.8	22.0	16	A-6	Clayey soils
Soil + 3% HL	49	72.0	24.3	13	A-6	
Soil + 1% PC	57	60.0	25.4	16	A-6	
Soil + 2% PC	48	59.5	20.1	11	A-5	Silty soils
Soil + 4% PC	41	58.1	14.1	6	A-4	

plastic bags were used in these analyses. The hydroge-ionic potential (pH) of soil and mixtures were determined in potassium chloride (KCl) solution in ratio of soil/solution suspension of 1/2.5 (volume/volume), at minimum of one hour of contact time and agitation before the potentiometric readings. Cation exchangeable capacity (CEC) of soil and mixtures were carried out in order to quantify the Calcium, Magnesium, Aluminum, Sodium and Potassium exchangeability. Calcium ( $\text{Ca}^{2+}$ ) and Magnesium ( $\text{Mg}^{2+}$ ) exchangeable were extracted by chloride potassium (KCl) solution (1 mol/L), with ratio of 1:20, and determined by an atomic absorption spectrometer, *Varian Spectra*, model 2020 FS. Aluminum ( $\text{Al}^{3+}$ ) cations were extracted in similar solution that was used in calcium and magnesium extraction; however, determination was performed by titration in NaOH (0.025 mol/L). Cations of Sodium ( $\text{Na}^+$ ) and Potassium ( $\text{K}^+$ ) were extracted by Mehlich-1 solution and determined via flame photometry.

### 2.2.3. Mechanical behavior parameters

UCS tests have been used in most of the experimental programs reported in the literature in order to verify the effectiveness of the stabilization, to access the importance of influencing factors in the strength of treated soils and to choose the best stabilizer percentage. Therefore, UCS failure and initial tangent modulus (up to 0.1%) were used in analyses of mechanical response after soil modification. UCS tests were carried out according to ASTM D2166/94 in cylindrical specimens with 10 cm diameter and 12.7 cm high, molded at the optimum compaction parameters of soil and mixtures. The tested specimens were rested during 7 days and 28 days. In accordance to DNER-ME 129 (1994), acceptance criteria of specimens were  $\pm 0.30 \text{ kN/m}^3$  for maximum dry unit weight, and  $\pm 0.5\%$  for optimum water content. Average of the failure stresses of three specimens were adopted as UCS values, and the acceptance criteria of UCS average value was  $\pm 10\%$  for each specimen. Initial tangent modulus was obtained from UCS tests stress-strain curves at strain levels up to 0.1%. Duncan & Chang (1970) hyperbolic models were fitted in order to eliminate inaccuracies and subjectivity of tests at these strain levels. Mechanical strength and swelling parameters from CBR tests were performed as recommended in DNIT-ME 049/94.

Resilient modulus (RM) tests were performed using cyclic triaxial tests following the procedure DNIT-ME 134/10, and were carried out in specimens of the lateritic soil treated with 2% of lime and cement that were cured during 7 days and 28 days. Bilinear models were fitted in the values obtained from triaxial tests, which were used in the mechanistic analyses.

### 2.2.4. X-ray diffractometry investigation (XRD)

Mineralogical characterizations of soils and mixtures were carried out using XRD analyses. Mixtures samples

used in this analysis were extracted from post-failure of UCS specimens after 7 days and 28 days of curing times, and prepared by breaking, sieving through the 2 mm sieve, and oven-drying at 105 °C. Clay-silt (diameter  $\leq 0.05 \text{ mm}$ ) and sand ( $0.05 < \text{diameter} \leq 2 \text{ mm}$ ) fractions were separated by sedimentation with sodium hexametaphosphate dispersant. The XRD analyses were conducted using an X-ray diffractometer from the Department of Soils at the Federal University of Vicosa. All samples were irradiated using Cobalt laminas (Co- $\text{k}\alpha$ ) and scanning intervals ranging from 4° to 50° 2 $\theta$ . The sand fraction samples were installed in excavated glass lamina without mineral orientation, and the clay-silt fraction samples were installed in flat glass lamina with mineral orientation (Gibbs, 1965).

### 2.2.5. Research data application in flexible pavement design

In the mechanistic analyses, it was used the finite-difference computational program ELSYM5 applied to two typical pavement configurations using modified soil mixtures as base and subbase layers. The main objective of these analyses was to evaluate fatigue failure conditions and elastic strains generated in asphalt layers. The two design configurations were here named as Design 1 and 2 (Fig. 3). Design 1 was composed of the following layers and thicknesses: asphalt (12.5 cm), granular base (15 cm), modified soil subbase (10 cm, 30 cm, 40 cm and 50 cm), and subgrade of untreated soil. Design 2 was a pavement structure with the layers: asphalt (12.5 cm), modified soil base (10 cm, 30 cm, 40 cm and 50 cm) and untreated local subgrade.

In this study, it was adopted the 82 kN axle dual wheel and the load repetition number of  $5 \times 10^7$  (for heavy traffic, the Brazilian standard requires at least a 12.5 cm thick hot mix asphalt concrete layer). The input elastic properties were obtained through iterative analyses by the relationship between the stress differences resulting from the mechanistic analyses and the RM calculated by the bilinear model. Therefore, the convergence between the inputs RM values (ELSYM5) and RM from bilinear models was considered in each configuration. RM parameters from bilinear fit are showed in Table 4.

Soares *et al.* (2000) refers to asphalt layer fatigue failure (hot mix asphalt concrete) of 0.55 MPa of allowable stress determined in the cyclic diametric compression test. Stress differences  $\sigma_{zz}$ ,  $\sigma_{xx}$  and  $\sigma_{yy}$  are indirectly related to tension stresses and elastic deformations of asphalt layers near fatigue failure. In this study, these stresses differences ( $\sigma_d = \sigma_{zz} - \sigma_{xx} - \sigma_{yy}$ ) were determined using the finite-difference computational program ELSYM5; however, fatigue failures of the modified soil layers were not evaluated in this work. Although, the fatigue failure of these layers may occur, it is expected that the modified soil layers do not show the high stiffness of the stabilized soil layers. Therefore, cracks may not occur. Further tests must be performed

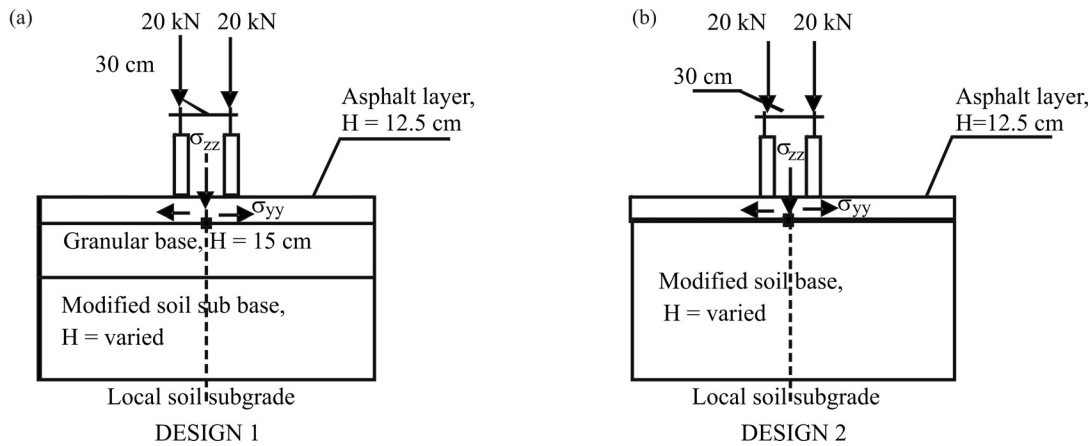


Figure 3 - Pavements mechanistic analyses: (a) Design 1 and (b) Design 2.

Table 4 - RM parameters from bilinear model.

Mixtures	RM parameters – bilinear model			
	K1	K2	K3	K4
Soil	130	73000	958	-79
Soil + 2% HL - 7 days	115	225000	5057	-579
Soil + 2% HL - 28 days	140	1175000	16111	-1591
Soil + 2% PC - 7 days	120	255000	10292	-1178
Soil + 2% PC - 28 days	140	720000	10389	-343

in order to assess the fatigue behavior of the modified soil layers.

### 3. Results and Discussion

#### 3.1. Workability

##### 3.1.1. Particles size distribution

Figure 4 shows particle size distribution curves of soil and mixtures. Results present reductions on the clay fraction (Fig. 4 and Table 3) and increases on the silt and fine sand fractions (Fig. 4), probably resulting from flocculation reactions. The alteration of particle size distribution curves occurs for all stabilizers. In general, the soil-lime mixtures showed higher reductions in the clay fraction than soil-cement mixtures, mainly with 3% of lime. Another interesting aspect is that addition of 1% of lime was as efficient as 3% of cement in the clay fraction reduction. Probably, calcium exchangeable concentration from hydrated lime favored the flocculation reaction. Additionally, the clay fractions reduced from 60% to 38% after addition of 3% lime even using dispersant in the sedimentation analysis.

##### 3.1.2. Atterberg limits

Figure 5 illustrates alterations on liquid ( $w_L$ ) and plastic ( $w_p$ ) limits promoted by addition of 0.5%, 1%, 2%, 4%,

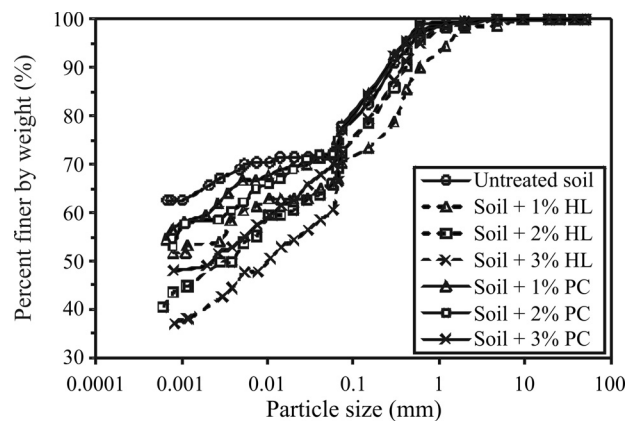


Figure 4 - Particle size distribution of lime (HL) and cement (PC) mixtures.

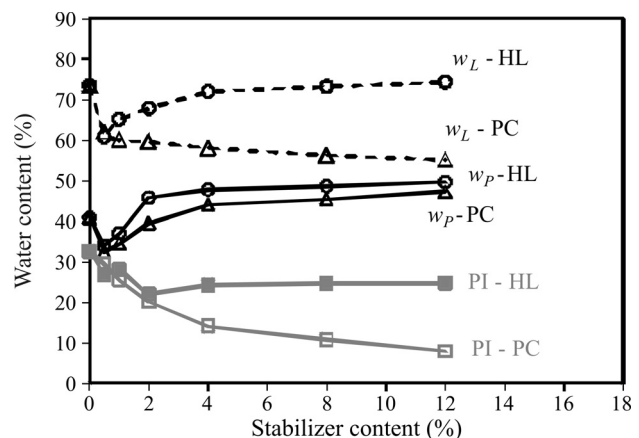


Figure 5 - Atterberg Limits vs. stabilizers contents.

8% and 12% of cement and lime. In general, content of 0.5% of both modifiers caused sudden decreases of  $w_p$  and  $w_L$  of soil. Thereafter, the  $w_L$  suffered increases after lime modification, whereas the cement promoted decreases. Probably, hydration reactions of cement can favor for this

behavior. On the other hand,  $w_p$  of soil increased after modification with lime and cement. In this set of results, curves in Fig. 5 showed that the modification of soil workability occurred with both modifier agents, and alterations promoted by lime were similar to cement when low contents were applied (up to 2%). In addition, the highest rates of decrease on PI occurred up to 2% of lime and cement, and soil stabilization with cement (from 4% to 12%) could provide higher alterations on PI due to hydration reaction effects. Chemical properties of mixtures supported the results from Atterberg limits, in which the CEC of mixtures with stabilizers contents from 1% to 3% did not change considerably (Fig. 6), and, simultaneously, PI of the lime mixture did not suffer significant alteration.

3.1.3. Chemical properties

The relationship between soil physic alterations and chemical parameters has been largely discussed in the technical literature (Bell & Coulthard, 1990; Rogers & Glenning, 2000). Specially, pH alterations of soils can establish mineralogical formations due to dissolution of soil mineral components, while the cationic exchangeable capacity (CEC) can explain cationic change reactions occurrence and, consequently, soil flocculation. Figure 5 pre-

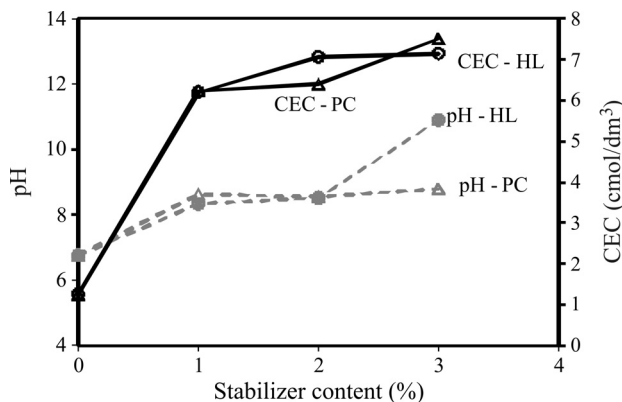


Figure 6 - pH and CEC values of soil modified with 1, 2 and 3% of lime and cement.

sents pH and CEC values of soil modified with lime and cement. The effects of pH in a clayey silt sand soil stabilized with lime are explicitly presented by Rogers & Glenning (2000), which reported that the minimum lime content to characterize the soil stabilization was 3%. After this lime content, called lime fixation point (LFP), further addition of lime did not produce significant change in the plastic limit, as reported previously by Hilt & Davidson (1960). In Fig. 6, CEC values of soil-lime mixtures were higher than soil-cement, which supports the highest particle size distribution changes showed by 3% lime mixtures. The pH of soil solution increased considerably after lime and cement modification (from 5.5 to 13), which can favor the minerals dissolution and, possibly, a formation of a new mineral gel.

3.1.4. Classification for roadway application

In order to quantify the modifications of soil caused by addition of lime and cement ranging from 0.5% to 12% in the roadways context, the mixtures were classified according to the USC (Fig. 7) and TRB (Fig. 7 and Table 3) systems. In the Unified system, plasticity modification did not promote changes in the classification groups of Casagrande plasticity chart, maintaining the material on the MH and OH group. Although cement did not change the classification group of the USC system, the cement modification caused dispersion of points inside the plot, and large contents of cement (4%, 8% and 12%) changed the mixture classification to the group OH. On the other hand, lime mixtures kept the classification in the group MH.

Figure 7b illustrates the TRB classification of soil after modification with lime and cement, while Table 3 presents the TRB classification considering the group index of mixtures. Lime and cement modification did not change the classification group. On the other hand, contents of 4%, 8% and 12% of cement provided  $w_p$  increases and  $w_L$  decreases, fitting these mixtures next to the A-5 group. The TRB classification considering group index reveals that the soil changes from A-7-5 to A-4 with addition of 4% of cement. Addition of lime showed to be less effective, since classified the soil as A-6.

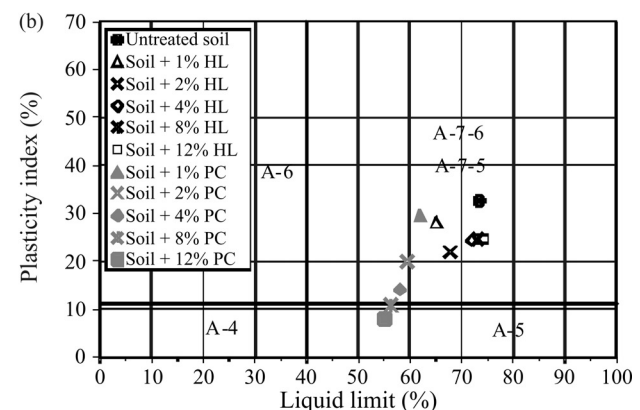
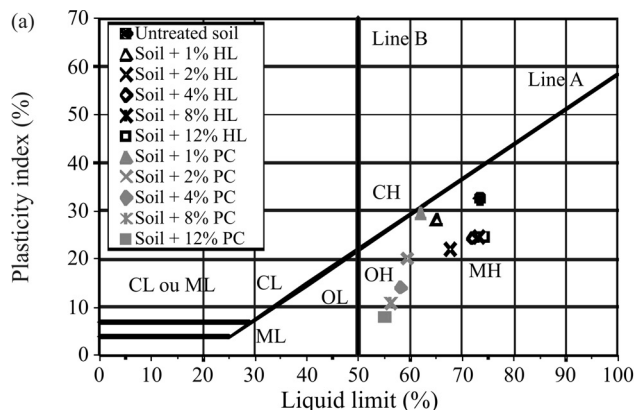


Figure 7 - Geotechnical classifications of modified soils: (a) USC, and (b) TRB systems.

3.1.5. Compaction parameters

Figure 8 presents the compaction curves of soil and its mixtures with 1%, 2% and 3% of lime and cement. Soil-cement mixtures showed higher values of maximum dry unit weight than the untreated soil, while soil-lime presented lower values when compared to untreated soil. The addition of lime caused increase of optimum water contents, while the addition of cement, in general, promoted decrease. In addition, gradual increases on both stabilizers percentage caused decreases of maximum dry unit weight in accordance with Osula (1996) and Osinubi & Nwaiwu (2006).

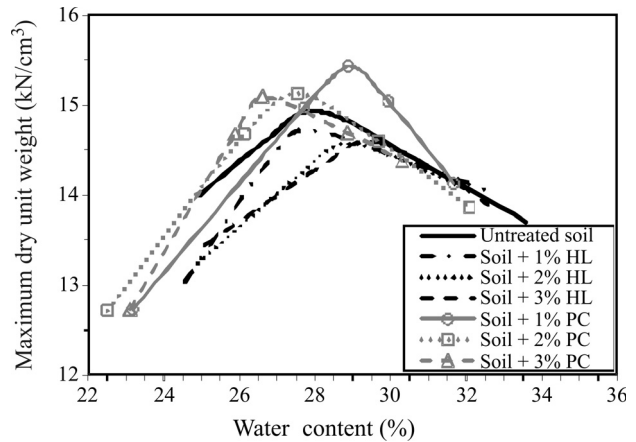


Figure 8 - Compaction curves of soil and mixtures.

3.2. Mechanical behavior

3.2.1. Unconfined compressive strength

Figure 9 shows results of unconfined compression tests at failure (Fig. 9a) and initial tangent modulus (Fig. 9b) for lime and cement soil modification, after 7 days and 28 days of curing times. Cement modification promoted higher increases in unconfined compressive strength (UCS) when compared with lime modification, for both curing times. Also, for both stabilizers, strength values after 28 days of cure were higher than for 7 days. In Fig. 9b, the variation of initial tangent modulus with addition of 1%,

2% and 3% of modified agents showed similar trends to those reported for maximum UCS (Fig. 9a).

Figures 10 and 11 illustrate the increase rates in mechanical strength and initial tangent modulus at 0.1%, respectively, caused by modification with 1%, 2% and 3% of lime and cement after 7 days (a) and 28 days (b) of curing. Increases rates were determined in relation to the untreated soil strength. Strength increases promoted by the addition

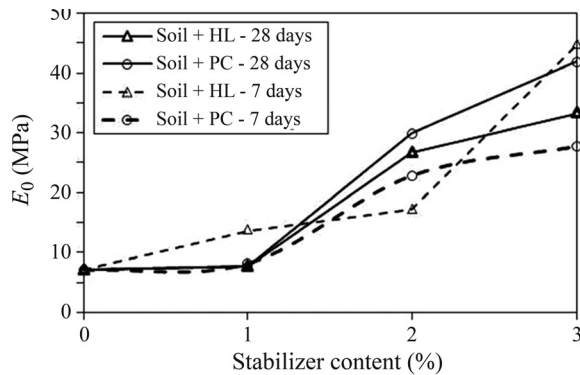
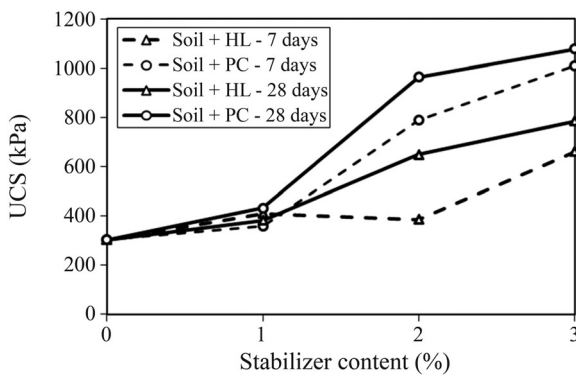


Figure 9 - UCS (a) and initial tangent modulus (b) of lime and cement mixtures, after 7 and 28 days of curing.

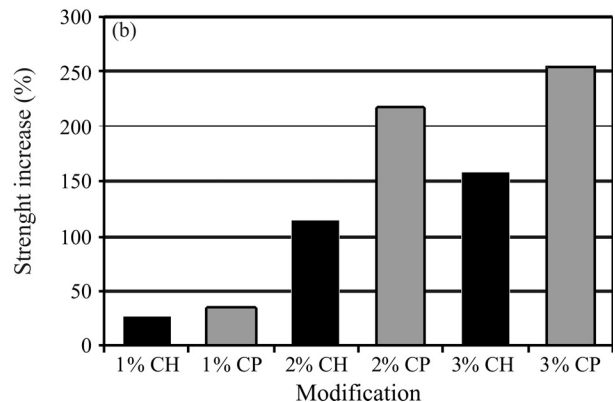
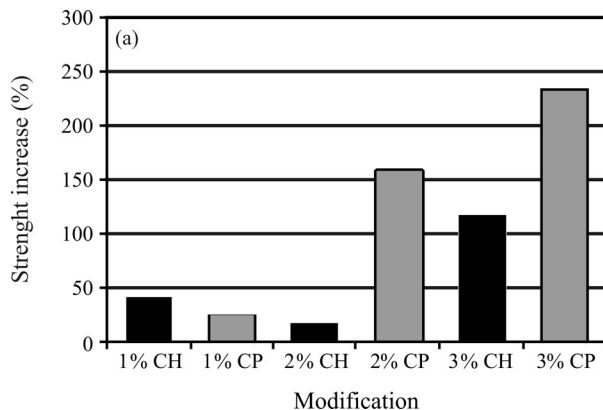
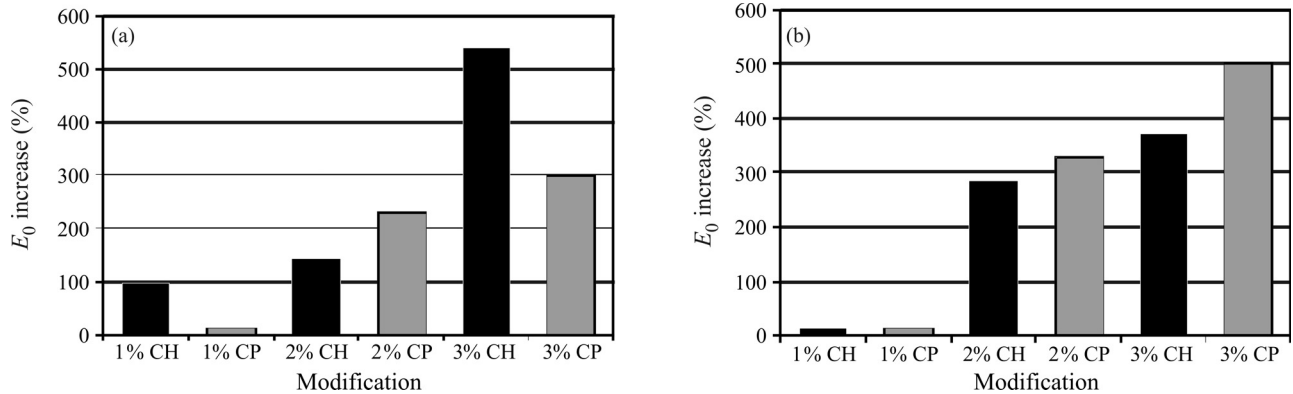


Figure 10 - Strength increase of mixtures specimens after 7 (a) and 28 (b) days of curing.



**Figure 11** - Initial tangent modulus increases of mixtures specimens after 7 (a) and 28 (b) days of curing.

of 1%, 2% and 3% of lime, in specimens cured after 7 days, were 42%, 17% and 118%, respectively. On the other hand, addition of 1%, 2% and 3% of cement provided increments of 26%, 166% and 233%, respectively (Fig. 10a). For specimens cured during 28 days, the addition of 1%, 2% and 3% of lime reveals increases of 26%, 114% and 159% in strength, while cement promoted increment of 35%, 218% and 255%, respectively (Fig. 10b). Therefore, the use of low contents of cement showed to be more effective than lime to improve the lateritic soil strength. In Fig. 11 increments of initial tangent modulus of soil-cement and soil-lime mixes are compared. Results show that the stiffness increments were higher than strength increments, presenting values around 500%.

### 3.2.2. CBR and swelling

CBR results and swelling parameters of mixtures with 2% and 4% of stabilizers are presented in Fig. 12. Results show that the cement modification is more efficient than the lime modification on the CBR responses, highlighting the highest increase of CBR in the mixture of lateritic soil with 4% of cement. Swellings of mixtures were very low in lime mixtures when compared to cement mixtures. Actually, lime modification eliminated the soil swell-

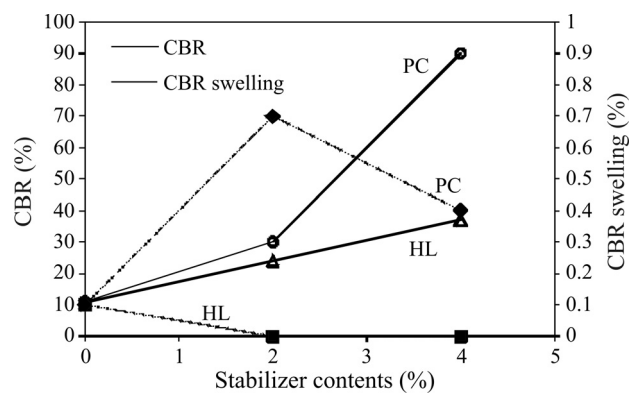


**Figure 12** - CBR results of modified soils.

ing. On the other hand, cement modification with 2% caused increases on the CBR swelling, and a sudden decrease after 4% of treatment.

### 3.3. XRD analysis

Figures 13 and 14 presents XRD analysis data of mixtures of clay-silt fractions (a) and sand fractions (b) at contents of 1%, 2% and 3% of lime and cement, respectively, after 7 days curing, while Figs. 15 and 16 show results of

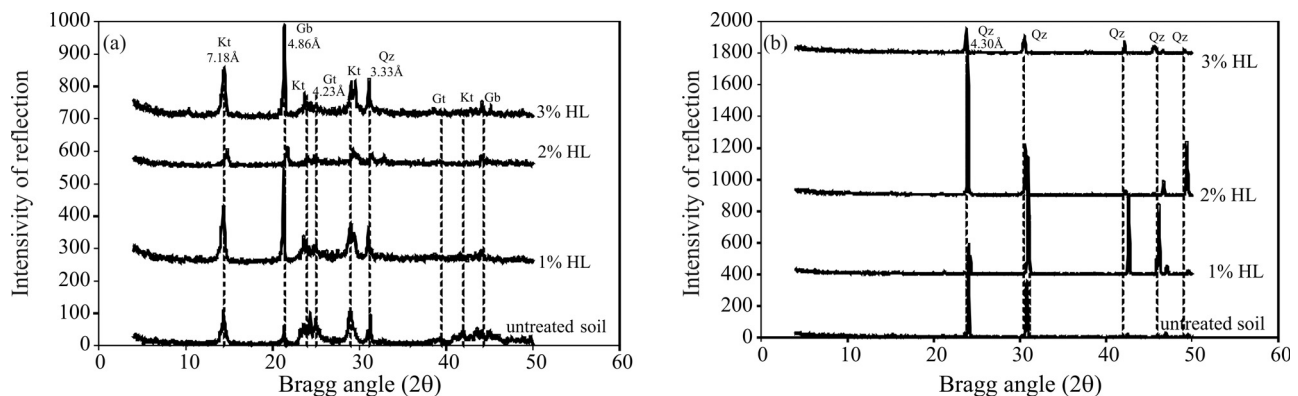


**Figure 13** - XRD data of silt-clay (a) and sand fraction (b) of the latosol and its mixtures with lime contents of 1%, 2% and 3% after 7 days of curing time.

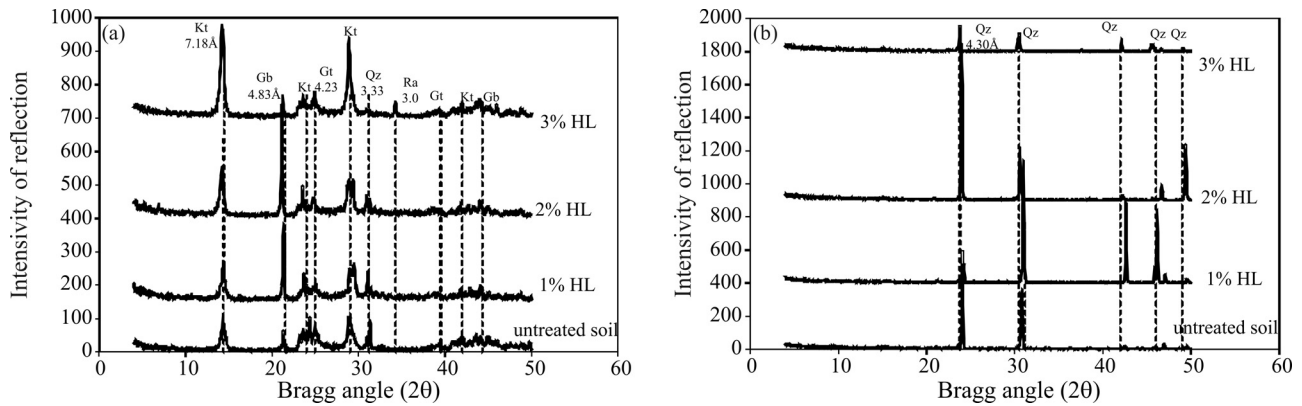


**Figure 14** - XRD data of silt-clay (a) and sand fraction (b) of the latosol and its mixtures with cement contents of 1%, 2% and 3% after 7 days of curing time.

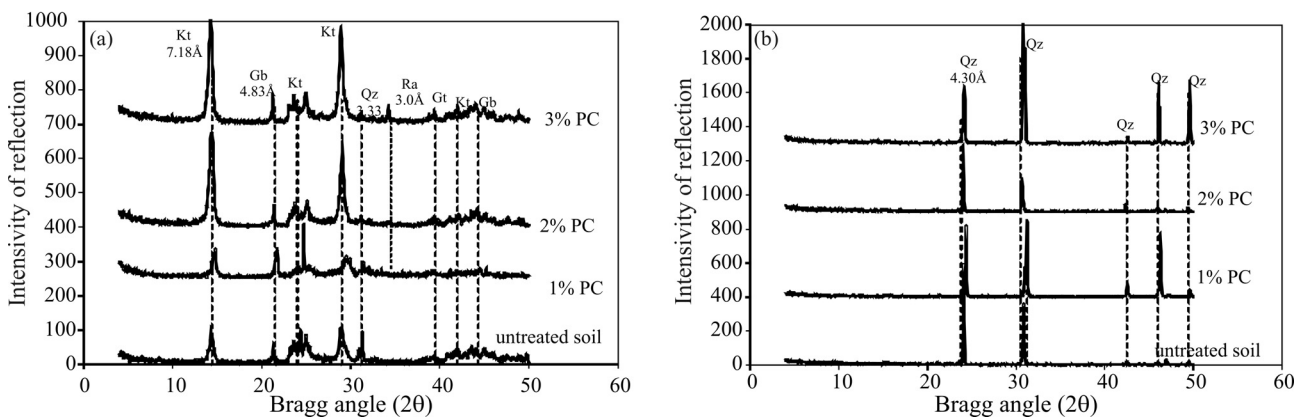


**Figure 15** - XRD data of silt-clay (a) and sand fraction (b) of the latosol and its mixtures with lime contents of 1%, 2% and 3% after 28 days of curing time.

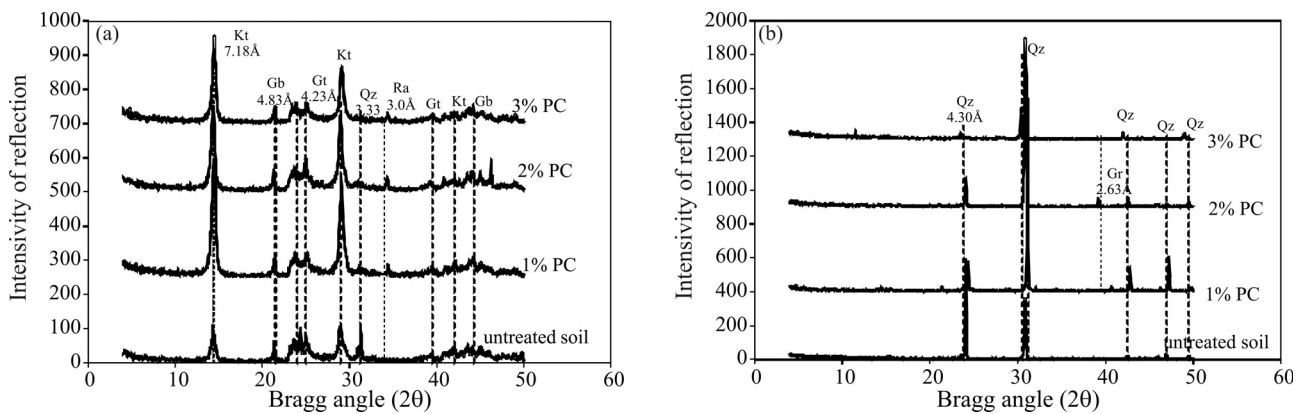


**Figure 16** - XRD data of silt-clay (a) and sand fraction (b) of the latosol and its mixtures with cement contents of 1%, 2% and 3% after 28 days of curing time.

clay-silt fractions and sand fractions of mixtures after 28 days of curing time. Results show that the utilization of low contents of lime in samples after 7 days of curing did not cause significant mineralogical alterations in the clay-silt and sand fractions. On the other hand, addition of 3% of cement favored formation of Calcium silicate, identified as

Rankinite, still after 7 days of curing (Fig. 14). For samples cured during 28 days, in the clay-silt fractions Calcium silicate appeared in mixtures of 3% of lime and 1%, 2% and 3% of cement. In the sand fractions, the formation of Calcium silicate aluminate was noted just in samples with 2% of cement. This mineral was identified as Grossular (Fig. 16).

### 3.4. Mechanistic analysis of flexible pavement layers with modified soil

Results from mechanistic analyses for the Designs 1 and 2 are showed in Figs. 17, 18 and 19. Figure 17 presents

the resilient modulus (RM) values obtained from the iterative process for the Designs 1 and 2. It can be noticed that soil modification applied in subbase of pavements (Fig. 3a) showed higher RM values than for base application as presented in Design 2 (Fig. 3b). Even though the cement modi-

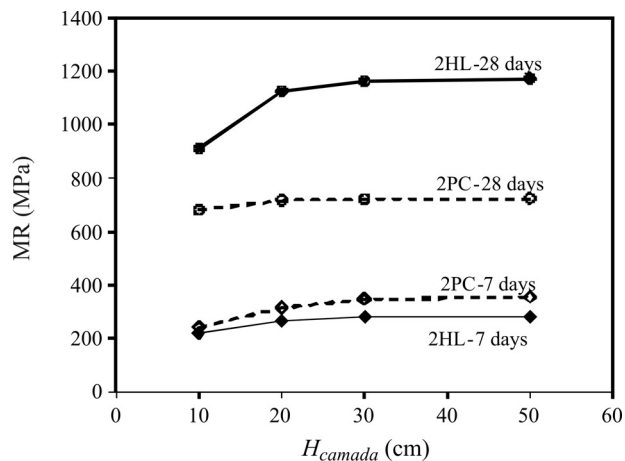
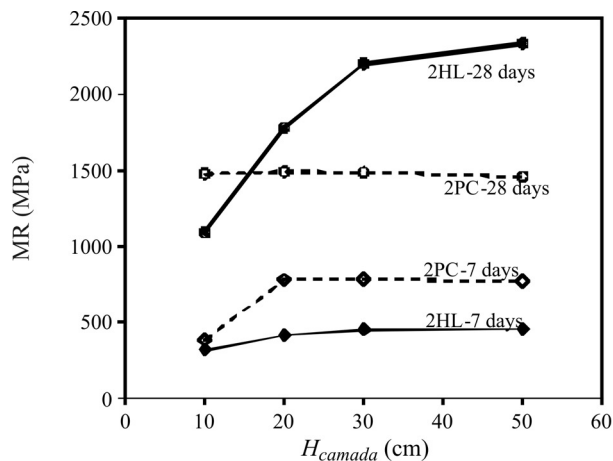


Figure 17 - RM values of mixtures of 2% of stabilizers and soil in the Design 1 (a) and Design 2 (b).

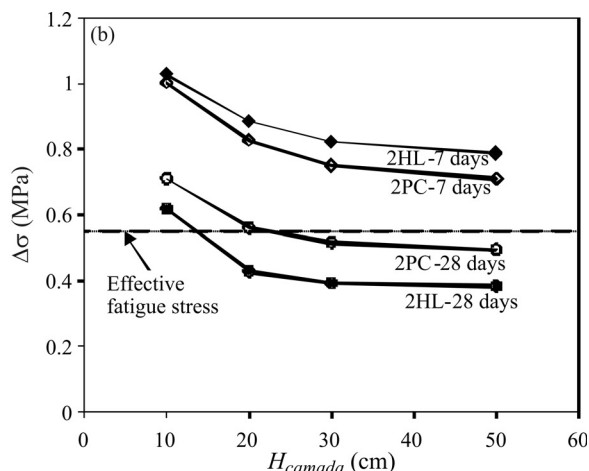
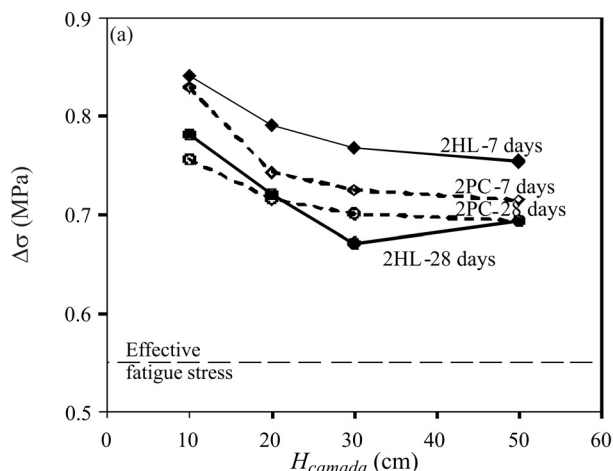


Figure 18 - Stress ( $\Delta\sigma$ ) and strain vs. base thickness of the Design 1.

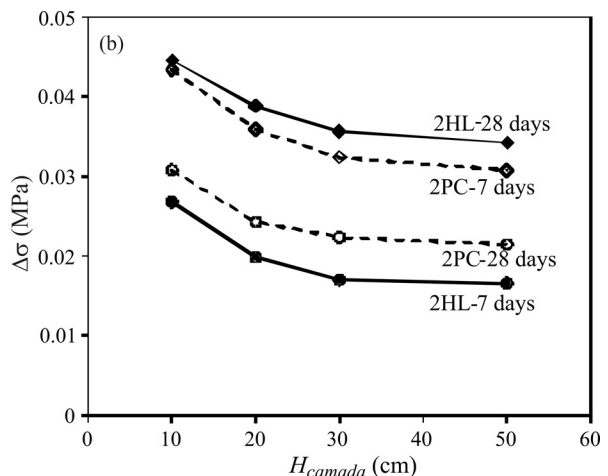
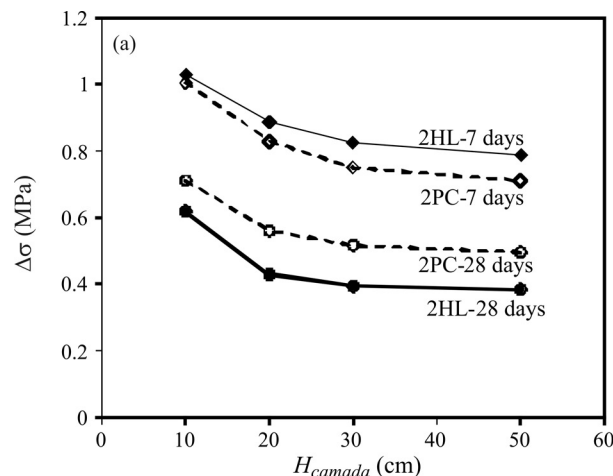


Figure 19 - Stress ( $\Delta\sigma$ ) and strain vs. base thickness of the Design 2.

fication has showed higher UCS values than lime modification, the RM values from lime modification were higher than those from cement modification after 28 days of curing. However, cement modification showed better response after 7 days of curing.

Input elastic properties are presented in Table 5.

Generally, the RM values of the modified soil with lime and cement after 28 days of curing were similar to the values of RM of sand soils with high bearing capacity. Nevertheless, the soil modification should be a good solution in situation where sand soils are not available.

Figure 18 shows the performance of Design 1 in the mechanistic analyses. The uses of higher layers favored to the decrease of the stress levels in the asphalt layer. However, regarding that the allowable stress level in asphalt layers with 12.5 cm is around 0.55 MPa, the configuration adopted in the Design 1 probably will results in cracking on the asphalt layer, even using higher subbase layers. Problems in this Design are higher resilient modulus in the subbase layer than in the base layer, favoring the cracking development.

In Fig. 19, it can be noticed that cracks can appear only when RM values with 7 days of curing time are considered in the designs. After 28 days of curing, cement and lime modification showed an excellent performance when considering modified base layers constructed with heights from 20 cm to 50 cm. Theoretically, fatigue failure will not occur and the stresses and strains levels were lower than that in Design 1. Hence, the use of 2% and 3% of lime and cement modifications may be an economical alternative for flexible pavement layers.

#### 4. Final Discussion

The use of low contents of lime and cement, here named soil modification technique, improved workability and mechanical behavior of the lateritic soil. Workability improvements were noted from analyses of plasticity properties and particle size distribution of mixtures. Lime and cement addition up to 2% of the stabilizers brought the highest alterations on plastic limit, and further additions did not change this parameter significantly. This behavior was confirmed by pH and CEC determinations. Additionally, cement was a more effective modifier of soil workability than lime after the lime fixation point. Explanations around this can come from hydration reactions of cement in short term. In contrast, the addition of lime provides higher alteration on grain size distribution than cement. In general, both stabilizers promoted improvement in soil handling with maximum alterations around 3% of lime and cement.

The cement provided significant improvement of strength and stiffness, and increased on compaction maximum dry unit weight. Nevertheless, the lime modification promoted increases in soil strength that can be useful in the applications suggested in this work. Still, the swelling elimination and initial tangent modulus increases can be a

**Table 5** - Input elastic parameters of materials used in mechanistic analyses.

Layers	Design 1		Design 2		
	RM (MPa)	$\nu$	RM (MPa)	$\nu$	
Asphalt layer	3000	0.3	3000	0.3	
Granular layer	300	0.35	300	0.35	
2% HL (7 days)	10 cm	201	0.25	197	0.25
	20 cm	203		212	
	30 cm	203	0.25	212	0.25
	50 cm	204		213	
2% HL (28 days)	10 cm	1330	0.25	760	0.25
	20 cm	1190		1010	
	30 cm	1170	0.25	1030	0.25
	50 cm	1155		1025	
2% PC (7 days)	10 cm	215	0.25	200	0.25
	20 cm	218		230	
	30 cm	217	0.25	229	0.25
	50 cm	219		228	
2% PC (28 days)	10 cm	750	0.25	645	0.25
	20 cm	720		693	
	30 cm	719	0.25	697	0.25
	50 cm	717		697	
Untreated soil	130	0.4	130	0.4	

considerable advantage of this modifier. In general, both materials demonstrated to be efficient with addition of 3%.

Findings from XRD analyses support the mechanical improvement of mixtures using low contents of lime and cement. Identification of new minerals forms was observed at the same stabilizers contents, responding for significant strength increases. Therefore, pH alterations of mixtures were sufficient to promote the dissolution of some minerals of soil and cementation of new formed gels.

This study was directed to the Brazilian regions showing occurrence of Red-yellow latosol; however, it is expected that the findings can apply to soils with similar mineralogical characteristics, chemical and physics properties. Regarding the RM and Poisson coefficient values adopted in the mechanistic analyses, soil modification in bases of pavement were efficient against asphalt layer fatigue failure, and showed to be an economical solution for local soil application. Applications in subbase of flexible pavement (asphalt) layers were not efficient in the mechanistic analyses because the subbase presented higher RM

than the granular base layer. However, if the elastic properties were inverted, the cracking problem could be avoided.

Even though the advantages of the lateritic soil modification, homogeneity of mixture in field applications can be an adverse aspect of the technique. Therefore, an intensive mixture process must be required in the field. Actually, the authors do not recommend the applications of contents of 1% of the modifiers. Probably, problems around homogeneity can be come up. However, the use of 2% and 3% and an intensive process of mixture can make the soil modification a good technique. The authors have not evaluated this aspect; however, they recommend implementation of an experimental field test before the final application.

## 5. Conclusions

Results support that modification of the tested soil with lime and cement is an efficient and economical technique for flexible pavement design and construction, and conclusions of the study are as follows:

- Low contents of lime and cement were efficient in workability changes of the Red-yellow latosol, highlighting highest alterations provided by addition of 3% of cement. Further additions of lime and cement do not change the soil PI.
- Chemical properties of mixtures were compatible with the plasticity behavior, showing that the lime fixation point is around 3% in this soil. Therefore, it can support the mineralogical alterations. Hydration reaction of cement favored to PI decreases;
- Lime modification eliminated the swelling of soil, while cement increased it with addition of 2% of cement;
- The soil modification promoted increase in strength and initial tangent modulus, mainly after 28 days of curing, where cement was more efficient material. The highest alterations in strength occurred at 2% and 3% of lime and cement, although addition of 1% was sufficient to provide 50% of the unconfined compressive strength increase compared to the untreated soil. Initial tangent modulus increases were significantly higher than the unconfined compressive strength increases generated by addition of low contents of stabilizers.
- It was noted that mineralogical alterations have occurred in samples that showed significant strength increases.
- Mechanistic analyses showed that the soil modification can be applied to the design of base of flexible pavements producing low elastic strain and stress levels. Additionally, the most efficient (economically and mechanically) configuration of pavements suggested in this study was the sub-grade improvement or modified soil base.

## Acknowledgments

The research described in this paper was supported by the Minas Gerais State Research Foundation (FAPEMIG), under Grant No. TEC APQ-0830-5.07/07 and by conces-

sion of scientific initiation scholarships (PROBIC FAPEMIG/UFV). The authors wish to thank the Brazilian Agency for Training of Superior Level People (CAPES) for the financial support during the first author graduate studies at the Federal University of Viçosa (UFV), Brazil.

## References

- ASTM (1994) Standard Test Method for Unconfined Compressive Strength of Cohesive Soil - D2166-98. ASTM International, West Conshohocken, Pennsylvania, USA, 6 pp.
- Bell, G. & Coulthard, J.M. (1990) Stabilization of clay soils with lime. *Engineering Geology*, v. 7:3, p. 125-140.
- Bhattacharja, S.; Bhatta, J.I. & Todres, H.A. (2003) Stabilization of Clay Soils by Portland Cement or Lime – A Critical Review of Literature. PCA R&D Serial N° 2066. Portland Cement Association, Skokie, 60 pp.
- Consoli, N.C.; Lopes, L.L. & Heineck, K.H. (2009) Key parameters for the control of lime stabilized soils. *Journal of Materials in Civil Engineering*, v. 21:5, p. 210-216.
- Cristelo, N.; Glendinning, S. & Jalali, S. (2009) Subbases of residual granite soil stabilized with lime. *Soils and Rocks*, v. 32:2, p. 83-88.
- DNER (1994) Soils - Determination of California Bearing Ratio in Non Handles Samples - ME 049 (in Portuguese). IPT - DNER, Rio de Janeiro, Brazil, 8 pp.
- DNER (1994) Soils – Compaction Using Non Handle Samples - ME 129 (in Portuguese). IPT - DNER, Rio de Janeiro, Brazil, 7 pp.
- DNIT (2010) Pavements - Soils - Determination of Resilient Modulus - ME 134 (in Portuguese). DNIT - Rio de Janeiro, Brazil, 11 pp.
- Drumm, E.C.; Boateng-Poku, Y. & Pierce, J.T. (1990) Estimation of subgrade resilient modulus from standard tests. *Journal of Geotechnical Engineering*, v. 116:5, p. 774-789.
- Duncan, J.M. & Chang, C.Y. (1970) Nonlinear analysis of stress and strain in soils. *Journal of the Soil Mechanics and Foundations Division*, v. 96:5, p. 1629-1653.
- EMBRAPA (1997) Methods of Chemical Analyses of Soils (in Portuguese). National Center of Soil Researches, Rio de Janeiro, 212 pp.
- Felt, E.J. & Abrams, M.S. (2004) Strength and Elastic Properties of Compacted Soil-Cement Mixtures. *Highway Research Board Bulletin*, p. 152-178.
- Galvão, C.B.; Elsharief, A.; Simões, G.F. (2004) Effects of lime on permeability and compressibility of two tropical residuals soils. *Journal of Environmental Engineering*, v.130:8, p. 883-885.
- Gibbs, R.J. (1965). Error due to segregation in quantitative clay mineral X-ray diffraction mounting techniques. *American Mineral*, v. 50:526, p. 741-751.
- Herrin, M. & Mitchell, H. (1961) Lime-soil mixtures. *Highway Research Board, Bulletin 304*, p. 99-121.

- Hilt, G.H. & Davidson, D.T. (1960) Lime fixation in clayey soils. Highway Research Board, Bulletin 262, p. 20-32.
- Kolias, S.; Kasselouri-Rigopoulou, V. & Karahalios, A. (2005) Stabilization of clayey soils with high calcium fly ash and cement. *Cement and Concrete Composites*, v. 27, p. 301-313.
- Kennedy, T.W.; Smith, R.; Holmgreen Jr, R.J. & Tahmouressi, M. (1987) An evaluation of lime and cement stabilization. *Transportation Research Record*, v. 119, p. 11-25.
- Ker, J.C. (1998) Latosols from Brazil: A review (In Portuguese). *Geonomos*, v. 5:1, p. 17-40.
- Moh, Z.C. (1965) Reactions of soil minerals with cement and chemicals. Highway Research. Board Record, v. 86, p. 39-61.
- ABNT (1984) Soil - Determination of Liquid Limit - NBR 6459 (in Portuguese). ABNT, Rio de Janeiro, Brazil, 6 pp.
- ABNT (1984) Soil - Particles Passing in 4.8 mm Sieve - NBR 6508 (in Portuguese). ABNT, Rio de Janeiro, Brazil, 8 pp.
- ABNT (1984) Soil - Determination of Plastic Limit - NBR 7180 (in Portuguese). ABNT, Rio de Janeiro, Brazil, 3 pp.
- ABNT (1984) Soil - Particle Size Distribution Procedures - NBR 7181 (in Portuguese). ABNT, Rio de Janeiro, Brazil, 13 pp.
- ABNT (1986) Soil - Compaction Tests Procedure - NBR 7182 (in Portuguese). ABNT, Rio de Janeiro, Brazil, 10 pp.
- Osinubi, K.J. & Nwaiwu, M.O. (2006) Compaction delay effects on properties of lime-treated soil. *Journal of Materials in Civil Engineering*, v. 18:2, p. 250-258.
- Osula, D.O.A. (1996) A comparative evaluation of cement and lime modification of laterite. *Engineering Geology*, v. 42:1, p. 71-81.
- Parreira, A.B.; Cunto, F.J.C.; Carmo, C.T. & Rodrigues, J.K. (1998) Resilient modulus of some pavement materials and prediction by unconfined compressive tests (in Portuguese). *Proc. 11th Brazilian Conference on Soil Mechanics and Geotechnical Engineering*, Brasília, pp. 149-155.
- Prusinski, J.R. & Brattacharja, S. (1999) Effectiveness of Portland cement and lime in stabilizing clay soils. *Journal of the Transportation Research Board*, v. 1652, p. 215-227.
- Rogers, C.D.F. & Glendinning, S. (2000) Lime requirement for stabilization. *Journal of the Transportation Research Board*, v. 1721, p. 9-18.
- San'tana, G.L.; Machado, C.C.; Carvalho, C.A.B.; Lima, D.C. & Fernandes, D.C.M. (2003) Resilient behavior of a clayey soil from Viçosa-MG in its natural state and after stabilization with cement and tar (in Portuguese). *Revista Árvore*, v. 27:3, p. 269-278.
- Sariosseiri, F. & Muhunthan, B. (2009) Effect of cement treatment on geotechnical properties of some Washington State soils. *Engineering Geology*, v. 104:2, p. 119-125.
- Soares, J. B.; Motta, L.M.G.; Paiva, J.A. & Branco, J.V.C. (2000) Mechanical properties of asphalt mixtures with particle size and asphalt concrete. *Asphalt Meeting in IBP*, Rio de Janeiro, 10 pp.
- Solanski, P.; Hhoury, N. & Zaman, M.M. (2009) Engineering properties and moisture susceptibility of silty clay stabilized with lime, class C fly ash, and cement kiln dust. *Journal of Materials in Civil Engineering*, v. 21:12, p. 749-757.

### List of Symbols

- Fd: Feldspate  
 Gr: Grossular  
 Gb: Gibbsite  
 Gt: Goethite  
 Kt: Kaulinite  
 Mi: Mica  
 UCS: Unconfined Compression Strength  
 Qz: Quartz  
 Ra: Rankinite  
 HL: Hydrated Lime  
 PC: Portland Cement  
 LFP: Lime fixation point  
 CBR: California Bearing Ratio  
 CEC: Cation Exchangeable Capacity  
 pH: Potential Hydrogenionic  
 TRB: Transportation research board  
 USC: Unified Soil Classification  
 MCT: Miniatura, Compactado, Tropical  
 RM: Resilient modulus



# Evaluation of Direct Shear Tests on Geogrid Reinforced Soil

A.S.F.J. Sayão, A.C.C.F. Sieira

**Abstract.** This paper presents a program of direct shear tests in soil reinforced with geogrids, carried out with large-scale equipment. A woven geogrid was placed in sandy soil and positioned with different inclinations inside the shear box. The strength parameters of the soil-geogrid interface were obtained from shear tests with the geogrid positioned horizontally in the sand. The direct shear tests with inclined reinforcement revealed the strength differences related to the reinforcement inclination, seeking to define the most favorable positioning of the geogrid for construction works in reinforced slopes. An analysis of the deformed configuration of the geogrid is presented, based on the measured position of the grid at the end of the shear tests. Finally, numerical simulations of the direct shear tests were carried out, allowing an assessment of the tensile forces acting on the inclined reinforcement. These studies allowed a clear definition of the soil region that is not distorted during the direct shear test, being subject to a simple translation only. The geogrid's displacements were found to be anti-symmetrical in relation to the failure plane. Shearing was concentrated at the central region of the specimen's height, with the upper and lower regions being simply subjected to translation, with no distortion. The inclination of the reinforcement within the soil has a significant influence, with the maximum strength occurring when the geogrid was positioned at 60° angle in relation to the failure plane.

**Keywords:** reinforced soil, geogrids, direct shear tests, numerical analyses.

## 1. Introduction

Geogrids are flat synthetic structures consisting of fully connected traction resistant elements in the form of a grid. In addition to the surface available for interface friction between the grid elements and the soil, geogrids also have a hollow area for the mobilization of soil-soil shear strength.

The interaction mechanism developed in the soil-geogrid interface depends on the physical and mechanical characteristics of the soil and the geogrid. A reinforced soil structure project requires knowledge of the interface strength parameters, which can be obtained from pullout, direct shear or inclined plane tests.

These test methods have basic differences in the boundary conditions, stress paths and failure mechanisms imposed to the specimen. The choice of one of these tests must take into account the similarity with the load conditions found in reinforced soil construction works. (Palmeira & Milligan, 1989). A comprehensive review on the advantages and limitations of these tests is presented by Palmeira (2009).

The direct shear tests herein described are aimed at the reproduction of two distinct mechanisms of interaction that occur in the soil-geogrid interface. The first involves the mobilization of interface friction, whereas its reproduction in the laboratory allows the strength parameters of the soil-geogrid interface to be obtained. The second mechanism consists of the mobilization of tensile loads in the

geogrid. Figure 1 illustrates the two different interaction mechanisms in geosynthetic reinforced soil.

In the first mechanism, the geogrid remains attached to the lower part of the enveloping soil, with the interface resistance being mobilized by the sliding of the upper soil mass in relation to the geogrid. In this case, the interface strength parameters ( $\phi'_{s/GGR}$  and  $c_{s/GGR}$ ) can be obtained from direct shear tests with the geogrid horizontally positioned in the test box.

Interface shear has been studied by several researchers. Bakeer *et al.* (1998) discussed the strength parameters obtained from direct shear and pullout tests for an aggregate-geogrid interface. Wasti & Ozduzgun (2001) compared results of horizontal reinforcement in direct shear tests to results of inclined plane tests (or tilt tests). Lui *et al.* (2009) reported on the results of shear tests with different soil-geogrid interfaces. Pitanga *et al.* (2009) studied the interface shear strength in inclined plane tests on from landfill cover materials. Slightly higher interface parameters have usually been found when obtained from direct shear tests with horizontal reinforcement as compared to inclined plane tests.

The second interaction mechanism occurs when the potential failure surface intercepts the geogrid. A laboratory simulation can be achieved in direct shear tests of soil specimens with reinforcement inclined in relation to the horizontal shear surface. The maximum tension of the geogrid occurs at the point where it is intercepted by the failure surface. In this mechanism, shear stresses on the soil-

A.S.F.J. Sayão, Associate Professor, Departamento de Engenharia Civil, Pontifícia Universidade Católica do Rio de Janeiro, Rio de Janeiro, RJ, Brazil. e-mail: sayao@puc-rio.br.

A.C.C.F. Sieira, Associate Professor, Departamento de Estruturas e Fundações, Universidade do Estado do Rio de Janeiro, Rio de Janeiro, RJ, Brazil. e-mail: sieira@uerj.br.

Submitted on December 2, 2010; Final Acceptance on April 3, 2012; Discussion open until September 30, 2012.

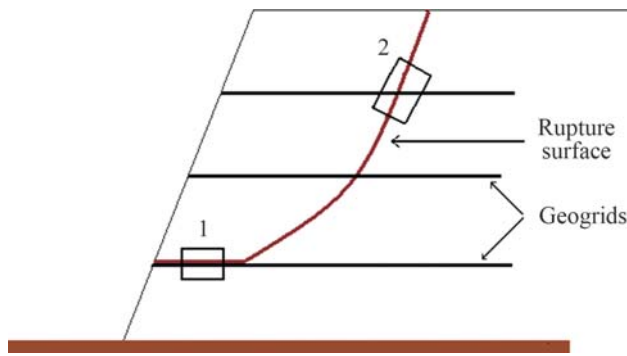


**Figure 1** - Soil-geogrid interaction mechanisms: (1) interface shear; (2) tension in reinforcement.

geogrid interface are absorbed by the tensioned reinforcement.

Figure 2 illustrates the direct shear test with an inclined reinforcement. The geogrid's function in a reinforced slope consists of overcoming the soil's incapacity to resist tensile stresses. When the failure surface intercepts the geogrid, this becomes tensioned, thereby giving the reinforced soil mass a stabilizing effect. The angle  $\theta$ , between the reinforcement and the failure surface, has a significant influence on the soil-geogrid resistance and changes from its initial value  $\theta_0$  to a final value  $\theta_f$  at the end of the shearing. This variation in  $\theta$  will depend on the magnitude of angular distortions and on the thickness of the shear zone, as illustrated in Fig. 3.

Bauer & Zhao (1994) presented results of direct shear tests with inclined reinforcement, using uniform sand and a polypropylene geogrid. Inclination angle  $\theta$  was shown to have a large influence on the soil-geogrid resistance. When compared to the non-reinforced soil, the maximum increase in strength occurred when the geogrid was positioned at  $\theta_0 = 60^\circ$  in relation to the failure plane.

Sayão & Teixeira (1995) carried out direct shear tests with an inclined unwoven geotextile for simulating the field condition of an embankment over soft clay. In these

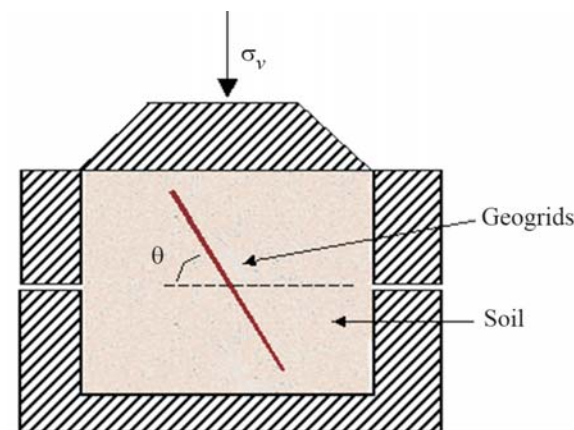


**Figure 2** - Direct shear tests with inclined reinforcement.

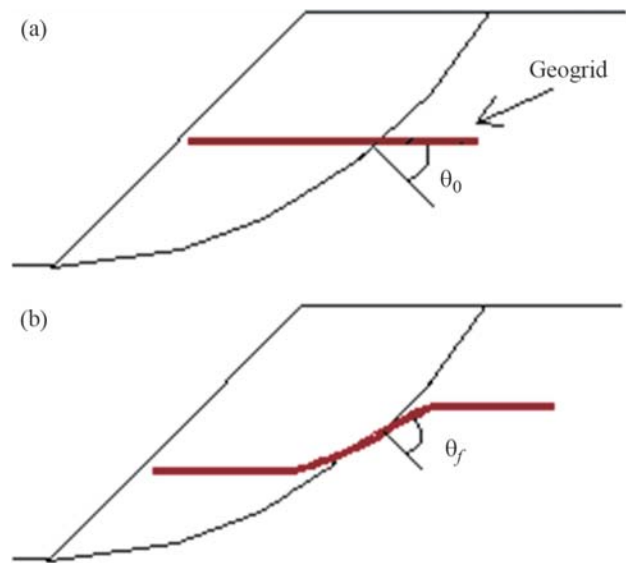


**Figure 3** - Reinforcement behavior in a shear zone. (a) initial condition; (b) distorted condition.

tests, the reinforcement was positioned at an inclined angle within the layered soil specimens, which were made of clay in the lower half and sand in the upper half. The shear strength parameters of the soil-geotextile interface were noted to vary with the geotextile inclination  $\theta$ , but further research on larger devices was suggested.

Palmeira (1999) also concluded that the most favorable orientation of the reinforcement element in large-size shear tests was  $60^\circ$ , because it coincided with the direction of the tensile strain increments of the unreinforced soil.

The main objective of this investigation was to obtain a clear definition of the soil region that is distorted during the direct shear test. This was achieved with shear tests with inclined reinforcement, in which the grid's displacements were measured for defining its deformed shape. The observations were complemented by numerical simulations of the direct shear tests.

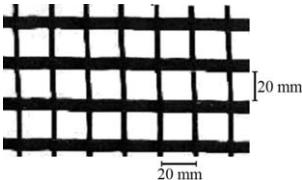
## 2. Materials

All tests were carried out with a geogrid reinforced sandy soil in large-scale direct shear apparatus at the Cedex geotechnical laboratory, in Spain.

### 2.1. Geogrid characteristics

The geogrid exhibits a 20 mm opening size and 70% of open area available for the mobilization of soil-soil friction during direct shearing. According to the manufacturer, this geogrid is bi-axially oriented, with woven fibers of high-tenacity polyester and low tendency to creep. The polyester filaments are coated with PVC for protecting the nucleus against damage during installation and working procedures. Nominal values for longitudinal and transversal tensile strengths are 97.0 kN/m and 29.4 kN/m, respectively. Table 1 shows the main physical and mechan-

**Table 1** - Physical and mechanical characteristics of geogrid.

Illustration		
Physical	Type of polymer	Polyester with PVC
	Manufacturing process	Woven
	Type of mesh	Square openings
	Openings of grid	20.0 mm
	Width of longitudinal elements	8.0 mm
	Width of transversal elements	3.0 mm
	Mechanical	Longitudinal tensile strength
Transverse tensile strength		29.4 kN/m
Tensile elongation at failure		12.8%
Longitudinal stiffness		750.0 kN/m

ical characteristics of geogrid used in the experimental program.

## 2.2. Sandy soil characteristics

The sand used in the experimental program consisted predominantly of quartz and feldspar and contained particles with a specific gravity  $G_s = 2.71$  and average diameter  $D_{50} = 0.7$  mm.

All sand specimens were compacted in the laboratory to a relative density  $D_r = 80\%$ , with water content  $w = 10 \pm 0.2\%$ , corresponding to a saturation degree  $S = 37\%$ . These values are typical for sandy embankments in reinforcement projects. Shear strength parameters of the sand were  $c' = 16$  kPa (cohesion) and  $\phi' = 33^\circ$  (friction angle). These parameters were obtained in the large size direct shear device under vertical confining stresses of 50, 100 and 200 kPa, for avoiding errors due to scale effects in the interpretation of reinforced test results.

## 3. Experimental Program

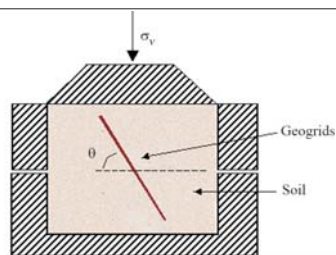
### 3.1. Direct shear tests

The experimental program consisted of twelve direct shear tests with the geogrid positioned at different inclinations inside the soil specimen, as shown in Table 2. Vertical confining stresses of 50, 100 and 200 kPa were imposed to each specimen configuration.

Direct shear tests with the horizontal geogrid ( $\theta = 0^\circ$ ) aimed at the simulation of interaction mechanism no. 1, as

**Table 2** - Direct shear tests program in reinforced soil.

Vertical confining stress, $\sigma_v$ (kPa)	Inclination of geogrid, $\theta$
50, 100 and 200	$0^\circ$
	$30^\circ$
	$60^\circ$
	$90^\circ$



shown in Fig. 1, for obtaining the soil-geogrid interface parameters (interface friction angle,  $\phi'_{s/GSY}$ , and soil-geogrid adhesion,  $c_{s/GSY}$ ). The shear tests with inclined reinforcement ( $\theta = 30^\circ, 60^\circ$  and  $90^\circ$ ) aimed at reproducing mechanism no. 2 and obtaining the shear strength variation as a function of the reinforcement inclination.

### 3.2. Equipment

Figure 4 shows the large size direct shear device used in the experimental program. The equipment used was originally developed in the Cedex Laboratory (Spain) to study the shear resistance of rockfill materials (Sayão *et al.*, 2005) and adapted to direct shear and pullout tests on soil specimens containing geosynthetic materials (Sieira & Sayão 2006, and Sieira *et al.* 2009).

The shear box is made of aluminum and divided into two halves with a square section with 1.0 m sides and a height of at least 0.70 m. The device is composed of two systems for vertical and horizontal load application. Each system consists of a hydraulic jack, a servo-control, a load cell and a displacement transducer.

The vertical hydraulic jack has a load capacity corresponding to a confining stress of 1.0 MPa. The vertical servo-control ensures the steadiness of  $\sigma_v$  during the test. The load signal applied to the test specimen is continually compared to the reference signal, which corresponds to the desired normal stress. Upon any difference between the two signals, the servo-control switches on the hydraulic jack to correct the applied vertical load. Increases in  $\sigma_v$ , produced by reductions in the contact area between the lower and upper halves of the shear box, can therefore be compensated.

The horizontal load system functions in a similar way. The horizontal servo-control guarantees a constant average shear strain rate during the test. The maximum elongation of the horizontal hydraulic jack piston is 300 mm. This was sufficient to produce a shear failure in all specimens tested in this experimental program.

### 3.3. Test procedure

Testing in the large size shear device is similar to the conventional direct shear tests: the upper half of the box remains immobile, while the lower half is displaced by the

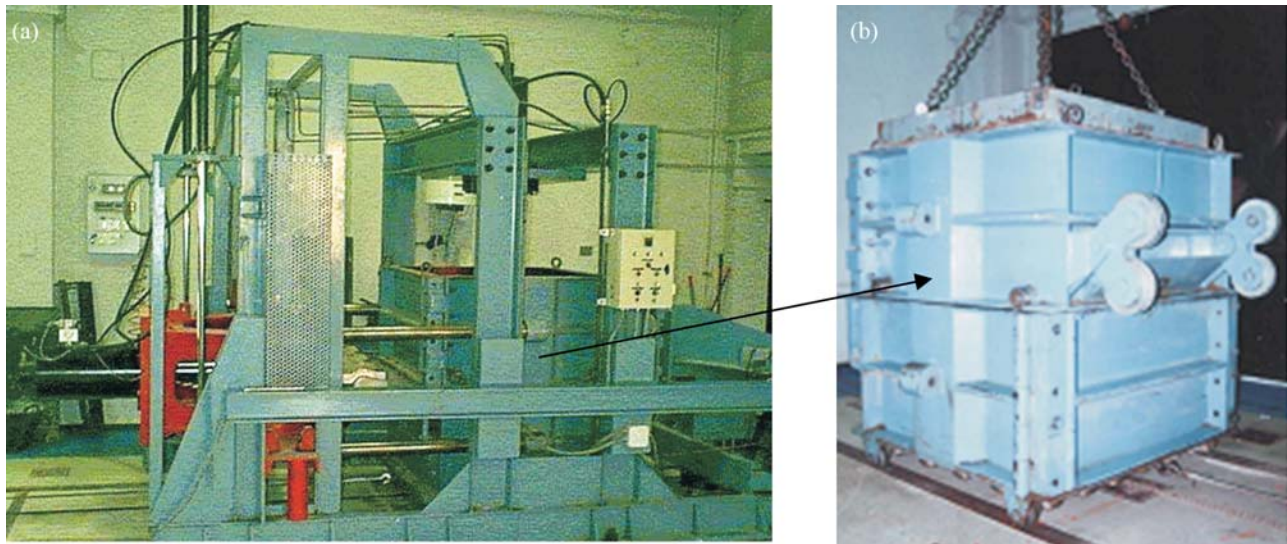


**Figure 4** - Large-scale direct shear test equipment. (a) lateral view; (b) detail of shear box.

horizontal hydraulic jack. More details about this equipment are given in Sieira & Sayão (2006).

Direct shear tests with inclined reinforcement were carried out with a dense silty sand ( $D_r = 80\%$ ), compacted in four successive layers. To achieve the prescribed relative density, the quantity of soil needed to fill a layer was statically compacted using the vertical jack until the required height was reached.

In direct shear with inclined reinforcement, the tests box was first totally filled with soil, and then the specimen was cut at the desired inclination and the soil removed was carefully kept separated. The geogrid was subsequently placed in position (Fig. 5) and the sand was placed for back filling the rest of the test box at the desired density.

After the specimen preparation, the top cap was put in position and the box placed inside the equipment. The hydraulic jacks were adjusted and the direct shear test was then started. Vertical confining stresses of 50, 100 and 200 kPa were applied during the direct shear tests, including the overload imposed by the cap weight.

### 3.4. Measurement of the internal displacement of the geogrid

The inner displacements and distortions of the geogrid in the shear box were evaluated at the end of the tests. Figure 6 schematically shows the geogrid configuration before and after a test with vertical reinforcement. Points A, B and C represent the positions of the vertical geogrid at the beginning of the shear test, while points A', B' and C' represent the deformed configuration of the geogrid upon completion.

This deformed configuration was obtained after careful dismantling of the soil specimen. The final positioning of different points of the geogrid was recorded in the test box. This final configuration of the distorted geogrid allows

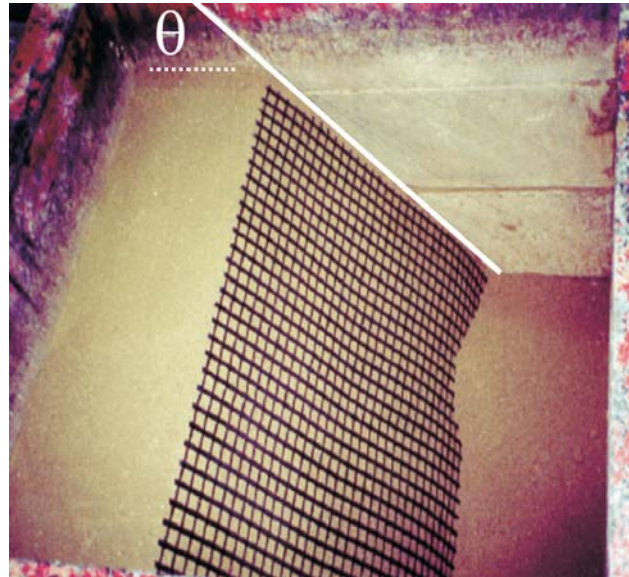


**Figure 5** - Upper view of the geogrid after positioning at  $\theta = 60^\circ$  in the shear box.

identification of three regions within the direct shear specimen: the central zone, where the shearing occurs, and the upper and lower external zones, where the soil is subject to a simple translation with no distortion.

## 4. Numerical Simulation of Tests with Inclined Reinforcement

The objective of the numerical simulations consisted in the visualization of mobilized stresses and strains in the geogrid at the end of the direct shear tests.

The first direct shear test simulation was done with non-reinforced sand. After the stress-strain parameters of

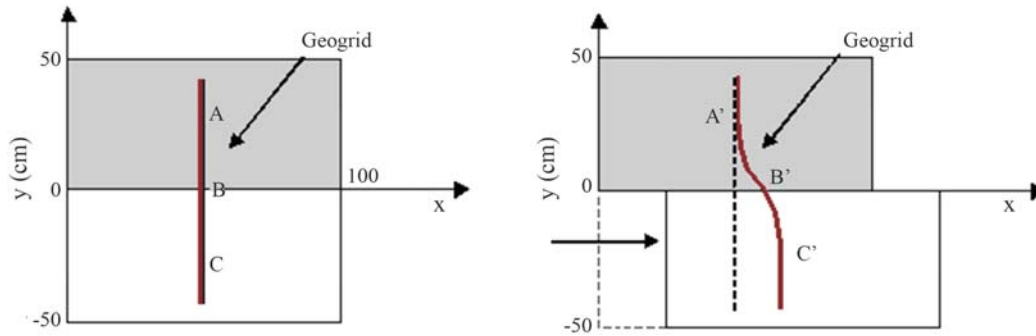


**Figure 6** - Configuration of the geogrid in the test box before and after shearing. (a) initial condition; (b) end of test.

the sand were correctly defined, the geogrid was introduced with the proper inclination in relation to the failure plane.

#### 4.1. Computer program

All simulations made use of the Plaxis computer program (Brinkgreve & Vermeer, 1998). The soil mass is divided in finite elements obeying pre-defined stress-strain relations and the reinforcement element requires only the axial stiffness as input parameter.

The use of a bi-dimensional program to represent the tri-dimensional geogrid may impose a restriction, as the mobilized passive resistance at transversal strips cannot be taken into account. However, in direct shear tests with inclined reinforcement, geogrids are basically subjected to tensile loading and the simulations with a 2D program are acceptable.

The direct shear tests were simulated by a finite element mesh with proper boundary conditions. Vertical confinement was simulated through a uniform load on the top horizontal boundary, which was free to move vertically. The shearing phase was then imposed by increasing the horizontal load on the vertical wall of the lower box, which was free to move horizontally. During this phase, all elements in the upper box could only move vertically.

#### 4.2. Stress-strain model

To represent the stress-strain behavior of the sand, a perfectly plastic model was adopted, using the Mohr-Coulomb failure criteria. This model requires the definition of five simple soil parameters: Young's modulus ( $E$ ), Poisson's ratio ( $\nu$ ), specific weight ( $\gamma$ ), effective cohesion ( $c'$ ) and effective friction angle ( $\phi'$ ).

Table 3 shows the parameters obtained for non-reinforced sand, as a function of the vertical stress, from large

**Table 3** - Geotechnical parameters of the sand.

$\sigma'_v$ (kPa)	$c'$ (kPa)	$\phi'$ (°)	$E$ (MPa)	$\nu$
50	16	33	3.5	0.3
100	16	33	8.0	0.3
200	16	33	17.0	0.3

size direct shear tests. Deformability parameters were determined numerically after adequately reproducing the shear test results, as indicated in Fig. 7.

For the analyses of tests with inclined reinforcement, the geogrid stiffness (750 kN/m) was determined from the unconfined tensile test results provided by the manufacturer.

The geogrid was introduced into the numerical analyses with different inclinations ( $0^\circ$ ,  $30^\circ$ ,  $60^\circ$  and  $90^\circ$ ) in relation to the failure plane. Irrespective of the inclination, boundary effects were avoided by positioning the geogrids 50 mm distant from the upper and lower borders.

Soil-geogrid interaction is modeled by interface elements. The type and magnitude of interaction are defined by an adequate value for the interface strength reduction factor ( $R_{inter}$ ). This factor may be defined as the ratio between the interface strength and the soil strength, as given by the equation:

$$R_{inter} = \frac{\tan \phi_{s/GGR}}{\tan \phi'} \quad (1)$$

where  $\phi_{s/GGR}$  = interface friction angle;  $\phi'$  = soil's friction angle.

In this investigation, a value of  $R_{inter} = 0.92$  was adopted based on results of direct shear tests with horizon-

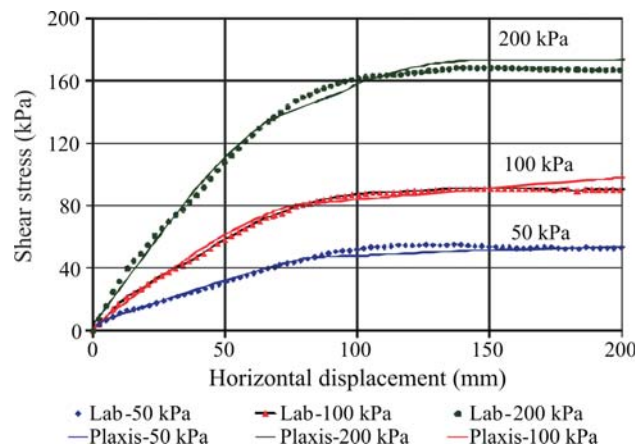


**Figure 7** - Numerical reproduction of direct shear tests in sand specimens.

tal reinforcement. These tests designate the shear strength at the soil-geogrid interface, as presented in the next section.

### 5. Experimental Results

#### 5.1. Shear strength

Results from direct shear tests are shown in Fig. 8 and corresponding strength parameters are presented in Table 4. In tests with inclined reinforcement ( $\theta > 0$ ), shearing does not occur on the soil-geogrid interface. Accordingly, the parameters  $c_{s/GGR}$  and  $\phi_{s/GGR}$  listed in Table 4 do not represent soil-geogrid interface adhesion and friction. They express the strength of the reinforced soil mass arising from the mobilization of tensile stresses in the geogrid.

Specimens with horizontal reinforcement ( $\theta = 0^\circ$ ) resulted in soil-geogrid parameters of  $c_{s/GGR} = 15.7$  kPa (adhesion) and  $\phi_{s/GGR} = 34.6^\circ$  (friction angle). These interface values were slightly lower than the strength parameters ( $c'$  and  $\phi'$ ) for the sandy soil, providing the following interaction coefficients:

$$\lambda_{s/GGR} = \frac{c_{s/GGR}}{c'} \tag{2}$$

$$f_{s/GGR} = \frac{\tan \phi_{s/GGR}}{\tan \phi'} \tag{3}$$

Figure 9 shows the variation in shear resistance due to the reinforcement inclination for three levels of vertical

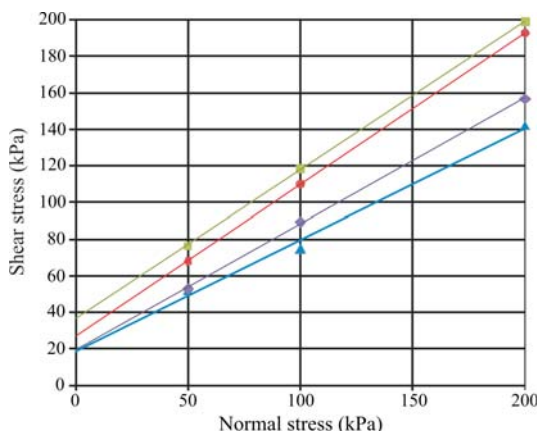


**Figure 8** - Direct shear test results in reinforced sand specimens with inclined geogrid.

**Table 4** - Strength parameters from direct shear tests.

$\theta$ ( $^\circ$ )	$c_{s/GGR}$ (kPa)	$\phi_{s/GGR}$ ( $^\circ$ )
0	15.7	34.6
30	26.8	36.0
60	36.2	39.1
90	19.2	35.0

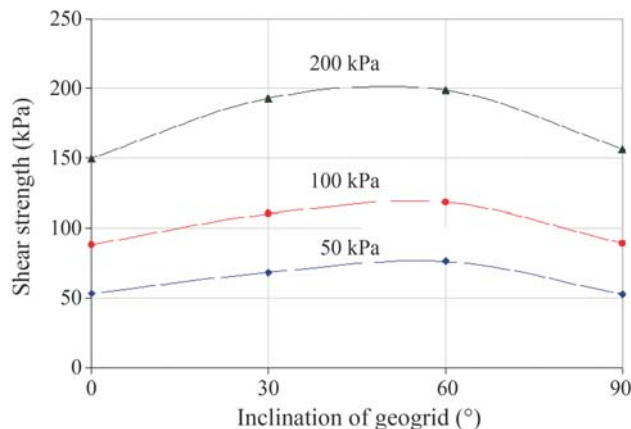


**Figure 9** - Variation of shear strength as a function of geogrid inclination.

confining stress (50, 100 and 200 kPa). The maximum variation corresponds to the optimal inclination of the geogrid (about  $55^\circ$  to  $60^\circ$  in Fig. 9). This conclusion may be in accordance with the classical Rankine’s theory, which predicts for vertical slopes a potential failure surface inclined by  $45^\circ + \phi'/2$  with the horizontal. For the sandy soil considered herein ( $\phi' = 37^\circ$ ), the theoretical optimum inclination of the reinforcement layer will then be  $\theta = 63^\circ$ . This is not far from the range of optimum geogrid inclinations (about  $55$  to  $60^\circ$ ) indicated in Fig. 9.

These results therefore suggest that, in reinforced soil, geogrid layers shall be placed at the horizontal direction. This will impose an angle of approximately  $60^\circ$  between the geogrid and the potential failure surface, resulting in maximum shear resistance mobilization.

Conclusions supporting that  $\theta = 60^\circ$  is the most favorable geogrid inclination relative to the shear surface were also reported by Jewell & Wroth (1987) and Palmeira (1999).

#### 5.2. Distortion of geogrid during shearing

Figure 10 illustrates the initial and final positions of the geogrid for tests with different levels of vertical stress ( $\sigma_v$ ) and different inclinations ( $\theta$ ) of reinforcement in relation to the failure surface. This figure illustrates only the upper half of the test box (the shaded half in Fig. 5). The displacements in the lower half of the shear box may be considered to be anti-symmetrical in relation to the upper box. It should be emphasized that the magnitudes of the horizontal displacement ( $dh$ ) indicated in Fig. 10 corresponds to the total displacement between the two halves at the end of shearing.

It can be noted that the shearing is concentrated in the central region, corresponding to approximately 35% of the box height. Outside this (*i.e.*, in the top and bottom regions, corresponding to the remaining 65% of the specimen), there is practically no distortion taking place in the soil or in the geogrid. In these external regions, dislocation of the

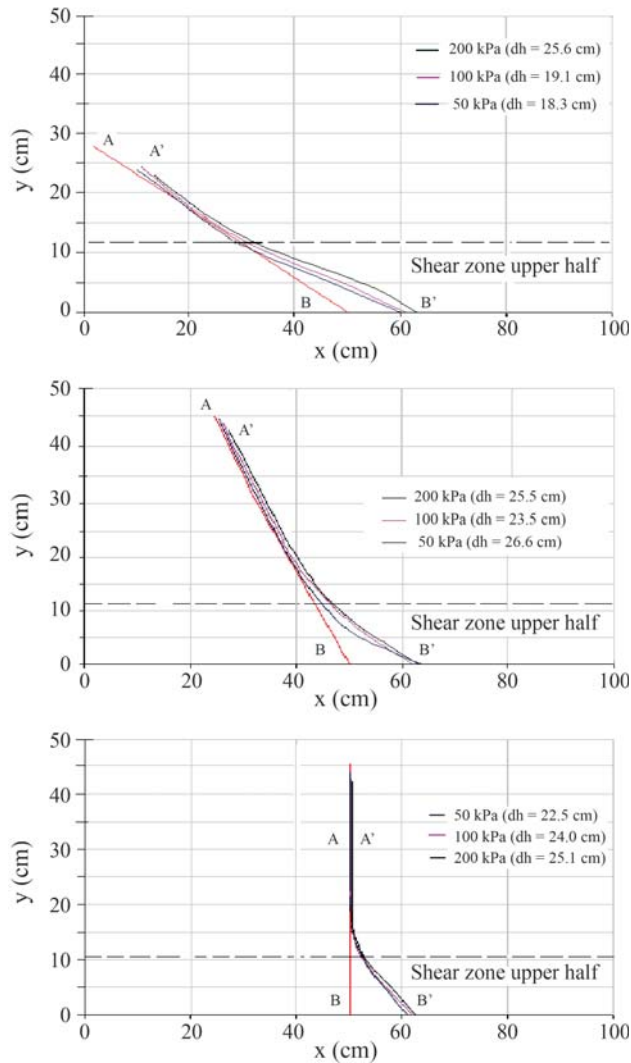


**Figure 10** - Final positions of geogrids in the upper half of direct shear box. (a) Geogrid at  $\theta = 30^\circ$ ; (b) Geogrid at  $\theta = 60^\circ$ ; (c) Geogrid at  $\theta = 90^\circ$ .

rigid box induces a simple translation of the geogrid mesh. This conclusion indicates that a small variation in the height of the box would not interfere with the results, since the volume subject to shearing is restricted to the internal part of the specimen.

It can also be noted that the geogrid's final displacements in the shearing zone increase slightly with the vertical confining stress. This may be clearly noted in Fig. 11. In fact, an increase in  $\sigma_v$  corresponds to an increase in shear stress and therefore to greater geogrid distortions at the end of the test. Consequently, greater tensile stresses in the geogrid are expected for higher levels of normal stress  $\sigma_v$ .

### 6. Numerical Analysis

Figure 12 shows the numerical predictions of the shear test results with the geogrid installed vertically in the soil specimen. The predicted curves do not exhibit a peak or

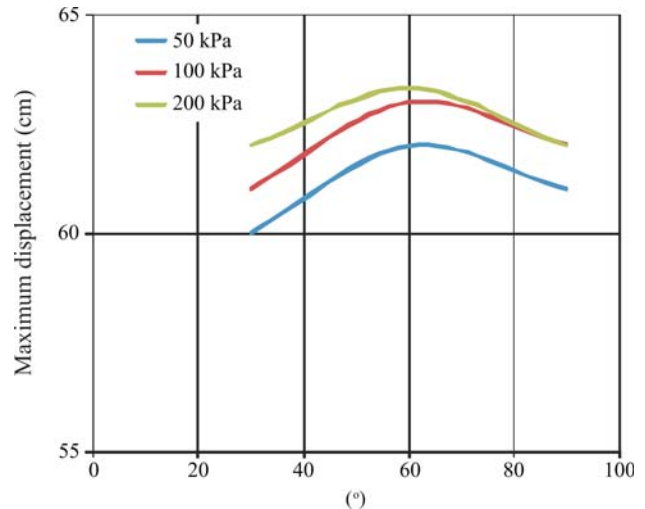


**Figure 11** - Final displacement of geogrid in the shearing surface as a function of inclination angle and confining stress.

a stabilization strength level. This behavior was observed in all simulations of the direct shear tests and is strictly related to the loading mechanism. After large displacements, the lower box tends to make contact with the upper box, imposing an additional constraint to the relative movement between the two boxes. For displacements smaller than 100, however, this restriction is negligible.

Figure 13 shows the deformed geogrid configuration, as predicted by the numerical analysis at the end of the  $\theta = 90^\circ$  tests with a confinement level of 200 kPa. It can be seen that the displacements are anti-symmetrical in relation to the failure plane. The predicted distortions of the geogrid are similar to what was observed in the laboratory. The shear zone, which may be defined as the region where the

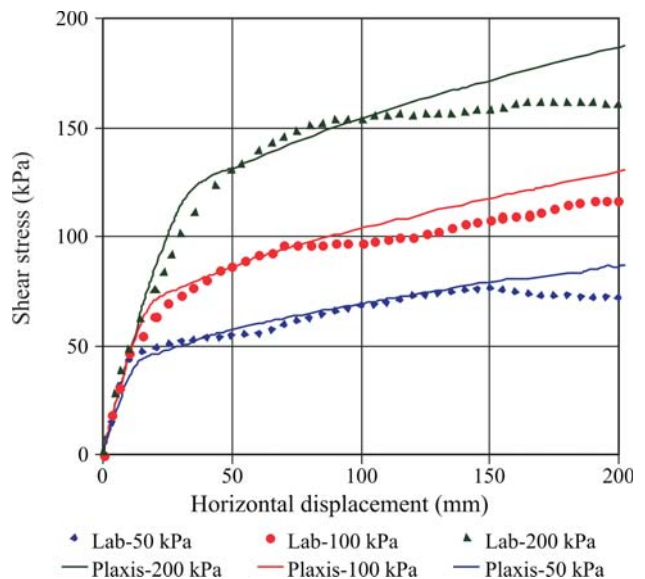


**Figure 12** - Reproduction of the direct shear tests with geogrid at  $\theta = 90^\circ$ .

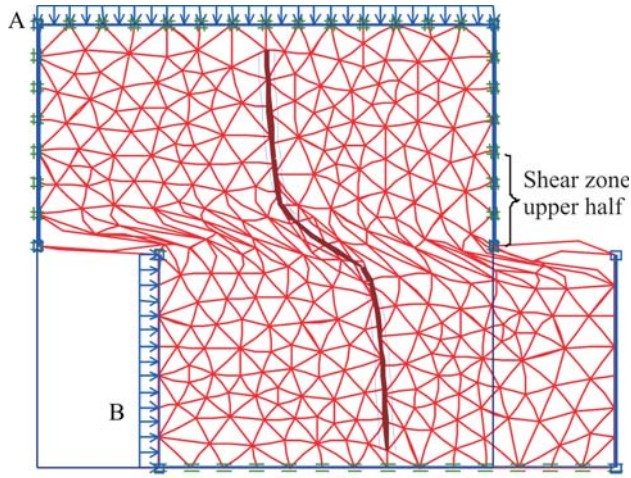


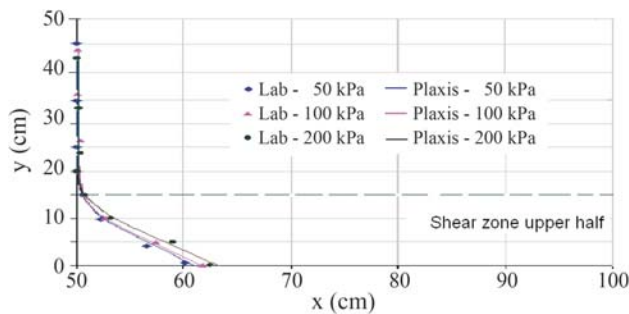
**Figure 13** - Deformed configuration of geogrid at inclination  $\theta = 90^\circ$ .

geogrid distortion occurs, corresponds to no more than 33% of the shear box height, as shown in the analysis of the experimental results.

The measured horizontal displacements were compared with those estimated through the numerical simulation. Figure 14 shows the upper right quadrant of the shear box with the final positions of the geogrid. Adequate agreement of the results can be observed, suggesting that the numerical analysis is capable of satisfactorily reproducing the laboratory tests.

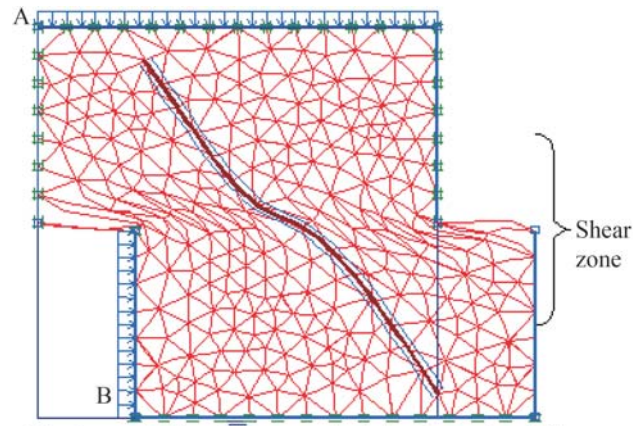
Figure 15 shows the deformed configuration of the geogrid, predicted at the end of the tests with  $\theta = 60^\circ$  and  $\sigma'_v = 100 \text{ kPa}$ . The relative displacement between the upper and the lower boxes was 243 mm. An anti-symmetric shape in relation to the failure plane is to be noted at the distorted geogrid. At the geogrid's extremities there was no distortion in the finite element mesh, indicating that these regions were not affected by shearing. Once again the shear zone corresponds to the central third of the total box height.

Figure 16 shows the points of the soil mass that reached the yield or failure condition in direct shear test simulations with the geogrid inclined at  $\theta = 30$  and  $60^\circ$ .



**Figure 14** - Predicted and measured displaced positions of geogrid at inclination  $\theta = 90^\circ$ .

These yielded points are observed to be confined to the specimen's central zone, which is away from the upper and lower undistorted regions of the soil within the shear box.



Maximum relative displacement of shear box:  $dh = 243 \text{ mm}$

**Figure 15** - Deformed configuration of the geogrid at inclination  $\theta = 60^\circ$ .

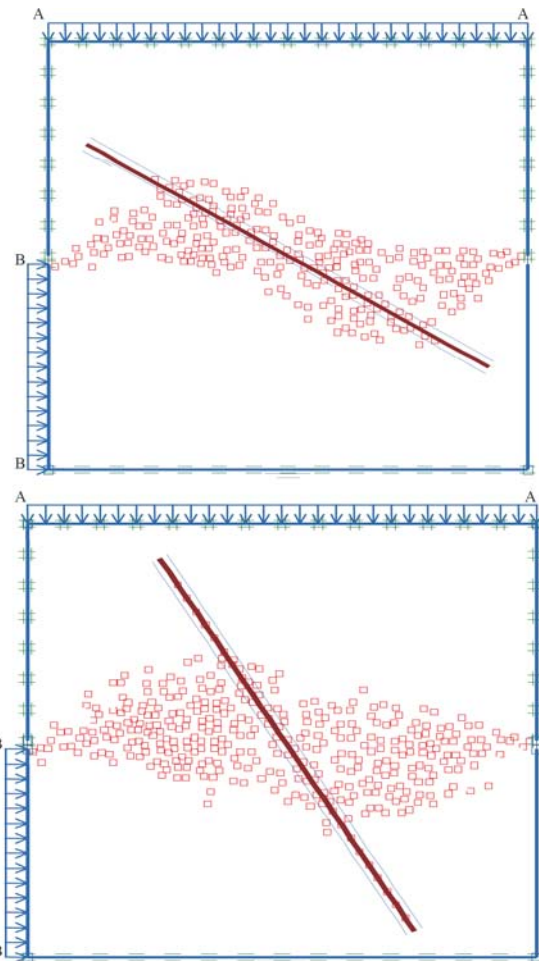


**Figure 16** - Soil elements that reached a yielding state in shear tests with inclined geogrid. (a) Geogrid at inclination  $\theta = 30^\circ$ ; (b) Geogrid at inclination  $\theta = 60^\circ$ .

Similar results were obtained from simulations with geogrid at other inclinations.

The numerical strain analysis, as well as the measurements of the geogrid displacements, indicates that the height of the direct shear box may be reduced without affecting the test results. The identification of the distorted region is particularly relevant in large scale tests, as it can allow a substantial reduction of the specimen volume to be used. In the case of the tests reported herein, this reduction can larger than 0.5 m<sup>3</sup>, which would be equivalent to at least 800 kg of compacted soil, with a relevant saving in time preparation of the soil specimen.

The tensile stresses in the geogrid at the end of the direct shear tests are shown in Fig. 17, for the three levels of vertical confining stress. The maximum tension value ( $T_{max}$ ) occurs in the central region of the geogrid, which is the region most demanded during shearing. Furthermore, the tensile stress tends to be annulled at the geogrid's extremities.

Higher levels of normal stress indicate higher tensile stress in the geogrid, as shown in Fig. 18. As the highest tensile stress was estimated to be 48 kN/m, in the test with the geogrid inclined at  $\theta = 60^\circ$ , maximum mobilization of the geogrid corresponded to about 50% of the maximum tensile strength of 97 kN/m.

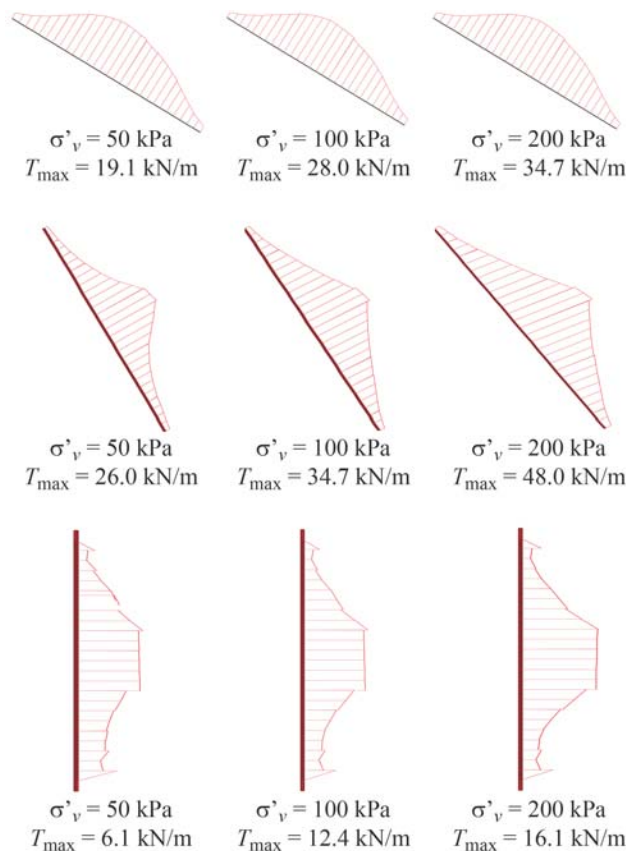


**Figure 17** - Tensile stresses along the geogrid at different inclinations to the failure plane. (a)  $\theta = 30^\circ$ ; (b)  $\theta = 60^\circ$ ; (c)  $\theta = 90^\circ$ .

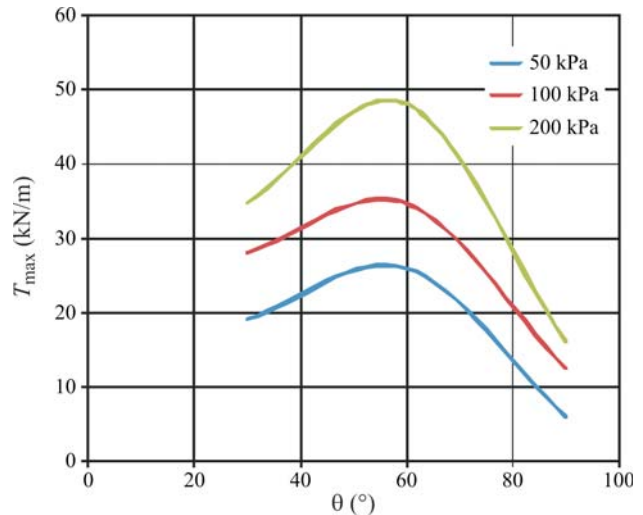


**Figure 18** - Variation of maximum tensile stress as a function of geogrid inclination and confinement.

## 7. Conclusions

This paper presents the results of a direct shear test program with inclined geogrids reinforcing the soil specimens. The tests were carried out using a large-scale device and the reinforcement was positioned with different inclinations within the shear box.

Numerical simulations using a finite element program were carried out with the aim of determining the deformed geogrid configuration and the tensile stresses in the geogrid.

The numerical and experimental results indicated that the geogrid's displacements were anti-symmetrical in relation to the failure plane. For the 1 m high soil specimen, shearing was concentrated approximately at the central one third of the specimen's height. The upper and lower regions of the specimen were simply subjected to translation, with no distortion taking place due to displacement of the shear box. This verification suggests that the large-scale direct shear tests may be carried out in equipment with a lower height, with a considerable reduction of the soil volume to be used in preparing the test specimens.

The analysis of stresses in the geogrid at the end of the tests indicated that the maximum tension value ( $T_{max}$ ) occurs in the central region of the geogrid, which is the region most demanded during shearing. A similar behavior for the three inclinations of geogrid in the box test was observed. The increase in confining stress test induces higher tensile stresses in the geogrid. The maximum tensile stress was predicted to be 48 kN/m, in the test with the geogrid inclined at  $\theta = 60^\circ$ . This value corresponds to around 50% of the reinforcement's peak strength.

The geogrid inclination in relation to the failure plane has a significant influence on the soil-geogrid resistance. The maximum increase in strength occurred when the geo-

grid was positioned at an angle of  $\theta = 60^\circ$  in relation to the failure plane. This is the most favorable geogrid inclination relative to the potential shear surface in reinforced soil projects.

### Acknowledgments

The research described herein was funded by the National Research Council of Brazil (CNPq). The authors are indebted to Maccaferri Brazil for supporting the research on geogrids, and to the Geotechnical Laboratory at Cedex (Spain) for the availability of experimental facilities.

### References

- Bakeer, R.M.; Sayed, S.M.; Cates, P. & Subramanian, R. (1998) Pullout and shear tests on geogrid reinforced lightweight aggregate. *Geotextiles and Geomembranes*, v. 16:2, p. 119-133.
- Bauer, G.E. & Zhao, Y. (1994) A realistic stress transfer model for geogrids in pullout. *Proc. 5<sup>th</sup> International Conference on Geotextiles, Geomembranes and Related Products*, Singapore, pp. 457-460.
- Brinkgreve, R.B.J. & Vermeer, P.A. (1998) *Plaxis, Finite Element Code for Soil and Rock Analyses*. Balkema, Rotterdam, Netherlands, 614 pp.
- Jewell, R.A., Wroth, C.P. (1987) Direct shear test on reinforced sand. *Geotechnique*, v. 37:1, p. 53-68.
- Lui, C.N.; Ho, Y.H. & Huang, J.W. (2009) Large scale direct shear tests of soil / PET-yarn geogrid interfaces. *Geotextiles and Geomembranes*, v. 27:1, p. 19-30.
- Palmeira, E.M. (1999) Execution and interpretation of laboratory tests on geosynthetic material (in Portuguese). *Proc. 1<sup>st</sup> South-American Symposium on Geosynthetics, ABMS-ISSMGE*, Rio de Janeiro, Brazil, v. 1, pp. 87-108.
- Palmeira, E.M. (2009) Soil-geosynthetic interaction: Modelling and analysis. *Geotextiles and Geomembranes*, v. 27:5, p. 368-390.
- Palmeira, E.M. & Milligan, G.W.E. (1989) Large scale direct shear tests on reinforced sand. *Journal Soils and Foundations (Japan)*, v. 29:1, p. 18-30.
- Pitanga, H.N.; Gourc, J.P. & Vilar, O.M. (2009) Interface shear strength of geosynthetics: evaluation and analysis of inclined plane tests. *Geotextiles and Geomembranes*, v. 27:6, p. 435-446.
- Sayão, A.S.F.J. & Teixeira, M.L. (1995) Use of geosynthetics for reinforcement of earthfills over soft soils (in Portuguese). *Proc. 2<sup>nd</sup> Brazilian Symposium on Applications of Geosynthetics, ABMS*, São Paulo, Brazil, pp. 169-180.
- Sayão, A.S.F.J.; Maia, P.C.A. & Nunes, A.L.L.S. (2005) Considerations on the shear strength behavior of weathered rockfill. *Proc. 16<sup>th</sup> International Conference on Soil Mechanics and Geotechnical Engineering, ISSMGE*, Osaka, Japan, v. 3, Section 2f, pp. 1917-1920.
- Seira, A.C.C.F. & Sayão, A.S.F.J. (2006) Pullout tests on mechanically damaged geogrids (in Spanish). *Revista Ingeniería Civil*, n. 141, pp. 63-72.
- Seira, A.C.C.F.; Gerscovich, D.M.S. & Sayão, A.S.F.J. (2009) Displacement and load transfer mechanisms of geogrids under pullout conditions. *Geotextiles and Geomembranes*, v. 27, n. 4, p. 241-253.
- Wasti, Y. & Ozduzgun, Z.B. (2001) Geomembrane-geotextile interface shear properties as determined by inclined board and direct shear box tests. *Geotextiles and Geomembranes*, v. 19:1, p. 45-57.

### List of Symbols

- $c'$  = effective cohesion of soil  
 $c_{s/GGR}$  = soil-geogrid adhesion parameter  
 $c_{s/GSY}$  = soil-geosynthetic adhesion parameter  
 $D_{50}$  = average diameter of soil particles  
 $D_r$  = relative density of soil  
 $E$  = Young's modulus  
 $f_{s/GGR}$  = soil-geogrid interaction coefficient  
 $G_s$  = specific gravity of soil particles  
 $R_{inter}$  = interface strength reduction factor  
 $S$  = saturation degree of soil  
 $T_{max}$  = maximum tensile load  
 $w$  = water content of soil  
 $\phi'$  = effective friction angle of soil  
 $\phi'_{s/GGR}$  = effective soil-geogrid interface friction angle  
 $\phi'_{s/GSY}$  = effective soil-geosynthetic interface friction angle  
 $\gamma$  = specific weight of soil  
 $\nu$  = Poisson's ratio  
 $\theta$  = inclination of geogrid in relation to failure surface  
 $\sigma_v$  = vertical confining stress  
 $\tau$  = shear stress

# Developing a System for Down-Hole Seismic Testing Together with the CPTU

O.P.M. Vitali, R.A.A. Pedrini, L.P.R. Oliveira, H.L. Giacheti

**Abstract.** This paper presents a system for performing down-hole seismic test together with the piezocone test in order to determine the shear wave velocity ( $V_s$ ) and for calculating the maximum shear modulus ( $G_0$ ); a basic parameter for analyzing the dynamic soil behavior and a reference value of the soil stiffness. The system components are described and tests results for checking the geophone response are also presented, both before and after installation into the probe. The system was used in down-hole tests carried out at three experimental research sites located in the interior of Sao Paulo State, Brazil, where in situ seismic test results are available. The  $V_s$  values measured in down-hole tests carried out with this system were consistent with those determined in cross-hole tests and with a commercial seismic piezocone, which enabled to validate the developed system.

**Keywords:** site investigation, maximum shear modulus, down-hole, CPTU.

## 1. Introduction

The down-hole seismic test is considered as an alternative to the cross-hole technique; a much more expensive and time consuming test procedure. According to Robertson *et al.* (1986), down-hole and cross-hole testing provide equivalent results.

The Seismic Cone test was developed in the early 1980's and was first tried by a seismologist at the Long Beach office of then ERTEC (Campanella & Howie, 2005). After that, the results of an initiative by Fugro Inc. with the University of British Columbia, where seismic transducers were added to the piezocone, enabling simultaneous performance of the seismic down-hole test along with the traditional CPTU test (Robertson *et al.*, 1986). This new test, called the seismic piezocone penetration test (SCPTU) was a success, because seismic and CPTU test data are complementary. In a seismic test the soil stiffness is determined, not estimated by correlations, complementing the piezocone test results. Both tests results can be used to delineate the nonlinear stress – strain relationship of the soil through a modified hyperbola (Mayne & Schneider, 2000). Giacheti (2001) highlights the potential that the ratio  $G_0/q_c$  has for the characterization of tropical soils. This ratio relates to the behavior of soil under small strains with its behavior under large deformations.

Despite the potential for interpretations from both down-hole and CPTU test results, in Brazil, there is not much test data on tropical soils, since the equipment available for performing seismic piezocone tests are mostly im-

ported. This has caused difficulties for performing SCPTU tests due to the high cost, plus the delay for maintenance, repairing and calibrations, since these all depend on imported parts and services.

## 2. The System for Down-Hole Seismic Testing

The developed system has five components described as follows:

- a) Machined steel probe which has three geophone compartments (0.5 m apart each);
- b) Data acquisition system;
- c) Software for data acquisition and interpretation;
- d) Electrical trigger; and
- e) Source for generating seismic waves.

The idea is to perform the CPTU test using a standard equipment and after that the down-hole seismic test is carried out driving a probe into the same borehole using our developed system. For this reason the diameter of the probe is greater than the standard cone. A description of each system along with their respective components and their tests and the test performance and data interpretations will be presented and discussed in this paper.

### 2.1. Test procedure

The test consists of pushing the probe continuously into the ground, the same way as it is done in a conventional piezocone test. At every 1 m a halt is made and the seismic testing is carried out. Shear waves are generated at the ground surface striking the source, which are captured by

O.P.M. Vitali, MSc, Departamento de Geotecnia, Escola de Engenharia de São Carlos, Universidade de São Paulo, Av. Trabalhador São Carlense 400, 13566-590 São Carlos, SP, Brazil. e-mail: opmvitali@gmail.com.

R.A.A. Pedrini, Engenheiro Civil, Departamento de Engenharia Civil, Faculdade de Engenharia de Bauru, Universidade Estadual Paulista "Júlio de Mesquita Filho", Av. Eng. L.E.C. Coube 14-01, 17033-360 Bauru, SP, Brazil. e-mail: rubenspedrini@gmail.com.

L.P.R. Oliveira, PhD, Professor, Departamento de Engenharia Mecânica, Escola de Engenharia de São Carlos, Universidade de São Paulo, Av. Trabalhador São Carlense 400, 13566-590 São Carlos, SP, Brazil. e-mail: leopro@sc.usp.br.

H.L. Giacheti, DSc, Professor, Departamento de Engenharia Civil, Faculdade de Engenharia de Bauru, Universidade Estadual Paulista "Júlio de Mesquita Filho", Av. Eng. L.E.C. Coube 14-01, 17033-360 Bauru, SP, Brazil. e-mail: giacheti@feb.unesp.br.

Submitted on March 12, 2011; Final Acceptance on April 3, 2012; Discussion open until September 30, 2012.

the geophones installed in the probe and the seismic data are recorded in a data acquisition system. The recommendations by Butcher *et al.* (2005) for performing these tests were followed.

During the preliminary tests of the system, the seismic probe spun with the addition of the rods. This rotation changed the axis of vibration of geophones affecting the quality of the recorded waves. This factor was considered to be the main cause for influencing the quality of the signals (Vitali *et al.*, 2010 and Vitali, 2011). This problem was solved by heavily holding the rods with a pipe wrench, preventing them from spinning during the operation of adding rods for pushing.

It was observed that those blows applied with great intensity generated waves of a higher amplitude and a lower quality than those generated from blows of a lower intensity (Vitali *et al.*, 2011). It is recommended to strike the source with less intensity, since it records waves with the main pulse of S waves free of distortions, which are easier to interpret.

## 2.2. Geophones

The three geophones are manufactured by Geospace Model GS-20DH OMNI. The main characteristics of these sensors include: natural frequency of 28 Hz, sensitivity of 35.4 V/(m/s) and spurious frequency of 400 Hz. It maintains the factory specifications for angles below 15 degrees to the axis of vibration, emphasising the importance of correct positioning of the geophones and keeping it so during the entire test.

Tests and calibrations were carried out in the laboratory to check if all three geophones matched the factory specifications, as well as seeing if they had the same response after installing them into the probe. This is fundamental for the interpretation by the true interval method (Butcher *et al.*, 2005). The test consisted of measuring the random vibrations produced by an electrodynamic vibrator with a geophone, an accelerometer and a laser dopler vibrometer (LDV), the measurements of which served as a reference for both sensors (accelerometer and geophone). The test results are shown in Fig. 1, where the transmissibility function, *i.e.*, the ratio between the geophone and accelerometer signals with respect to the LDV in the frequency domain, is used in order to verify the calibration factor of those sensors using a broad frequency band. As it can be seen the geophones presented an identical response consistent with the calibration curve supplied by the manufacturer.

As mentioned before, the response of the geophone and accelerometer were divided by the LDV signal, which is much more accurate and reliable, therefore the dimensionless value was obtained, which is known as transmissibility. It is important to mention that the accelerometer signal had to be integrated in order to obtain the same curve, which was done in the frequency domain. As a result

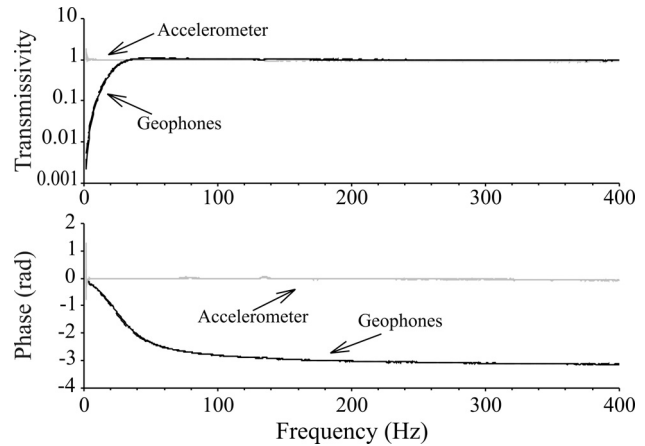


**Figure 1** - Test results of the geophone calibration.

of the direct ratio of those two signals, the transmissibility (as any other transfer function or frequency response function) is a complex number, presenting amplitude and phase information. It was observed that for frequencies above 28 Hz, which is the natural frequency of the geophones, that the amplitude response for the three geophones is constant and identical to the response of the laser, hence transmissibility equals one. According to Campanella & Stewart (1992), shear wave frequencies are between 40 Hz and 120 Hz, so these sensors are appropriate for their registration.

It is also important to notice that the transmissibility analysis allows one to observe not only the amplitude but also the phase behaviour between the two signals. In this study, there was no difference between the phases of the three geophones used. Differences between the phases would indicate *delays* in the time domain, which compromises the use of the true interval method, described in item 2.9.

## 2.3. Seismic probe

A machined steel seismic probe was built with three compartments (0.5 m apart each) welded to two rods, for installation of the geophones in an uniaxial configuration (Fig. 2). In this manner, three recordings are registered at different depths for the same stroke, increasing the possibilities of testing interpretation and getting a more detailed  $V_s$  profile (at every 0.5 m interval). In a uniaxial configuration, it is essential to maintain the axis of vibration of the geophones parallel to the direction of the strike and maintain this position during the entire test; this factor is considered as the most important factor for the success of the test (Vitali *et al.*, 2010).

Tests were conducted in the laboratory to assess whether the installation of the geophones into the probe interferes with the quality of the recorded data. The probe was suspended with an elastic rope, simulating a free-free boundary condition, and accelerometers were installed under the geophone compartments, aligned with the geophones axis.



**Figure 2** - Photo of the seismic probe.

The test was carried out by hitting each geophone's compartment with a small hammer instrumented with a load cell. Frequency response functions (FRF) of acceleration over force and geophone velocity over force were calculated and used to compare the geophone's dynamic behaviour with that of the accelerometer's behaviour.

The FRF relates the impulse, measured by the instrumented hammer, with the structure vibration, measured by the geophone fixed in the probe and by the reference accelerometer, therefore, identical FRFs mean that the geophones fixed in the probe present the proper response. Again, FRFs are also complex numbers, which present amplitude and phase behaviour and, differ from the transmissibility functions – used during the calibration phase – the FRFs could also provide some valuable information on the probe dynamics, such as its free-free resonances. Figure 3 shows a photo of the accelerometer attached to the geophone's compartment and Fig. 4 shows the testing data for comparing the response of the geophone with the accelerometer.

It can be seen in Fig. 4, that for frequencies higher than 30 Hz, the response of the geophones and accelerometers is essentially identical. The difference of 180° observed in the phase is due to the positioning of the sensors to the axis of vibration. It can therefore be concluded that the geophones installed into the probe provided reliable answers. It is worth mentioning that in the case of the other two compartments, the geophones also responded identically with the accelerometers.

Rubber o-rings were installed in geophone's compartment and liquid silicone was used in the connection with the rods. The probe was immersed in a PVC pipe filled with water and submitted to 750 kPa pressure for an hour to check the probe tightness. During this time, it was observed that there was no decrease in applied pressure, indicating no leakage and guaranteeing the probe water tightness.

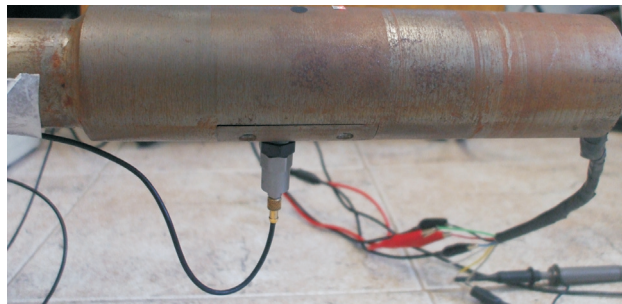


**Figure 3** - Photo of the accelerometer attached to the geophone's compartment.

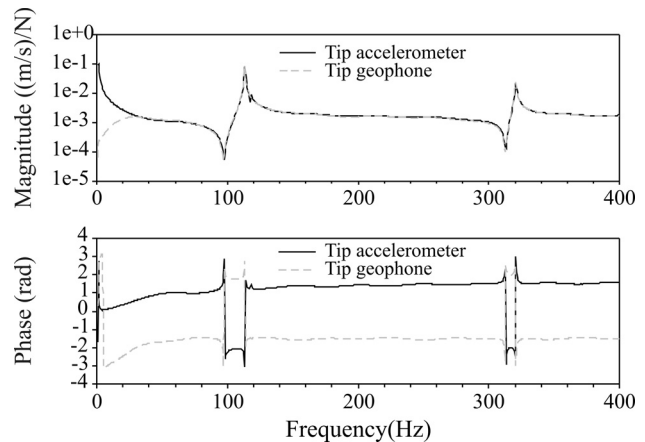


**Figure 4** - Comparison between the FRFs of the geophone and accelerometer installed at the probe tip for the blow applied at the tip.

## 2.4. Data acquisition

Initially a 12 bit resolution with 16-channel analog-digital module was used for data acquisition. This equipment is the model ADS2000, with a signal conditioner model AI-2161, manufactured by Lynx Electronic Technology. The data acquisition software in Visual Basic was developed by Pedrini *et al.* (2010).

This system permits a maximum data acquisition frequency of 15 kHz, which is lower than the minimum value recommended by Butcher *et al.* (2005), which was 20 kHz. Although this data acquisition system presented a good performance it was replaced by another system from National Instruments; NI USB-6251 model. This device also has 16 channels but with a sampling rate of 1.25 MHz per channel and with 16 bit resolution. New software was developed for data acquisition and interpretation using the Labview platform. The decision for using this new system was the high capability it had for data acquisition with a relatively low cost. Two channels were used for each geophone to allow differential reading to enhance the recorded data quality. During the event, one channel provides the sensor signal plus noise while the other provides the inverted sensor signal plus noise. So, the recorded signal is the difference of the two signals, which corresponds to the duplicate sensor signal free of the noise. This approach is desirable but is not mandatory, as the noise can be removed with digital filtering. Figure 5 compares the field noise registered with differential and conventional reading, where the lowest noise intensity is noticeable for the differential reading.

According to the Sampling Theorem of Nyquist, the minimum sampling rate that does not corrupt the signal must be, at least, double of the existing maximum frequency in the signal (aliasing phenomenon).

Some data acquisition systems have an anti-aliasing filter, which prevents the registration of frequencies above half of the maximum sampling frequency of the board. However, the data acquisition system from National Instruments does not have an anti-aliasing filter, so it is essential to use a high sampling frequency in order to adequately sample the signal.

In two tests carried out in the experimental research site from Unesp, a sampling frequency of 40 kHz was used; double the minimum sampling frequency recommended by Butcher *et al.* (2005), and the results were corrupted due to aliasing phenomenon. It happened because this site is quite close to the meteorological radar station from Unesp (IPMet), which generates signals that interfere with the seismic wave records. In another test campaign carried out at the same site, this problem was avoided by using 150 kHz sampling frequency, which ensured an appropriate signal and an excellent resolution in time domain, fundamental for the application of the cross correlation method, described in

item 2.9. Figure 6 shows a signal corrupted by the aliasing phenomenon. It is noteworthy that this phenomenon does not occur in this particular site using the data acquisition system from Lynx because it has an anti-aliasing analog filter on board.

### 2.5. Signal processing

Butcher *et al.* (2005) recommend recording the signal without any modifications. This recommendation was followed and then a digital filter (which does not cause delay on the signal) was used to remove noise.

The application of digital filter Butterworth low-pass type of third order with cutoff frequency of 400 Hz (corresponding to the spurious frequency of the geophones) completely removed the signal noise without distorting the main pulse of S waves, which occurs between the frequencies of 40 and 120 Hz (Campanella & Stewart, 1992). It provided a fairly reliable data interpretation (Fig. 7).

The software for data acquisition was prepared using the Labview platform. This software presents the original and filtered signal on the computer screen during the execution of the test, allowing visual inspection of signals before recording the data.

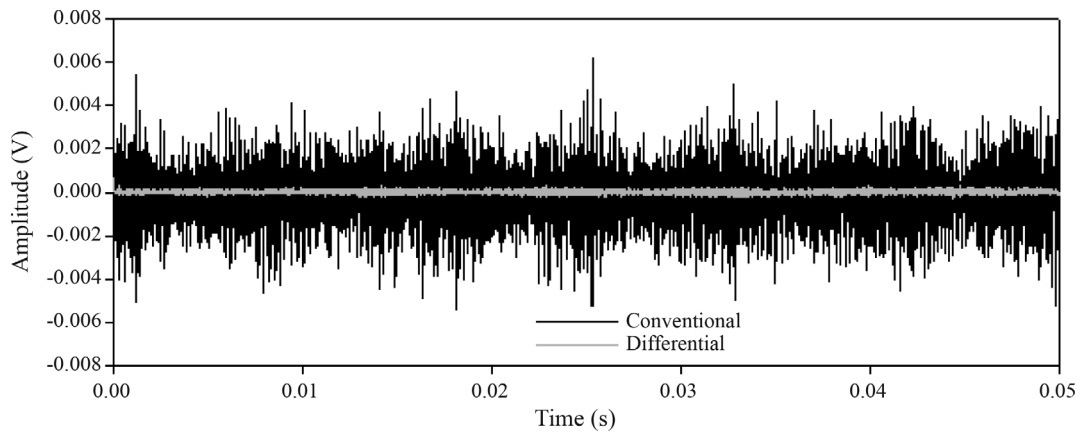


**Figure 5** - Noise registered with differential and conventional reading in Unesp experimental research site using 100 kHz data acquisition frequency.

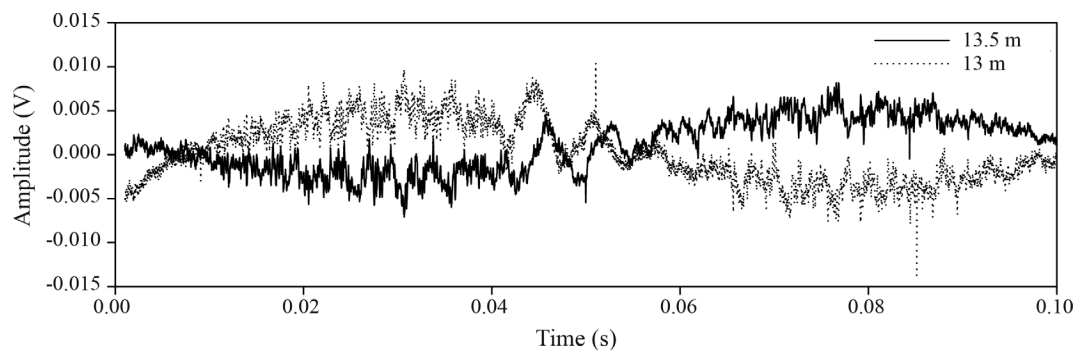


**Figure 6** - Recorded signals at the Unesp experimental research site using 40 kHz data acquisition frequency, twice the recommended minimum frequency, which were corrupted due to the aliasing phenomenon.

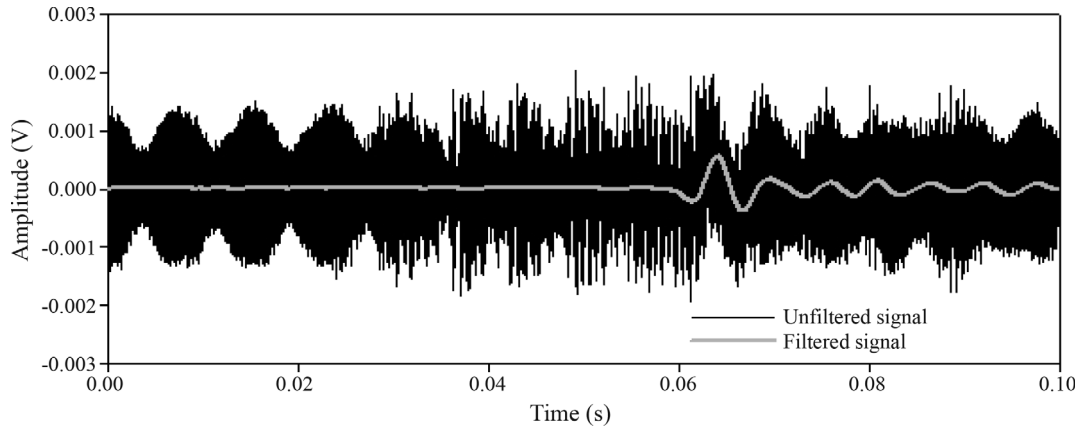


**Figure 7** - Comparing the signal with and without the Butterworth low-pass digital filter of third order with a cutoff frequency of 400 Hz. Signal recorded at 20 m depth in the Unesp experimental research site using 150 kHz sampling frequency.

## 2.6. Trigger

The trigger device has the function of triggering the data acquisition system when the seismic event is generated. At the moment the hammer hits the seismic source, the circuit is closed and an electrical signal triggers the data acquisition system. After applying the strike, the trigger automatically resets itself for a new event. Campanella & Stewart (1992) compared several trigger devices and concluded that an electrical trigger is the simplest and most reliable device to be used.

## 2.7. Equipment for piezocone tests

A multi-purpose pushing device manufactured by Paganí Geotechnical Equipment was used to perform piezocone and seismic tests. This equipment has a pushing capacity of 150 kN and it is anchored to the ground by two 4 m long anchors. It is noteworthy that pushing the seismic probe into the ground ensures a perfect contact between the sensor and the soil, which is fundamental for good quality of the recorded signals.

## 2.8. Seismic source

The seismic source consists of a steel bar placed on the ground by the pushing equipment, which is struck by a 2 kg sledgehammer. This type of source is suitable for generating predominantly S waves and allows generating reversed polarity waves striking both sides of the bar.

This source can be positioned behind or in the front of the pushing equipment. The rear leveling rod provides a higher vertical load than the front leveling rod ensuring a better contact with the ground, however, in the rear case, the source will be 1.8 m away from the hole and this horizontal distance will provide reliable  $V_s$  results only after 4 to 5 m depths are reached, as shown by Butcher & Powell (1996). These authors recommended the use of a horizontal distance less than 1 m between the seismic source and the borehole. When the source is placed in front of the pushing equipment, the horizontal distance is 0.3 m. In several tests,

two seismic sources were placed, one in front and another in the rear of the pushing equipment in order to assess the best position for this source. Figure 8 shows a picture of the seismic source positioned in the rear of the pushing equipment and Fig. 9 show two graphics to compare the results with the waves generated simultaneously with the seismic source positioned in the rear of the pushing equipment (1.8 m) and at the front (0.3 m). The analysis of these data showed that in some tests higher shear wave velocities were calculated with the source 1.80 m from the hole up to about 6 m, as described by Butcher & Powell (1996). The  $V_s$  profiles obtained with the seismic source in the front were smoother, so this position was considered more appropriate and it was recommended for routine jobs. It is noteworthy that the closer the source is, the smaller will be the difference between the paths traveled by the waves ( $L_1 - L_2$ ) (Eq. 1) of the spacing between the geophones, reducing errors associated with wave propagation in soil.



**Figure 8** - Photo of the seismic source placed in the rear of the pushing equipment.

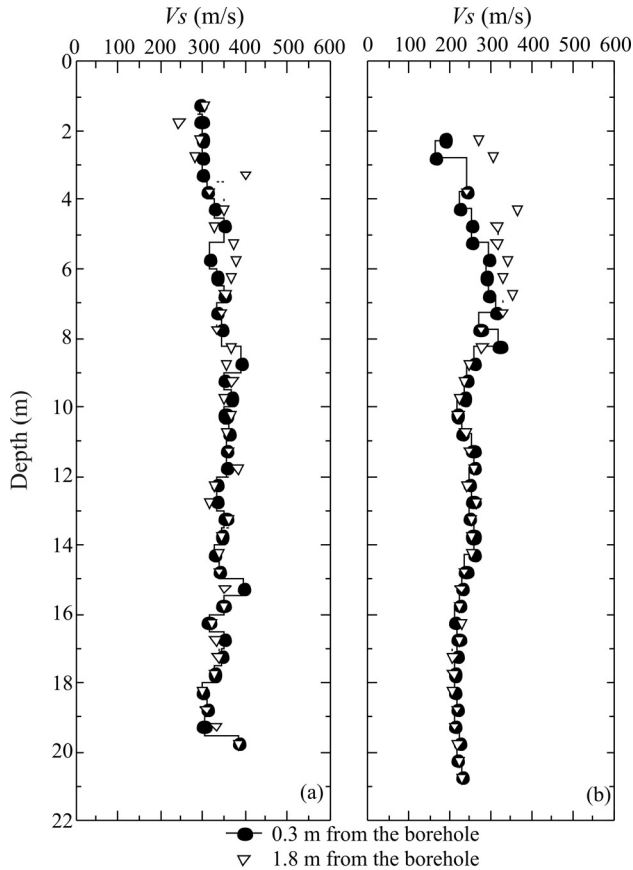


**Figure 9** -  $V_s$  values calculated with the seismic source 0.3 m and 1.8 m from the borehole in tests conducted at the (a) Unesp experimental research site and at the (b) Unicamp experimental research site.

### 2.9. Data interpretation

The shear wave velocities ( $V_s$ ) were calculated by the time interval method recommended by Butcher *et al.* (2005). The time interval ( $\Delta T = T_2 - T_1$ ) is the difference between the first arrival time of seismic waves to the transducers at two distances from the source ( $\Delta L = L_2 - L_1$ ). The difference between the distances traveled by the S waves, assuming a linear pathway, divided by the time interval provides the shear wave velocity ( $V_s$ ), given by the Eq. 1.

$$V_s = \frac{L_2 - L_1}{T_2 - T_1} \quad (1)$$

Data interpretation was made using the cross correlation method, selecting a complete revolution of the main S wave pulse as recommended by Vitali *et al.* (2010). Details on the interpretation of down-hole seismic tests are presented by these authors. According to Campanela & Stewart (1992), “the cross-correlation of signals at adjacent depths is determined by shifting the lower signal, relative to the upper signal, in steps equal to the time interval between the digitized points of the signals. At each shift, the sum of

the products of the signal amplitudes at each interval gives the cross correlation for that shift. After shifting through all of the time intervals, the cross correlation can be plotted versus the time shift, and the time shift giving the greatest sum is taken as the time shift interval used to calculate the interval velocity”. This method presents the advantage of using the entire recorded signal to calculate the time interval; however, a software is necessary for data reduction and interpretation.

The true time interval is obtained recording the responses received by two sensors placed at two different depths resulting from the same seismic event. This method eliminates errors associated with inaccuracies in the trigger device, variations in the generated waves and inaccuracies in depth measurements. This technique requires the use of seismic transducers with identical responses. Figure 10 presents a schematic illustration of the true interval method.

Shear wave velocity values were calculated using data acquisition software developed by the use of the Labview platform. This software uses the cross correlation method and filters the signals from the three geophones. The  $V_s$  values are calculated with the three possible combinations of true interval method and recorded in a text file (\*.txt) throughout the test. So, the step for the data interpretation is almost simultaneous to the test execution, giving plenty of speed and convenience for the test.

The way the seismic probe was designed and built allows obtaining two  $V_s$  values with the geophones spaced 0.5 m and one  $V_s$  value with the geophones spaced 1 m for every single seismic event. Making the comparison of the results obtained using different geophone spacing was not found in any of the relevant literature on this subject. It was assumed that the results are similar and the use of smaller geophone spacing would be more appropriate because the waves would be more similar, facilitating the application of

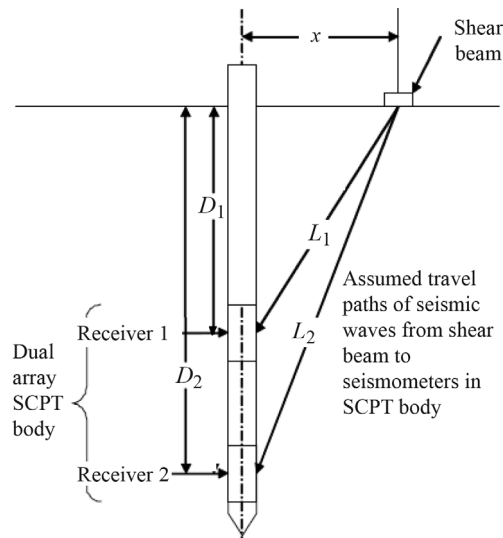


**Figure 10** - Down-hole SCPT test with two seismic sensors at different depths (Butcher *et al.*, 2005).

the cross correlation method. The trajectory followed by seismic waves ( $L_1 - L_2$ ) would be closer to the spacing of the geophones, reducing errors associated with wave propagation path. Figure 11 demonstrates this comparison, which shows that the results were indeed equivalent.

### 3. System Validation

Several tests were conducted at the experimental research sites from Unesp, Unicamp and USP to validate the system. These sites were chosen because there is already cross-hole and SCPT test data available (Giacheti *et al.* 2006a; Giacheti *et al.* 2006b; Giacheti *et al.*, 2007) and this served as a reference for the comparison.

The tests performed at the Unesp and Unicamp experimental research sites used the National Instruments data acquisition system and the seismic source was positioned in front of the pushing equipment, 0.3 m away from the hole. The tests carried out at the USP experimental research site were carried out in 2009, a year before the others, the data acquisition system from Lynx was used and the seismic source were positioned in the rear of the pushing equipment, 1.8 m apart from the hole.

#### 3.1. Unesp experimental research site

Giacheti (2001) describes the soil at the Unesp experimental research site, located in the city of Bauru, São Paulo, Brazil as a red sand clayey soil, classified as SM-SC. It is a porous and collapsible soil, the density increases with

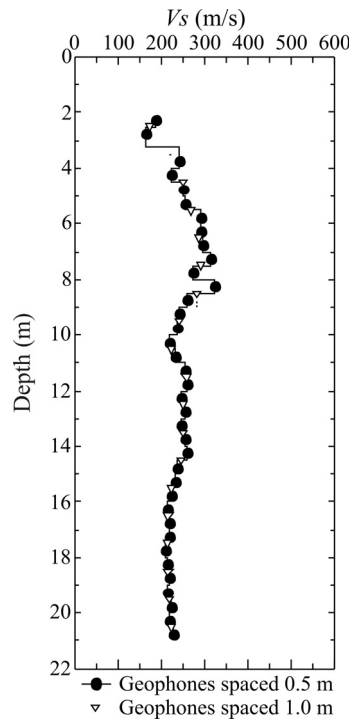


**Figure 11** -  $V_s$  profiles with the geophones spaced 0.5 m and 1.0 m in tests carried out at the (a) Unesp experimental research site and at the (b) Unicamp experimental research site.

depth and the soil has a lateritic behavior up to about 13 m depth. Giacheti *et al.* (2006a) highlights the heterogeneity of the soil, observed throughout the electrical CPT testing data. Figure 12 shows the position of field tests conducted at this site, previously discussed in this paper.

Some filtered signals obtained at different depths, during the down-hole test DH2 using the developed system are shown in Fig. 13. It demonstrates that all three different geophones provided signals with excellent quality. It is noteworthy that, in general, it is possible to get recordings of similar quality for all the three geophones.

Figure 14 shows the results obtained at this site for two cone tests (CPT1 and CPT2), a commercial seismic cone (SCPT), a cross-hole testing data (CH) and two down-hole tests carried out using the developed system (DH1 and DH2).

The DH2 test was carried out positioning the pushing equipment parallel to the alignment of the cross-hole test holes while the test DH1 was carried out perpendicular to this alignment, aiming to evaluate possible soil anisotropy.

Figure 14 also allows comparing down-hole test data using the developed system with those results obtained from other seismic tests using commercial equipment (cross-hole and SCPT). Considering the cross-hole and SCPT testing data, note that:

- a) The DH1 test provided very similar results, with an average difference of 5.8% from cross-hole with little variation of this difference over the depth;
- b) For the DH2 test results the average difference was 14.7% from cross-hole up to 7 m depth, and 5.9% from 7 m to 15 m depth; and
- c) Comparing the SCPT test results with the cross-hole, the difference was 9.2% up to 10 m depth and 18.2 up to 15 m.

The observed differences were associated to soil heterogeneity in this particular experimental research site, as highlighted by Giacheti *et al.* (2006a), as well as possible soil anisotropy.

#### 3.2. Unicamp experimental research site

The Unicamp experimental research site is located at Campinas, São Paulo State, Brazil. This site is basically composed of two distinct layers. The first layer extends up to about 6 m depth and consists of a red silty clay soil, porous, collapsible and with lateritic behavior. Below this layer there is a diabase residual soil with a clayey silt tex-

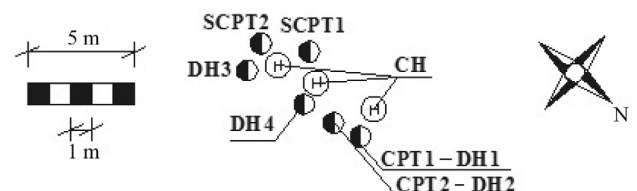


**Figure 12** - Test locations at the Unesp experimental research site.

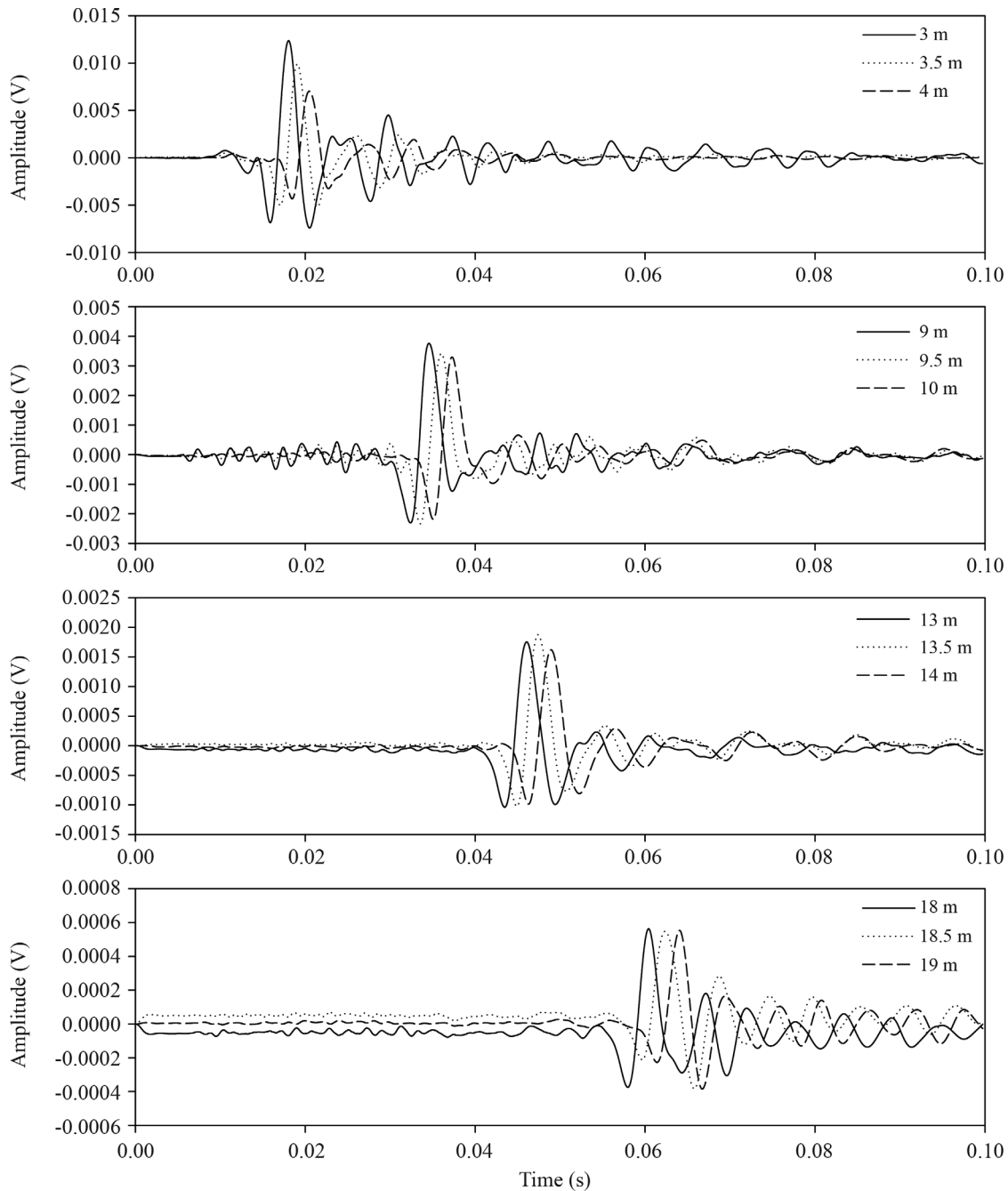
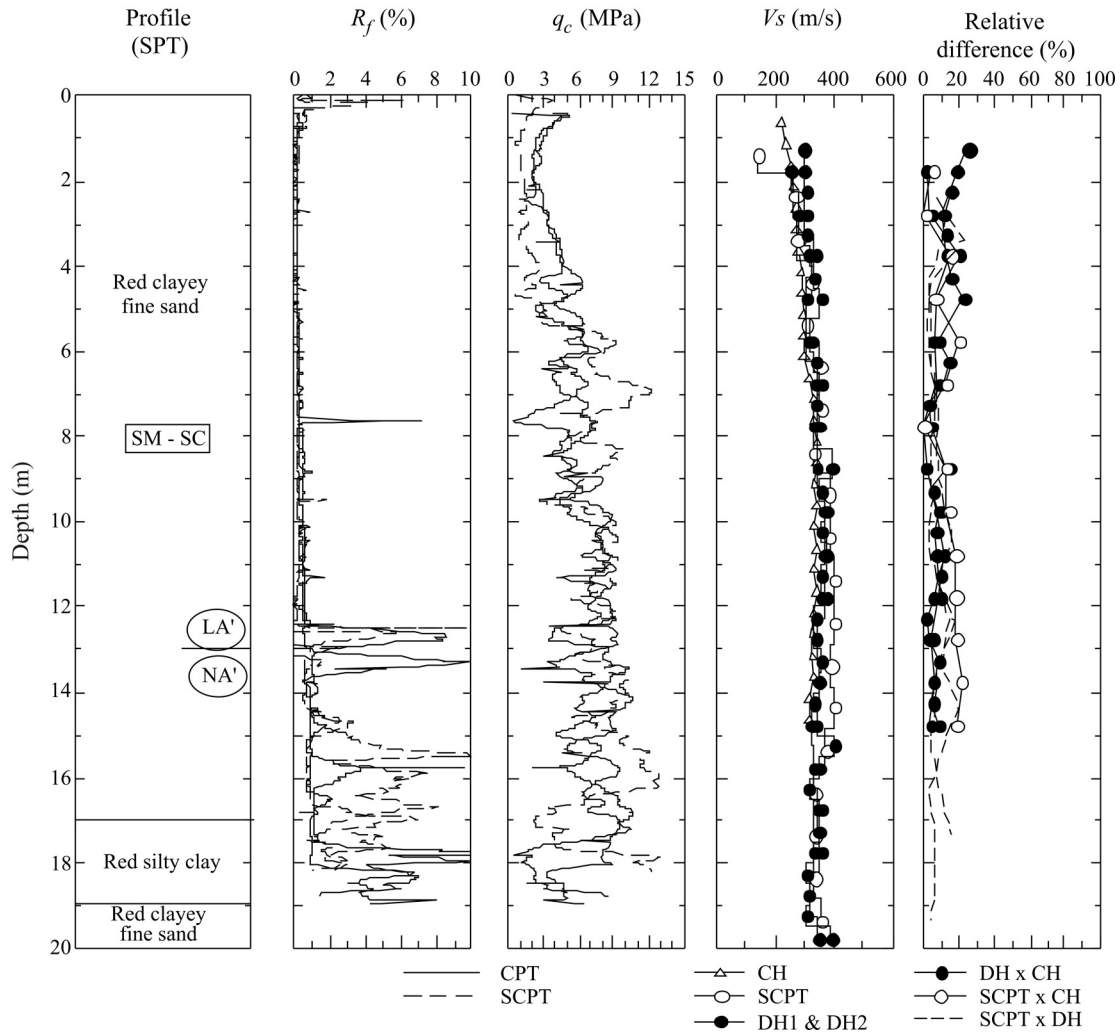


**Figure 13** - Filtered signals using the developed system for down-hole seismic test (DH2) performed at the Unesp experimental research site.

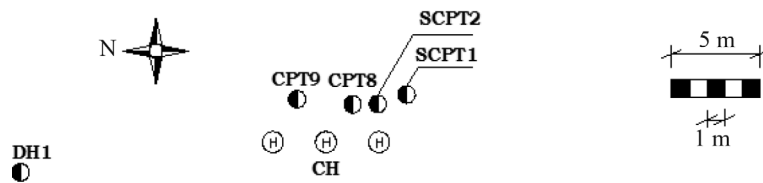
ture (Giacheti, 2001). Figure 15 shows the location of field tests conducted at this site already discussed in this paper. The DH2 test was carried out up to around 7 m depth in a new experimental research site about 300 m away from where the other tests were performed.

Figure 16 shows results of two cone tests (CPT8 and CPT9), two commercial seismic cone tests (SCPT1 and SCPT2), a cross-hole test (CH) and one of the two down-hole tests (DH1) carried out using the developed system for the Unicamp site.

It is observed in Fig. 16 that the seismic test results had excellent consistency. There is a great dispersion of both the values of  $V_s$  and tip resistance ( $q_c$ ), indicating a high local soil variability up to about 9 m depth. The average differences of down-hole test results DH1, DH2, SCPT1, SCPT2 compared with the cross-hole test result (CH) were respectively 22.4%, 19.4%, 9.3% and 14.8%. From 9 m to 17 m depth, where residual soil occurs, there is excellent consistency between the down-hole seismic test results SCPT1 and SCPT2 and for the DH1, with a mean



**Figure 14** - CPT, cross-hole and down-hole tests results using commercial equipment and the developed system at the Unesp experimental research site. DH = down hole using developed system; SCPT = seismic CPT using commercial system; CH = cross hole using commercial system.



**Figure 15** - Location of field tests carried out at the Unicamp experimental research site.

relative difference of 5.8%. Also noteworthy is the similarity of the results of  $q_c$  values in this region, indicating homogeneity of the geotechnical properties from this layer. After 17 m depth the cone reaches a silty fine sand layer, there is an increase in the relative differences of both  $V_s$  and  $q_c$  values and the average difference between the down-hole DH1 test result for the two seismic cone tests (SCPT1 and SCPT2) were 18.0% and 9.8%.

### 3.3. USP experimental research site

According to Giacheti (2001), the soils in this research site, located at São Carlos city, São Paulo State, Brazil, consist of a porous and collapsible clayey fine sand up to about 6.5 m depth, followed by a layer of residual soil of Bauru sandstone. These two distinct layers are divided by pebbles. Giacheti *et al.* (2006b) discussed the variation

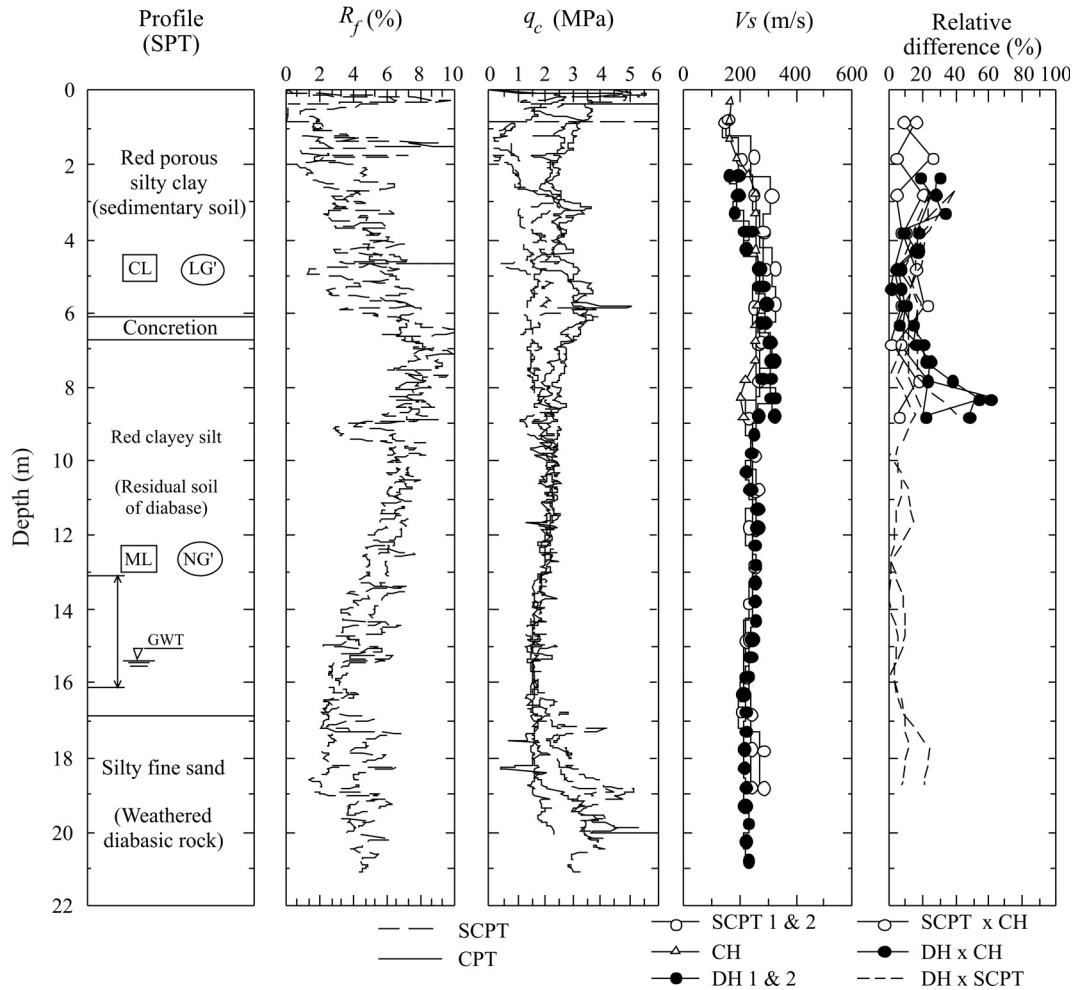


**Figure 16** - CPT, cross-hole and down-hole tests results using commercial equipment and the developed systems at the Unicamp experimental research site. DH = down hole using developed system; SCPT = seismic CPT using commercial system; CH = cross hole using commercial system.

observed in the  $q_c$  and  $R_f$  values obtained in CPT tests conducted at this location. Figure 17 shows the location of the field test carried out at the USP research site and discussed in this paper. Figure 18 shows test results of three CPT tests (CPT1, CPT2 and CPT3), three commercial seismic cone tests (SCPT1, SCPT2 and SCPT3), two cross-hole tests (CH1 and CH2) and two down-hole tests carried out using the developed system (DH1 and DH2).

It can be observed in Fig. 18 that the average difference between the down-hole DH1 and DH2 test results, with the cross-hole CH1 test results was 7.7% and 6.3%, respectively. It is also possible to observe in this figure that the average relative difference from cross-hole CH2 and CH1 was 7.9%, which is in the same range obtained with the developed system, indicating that down-hole and cross-hole provide similar results at this site.

This similarity was not observed in the first 2 and 3 m depth points, probably because of the position of the seismic source, which was kept at a distance of 1.8 m away

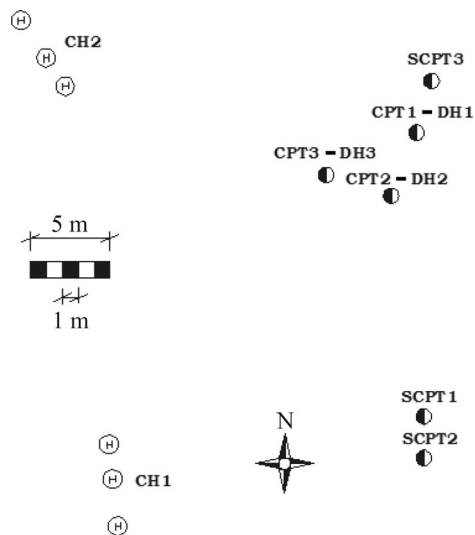


**Figure 17** - Location of the field tests carried out at the USP experimental research site.

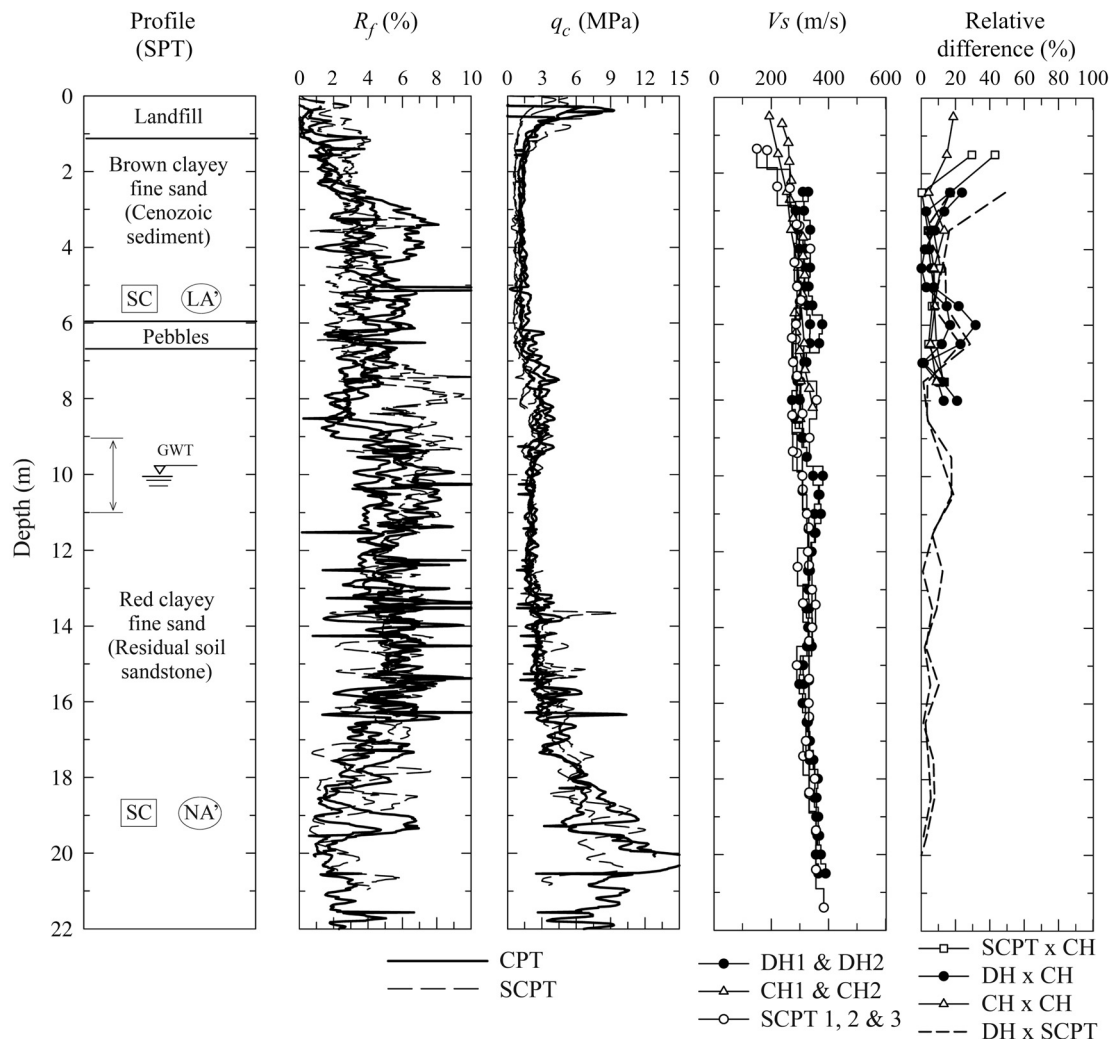


**Figure 18** - CPT, cross-hole and down-hole tests results using commercial equipment and the developed systems at the USP experimental research site. DH = down hole using developed system; SCPT = seismic CPT using commercial system; CH = cross hole using commercial system.

from the hole. This difference was also observed in the pebble layer, between 5 and 7 m depth, where the average values between the DH1 and DH2 test results compared with the CH1 test were respectively 25.4% and 14.6%. It is important to point out that in this region the signals from the down-hole seismic tests had low quality, which was associated with interference from the pebble layer in the pathway of the seismic waves.

There are no cross-hole test results below 8 m depth. However, it was possible to verify the consistency between the  $V_s$  values calculated using the down-hole test with the developed system and with a commercial seismic cone (Giacheti *et al.* 2006b) since the average relative difference was 6%. The average results between 9 and 11 m depth were of 15.5%. This region corresponds to a zone of groundwater level variation, so considering that the tests were conducted at different seasons of the year; it is believed, based on our judgment, that this difference can be

associated with a possible variation in soil suction, that could affect the soil stiffness and, consequently, the shear wave velocity.

#### 4. Conclusions

The system developed for performing the seismic down-hole test right after and in the same hole of a CPT test proved to be very reliable.

The last version of the data acquisition software using Labview platform, which also includes interpretation using cross correlation and the true interval methods simultaneously to the testing execution was significantly improved. Using this software the later step of data processing and interpretation was eliminated through the test procedure becoming faster and easier to be conducted.

The laboratory test showed that the geophones have the same response and their installation in the seismic probe

did not interfere in their seismic response, which is essential for using the true interval method.

The use of a seismic probe which has three geophones 0.5 m apart was very interesting because it allows obtaining a more detailed  $V_s$  profile, which is important for identifying different rigidity layers without requiring a longer test. The  $V_s$  values calculated with a spacing of 1 m and 0.5 m were considered similar.

The National Instruments data acquisition system and the developed software in the Labview platform were considered appropriate since this system presented a good performance at a relatively low cost. Since the data acquisition system does not have a low pass filter, the use of a high data acquisition frequency is necessary to avoid the aliasing phenomenon, which may compromise the test data. A high data acquisition frequency ensures an adequate sampling including the noise interference, which can be removed with digital filtering. Another possibility is to use an analog filter, which filters the signal at the time of acquisition; however, it should be verified that this filter does not cause delay in the signal arrival. The use of 150 kHz data acquisition frequency was considered adequate, ensuring appropriate sampling and an excellent resolution in time domain. This very high frequency is interesting for interpretation throughout the cross correlation method. It is recommended using the highest data acquisition rate allowed by the system in use and also a digital filter for noise removal.

The best results were obtained with the seismic source positioned in front of the pushing equipment, 0.3 m away from the hole, which can be considered consistent with the Butcher *et al.* (2005) recommendation. The seismic source closer to the hole makes the difference between the distances travelled by the seismic waves closer to the spacing between the geophones, reducing the error associated with the wave propagation pathways.

It was observed that the reliability of down-hole test results is directly related to the quality of the recorded signals, which heavily relies on the care taken during testing procedure and interpretation. The most significant factor for guaranteeing good quality seismic data was to keep the position of the axis of vibration of the geophones parallel to the blow direction. The recommended procedure is to secure with force the test rod using a pipe wrench, ensuring the maintenance of the correct position of the geophones during all tests. The intensity which the hammer hits the seismic source also influences the signal quality. It was observed that applying strokes with a lower intensity, generates the best waves, which are preferable because they facilitate all data interpretation.

The consistency between the results obtained in the down-hole tests conducted with the developed system with the results of SCPT tests performed with commercial equipment and with those obtained in cross-hole tests allowed validation of the system.

## Acknowledgments

The authors thank FAPESP, CNPq and CAPES for the funding of their research. Also thanks to Thiago Mota Ramos and Francisco Avesani, for their assistance and to the engineer Jorge Nicolau, from EESC – USP, for his support on developing the data acquisition system, hardware and Labview software.

## References

- Butcher, A.P.; Campanella, R.G.; Kayne, A.M. & Mas-sarch, K.R. (2005) Downhole seismic cone procedure to measure shear wave velocity - The guideline. The International Society for Soil Mechanics and Geotechnical Engineering, Technical Committee No. 10: Geophysical and Geotechnical Engineering Testing, 5 pp.
- Butcher, A.P. & Powell, J.J.M. (1996) Practical considerations for field geophysical techniques used to ASSESS ground stiffness. *Advances in Site Investigation practice*. Thomas Telford, London, pp.701-714.
- Campanella, R.G. & Howie, J. (2005) A Practical Applications of the Cone Penetration Test, a Manual on Interpretation of Seismic Piezocone Test Data for Geotechnical Design. U.B.C. Civil Engineering Department, 305 pp.
- Campanella, R.G. & Stewart, W.P. (1992) Seismic cone analysis using digital signal processing for dynamic site characterization, *Canadian Geotechnical Journal*, v. 29:3, p.477-486.
- Giacheti, H.L. (2001) Field Tests in Site Investigation: Study and Considerations to the Applicability for Tropical Soils (in Portuguese). Associate Professor Thesis, Faculty of Engineering, Unesp, Bauru, 301 pp.
- Giacheti, H.L.; De Mio, G.; Dourado, J.C. & Malagutti, W. (2006a) Comparing down-hole and cross-hole seismic tests results on the Unesp Bauru experimental research site (in Portuguese). *Proc. XIII Brazilian Congress of Soil Mechanics and Geotechnical Engineering*, Curitiba, v. 2. pp. 669-674.
- Giacheti, H.L.; De Mio, G. & Peixoto, A.S.P. (2006b) Seismic cross-hole and CPT Tests in the Tropical Soil Site. *Proc. ASCE GeoCongress*, Atlanta, CD-Rom, pp. 1-6.
- Giacheti, H.L.; Peixoto, A.S.P. & De Mio, G. (2007) Cross-hole and SCPT tests in a tropical soil from Campinas, SP, Brazil. *Proc. XIII Panamerican Conference on Soil Mechanics and Geotechnical Engineering*, Isla Margarita, CD-Rom, pp. 1-6.
- Mayne, P.W. and Schneider, J.A. (2000) Evaluating axial drilled shaft response by seismic cone. *Foundations & Ground Improvement*, GSP 113, ASCE, Reston, pp. 655-669.
- Pedrini, R.A.A.; Vitali, O.P.M. & Giacheti, H.L. (2010) Software for analysis of seismic records in down-hole tests with the seismic piezocone (in Portuguese). *Proc.*

- XV Brazilian Congress of Soil Mechanics and Geotechnical Engineering, Gramado, CD-Rom, pp. 1-8.
- Robertson, P.K.; Campanella, R.G.; Gillespie, D. & Rice, A. (1986). Seismic CPT to measure in-situ shear wave velocity, *Journal of Geotechnical Engineering, ASCE*, v. 112:8, p. 791-804.
- Vitali, O.P.M.; Pedrini, R.A.A. & Giacheti, H.L. (2010) Factors affecting the determination of maximum shear modulus in down-hole seismic tests with piezocone (in Portuguese). Proc. XV Brazilian Congress of Soil Mechanics and Geotechnical Engineering, Gramado, CD-Rom, pp. 1-8.
- Vitali, O.P.M.; Pedrini, R.A.A. & Giacheti, H.L. (2011) Shear wave velocity in down-hole seismic tests: Equipment and factors affecting the test data. Proc. 14th Pan-American Conference on Soil Mechanics and Geotechnical Engineering, 2011, Toronto, CD-Rom, pp. 1-7.
- Vitali, O.P.M. (2011) Developing a System for Down-Hole Seismic Test Together with the Piezocone (in Portuguese). M.Sc. Thesis, Departamento de Geotecnia, Escola de Engenharia de São Carlos, São Carlos, 114 pp.



# Estimating Young Moduli in Sands from the Normalized $N_{60}$ Blow Count

A. Conde de Freitas, M. Pacheco, B.R. Danziger

**Abstract.** This paper presents statistical correlations between the static Young modulus  $E_s$  and the normalized SPT penetration resistance  $N_{60}$  (corresponding to 60% of the theoretical energy of the SPT test) for preliminary estimation of settlements in sedimentary sands. The correlations have been established through the statistical interpretation of many experimental studies available in the literature, based on power regression analyses. Equations and charts are presented to estimate the mean value  $E_s$  and related statistical limits of  $E_s$  as a function of  $N_{60}$ . The obtained correlations have been used to compare the calculated settlements of a rigid raft bearing on a multi-layered sand deposit (comprising distinct relative densities) with the measured settlements in eight points underneath the raft.

**Keywords:** sand compressibility, normalized SPT, Young modulus, correlations.

## 1. Introduction

The use of seismic tests to obtain correlations between the shear wave velocity  $V_s$  and  $N_{SPT}$  is widely used in foundation engineering. However, most of the published correlations do not provide the statistical inferences used to support the published results. Also, many of these correlations do not take into consideration normalized  $N_{60}$  blow counts, causing a large scatter of the data compiled from different countries.

Hanumantharao & Ramana (2008) compiled several correlations between  $V_s$  and  $N_{SPT}$  (uncorrected) worldwide for different soil types. It is well known that the low amplitude shear modulus ( $G_{max}$ ) is directly related to the shear wave velocity and to the density of the soil through which the wave travels (Richart *et al.*, 1970). Thus,  $G_{max}$  is estimated by measuring the shear wave velocity and the soil density to predict the stress-strain behavior of soils under low amplitude dynamic excitation. Unfortunately the use of seismic tests is not yet widespread in Brazil, while the SPT is still the most used technique for site investigation there and in many other countries, what supports the development of several correlations between  $V_s$  and  $N_{SPT}$  worldwide. Anbazhagan & Sitharam (2010) developed recent relationships between  $V_s$  and  $N_{SPT}$  and pointed out that better correlations could be obtained by correlating  $N_{SPT}$  and  $G_{max}$  also to the overburden stress.

The most common relationship between  $V_s$  to  $N_{SPT}$  is of the type given by Eq. 1, although Eq. 2 is also commonly used. In both equations  $A$ ,  $B$  and  $C$  are regression constants and  $N$  may represent either  $N_{SPT}$  or  $N_{60}$ .

$$V_s = A \cdot N^B \quad (1)$$

$$V_s = C + A \cdot N^B \quad (2)$$

The correlations compiled by Hanumantharao & Ramana (2008) for sands have been used to form the database of the present paper, along with further correlations by Ohsaki & Iwasaki (1973), Jafari *et al.* (2002), Athanapoulos (1995), Wride & Robertson (1997), Wride *et al.* (2000) and Robertson *et al.* (2000). In this paper, a power regression analysis (Eq. 1) is used to relate statistically  $V_s$  to  $N_{60}$ . It is worth noting that the velocity of the shear wave can be determined reliably by seismic field tests such as crosshole, downhole, uphole, seismic piezocone, seismic refraction, among others. The velocity  $V_s$  and all parameters related to  $V_s$  are limited to small strains, of the order of 10<sup>-4</sup>% (Barros, 1997).

Hanumantharao & Ramana (2008) mention that the measured shear wave velocities obtained from different field methods differ only by the order of 10 to 15%. This may be regarded as negligible when compared to the uncertainties to estimate dynamic moduli and make feasible the use of correlations between  $V_s$  and  $N_{60}$ , even when  $V_s$  is determined by different field techniques. Giachetti *et al.* (2006) and Moura (2007) reported a difference of only 6.7% in the average shear wave velocity determined by downhole and crosshole tests in a fine clayey sand from the region of Bauru (State of São Paulo, Brazil).

Starting from published correlations between  $V_s$  and  $N_{SPT}$ , regression equations relating  $G_{max}$  and  $E_{max}$  (small strain dynamic Young modulus) to  $V_s$  are readily obtained by well known equations of the classical theory of elasticity. Further correlations between  $E_{max}$  and the static Young modulus  $E_s$ , according to Buzdugan (1972), enable the final correlations

A. Conde de Freitas, Visiting Professor, Departamento de Estruturas e Fundações, Faculdade de Engenharia do Estado do Rio de Janeiro, Maracanã, R.J., Brazil. e-mail:alessandra.conde@uol.com.br.

M.P. Pacheco, Professor, Departamento de Estruturas e Fundações, Faculdade de Engenharia do Estado do Rio de Janeiro, Maracanã, R.J., Brazil. e-mail:marcus\_pacheco@terra.com.

B.R. Danziger, Associate Professor, Departamento de Estruturas e Fundações, Faculdade de Engenharia do Estado do Rio de Janeiro, Maracanã, R.J., Brazil. e-mail:brdanzig@uerj.br.

Submitted on March 15, 2011; Final Acceptance on April 3, 2012; Discussion open until September 30, 2012.

between the static Young modulus  $E_s$  and the corrected  $N_{60}$  blow count for sands, as proposed in this paper.

## 2. Regression Equations Relating $E_{max}$ to $N_{60}$

Hanumantharao & Ramana (2008) compiled several correlations between  $V_s$  and  $N_{SPT}$  for clayey and sandy soils. In the present paper, however, emphasis is given only to correlations in sands, according to Table 1. Wride *et al.* (2000) and Robertson *et al.* (2000) summarized the Canlex research project (Canadian Liquefaction Experiment) whose main objective was the study of soil liquefaction in saturated sandy soil. From the Canlex database some correlations between shear wave velocity  $V_s$  and  $N_{60}$  have been established and presented in the research report from different sites, also included in Table 1. The fourth column in Table 1 refers to the range of  $N_{SPT}$  corresponding to the sands investigated by each author. The fifth column refers to the range of  $N_{60}$  for the correlations established in the Canlex research project.

Selection of appropriate correction factors are required to convert  $N_{SPT}$  into  $N_{60}$  to normalize the correlations in Table 1 according to the actual energy delivered during the SPT test in each country. Several authors have proposed correction factors to account for the actual energy transmitted to the rods in the SPT test (De Mello, 1971; Kovacs *et al.*, 1977; Palacios, 1977; Schmertmann & Palacios, 1979; Belincanta, 1985; Danziger *et al.*, 2008, among others). The ISSMFE (1989) established 60% of the theoretical potential energy as the international reference. Therefore,  $N_{SPT}$  should be converted to  $N_{60}$  by the expression:

$$N_{60} = N_{SPT} \frac{E}{E_{60}} \quad (3)$$

In Eq. 3  $E$  represents the actual energy delivered to the rods in the SPT test and  $E_{60}$  refers to 60% of the theoreti-

cal potential energy of the SPT hammer. If the energy  $E$  is measured, the above expression should be used. Otherwise, an estimated value for  $E$  based on past experience is required. Therefore, correcting  $N_{SPT}$  is essential to compare correlations from different countries. Décourt (1989) pointed out that the energy just below the anvil ( $E$ ) can be obtained as:

$$E = e_1 e_2 e_3 \quad (4)$$

where  $e_1, e_2, e_3$ , are the efficiencies (or correction factors). The efficiency factor  $e_1$  relates the kinetic energy just before the impact, being mainly dependent on the way the hammer is lifted and released. Values of  $e_1$  suggested by Décourt (1989) are shown in Fig. 1.

The factor  $e_2$  is the ratio between the energy just below the anvil and the kinetic energy just before the impact and it is dependent on the anvil mass (Skempton, 1986). Figure 2 summarizes the main results (Décourt, 1989).

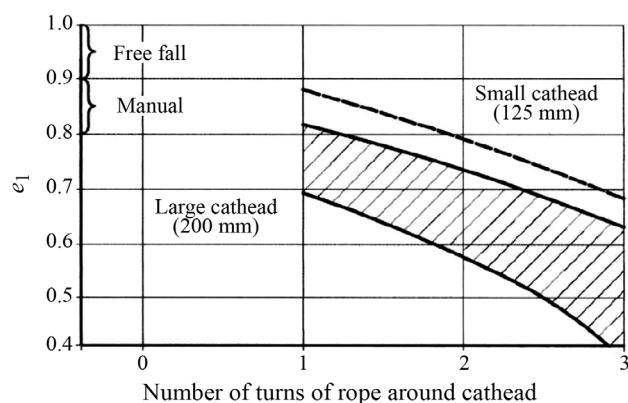


**Figure 1** - Efficiency factor  $e_1$  (adapted by Décourt, 1989, from Skempton, 1986).

**Table 1** - Correlations between  $V_s$  and  $N_{SPT}$  in sands (adapted from Hanumantharao & Ramana, 2008), including other data.

Author	$V_s$ (m/s)	Country	$N_{SPT}$ range	$N_{60}$ range
Ohta <i>et al.</i> (1972) <sup>(a)</sup>	$87.0N_{SPT}^{0.36}$	Japan	1 to 50	
Ohsaki & Iwasaki (1973)	$59.0N_{SPT}^{0.47}$	Japan	1 to 50	
JRA (1980) <sup>(b)</sup>	$80.0N_{SPT}^{0.33}$	Japan	1 to 50	
Seed <i>et al.</i> (1983)	$56.4N_{SPT}^{0.50}$	USA	1 to 50	
Sykora & Stokoe (1983)	$106.7N_{SPT}^{0.27}$	USA	1 to 50	
Lee (1990)	$57.0N_{SPT}^{0.49}$	USA	1 to 50	
Massey – Fraser River Delta <sup>(c)</sup>	$92.9N_{60}^{0.25}$	Canada		9 to 21
Kidd – Fraser River Delta <sup>(c)</sup>	$83.7N_{60}^{0.25}$	Canada		13 to 43
J-Pit – Syncrude <sup>(c)</sup>	$92.8N_{60}^{0.25}$	Canada		2 to 29
LL Dam – HVC Mine <sup>(c)</sup>	$102.9N_{60}^{0.25}$	Canada		2 to 7
Highmont Dam – HVC Mine <sup>(c)</sup>	$95.4N_{60}^{0.25}$	Canada		3 to 13

<sup>(a)</sup>from Ohsaki & Iwasaki (1973). <sup>(b)</sup>from Jafari *et al.* (2002). <sup>(c)</sup>CANLEX Research.

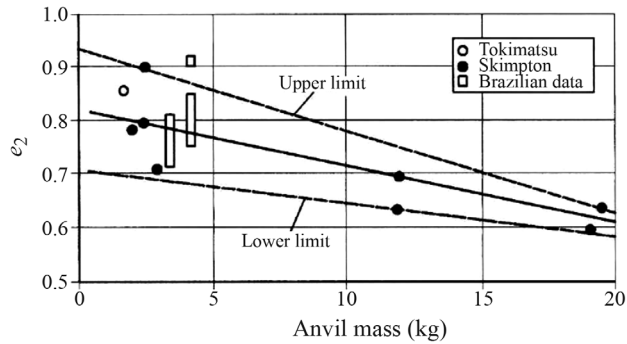


**Figure 2** - Efficiency factor  $e_2$  as a function of the anvil mass (Décourt, 1989).

The efficiency factor  $e_3$  is due to the rod length. According to Schmertmann & Palacios (1979) the driving energy would only be fully transmitted to the rods if they had a minimum critical length. This would occur because in most cases the first compression wave pulse is reflected in the lower end of the sampler as a tension wave. Therefore the tension wave induces a separation between the hammer and the rods, preventing further transfer of energy. Recent researches, however, have shown that the subsequent (secondary) impacts in the same blow contribute to full energy transmission, indicating that the energy just below the anvil is independent of the length of the rod stem, and thus the factor  $e_3$  should be taken as unity.

Odebrecht (2003) and Odebrecht *et al.* (2005) have shown that the potential energy resulting from the penetration of the sampler should be added to the nominal potential energy, which is significant mostly in case of small rod lengths in soft clays and loose sands.

Aoki & Cintra (2000) pointed out that the energy producing the sampler penetration (which is associated to the  $N$  value) is the one that reaches the sampler, and not the one below the anvil. Thus, the corresponding energy loss over the rods should also be taken into account. Thus another factor  $e_4$  that quantifies the energy loss over the rods should also be included in Eq. 4. Unfortunately, very few data is available about this factor (*e.g.*, Cavalcante, 2002; Odebrecht, 2003; Johnsen & Jagello, 2007).

It turns out that the only reliable way to quantify the SPT energy losses is by proper measurement of the actual energy delivered to the sampler. In this paper,  $N_{60}$  values are assigned according to average correction factors  $C$  reported by Décourt *et al.* (1989), as shown in Table 2. For example, the value  $C = 1.05$  (USA) in Table 2 refers to the average value for 0.75 (donut/rope-cathead); 1.00 (safety/hope/cathead) and 1.40 (safety/free fall). The correction factor  $C$  is given by:

$$C = \frac{E}{E_{60}} \quad (5)$$

$$N_{60} = C \cdot N_{SPT} \quad (6)$$

**Table 2** - Correction factors  $C$  – (adapted from Décourt *et al.*, 1989).

Country	$C$
Argentina	0.75
Brazil	1.20
China	1.00
Colombia	0.83
Japan	1.27
Paraguay	1.20
U.K.	0.92
U.S.A.	1.05
Venezuela	0.72

For the Brazilian SPT, Décourt (Table 2) proposed:

$$N_{60} = 1.20 \cdot N_{SPT} \quad (7)$$

Further research based on actual energy measurements on the SPT hammers mostly used in Brazil (*e.g.*, Belincanta, 1985, 1998; Cavalcante, 2002; Odebrecht, 2003) has indicated:

$$N_{60} = 1.37 \cdot N_{SPT} \quad (8)$$

Equations 7 and 8 are used in Session 3 to enable correlations for practical application in Brazil. Hanumantharao & Ramana (2008) pointed out that most correlations may produce acceptable  $V_s$  predictions for  $N_{SPT}$  values up to 40. According to the Authors experience in settlement predictions based on  $N_{SPT}$ , the correlations above require good engineering judgment for  $N_{SPT} > 30$  and should be avoided for  $N_{SPT}$  above 50 or below 4.

To relate  $E_{max}$  to  $N_{60}$ , the following equations of the classical theory of elasticity are used:

$$E_{max} = 2 \cdot G_{max} \cdot (1 + \nu) \quad (9)$$

$$G_{max} = V_s^2 \cdot \rho \quad (10)$$

From Eqs. 9 and 10:

$$E_{max} = 2 \cdot \left( V_s^2 \cdot \frac{\gamma}{g} \right) \cdot (1 + \nu) \quad (11)$$

In the equations above  $\nu$  is the Poisson ratio,  $\rho$  the soil unit mass,  $\gamma$  the soil unit weight and  $g$  the acceleration of gravity. Equation 11 enables to relate  $E_{max}$  to  $N_{60}$  by assigning a power regression curve to  $V_s$  (Eq. 1). Therefore, each pair  $N_{60} \times E_{max}$  (for each regression equation in Table 1) is plotted in Fig. 3 for all integer  $N_{SPT}$  and  $N_{60}$  values according to the ranges given by the two last column of Table 1.  $N_{SPT}$  values are corrected to  $N_{60}$  according to Table 2. The points in Fig. 3 have been plotted by assigning  $\nu = 0.3$ ,  $\gamma = 18 \text{ kN/m}^3$  and  $g = 9.8 \text{ m/s}^2$  in Eq. 11.

According to Conde de Freitas (2010) the soil specific weight increases only moderately with  $N_{60}$ , with minor

impact on Eqs. 9, 10 and 11. Therefore, a constant value  $\gamma = 18 \text{ kN/m}^3$  was assigned throughout this work.

Attention should be pointed out that Eqs. 9 and 10 have been derived from the classical theory of elasticity that assumes a constant modulus for soil mass. Such a simplification is only justified in the proposed correlations as long as its use has been conceived as preliminary settlement estimations.

To fit a regression power curve through the 357 points in Fig. 3a, a transformed linear regression analysis is carried out by plotting  $\log(N_{60})$  x  $\log(E_{\max})$ , as in Fig. 3b (Conde de Freitas, 2010). The desired regression power curve in Fig. 3a is readily determined by mapping back the linear regression curve (Fig. 3b) into the original plot ( $N_{60}$  x  $E_{\max}$ ), producing:

$$E_{\max} = 24975 \cdot N_{60}^{0.75} \text{ (kPa)} \quad (12)$$

For comparison, an alternative relationship between  $N_{SPT}$  (uncorrected) and  $E_{\max}$  is readily obtained from Eq. 13 below, widely used in the oil industry in Brazil for design of foundations for machinery (Petrobras, 2008; Machado, 2010):

$$G_{\max} = 12000 \cdot N_{SPT}^{0.80} \text{ (kPa)} \quad (13)$$

From Eqs. 9 and 13:

$$E_{\max} = 31200 \cdot N_{SPT}^{0.80} \text{ (kPa)} \quad (14)$$

Equations 12 and 14 are compared in Session 3 to estimate the static Young modulus  $E_s$ , the main objective of this paper. Experimental data by Machado (2010) has confirmed the adequacy of Eq. 13 to estimate the shear modulus  $G_{\max}$  for design of foundations for machinery.

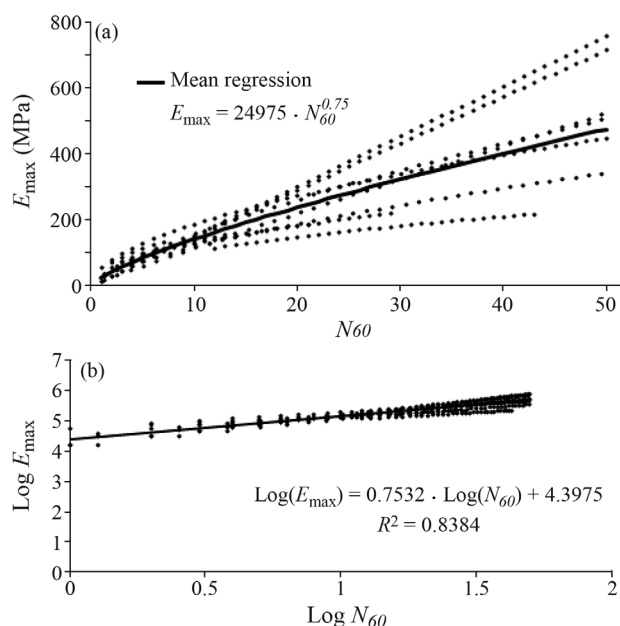


**Figure 3** - (a).  $N_{60}$  vs.  $E_{\max}$  points for sands and corresponding power regression curve and (b). Transformed linear regression  $\log(N_{60})$  vs.  $\log(E_{\max})$  (Conde de Freitas, 2010).

Statistical limits for the points in Fig. 3a have been determined in Fig. 4 (Conde de Freitas, 2010) according to Neter *et al.* (1982); Pacheco & Lima (1996), for  $n$  standard deviations about the mean regression curve ( $n$  ranging from 0.5 to 2).

### 3. Static Young Moduli

Equations 12 and 14 are applicable to engineering problems related to small strains, as in dynamic analyses of foundations for machinery. For static problems, however, a reduction factor is to be applied to the dynamic modulus  $E_{\max}$  to estimate the corresponding static Young modulus  $E_s$ . Laboratory tests on reconstituted samples in sands indicate that the dynamic shear modulus may be reduced more than tenfold for shear deformations of  $10^{-3}\%$  to 1% (Barros, 1997; Moura, 2007). According to Kulhawy & Mayne (1990); Moura (2007), the shear modulus for static loads is about 5 to 10%  $G_{\max}$ . A similar reduction is also reported by Sitharam *et al.* (2004), Fig. 5. Therefore it is important to keep in mind that estimates of  $E_s$  (or  $G_s$ ) should be made according to the range of shear deformation expected for each problem under consideration (Silveira *et al.*, 2006).

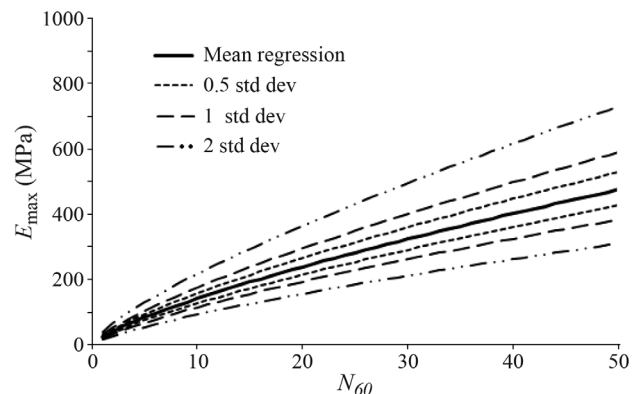


**Figure 4** - Statistical limits for  $E_{\max}$  from the points in Fig. 3a (adapted from Conde de Freitas, 2010).

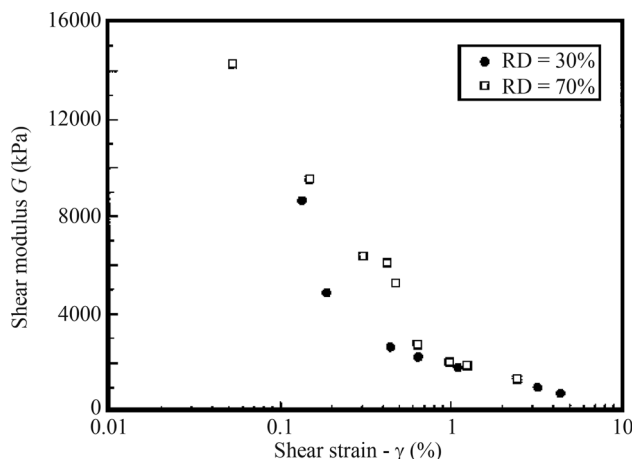


**Figure 5** - Shear modulus vs. shear deformation for Ahmedabad sand for two relative densities (Sitharam *et al.*, 2004).

Buzdugan (1972) summarized the range of variation of dynamic ( $E_{max}$ ) and static ( $E_s$ ) Young moduli (Table 3) for foundation design. An average ratio  $E_{max}/E_s = 3$  is inferred from Table 3 to estimate  $E_s$  from Eqs. 12 and 14 in sands. This ratio is recommended only to well-designed foundations whose applied pressure is far from failure, as expected in large dimension foundations like rafts, tanks and silos. The ratio  $E_{max}/E_s$  is expected to increase for smaller safety factors (larger shearing strains) and therefore good engineering judgment and experience are required for practical use of the correlations proposed herein. Furthermore, the ratio  $E_{max}/E_s$  increases for clayey soils (Buzdugan, 1972). Therefore, the ratio  $E_{max}/E_s = 3$  as well the correlations presented in this paper should also be restricted to sedimentary pure sands with negligible amount of fines, considering that even small percentages of fines are likely to produce higher  $E_{max}/E_s$  ratios.

The regression curves in Fig. 4 ( $N_{60} \times E_{max}$ ) are converted into  $N_{60} \times E_s$  in Fig. 6 for  $E_{max}/E_s = 3$ . The corresponding mean power curve in Fig. 6 (determined from Eq. 12) is given by:

$$E_s = 8325 \cdot N_{60}^{0.75} \text{ (kPa)} \quad (15)$$

For comparison, the static modulus  $E_s$  estimated from Eq. 14 for  $E_{max}/E_s = 3$  is:

$$E_s = 10400 \cdot N_{SPT}^{0.80} \text{ (kPa)} \quad (16)$$

For practical applications using the Brazilian SPT, curve (a) in Fig. 6 is obtained from Eq. 16 for  $C = 1.20$  (Eq. 7), as:

$$E_s = 8988 \cdot N_{60}^{0.80} \text{ (kPa)} \quad (17)$$

Alternatively, curve (b) in Fig. 6 is obtained from Eq. 16 for  $C = 1.37$  (Eq. 7), as:

$$E_s = 8084 \cdot N_{60}^{0.80} \text{ (kPa)} \quad (18)$$

Curve (a) in Fig. 6 is very close to the curve corresponding to 1.0 standard deviations above the mean curve, whereas curve (b) nearly coincides with the curve corresponding to 0.5 standard deviations above the mean curve. The good agreement between curves (a), (b) and the mean curve given by Eq. 15 seems to indicate that the regression curves in Fig. 6 provide a simple and reasonable statistical procedure to estimate  $E_s$ , in addition to providing a simple way to account for the uncertainty in the predictions (varia-

**Table 3** - Ranges of static and dynamic moduli for sands (adapted from Buzdugan, 1972).

Soil type	Young Modulus ( $\times 10^5 \text{ N/m}^2$ )				$E_{max}/E_s$	
	$E_s$ (static)		$E_{max}$ (dynamic)		Lower range	Upper range
(1) Loose sand (rounded grains)	400	800	1500	3000	3.75	3.75
(2) Loose sand (angular grains)	500	800	1500	3000	3.00	3.75
(3) Medium dense sand (rounded grains)	800	1600	2000	5000	2.50	3.13
(4) Medium dense sand (angular grains)	1000	2000	2000	5000	2.00	2.50
(5) Clean gravel (no sand fraction)	1000	2000	3000	8000	3.00	4.00
(6) Gravel (angular grains)	1500	3000	3000	8000	2.00	2.67
Lower and upper mean $E_{max}/E_s$	2.71	3.30				
Global mean $E_{max}/E_s$	3.00					

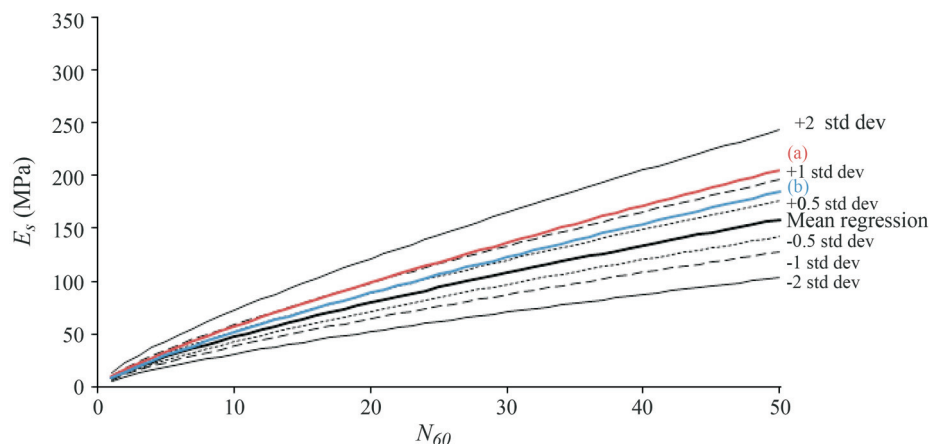


**Figure 6** - Static modulus  $E_s$  for sands ( $E_{max}/E_s = 3$ ), adapted from Conde de Freitas (2010).

tions of  $n$  standard deviations about the mean). Equations 15, 17 and 18 indicate that the static Young modulus  $E_s$  can be expressed in round numbers by:

$$E_s = 8000 \cdot N_{60}^{0.80} \text{ (kPa)} \quad (19)$$

It should be pointed out that the Young modulus  $E_s$  increases with depth in nearly normally consolidated sand deposits and this can be easily accounted for in FE modeling. In the present study, however, the variation of  $E_s$  with depth was modeled by Eq. 19 after subdividing the sand deposit into several thin layers represented by individual average  $N_{60}$  values which account indirectly for the overconsolidation condition.

#### 4. Settlement Analysis of a Raft on Multilayered Sand Deposit

The following is an application of Eq. 19 to predict the settlements of an instrumented nearly rigid raft bearing on a sedimentary sand deposit investigated by Lopes et al. (1994), and Lopes (2000). Those authors describe the measured settlement of a raft foundation during a period up to 3 years after completion of the structure. The raft supports the building housing a diesel power generator and applies to the soil a net uniform pressure  $\Delta p = 123 \text{ kN/m}^2$  (building + generator). The raft dimensions (16.6 m x 27.0 m) and the instrumentation points are shown in Fig. 7 (Lopes et al., 1994).

The sand deposit has been subdivided into six layers whose deformation parameters have been assigned in Table 4 according to the normalized  $N_{60}$  blow count obtained from Fig. 8.

The soil profile is subdivided into six moderately inclined sand layers interpreted from the SPT boring logs, as depicted in Fig. 9 (input geometry to the finite element program Plaxis 3-D Foundation). The raft bears on top of the sand deposit above which was placed a 4-m high fill. The water table is assumed to coincide with the base of the raft (4 m below the fill surface). The Young modulus for each sand layer is estimated by Eq. 19 taking the average normalized  $N_{60}$  blow counts in Table 4. Other input parameters to the numerical analysis are listed in Table 5.

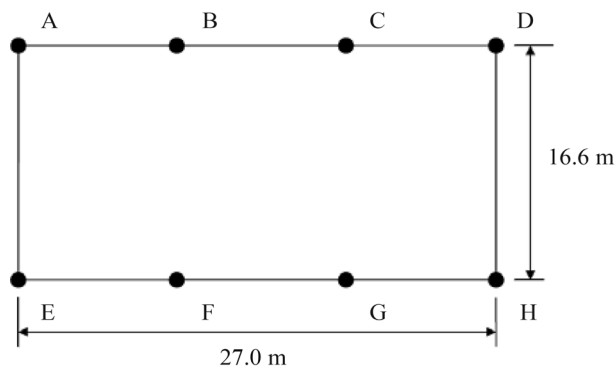


Figure 7 - Raft dimensions and location of the instrumentation points.

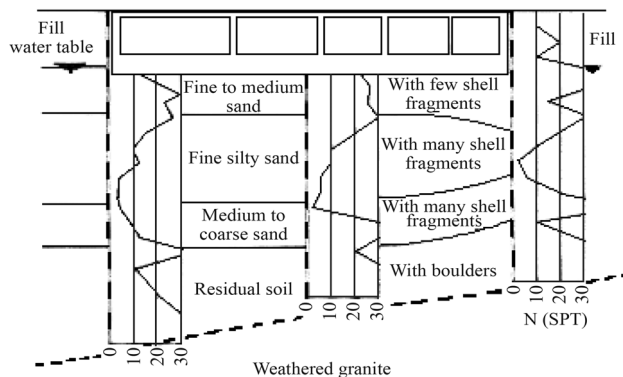


Figure 8 - Soil profile, Lopes et al. (1994).

Table 4 - Deformation parameters for the sand deposit.

Layer	Average thickness (m)	Normalized blow count $N_{60}$	Young modulus $E_s$ (kN/m <sup>2</sup> )
Sand 1	3	22	95000
Sand 2	2	18	80000
Sand 3	2	10	50000
Sand 4	2	4	24000
Sand 5	2	6	34000
Sand 6	1	17	77000

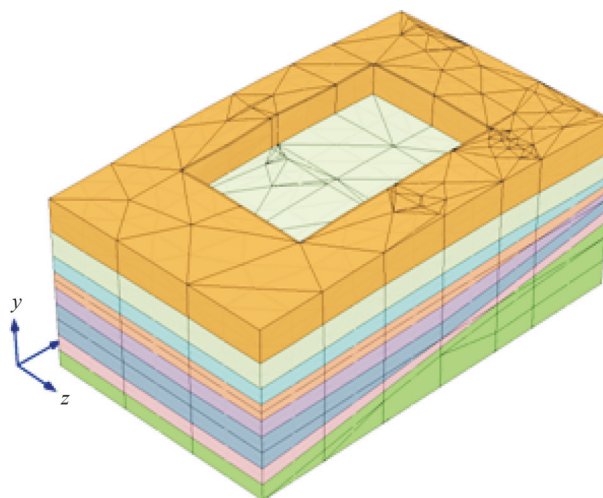


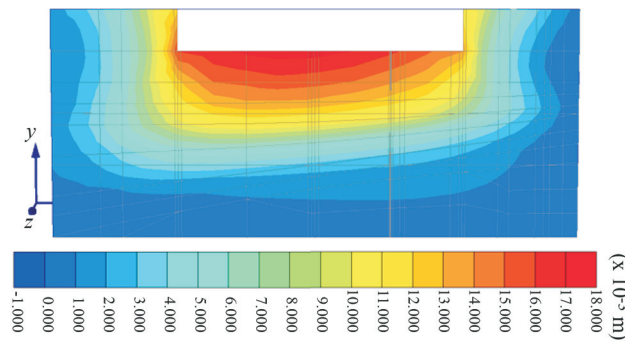
Figure 9 - Raft bearing on multilayered sand deposit.

In Table 5,  $\gamma_t$  is the total (saturated) unit weight,  $\gamma_h$  the natural (non saturated) unit weight,  $\nu$  the Poisson ratio,  $c$  the cohesion and  $\phi$  the friction angle.

Figure 10 shows the displacement contours at a longitudinal cross section passing through the center of the raft. The measured and the calculated displacements at the instrumentation points are shown in Table 6. It is seen that the calculated values are in reasonably good agreement with

**Table 5** - Input parameters for the FEM analysis (program Plaxis 3-D Foundation).

Layer	$\gamma_t$ (kN/m <sup>3</sup> )	$\gamma_h$ (kN/m <sup>3</sup> )	$E_s$ (kN/m <sup>2</sup> )	$\nu$	$c$ (kN/m <sup>2</sup> )	$\phi$ (°)
Fill	-	18	20000	0.30	5	30
Sand 1	20	-	95000	0.30	1	37
Sand 2	20	-	80000	0.30	1	35
Sand 3	20	-	50000	0.30	1	35
Sand 4	19	-	24000	0.35	1	30
Sand 5	19	-	34000	0.35	1	30
Sand 6	20	-	77000	0.30	1	35
Residual	18	-	200000	0.30	20	37
Raft (concrete)	25	-	$2.5 \times 10^7$	0.20	linear elastic	


**Figure 10** - Displacement contours, longitudinal cross section through the center of the raft.

the measured results at the instrumentation points, whereas the average settlement (15.06 mm) coincide.

Equation 19 may also be useful to estimate the oedometric modulus  $E_o$  in sands. From the theory of elasticity:

$$E_o = \frac{E_s(1-\nu)}{(1-2\nu)(1+\nu)} \quad (20)$$

Combining Eqs. 19 and 20 for  $\nu = 0.3$ :

$$E_o \cong 1.35 \cdot E_s = 10800 \cdot N_{60}^{0.80} \quad (21)$$

Equation 22 below and Eq. 21 are used to estimate the one-dimensional settlement ( $r$ ) of the 6-layer sand in Fig. 9 under the raft pressure  $\Delta p = 123 \text{ kN/m}^2$ .

$$r = \sum_{i=1}^6 \frac{\Delta p \cdot h_i}{E_{oi}} \quad (22)$$

The thicknesses  $h_i$ , the oedometric moduli  $E_{oi}$  and the settlement  $r_i$  for each sand layer are shown in Table 7. The estimated total settlement is  $r = 22.87 \text{ mm}$ . This is higher than the average measured settlement of 15.06 mm due to the assumption of infinite loading and also because Eq. 22 does not consider the confinement provided by the 4-m

**Table 6** - Measured vs. calculated settlements.

Point	Settlement (mm)		
	Measured	Calculated (3-D FEM analysis)	Deviation from mean settlement (%)
A	19.5	14.5	33.20
B	17.5	15.5	13.28
C	12.5	14.0	-9.96
D	9.8	12.0	-14.61
E	20.0	16.5	23.24
F	17.5	18.0	-3.32
G	13.7	17.0	-21.91
H	10.0	13.0	-19.92
Average	15.06	15.06	

high fill and the stiffness of the raft (both accounted for in the FEM analysis).

To account for those effects, the following equation from the theory of elasticity modified by Barata (1962, 1984, 1986) is used:

$$r = \frac{\lambda \cdot c_{\Delta} \cdot \Delta p \cdot B \cdot (1-\nu^2) \cdot I}{E_s} \quad (23)$$

The following values are plugged in Eq. 23 (Barata, 1962, 1984, 1986);  $\lambda = 0.96$  (Mindlin's coefficient);  $c_{\Delta} = 1.09$  (shape factor, rigid foundation);  $\Delta p = 123 \text{ kN/m}^2$ ;  $B = 16.6 \text{ m}$  (foundation width);  $\nu = 0.3$  (Poisson ratio);  $I = 0.63$  (influence factor accounting for a rigid boundary about 12 m below the raft);  $E_s = 61500 \text{ kN/m}^2$  (weighted mean static Young modulus, according to Table 4). The settlement estimated by Eq. 23 is  $r = 19.9 \text{ mm}$ . This is about 33% higher than the average FEM predictions (which coincided with the average measured settlement) and 15% lower than the estimated 1-D settlement.

The settlements estimated by the three models above are superimposed on Burland and Burbidge chart in Fig. 11

**Table 7** - Deformation parameters for the sand deposit.

Layer	Average thickness (m)	Normalized blow count $N_{60}$	Oedometric modulus $E_o$ (kN/m <sup>2</sup> )	1-D settlement (mm) (*)
Sand 1	3	22	128045	2.88
Sand 2	2	18	109054	2.26
Sand 3	2	10	68143	3.61
Sand 4	2	4	32739	7.51
Sand 5	2	6	45284	5.43
Sand 6	1	17	104180	1.18
			$\Sigma$	22.87

(\*) Eqs. (21), (22).

(Burland & Burbidge, 1985; Sivakugan & Pacheco, 2011). Considering that Burland and Burbidge chart provides an upper bound for the expected settlements, the results shown in Fig. 11 seem to indicate the adequacy of the estimated Young moduli according to Eq. 19 to calculate the raft settlements.

## 5. Conclusions

This paper presents correlations between the static Young modulus  $E_s$  and the normalized penetration resistance  $N_{60}$  for pure sands, aiming at preliminary settlement predictions. The proposed correlations can also be extended to preliminary estimates of the oedometric modulus  $E_o$  in pure sands.

The correlations in this paper are limited to the statistical interpretation of several results published in the literature. Therefore, practical application of equations and charts presented in this paper should be supported further by load tests and other *in-situ* tests. Eq. 19 is generally suited to applied pressures sufficiently far from failure, as expected in well-designed rafts and foundations for tanks and silos where reasonably low static shearing strains result. For higher shearing strains, it is recommended to select  $E_s$  values below the mean trend equation in Fig. 6. In

contrast,  $E_s$  values above the mean trend curve should be used with increased caution and only when supported by load tests.

The proposed correlations have been used to predict satisfactorily the settlements of a nearly rigid raft supporting the structure of a diesel power generator on sedimentary sand. Good predictions have been obtained by 3-D FEM analysis taking  $E_s$  values from Eq. 19. Reasonable predictions have also been achieved by one-dimensional calculations using the oedometric modulus  $E_o$  (Eqs. 21 and 22) and the elasticity equation modified by Barata (Eq. 23). The results coming from the three models plotted satisfactorily on Burland and Burbidge chart, indicating that the proposed correlations are useful for preliminary estimation of settlements in sedimentary sands.

## References

- Anbzhagan, P. & Sitharam, T.G. (2010) Relationship between low strain shear modulus and standard penetration test N values. *Geotechnical Testing Journal*, ASTM, v. 33:2, p. 1-15.
- Aoki, N. & Cintra, J.C.A. (2000) The application of energy conservation Hamilton's principle to the determination of energy efficiency in SPT tests. *Proc. 6th International Conference on the Application of Stress-Wave Theory to Piles*, São Paulo, pp. 457-460.
- Athanasopoulos, G.A. (1995) Empirical correlations  $V_{so}$  - NSPT for soils of Greece: A comparative study of reliability. *Proc. 7th Int. Conf. on Soil Dyn. Earthquake Engg. Computation Mechanics Publications*, Southampton, pp. 19-25.
- Barata, F.E. (1962) An attempt to rationalize the problem of allowable bearing pressure of shallow foundations (in Portuguese). *Tese de Livre Docência*, Escola Nacional de Engenharia, Universidade do Brasil.
- Barata, F.E. (1984) *Propriedades Mecânicas dos Solos: Uma Introdução ao Projeto de Fundações*. 1ª ed. Livros Técnicos e Científicos, Rio de Janeiro, 152 pp.
- Barata F.E. (1986) *Settlements of Buildings on Shallow Foundations on Soil of Drained Behavior Considering the Structural Rigidity* (in Portuguese). *Tese de Con-*

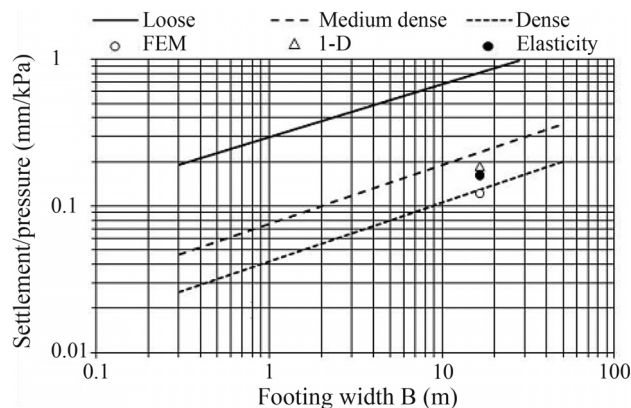


**Figure 11** - Burland and Burbidge chart: upper limits of settlement per unit pressure (Burland & Burbidge, 1985; Sivakugan & Pacheco, 2011).

- curso para Professor Titular, Departamento de Construção Civil, Escola de Engenharia, UFRJ, Rio de Janeiro, 77 pp.
- Barros, J.M.C. (1997) Dynamic shear modulus in tropical soils (in Portuguese). Tese de Doutorado, Escola Politécnica, Universidade de São Paulo, São Paulo, 637 pp.
- Belincanta, A. (1985) Dynamic Energy in SPT: Results from a Theoretical-Experimental Investigation (in Portuguese). Dissertação de MSc, EPUSP, São Paulo, 217 pp.
- Belincanta, A. (1998) Evaluation of the Factors Intervening the Penetration Resistance of the SPT (in Portuguese). Tese de DSc, Escola de Engenharia de São Carlos, Universidade de São Paulo, São Carlos, 141 pp.
- Burland J.B. & Burbidge, M.C. (1985) Settlement of foundations on sand and gravel. ICE proceedings, Part 1, v. 78:6, p. 1325-1381.
- Buzdugan, G. (1972) Dynamique des Foundations de Machines. Éditions Eyrolles, Paris, 438 pp.
- Cavalcante, E.H. (2002) Theoretical – Experimental Investigation of the SPT (in Portuguese). Tese de DSc, COPPE/UFRJ, Rio de Janeiro, 410 pp.
- Conde de Freitas, A. (2010) Contribution to the Study of the 3D Installation and Group Effect of Piles in Sands (in Portuguese). Tese de MSc, Programa de Pós-Graduação em Engenharia Civil, Universidade do Estado do Rio de Janeiro, Rio de Janeiro, 231 pp.
- Danziger, F.A.B.; Danziger, B.R. & Cavalcante, E.H. (2008) Reflections Concerning the Energy in SPT and the Significance of the N Value in Particular Circumstances (in Portuguese). Proc. XIV Congresso Brasileiro de Mecânica dos Solos e Engenharia Geotécnica, Cobramseg, Búzios, 11 pp.
- Décourt, L. (1989) The standard penetration test - State-of-the-art. Proc. XII ICSMFE, Rio de Janeiro, v. 4, pp. 2405-2416.
- Décourt, L.; Belincanta, A. & Quaresma Filho, A.R. (1989) Brazilian experience on spt, supplementary contributions by the brazilian society of soil mechanics. Proc. XII ICSMFE, Rio de Janeiro, pp. 49-54.
- De Mello, V.F.B. (1971) Standard penetration test. In: Proceedings of the IV Panamerican Conference on Soil Mechanics and Foundation Engineering, Porto Rico, v. 1, pp. 1-86.
- Giachetti, H.L.; Mio, G. De; Dourado, J.C. & Malagutti Filho, W. (2006) Comparison of the results of down-hole and cross-hole seismic tests in the experimental research field in UNESP, Bauru (in Portuguese). Proc. XIII Congresso Brasileiro de Mecânica dos Solos e Engenharia Geotécnica - Cobramseg, Curitiba, pp. 669-674.
- Hanumantharao, C. & Ramana, G.V. (2008) Dynamic soil properties for microzonation of Delhi, Índia. J. Earth Syst. Sci., v. 117:S2, p. 719-730.
- ISSMFE (1989) International Reference Test Procedure for the Standard Penetration Test (SPT), In: Report of the ISSMFE - TC 16 - Technical Committee on Penetration Testing of Soils, with Reference Test Procedures - CPT- SPT - DP - WST - pp. 17-19.
- Jafari, M.K.; Shafife, A. & Razmkhah, A. (2002) Dynamic properties of fine grained soils in south of Tehran. Soil Dyn. Earthquake Engg., v. 4:1, p. 25-35.
- Johnsen, L.F. & Jagello, J.J. (2007) Discussion of energy efficiency for standard penetration tests, Journal of Geotechnical and Geoenvironmental Engineering, ASCE, v. 133:4, p. 486-487.
- Kovacs, W.D.; Evans, J.C. & Griffith, A.H. (1977) Towards a More standardized SPT. Proc. IX ICSMFE, Tokyo, v. 2, pp. 269-276.
- Kulhawy, F.H. & Mayne P.H. (1990) Manual on Estimating Soil Properties for Foundation Design. Cornell University, New York, 308 pp.
- Lee, S.H.H. (1990) Regression models of shear wave velocities. Journal of Chinese Institute of Engineers, v. 13:5, p. 519-532.
- Lopes, F.R, Sousa, O.S.N. & Soares, J.E. (1994) Long-term settlement of a raft foundation on sand. Geotechnical Engineering, v. 107:1, p. 11-16.
- Lopes, F.R. (2000) Design of raft foundations on Winkler springs. Hemsley, J.A. (ed) Design Application of Raft Foundation, chap. 5, Thomas Telford, London, pp. 127-154.
- Machado, F.G. (2010) Study of the Behavior of Foundations Submitted to Vibration Machines (in Portuguese). Dissertação de Mestrado, COPPE, UFRJ, Rio de Janeiro, 149 pp.
- Moura, A.S. (2007) Evaluation of Shallow Foundation Design Methodology of Aerogenerators Embedded in Dense Sand (in Portuguese). Tese de Doutorado, publicação G.TD-051/07, Departamento de Engenharia Civil, Universidade de Brasília, Brasília, 323 pp.
- Neter, J.; Wasserman, W. & Whitmore, G.A. (1982) Applied Statistics, 2nd ed. Allyn and Bacon Inc., Boston 743 pp.
- Odebrecht, E. (2003) SPT Energy Measurements (in Portuguese). Tese de D.Sc., UFRGS, Porto Alegre, 230 pp.
- Odebrecht, E.; Schnaid, F.; Rocha, M.M. & Bernardes, G.P. (2005) Energy efficiency for standard penetration tests. Journal of Geotechnical and Geoenvironmental Engineering, ASCE, v. 131:10, p. 1252-1263.
- Ohsaki, Y. & Iwasaki, R. (1973) Dynamic shear moduli and Poisson's ratio of soil deposits. Soils and Foundation, v. 13:4p. 61-73.
- Pacheco, M.P. & Lima, L.S.A. (1996) An statistical criteria for investigation of geotechnical tests (in Portuguese). Solos e Rochas, v. 19:3. p. 177-188.
- Palacios, A. (1977) Theory and Measurements of Energy Transfer During Standard Penetration Test Sampling. Ph.D. Thesis, University of Florida, Gainesville, 391 pp.

- Petrobrás (2008) N 1848 REV. B– Design of Machine Foundations. CONTEC – SC-04. 51 pp. Projeto de Fundações de Máquinas.
- Richart, F.E.; Hall, J.R. & Woods, R.D. (1970) *Vibrations of Soils and Foundations*, Prentice-Hall, Inc. Englewood Cliffs, New Jersey, 414 pp.
- Robertson, P.K.; Wride, C.E.; List, B.R.; Atukorala, U.; Biggar, K.W.; Byrne, P.M.; Campanella, R.G.; Cathro, D.C.; Chan, D.H.; Czajewski, K.; Finn, W.D.L.; Gu, W.H.; Hammamji, Y.; Hofmann, B.A.; Howie, J.A.; Hughes, J.; Imrie, A.S.; Konrad, J.-M.; Küpper, A.; Law, T.; Lord, E.R.F.; Monahan, P.A.; Morgenstern, N.R.; Phillips, R.; Piché, R.; Plewes, H.D.; Scott, D.; Sego, D.C.; Sobkowicz, J.; Stewart, R.A.; Watts, B.D.; Woeller, D.J.; Youd, T.L. & Zavodni, Z. (2000) The CANLEX project: summary and conclusions. *Canadian Geotechnical Journal*, v. 37:3 p. 563-591.
- Schmertmann, J.H. & Palácios, A. (1979) Energy dynamics of SPT. *Journal of the Soil Mechanics and Foundation Division, ASCE*, v. 105:GT8, p. 909-926.
- Seed, H.B.; Idriss, I.M.; Arango, I. (1983) Evaluation of liquefaction potential using field performance data. *Journal of Geotechnical Engineering*, v. 109:3, p. 458-482.
- Silveira, R.M. da S.; Barros, J.M. de C. & Amaral, C. dos S. (2006) Shear Modulus Decrease with Deformation of a Remoulded Marine Clay (in Portuguese). *Proc. XIII Congresso Brasileiro de Mecânica dos Solos e Engenharia Geotécnica - Cobramseg, Curitiba*, 6 pp.
- Sitharam, T.G.; Govindaraju, L. & Sridharan, A. (2004) Special section: Geotechnics and Earthquake Hazards Dynamic properties and liquefaction potential of soils. Department of Civil Engineering, Indian Institute of Science, Bangalore, India. *Current Science*, v. 87:10 p. 1370-1378.
- Sivakugan, N. & Pacheco, M. (2011) Design of shallow foundations. Das, B. (ed), *Geotechnical Engineering Handbook*, Chapter 3, Ross Publishers, Florida, pp. 302-355.
- Skempton, A.W. (1986) Standard penetration test procedures and the effects in sands of overburden pressure, relative density, particle size, ageing and overconsolidation. *Géotechnique*, v. 36:3, p. 425-447.
- Sykora D.W. & Stokoe K.H. (1983) Correlations of in situ measurements in sands of shear wave velocity, soil characteristics, and site conditions. In: University of Texas. *Geotechnical Engineering Report: GR 83-33*, Austin, 484 pp.
- Wride, C.E. & Robertson, P.K. (1997) *CANLEX, The Canadian Liquefaction Experiment*. 5 volumes. Bi Tech Publishers Ltd, Canada, 1082 pp.
- Wride, C.E.; Robertson, P.K.; Biggar, K.W.; Campanella, R.G.; Hofmann, J.M.O.; Hughes, J.M.O.; Kupper, A. & Woeller, D.J. (2000) Interpretation of in situ test results from the CANLEX sites. 2000. *Canadian Geotechnical Journal*, v. 37, p. 505-529.

# The Influence of the Relative Density of Sands in SPT and CPT Correlations

J.M.S. Souza, B.R. Danziger, F.A.B. Danziger

**Abstract.** Correlations between CPT and SPT in sands are presented in this paper for different sand densities. Such proposition is based on the experience obtained with the use of piezocone whose penetration in sands occurs commonly under drained condition. The SPT penetration, on the other hand, is much faster, occurring under a partially drained condition. Due to the high loading velocities, much higher than that of the CPT, the SPT test can generate positive excess pore pressures in loose sands and negative excess pore pressures in dense sands. In this way, the  $N$  value may be higher than if the test were carried out in a drained condition, for dense sands, and smaller for loose sands. The same does not occur for the  $q_c$  value of CPT. So, the trend would be of greater  $q_c/N_{60}$  ratio for loose sands than for dense sands with the same grain size distribution. The results confirm distinct correlations for different sand densities. The  $q_c/N_{60}$  ratio of 0.5 MPa/blows/0.30 m for sands, obtained from Danziger & Velloso (1995) regardless of the sand density, is consistent with the value obtained in the present research for the whole data, if no distinction of density is made. For distinct sand densities, the  $q_c/N_{60}$  ratio was found to be 0.7; 0.5; and 0.4 MPa/blows/0.30 m, respectively for loose, medium and dense sands. While most of the correlations in the literature depend only on grain size, the results presented in this paper show that the sand density is of fundamental importance and should also be considered to interpret CPT and SPT correlations.

**Keywords:** SPT, CPT, correlations, sands, relative density.

## 1. Introduction

CPT and SPT correlations have practical applications in many geotechnical areas, especially in foundation design.

The existing correlations between cone tip resistance,  $q_c$ , and SPT  $N$  value in sedimentary sands are usually based solely on soil grain size (Fig. 1).

In fact, the suggestion of Robertson *et al.* (1983) is quoted extensively in the literature. This is shown in Fig. 1, together with data obtained by Politano *et al.* (1998, 2001) and Viana da Fonseca & Coutinho (2008) for residual soils. The figure shows that the data obtained in residual soils do not follow the trend shown by Robertson *et al.* (1983).

Mitchell & Brandon (1998) emphasized that the ratio  $q_c/N_{60}$  does not correlate uniquely with mean grain size ( $D_{50}$ ). They suggest that site specific determinations should be developed if a  $q_c/N_{60}$  value is needed so that it results can be used with  $N_{60}$  value property correlations, or vice versa. Mitchell & Brandon (1998) quoted Kulhawy & Maine (1990), as shown in Fig. 2, with a rather broad band when a large number of data points from tests at many sites are examined.

Mitchell & Brandon (1998) pointed out that the  $q_c/N_{60}$  based on mean particle size may involve significant uncertainty. They suggested that site specific  $q_c/N_{60}$  values based on median values for relatively thick homogeneous layers may be more reliable.

The use of the piezocone, instead of the CPT, brings a new feature to the correlation analysis, since the pore pressure is also measured. In fact, it is generally accepted that the piezocone tests in sands occur in a drained condition, which is easy to verify with the pore-pressure measurement. On the other hand, the much faster velocity in the SPT procedure, even in sands, results in a test condition usually considered as partially drained (*e.g.* Youd *et al.*, 2001).

The main objective of the present paper is to show an alternative interpretation of CPT and SPT correlations by taking into account distinct sand densities.

The SPT is more influenced by the change in shear stresses than normal stresses. Due to a much higher loading velocity, the SPT generates positive excess pore pressures in loose sands and negative excess pore pressures in dense sands. As a result, the  $N$  value may be higher than if the test were carried out in a drained condition, for dense sands, and smaller for loose sands. The same does not occur for the  $q_c$  value of CPT. Therefore, the trend would be of greater  $q_c/N_{60}$  ratio for loose sands than for dense sands with the same grain size distribution. Taking these points into consideration, the paper presents and discusses the correlations obtained in sedimentary sandy layers of variable relative densities. The data have been selected from sites where the database has been extracted from layers of high thickness and a satisfactory soil characterization has been available.

J.M.S. Souza, MSc, Engenheiro Civil, Universidade do Estado do Rio de Janeiro, Rio de Janeiro, RJ, Brazil. e-mail: jeffson\_souza@hotmail.com.

B.R. Danziger, Associate Professor, Departamento de Estruturas e Fundações, Faculdade de Engenharia, Universidade do Estado do Rio de Janeiro, Maracanã, RJ, Brazil. e-mail: brdanzig@uerj.br.

F.A.B. Danziger, Associate Professor, COPPE and Escola Politécnica, Universidade Federal do Rio de Janeiro, Rio de Janeiro, RJ, Brazil. e-mail: danziger@coc.ufrj.br.

Submitted on August 25, 2011; Final Acceptance on April 4, 2012; Discussion open until September 30, 2012.

The data from the tests in layers of small thickness or containing sandy soils with high percentage of fines have been discarded. The inclusion of these data could compromise the quality of the analysis, which aimed to determine the influence of relative density of pure sands or sands with low fines content in the correlations.

In fact, Mitchell & Brandon (1998) also reported that the presence of layers of different density and strength within a soil profile may have a significant influence on the measured values of cone penetration resistance. According to them, the cone “senses” the presence of a different underlying layer when it reaches a few diameters of the layer boundary. The layer effect is likely to be conservative in

that the measured resistance of dense layers will be lower than its real value, whereas that measured in loose layers will be reasonably close to the correct value. The authors also pointed out that the layer effect could lead to incorrect soil identification if tip and friction ratio based classification charts are used.

Depending on the SPT equipment, the actual energy delivered by the rods may also influence the test results. Faster automatic equipments may present different conditions from manual equipments routinely used.

## 2. Geotechnical Characterization of the Test Sites

Most interpretations of the soil stratification profile have been based on soil classification from SPT samples or obtained indirectly from the piezocone results. It is worth emphasizing that Robertson & Campanella (1983) reported that tests conducted by Schmertmann (1978) in calibration chambers showed that the cone tip senses an interface region between 5 and 10 cone diameters ahead and behind the tip. Robertson & Campanella (1983) called attention to the fact that if the sandy layer has a thickness less than about 70 cm and is located between two soft clay deposits, the cone penetration resistance may not reach its full value within the sand because of the close proximity of the adjacent interfaces. In fact, Mitchell & Brandon (1998) also reported that the presence of layers of different density and strength within a soil profile may have a significant influence on the measured values of cone penetration resistance. According to them, the cone “senses” the presence of a different underlying layer when it reaches a few diameters of the layer boundary. In the present analysis all data from layers with thickness smaller than 1 m has been discarded. Table 1 lists the locations of the sites whose data have been included in the database.

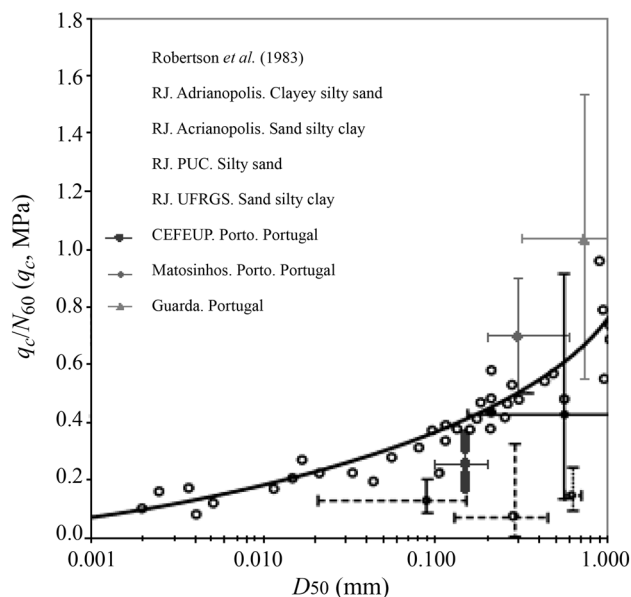


**Figure 1** -  $q_c/N_{60}$  and  $D_{50}$  relationship from Robertson et al. (1983) with data from residual soils, extracted from Politano et al. (1998, 2001) and Viana da Fonseca & Coutinho (2008).

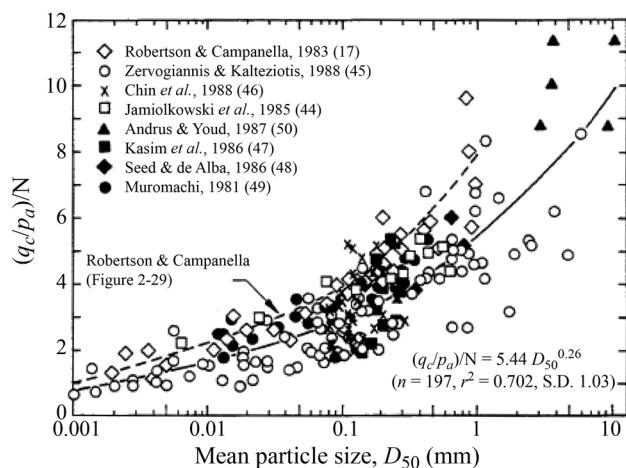


**Figure 2** -  $q_c/N$  correlations based on mean particle size from Kulhawy & Mayne (1990), as quoted by Mitchell & Brandon (1998).

**Table 1** - Sites from the database.

Region	Site
Brazil	Port of Açú - São João da Barra, Rio de Janeiro
	Presidente Dutra Highway km 36 - Queimados, Rio de Janeiro
	Industrial Construction in Rio de Janeiro West Zone
	Presidente Dutra Highway, km 163 to 165 Jacareí, São Paulo
USA	University of Florida
	San Francisco Bay
Canada	Mildred Lake Settling Basin - Syncrude
	Massey and Kidd - Fraser River Delta
	J-Pit - Syncrude
	LL Dam and Highmont Dam - HVC Mine

### 2.1. Port of Açú - RJ

The Port of Açú is located in São João da Barra, 30 km from Campos dos Goytacazes, in the State of Rio de Janeiro. The Port of Açú will have an important role to export Brazilian ore.

Several SPT test and nine piezocone tests have been performed in part of the site. The soil profile in this region shows a thick superficial layer of sand, up to 10 to 15 m deep, over a layer of organic clay of low strength with 5 m thick. Underlying the clay occur layers of high density sands.

### 2.2. President Dutra Highway, km 36 - Queimados - RJ

This area of the highway is located in the town of Queimados, nearly 40 km from the City of Rio de Janeiro.

Five vertical adjacent SPT and CPT tests have been performed. No laboratory tests have been available to better characterize the investigated soils.

The geotechnical profile consists of a superficial low strength clay layer, 2.5 m thick, overlying a sandy deposit of medium to high density 14 m thick. Below that depth residual soils can be found. In some borings small layers of very soft clay are present, between the sandy layers.

### 2.3. Industrial construction in the Rio de Janeiro West Zone

The soil profile in this site consists of a sedimentary superficial soft clay deposit of low consistency, nearly 14 m thick, over the sandy stratum with thicknesses ranging from 6 to 20 m. Small lenses of very soft clay are present, within the sand deposit.

### 2.4. President Dutra Highway - Jacareí - SP

In the President Dutra highway, close to the city of Jacareí, State of São Paulo, CPTU tests have been performed in the central region of the highway and at each side, forming 4 transversal sections to the axis of the highway. A total of eight CPTU tests have been included in the database.

The tests aimed at characterizing the quaternary sediments presented at the site. Adjacent to the CPT tests, SPT tests have also been performed. The SPT blow counts were obtained every 0.5 m depth. Some samples collected by the surveys were submitted to grain size tests. It has been possible, then, to verify the low content of fines in the sandy soil away from the boundary of the neighboring layers.

The CPTU tests have been performed in previously leveled ground next to the SPT tests. Therefore, the reference depths were the same both for the CPTU and SPT tests.

Figure 3, extracted from Danziger *et al.* (1998), illustrates the local geotechnical profile and compares SPT 17 and CPTU 6. The soil of the upper sand layer, between 7.5 to 8 m depth, is composed of 34% of soil passing through 200 # sieve, 56% of fine sand and 10% of medium sand.

However, even with the great predominance of the sandy fraction, excess pore-pressure has been developed, including negative pore-pressure, indicating undrained or partially drained behavior. The second layer of sand, on the other hand, between 8 to 10 m depth, presented a drained behavior. The grain size distribution of the material shows only 2% passing through 200 # sieve, 12% of fine sand, 71% of medium sand and 15% of coarse sand. The drained behavior is therefore fully justified.

This figure helps to explain the importance of verifying carefully the data points before including them in the database, as the authors intended to do.

### 2.5. University of Florida - USA

These data were obtained by Palacios (1977) at three sites on the campus of the University of Florida. Palacios' research accounted for energy measurements in SPT tests.

In the three sites the soil profile indicated superficial sandy layers of great thickness. Atterberg limits and grain size analyses were performed with indication of soil classification by the unified system. In the three sites the most superficial layer was classified as SP, which corresponds to a sandy soil with less than 5% of fines, poorly graded. The underlying sandy layer, on the other hand, was classified as SC - SP in sites A and B. This means that there are parts of sandy clay, SC, with more than 12% of fines and parts of sand with less than 5% of fines, poorly graded. On site C the whole soil profile is sandy, with the lower layer containing sands classified as SC, with more than 12% of fines.

Palacios (1977) performed CPT tests, not CPTU tests. Moreover, Palacios (1977) did not include, for the whole database, the grain size characteristics of the sandy soil. It was not possible to discard the data from sands containing high fines content. An aspect that motivated the authors to analyse Palacios (1977) data was the fact that the SPT have been performed with the sampler with liner removed. With the removal of the liner, the internal friction in the sample is smaller, resulting in a lower  $N$  value. The authors expectation was that the ratio  $q_c/N_{60}$  would be greater with the use of the sampler with the liner removed. The authors decided to analyze the data from Palacios (1977) in order to verify if the higher values of the ratio  $q_c/N_{60}$  would be also sensitive to the relative density of the sand. However, data from Palacios (1977) were not included in the global analysis, as is further emphasized in the paper.

### 2.6. San Francisco Bay - USA

The soil profile where Kasim *et al.* (1986) conducted their experiments consisted of a deposit of sand from a recent hydraulic landfill (pumped 16 years before), 5.5 m thick, overlying a deposit of natural Pleistocene sand. The hydraulic fill was classified as SM, silty sand, with nearly 10% of fines. The natural sand deposit was classified as SM, silty sand, and occasionally as SM-SC, clayey silty sand, with fine content of the order of 20%.

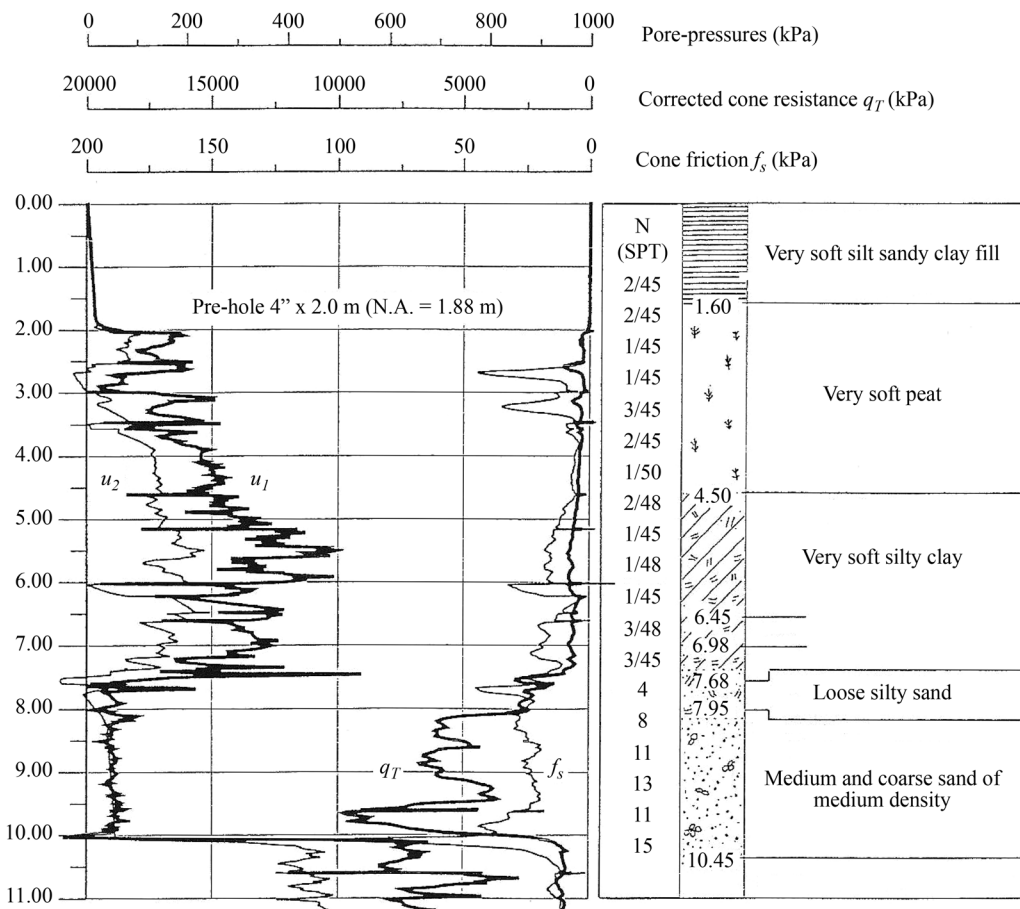


Figure 3 - Comparison between the SPT-17 test and CPTU 6 (Danziger et al., 1998).

The tests have been performed with electrical cone, without the measurement of pore-pressure.

It should be emphasized that the authors have found the same trend of Robertson & Campanella (1983): the reduction of  $q_c/N_{60}$  with  $D_{50}$ , as in Fig. 1, but with a large dispersion. The authors attributed the large dispersion to the variability found in the penetration tests and also in other soil properties not completely defined by grain size. The soil properties not completely defined by grain size distribution also support Mitchell & Brandon (1998) feelings. It also justifies the idea that motivated the main objective of this paper: to investigate the effect of relative density in the  $q_c/N_{60}$  correlation in sands.

2.7. Canlex - Canadá

Wride et al. (2000) and Robertson et al. (2000) summarize the Canlex project (The Canadian Liquefaction Experiment), a research project developed over a period of 5 years, whose main objective was to study the phenomenon of liquefaction of soil, likely to occur in saturated sandy soils, characterized by a large shear strength and soil stiffness loss resulting in significant deformation.

Canlex research project was divided into phases, each phase representing a new location or a different purpose.

Each phase included a series of activities, with many field and laboratory tests being performed. Only the data of interest to the present analysis have been obtained from the Canlex reports and included in the database.

The deposits of sand covered in the Canlex research project are from the Holocene (less than 11,000 years old). The age of the deposits ranges from 2 months to 4,000 years. Table 2 illustrates the different ages of the deposits analyzed. They consist of normally consolidated sands without cementation, composed mainly of quartz grains with small amount of feldspar and mica. They are

Table 2 - Ages of each deposit of CANLEX research (Robertson et al., 2000).

Phase	Location	Site	Deposit Age
I	Syncrude	Mildred Lake	12 years
II	Fraser River delta	Massey	200 years
		Kidd	4,000 years
III	Syncrude	J-Pit	2 months
IV	HVC Mine	LL Dam	5 years
		Highmont Dam	15 years

uniform sands, with  $D_{50}$  ranging from 0.16 to 0.25 mm and generally containing percentage of fines less than 15%, with some samples showing fines content less than 5%.

Table 3, taken from Robertson *et al.* (2000), illustrates the main characteristics of the various deposits, allowing the observation that it consists, in general, of deposits with low fines content.

Energy measurements have been performed in SPT tests. The energy measured in the 6 sites of the research ranged from 50 to 80%.

The ISSMFE (1989) has established 60% of the theoretical potential energy as the international reference. Once performed the SPT test, the  $N$  value must be converted to  $N_{60}$  by the expression:

$$N_{60} = N \frac{E}{E_{60}} \quad (1)$$

where  $E$  = measured energy corresponding to  $N$  value and  $E_{60}$  = 60% of the theoretical potential energy of 474 J (ISSMFE, 1989).

Energy correction has been made from the efficiency obtained from each  $N$  value included in the database.

### 3. Description of the Criteria for Data Selection

#### 3.1. Grain size

The authors discarded the soil data with finer content higher than 12%. According to Souza Pinto (2000), the behavior of sands with finer content of this order is determined by the contact between grains. On the other hand, sands with higher percentage of fines usually have their behavior most influenced by the clay fraction, and their behavior is much more similar to that of clays.

#### 3.2. Layer thickness

Data obtained from layers of sands of low thickness were not considered appropriate. In such cases the data are influenced by adjacent layers, mainly in presence of thin soils, especially soft clays, as quoted by Mitchell & Brandon (1998) and Robertson & Campanella (1983), already cited. Horizons of small thickness were present in most sites. In such situations, the presence of higher fines content

is evident, indicating an undrained behavior in the piezocone test.

### 3.3. The $B_q$ parameter

In the absence of the characterization tests for most data, the pore-pressure parameter  $B_q$  from the piezocone is an important tool in verifying the soil behavior.

Senneset & Janbu (1984) have a proposal for soil classification based on the corrected cone resistance,  $q_T$ , and the pore-pressure parameter  $B_q$ . This proposal is based on the fact that the generation of excess pore-pressure is an excellent indication of the type of soil penetrated.

The authors made use of the  $B_q$  parameter (Eq. 2) in cases where grain size analyses were not available in order to decide if the results would be incorporated into the database. The authors made use of the classification procedure from Senneset *et al.* (1989) and also that from Robertson *et al.* (1986), Figs. 4 and 5.

$$B_q = \frac{u - u_0}{q_T - \sigma_{v0}} \quad (2)$$

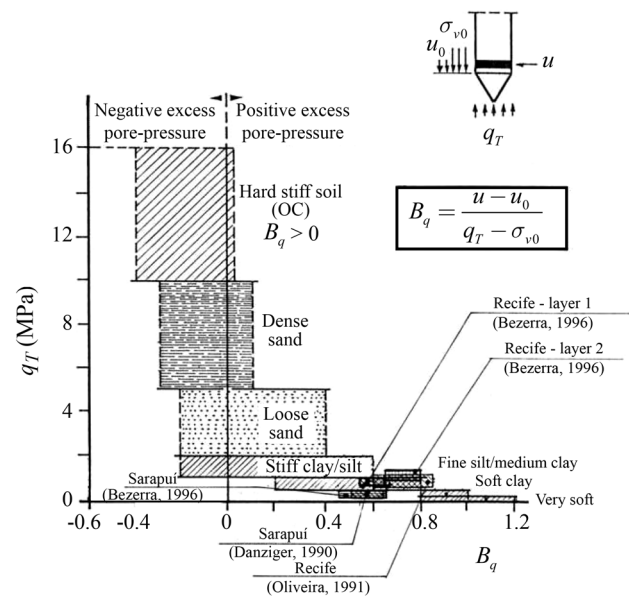
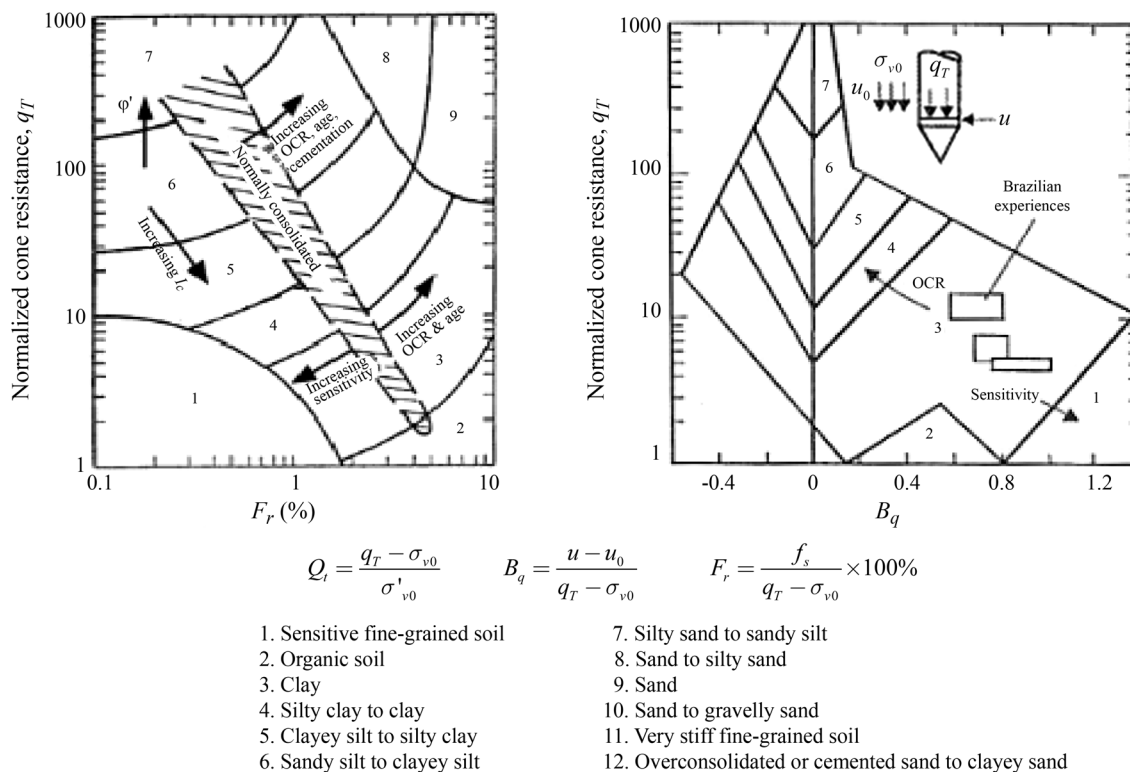


Figure 4 - Soil classification by Senneset *et al.* (1989), including data from Bezerra (1996) and Oliveira (1991), as quoted by Danziger & Schnaid (2000).

Table 3 - Index properties of CANLEX deposits (Robertson *et al.*, 2000).

Local	$e_{max}$	$e_{min}$	$G_s$	$D_{50}$ (mm)	$C_u (D_{60}/D_{10})$	% fines < # 200 mm
Mildred Lake	0.958	0.522	2.66	0.15	2.22	≈10
Massey	1.100	0.700	2.68	0.20	1.57	< 5
Kidd	1.100	0.700	2.72	0.20	1.78	< 5
J-Pit	0.986	0.461	2.62	0.17	2.50	≈15
LL Dam	1.055	0.544	2.66	0.20	2.78	≈8
Highmont Dam	1.015	0.507	2.66	0.20	4.00	≈10



**Figure 5** - Proposal for classification of soils from Robertson *et al.* (1986), including the Brazilian experience, as cited by Schnaid (2000).

where  $u$  is the pore-pressure measured at the base of the cone,  $u_0$  is the hydrostatic pressure and  $\sigma_{v0}$  is the total vertical stress (see Fig. 4).

Meireles (2002) reports that Robertson & Campanella (1983) consider the determination of the soil profile as the main application of the CPTU data. The authors commented that traditionally the soil classification has been related to the tip resistance,  $q_c$ , and friction ratio,  $(f_s/q_c) * 100\%$ ,  $f_s$  being the side friction. Several charts have been developed based on the fact that sandy soils usually present high tip resistance and low friction ratio, while clayey soils often present low tip resistance and high friction ratio.

Robertson *et al.* (1986) proposed the simultaneous use of two diagrams for soil classification, Fig. 6. The first is a graph of corrected cone tip resistance vs. friction rate,  $(f_r/q_T), f_r$  being the corrected lateral friction. The second is a graph of corrected cone tip resistance vs. pore-pressure parameter,  $B_q$ . According to the authors, occasionally a particular soil can be classified in different ways in both graphs. In fact, in such circumstance a more appropriate analysis is necessary in order to classify the soil in a satisfactory way. The authors reported that both the rate and the way in which the excess pore-pressure dissipates during an interruption in the penetration are of help in soil classification.

In the present paper the authors discarded the  $B_q$  values outside the interval (-0.1, +0.1) in order to assure a drained behavior for the soil under analysis.

According to Meireles (2002), Robertson (1991) modifies the second graph in order to incorporate more negative values of  $B_q$ , Fig. 7. According to the author this modification provides a better fit for many of the prior experience. The author also included in the same graph the Zone 2 for organic soil and peat, which was missing in the original published graph.

#### 4. The Correspondence of the Two Tests

Using the same procedure adopted by Politano (1999) and Politano *et al.* (1998, 2001), aiming at analyzing the values of  $q_T$  and  $N$  in the same depths, the  $q_T$  were taken at each meter depth plus 0.30 m. This follows from the fact that the  $N$  values are measured between the depths of A +0.15 m and A +0.45 m, being A an entire number corresponding to a given depth, *i.e.*  $N$  corresponds to an average depth of A +0.30 m, as shown in Fig. 8.

At this way, the  $N$  value for the last 0.30 m of penetration ( $N$ ) was obtained directly from the boring report, while in the piezocone tests the values of  $q_T$  were considered corresponding to A +0.30 m depth, following the trend of the  $q_T$  curve, avoiding the use of discrepant results.

#### 5. Data Handling

The data were grouped according to the relative density of the sand.

The relative density was estimated considering the influence of the vertical effective stress. First, the value of  $N_{60}$ , the number of blows related to the standard energy of

60% of the theoretical potential energy, was estimated from the Eq. 3. For the Brazilian data, the value of 1.37 in Eq. 3 is an average value based on energy measurements carried

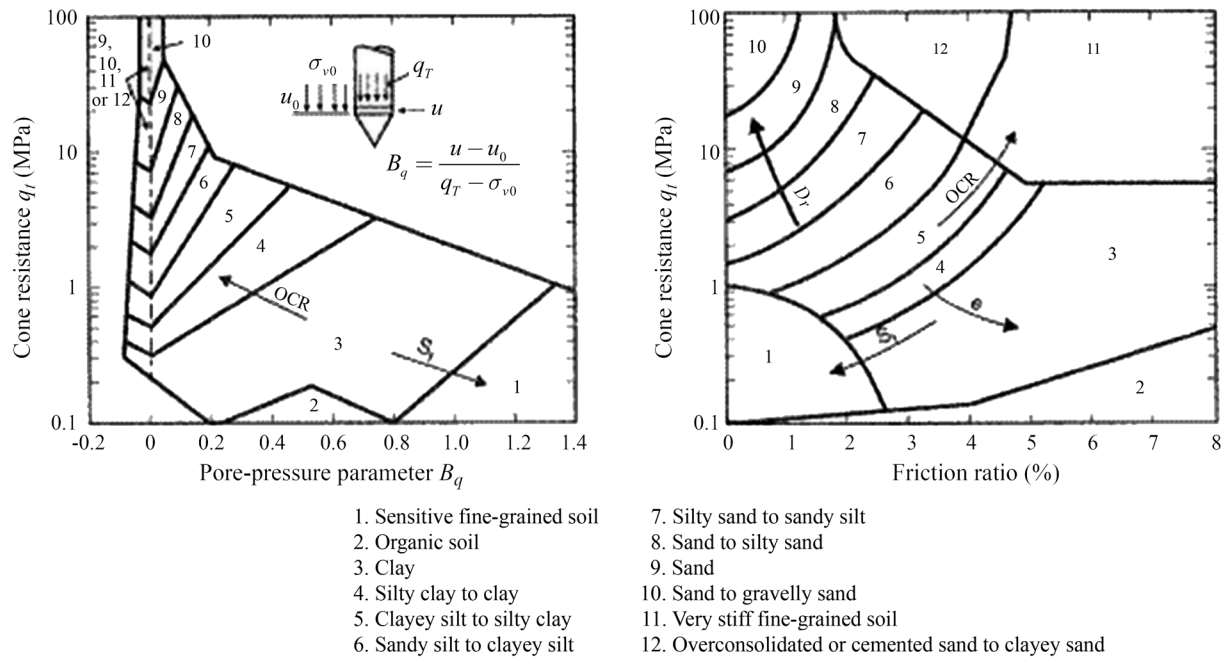


Figure 6 - Proposal for soil classification. Robertson *et al.* (1986).

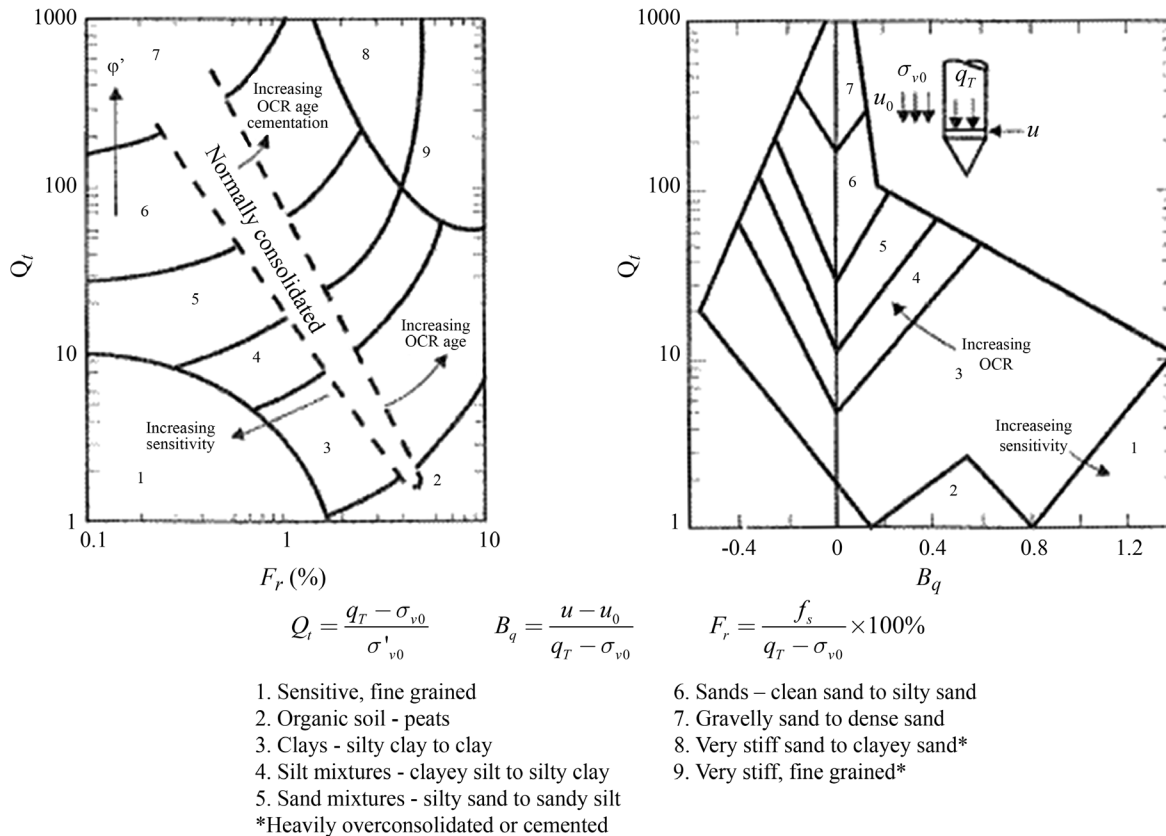
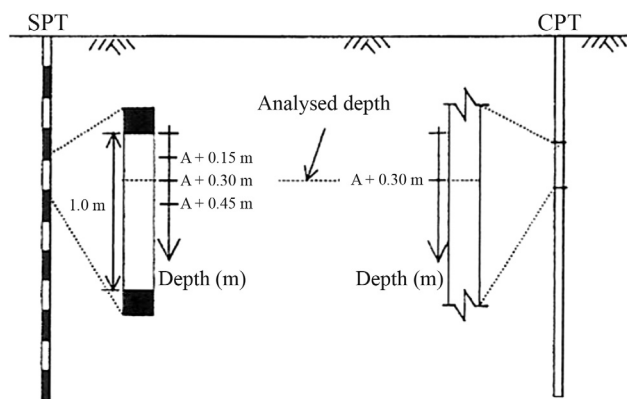


Figure 7 - Proposal for soil classification - Robertson (1991).



**Figure 8** - Illustration showing how the data have been obtained (extracted from Politano (1999) and Politano et al. 1998, 2001).

out in equipments used routinely in Brazil (e.g., Belincanta, 1985, 1998, Cavalcante, 2002, Odebrecht, 2003, Odebrecht et al., 2005).

$$N_{60} = 1.37N_{SPT} \quad (3)$$

From  $N_{60}$ , the value of  $(N_1)_{60}$  were estimated, which means the value of  $N_{60}$  normalized for a vertical effective stress of 100 kPa, through Eq. 4:

$$(N_1)_{60} = C_N N_{60} \quad (4)$$

where  $C_N$  is given by Eq. 5, from Seed & Idriss (1982). Kaeyn et al. (1992) recommend that the value of  $C_N$  should not exceed 1.7.

$$C_N = \frac{2.2}{\left(1.2 + \frac{\sigma'_{v0}}{p_a}\right)} \quad (5)$$

In Eq. 5,  $\sigma'_{v0}$  is the vertical effective stress and  $p_a$  is a reference pressure of 100 kPa. After the estimation of  $(N_1)_{60}$ , the relative density  $D_r$  is obtained from Eq. 6 from Kulhawy & Mayne (1990).

$$\frac{(N_1)_{60}}{D_r^2} = 60 + 25 \log D_{50} \quad (6)$$

The value of  $D_{50}$  for use in Eq. 6 was based on results of particle size distribution, when available. In cases where there was no information on the soil particle size, the value of  $D_{50}$  was estimated as 1 mm.

It should be noted that the Eq. 6 refers to a normally consolidated and not aged deposit. The second term of the expression represents the factor  $C_p$ , relative to the size of the particles.

Some investigations have been made by conducting some analysis including an equation that contains the age of the deposit, also reported by Kulhawy & Mayne (1990). As this information was not available in most of the database, a sensitivity analysis has been made in order to verify the influence of the age on relative density. The influence of the

age is given by the factor  $C_A$ , which must be applied according to the Eq. 7, the factor  $C_{ov}$  in Eq. 8 being related to over consolidation and the factor  $C_p$  due to the particle size.

$$C_A = 1.2 + 0.05 \log \left( \frac{t}{100} \right), t \text{ in years} \quad (7)$$

$$D_r^2 = \frac{(N_1)_{60}}{C_A \cdot C_p \cdot C_{ov}} \quad (8)$$

Considering a deposit with ages ranging from 1 to  $10^8$  years, in comparison to a not aged deposit, the results are shown in Table 4. The difference in the estimation of relative density for a value of  $(N_1)_{60} = 20$  is also shown in Table 4. It can be observed that a change in age from 1 to  $10^8$  years represents an increase of 36% in the  $C_A$  factor, resulting in a reduction of only 0.08, or 8%, on the relative density. Although these changes, if incorporated into the database, would cause a small increase in the number of data of sands with lower relative density and a small reduction in the number of data corresponding to sands of greater relative density, its influence in the  $q_c/N_{60}$  ratio is not significant at all. For the deposits with age information available, its influence has been considered in the determination of the relative density.

With the value of the relative density determined by Eq. 8, the data were classified according to Table 5, obtained from Terzaghi & Peck (1967).

**Table 4** - Sensitivity analysis of the influence of the factor  $C_A$  in  $D_r$ .

$t$ (years)	$C_A$	$D_r^2$
1	1.10	0.30
10	1.15	0.29
$10^2$	1.20	0.28
$10^3$	1.25	0.27
$10^4$	1.30	0.26
$10^5$	1.35	0.25
$10^6$	1.40	0.24
$10^7$	1.45	0.23
$10^8$	1.50	0.22

**Table 5** - Relative density of the sands (Terzaghi & Peck, 1967).

Relative density	$D_r$ (%)
Very loose	0 a 15
Loose	15 a 35
Medium	35 a 65
Dense	65 a 85
Very dense	85 a 100

## 6. Testing Data

### 6.1. For each site

In establishing the correlations 41 SPT tests and 41 CPTU have been considered, including 319 data points ( $N_{60}$ ,  $q_T$ ),  $N_{60}$  being the corrected  $N$  value for an efficiency of 60% and  $q_T$  the corrected cone resistance. In most cases these data corresponded to metric intervals, since this is the usual practice in Brazil. It should be noted that the value of  $q_T$  in the case of sands is almost equal to  $q_c$ . For this reason, the designation  $q_c$  is also used in the present paper.

A linear correlation passing through the origin was initially established. According to Bussab (1988), the equation that determines the angular coefficient  $K_c$  of the linear correlation passing through the origin is given by:

$$K_c = \frac{\sum N_{60} q_c}{\sum (N_{60})^2} \quad (9)$$

In cases of small number of data (less than 9 data sets) the correlation has not been established. It has been preferred to calculate only the average value of the statistical distribution of the ratio  $q_c/N_{60}$ , designated as  $K_m$ . Souza

(2009) presented the results in tables and graphs. In the present paper the results are only shown graphically. In Figs. 9 to 15 the values of  $K_c$  and  $K_m$  are presented for each density range and data site.

### 6.2. For all sites

The results of University of Florida from Palacios (1977) showed the great influence of the liner removal on the measured

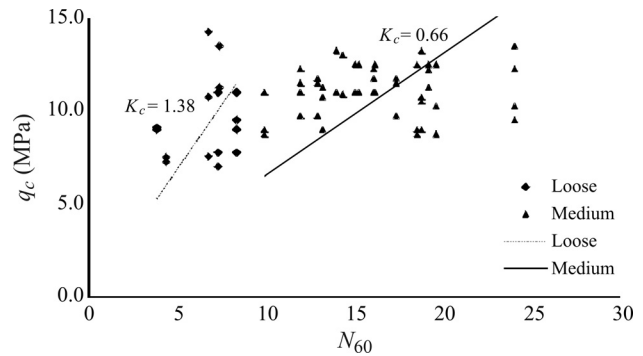


Figure 11 - University of Florida,  $K_c$  values for loose and medium sands.

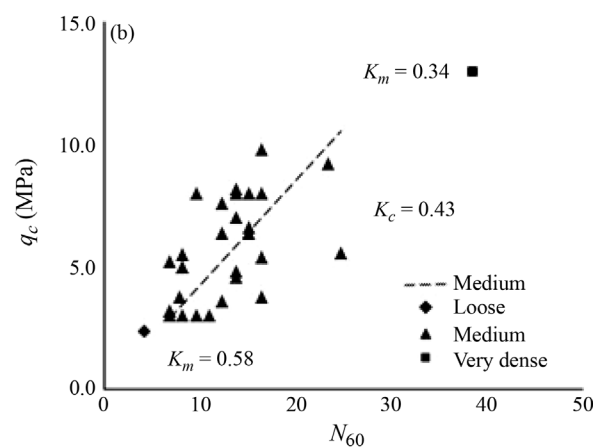
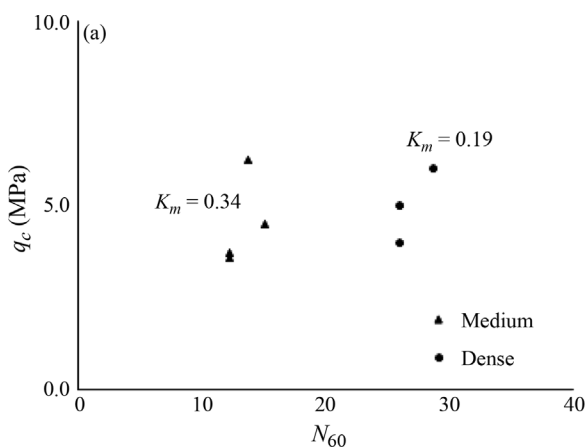


Figure 9 -  $K_m$  and  $K_c$  values for loose, medium, dense and very dense sands. (a) Port of Açú. (b) President Dutra, Queimados.

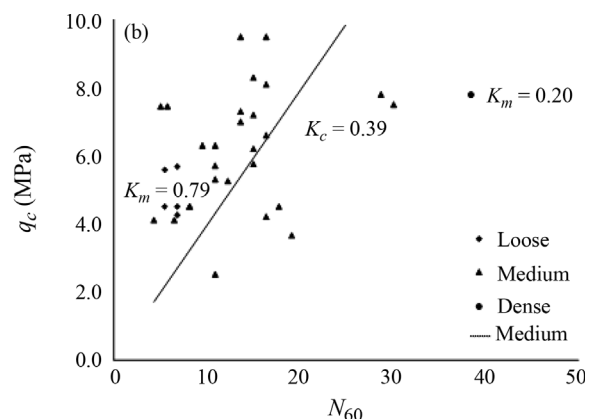
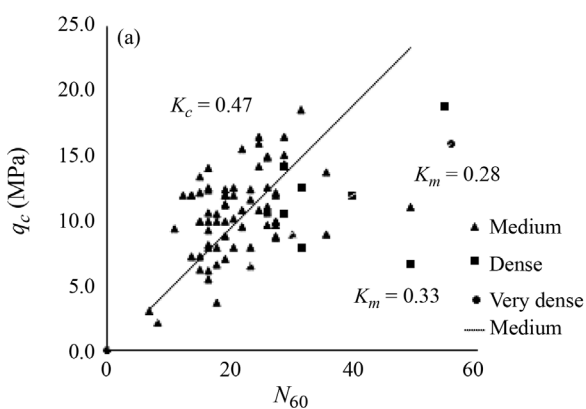
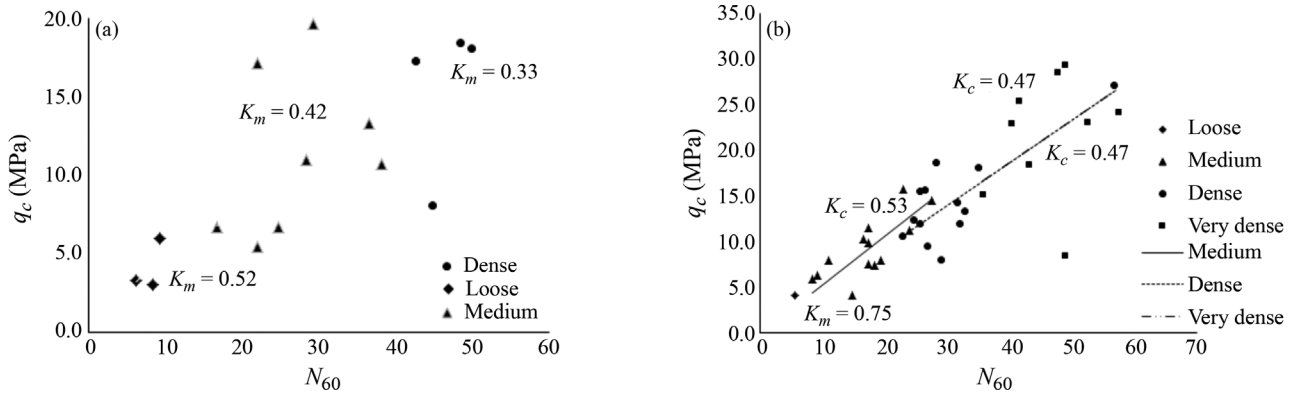
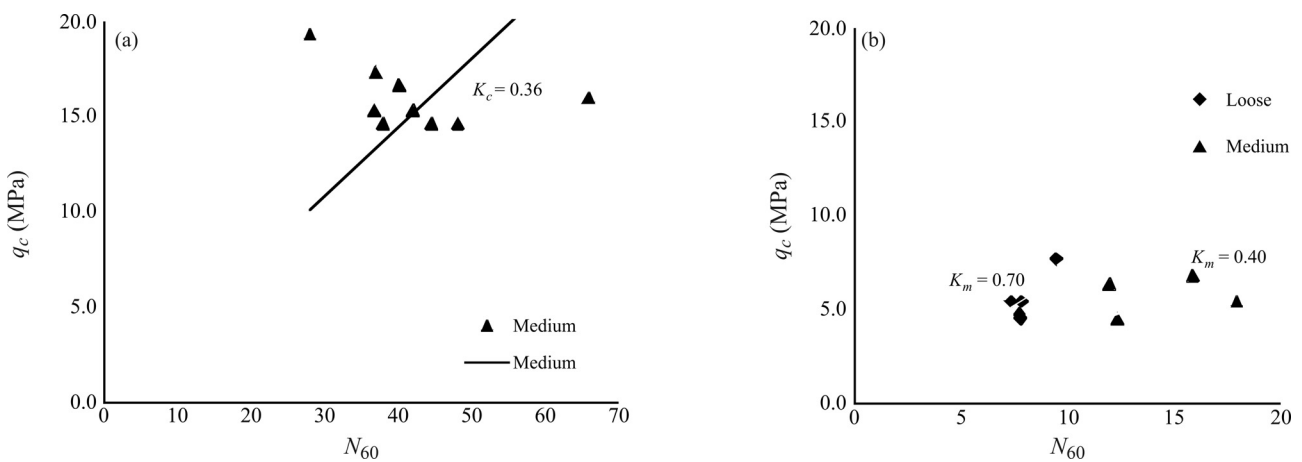


Figure 10 -  $K_m$  and  $K_c$  values for loose, medium, dense and very dense sands. (a) Industrial construction in the West Zone of Rio de Janeiro. (b) Banhado do Jacareí.



**Figure 12** -  $K_m$  and  $K_c$  values for loose, medium, dense and very dense sands. (a) Natural sand from San Francisco Bay. (b) Hydraulic Fill from San Francisco Bay.



**Figure 13** -  $K_c$  and  $K_m$  value for loose and medium sands. (a) Canlex, Mildred Lake. (b) Canlex, Massey.

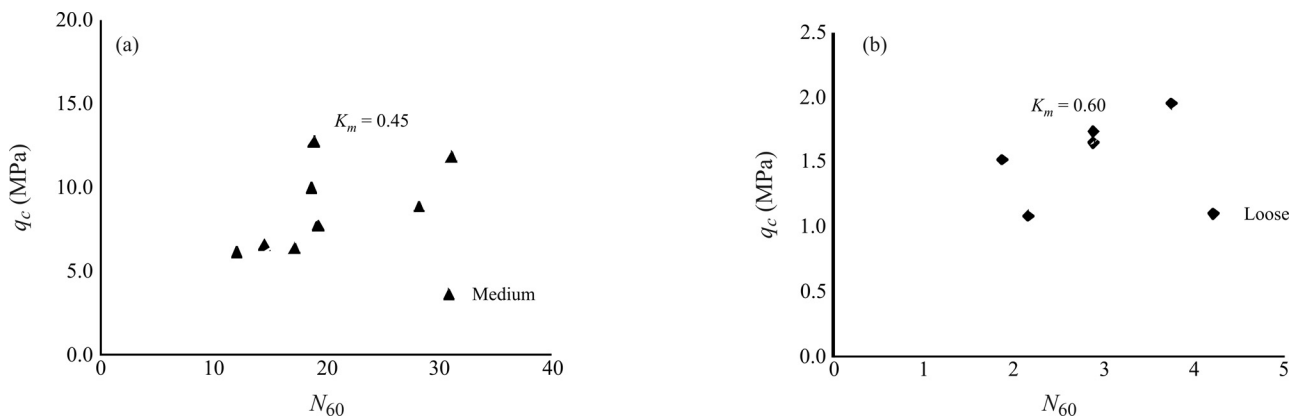


**Figure 14** -  $K_m$  value for loose and medium sands. (a) Canlex, Kidd. (b) Canlex, J-Pit.

$N$  values. In fact, Fig. 11 shows the higher values of  $K_c$  compared to the other data. For that reason, the results from University of Florida were excluded from the “all sites” database. The remaining data, including 255 data points ( $N_{60}$ ,  $q_c$ ) were grouped for a comprehensive analysis, with results summarized in Table 6. In this table, the numbers of data included in each correlation is also shown in parentheses. The last column in Table 6 corre-

sponds to the median  $K$  value, representing the value with 50% of the data with  $q_c/N_{60}$  inferior and 50% superior to it.

For very dense sands the data points are very few and the  $K_c$  value in Table 6 should be considered with caution. The corresponding Figs., 16 to 19, are shown below.

For the whole database an analysis was also made using a potential correlation, for all the density range. Based

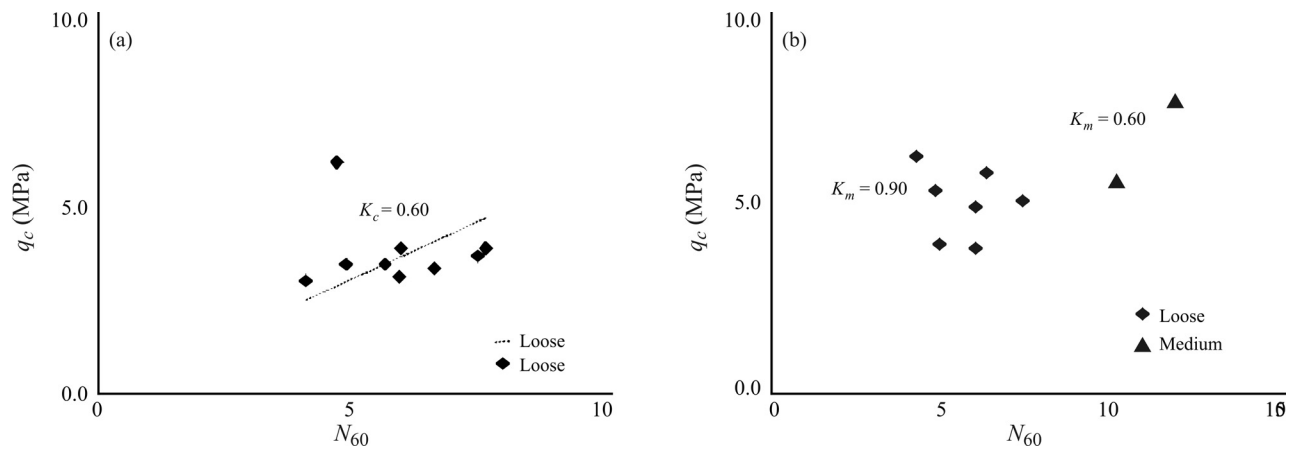


Figure 15 -  $K_c$  and  $K_m$  value for loose and medium sands. (a) Canlex, LL Dam. (b) Canlex, Hightmont Dam.

Table 6 - Analysis of the whole database.

Sand density	$K_c$ (MPa)	$K_m$ (MPa)	$K_{median}$ (MPa)
Loose (37)	0.69	0.72	0.66
Medium (179)	0.44	0.46	0.44
Dense (28)	0.36	0.37	0.37
Very dense (11)	0.40	0.44	0.43
Whole database (255)	0.41	0.51	0.50

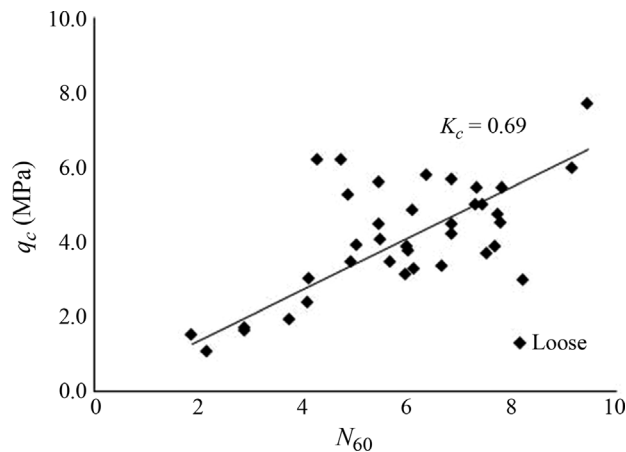


Figure 16 -  $K_c$  value for loose sands, whole database.

on 255 data points, the following expression has been obtained:

$$q_c = 1.06N_{60}^{0.71} \quad (10)$$

$q_c$  given in MPa, Figs. 20 and 21.

## 7. Data Interpretation

### 7.1. Relative density

The expectation of the authors, highlighted in the introduction, was that the SPT test is more influenced by the

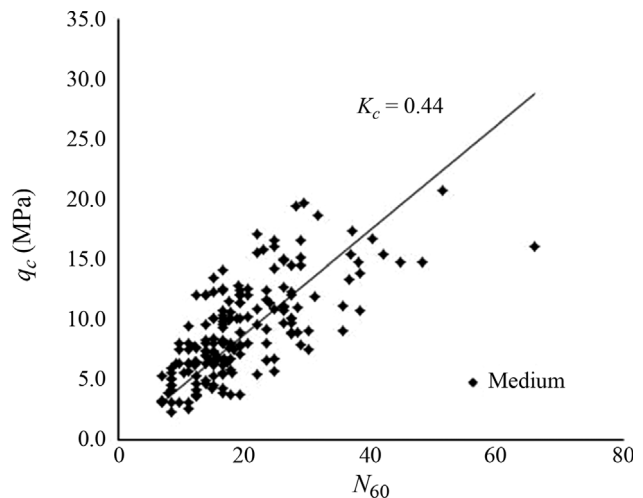


Figure 17 -  $K_c$  value for medium sands, whole database.

increases in shear stress (due to the unplugged behavior in sands in most of the length of the sampler) than by increases in normal stress. Given the high rate of loading, much higher than in the CPT, the SPT test can generate positive excess pore-pressures in loose sands and negative excess pore-pressures in dense sands. Thus, the  $N_{60}$  must be greater than it would be if the test was performed in drained conditions, in the case of dense sands, and lower in the case of loose sands. The same is not true for the values of  $q_c$  from the CPT (or CPTU). Therefore, the tendency would be for

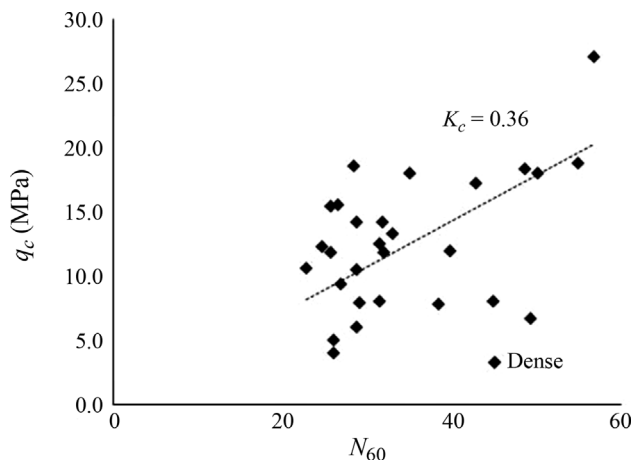


Figure 18 -  $K_c$  value for dense sands, whole database.

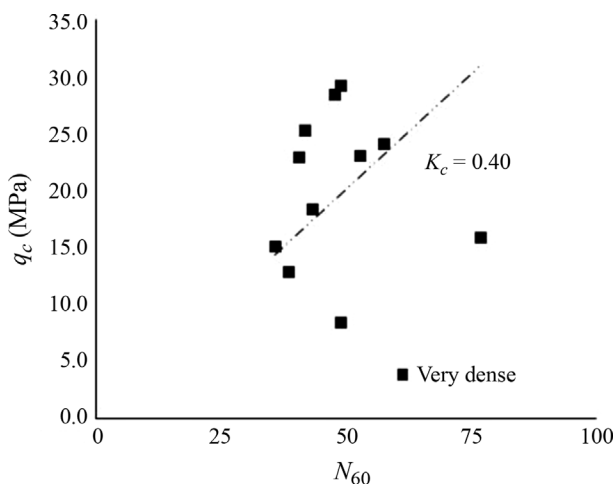


Figure 19 -  $K_c$  value for very dense sands, whole database.

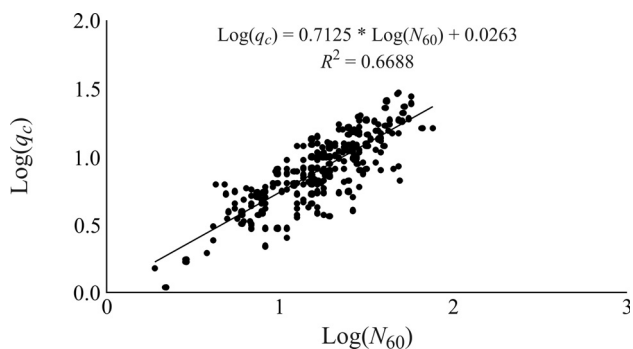


Figure 20 - Linearization of the potential correlation for the whole database.

higher values of the  $q_c/N_{60}$  in loose sands and lower values in dense sands for the same grain size.

Schmertmann (1976), as cited by Palacios (1977), found that the sampler penetration velocity could vary from about 4.60 m/s to 0.45 m/s, with an average of 1.20 m/s. On the other hand, the CPT penetration rate is 1.20 m/min, a factor of 60 slower. The author noted that in some soils, the

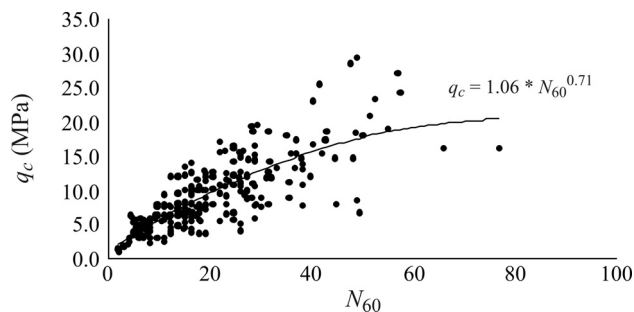


Figure 21 - Potential correlation for the whole database.

different pore-pressure effects due to these different rates of penetration will cause errors; the most serious are likely to occur in loose saturated sands, where the SPT might liquefy the soil, and yield a very low blow count in relation to  $q_c$ . That is precisely what Table 6 shows, not only for loose sands, but also for the other density ranges. The  $q_c/N_{60}$  ratio is strongly influenced by the density, and not only by the grain size as the existing correlations illustrated. Figures 9 to 15 have also shown that this behavior has been observed in all sites.

In fact, Table 6 shows that the value of  $K = q_c/N_{60}$  decreases with increasing density. It is interesting to note that this same behavior has been observed in all the deposits from the database, not only for  $K_c$  but also for  $K_m$ .

### 7.2. Liner removal

Only on the deposit of the University of Florida, whose data were obtained from Palacios (1977), the database included measurements of the SPT  $N$  values with the liner removed. In Brazil the use of the liner is not usual. Schmertmann (1979) observed that the liner removal reduces the relative importance of lateral friction, showing experimental results which confirmed his theory. It should be noted that the results of the  $q_c/N_{60}$  of the deposit studied by Palacios (1977), with the liner removed, were nearly twice those of the other deposits, where the liner was not removed. As the removal of the liner practically eliminates internal resistance, the value of  $N_{60}$  with the liner removed should be lower than that obtained with the use of the liner, with the sampling unplugged. Consequently the value of  $K$  should be greater, with the removal of the liner, when compared to the value of  $K$ , for the same soil. One should note that this was exactly what happened with the database of Palacios (1977), Fig. 11, when compared to the rest of the database analyzed in this paper.

### 7.3. The analysis of the global database

Excluding the results presented by Palacios (1977), which showed the great influence of the liner removal in the measured values of  $N_{60}$ , all the other results, including 255 data points ( $N_{60}, q_c$ ) were grouped for a global analysis, for each density range. The results, presented in Table 6, con-

firming the trend observed in individual deposits: a reduction of  $K$  has been observed with increasing soil density.

A value of  $K$  in MPa/blows/0.30 m close to 0.7 has been obtained for loose sands, 0.5 for medium sands, 0.4 for dense and very dense sands and 0.5 for the whole database, regardless its density.

#### 7.4. The potential correlation

From Eq. 10, and based on the average  $N_{60}$  of each density range suggested by the Brazilian Code, ABNT (2001), which presents 5 density ranges, one can obtain the values of Table 7.

The values obtained by the potential correlation expressed by Eq. 10 are close to those obtained with the linear correlation for each density range. The advantage of the potential correlation is that a single equation can represent the tendency of distinct  $K$  values for the various densities.

The authors suggest the direct use of the potential equation in future applications of correlations between the CPT and SPT in sands.

#### 7.5. The consequences for foundation design

The results obtained in the present paper have a great impact in foundation design. In fact, some design methods use direct correlations between the results of SPT and CPT. While in the traditional correlations the values of  $q_c/N_{60}$  depend solely on grain size, the results observed show that the density is of fundamental importance in correlations and should therefore be considered.

In particular, the analysis indicate that the value of  $K$  equal to 0.7 MPa/blows/0.30 m for sands, as commonly used in Brazil in the Aoki & Velloso (1975) method for estimating bearing capacity of piles, is more characteristic of loose sands. In fact, Danziger & Velloso (1995) found a  $K$  value of 0.5 MPa/blows/0.30 m for an extensive database covering all density ranges. It is interesting to note that the value of  $K$ , obtained from Table 6 for the overall analysis, is equal to 0.5 MPa/blows/0.30 m. The results presented herein also indicate that the value of  $K$  of 0.5 MPa/blows/0.30 m for sands found by Danziger & Velloso (1995) is consistent with the overall analysis shown in the present paper. In the case of a pile driven through a sedimentary low consistency deposit and embedded into an underlying dense sand, with a  $K$  value in the order of 0.4, according to

the present paper, the use of a  $K$  value of 0.7, as suggested in Aoki & Velloso (1975) method, would lead to a very unsafe design.

The comparison made also reinforces the experience that the tip resistance of the mechanical cone is similar to corresponding values of the electrical cone test (and piezocone). Indeed, the correlations established by Costa Nunes & Fonseca (1959), which served as the basis for Aoki & Velloso (1975) bearing capacity method and the correlations of Danziger & Velloso (1995), were both based on data from the mechanical cone, while the present correlations consider the CPT and piezocone, equivalent to the electrical cone.

### 8. Conclusions

The present paper presented the analysis of nearly 319 data points ( $q_c, N_{60}$ ) from cone tip resistance (mainly CPTU) and dynamic SPT in sands. The main purpose of the analysis was to investigate the influence of the relative density of the sand in the establishment of correlations between  $q_c$  and  $N_{60}$ . The results confirmed the author's initial expectation that relative density has a great influence on the correlations. The main conclusions are:

- i) The value of  $K = q_c/N_{60}$  decreases with increasing relative density of the sand. In the overall analysis, including the database from all sand deposits, an approximate value for  $K$ , in MPa/blows/0.30 m of 0.7 has been obtained for loose sands, 0.5 for medium sands and 0.4 for dense and very dense sands. The analysis with all database indicated 0.5 for  $K$  regardless the relative density.
- ii) Data from Palacios (1977), who registered the  $N_{60}$  with liner removed, indicated the same trend of reduction of the  $K$  value with relative density. However, the  $K$  values were almost twice those found in other deposits, where the  $N_{60}$  have been obtained without the liner removal.
- iii) The results have great impact on foundation design, as long as some design methods of bearing capacity estimation use  $q_c$  vs.  $N_{60}$  correlations. While traditional correlations of  $q_c/N_{60}$  are based solely on grain size, the results shown in the present paper illustrate that the relative density is of fundamental importance and should therefore be considered. The tests performed indicate that the value of  $K$  equal to 0.7 MPa/blows/0.30 m for sands, as used in Aoki & Velloso (1975) method for pile bearing capacity estimation

**Table 7** - Values of  $K$  obtained from Eq. (10).

Density	$N_{SPT}$	$N_{60}$	$q_c$ (MPa)	$K = q_c/N_{60}$
Loose	2 ( $\leq 4$ )		2.2	0.79
Low density	6 (5 to 8)		4.7	0.58
Medium	13 (9 to 18)	$1.37 \times N_{SPT}$	8.2	0.46
Dense	30 (19 to 40)		14.9	0.36
Very dense	> 40		> 18.0	< 0.34

is more characteristic of loose sands. For piles in sands with higher density, the use of smaller values of  $K$  is suggested. As an alternative, a potential correlation is presented, which allow with a single expression the estimation of  $q_c$  for the whole density range.

## References

- ABNT (2001) Soil - Simple Soil Boring for Soil Reconnaissance with SPT - Test Procedure (in Portuguese). NBR 6484.
- Aoki, N. & Velloso, D.A. (1975) An approximated method to estimate the bearing capacity of piles. Proc. of the V Panamerican Conference on Soil Mechanics and Foundation Engineering, Buenos Aires, v. 5, p. 367-377.
- Belincanta, A. (1985) Dynamic Energy on SPT: Results From a Theoretical-Experimental Investigation (in Portuguese). MSc Thesis, Escola Politécnica, Universidade de São Paulo, São Paulo, 217 pp.
- Belincanta, A. (1998) An Evaluation of the Factors Intervening in the Penetration Resistance in SPT (in Portuguese). DSc Thesis, Escola Politécnica, Universidade de São Paulo, São Paulo, 141 pp.
- Bezerra, R.L. (1996) Development of the Three Generation Piezocone at COPPE, UFRJ (in Portuguese). DSc Thesis, COPPE, UFRJ, Rio de Janeiro, 426 pp.
- Bussab, W. (1988) Quantitative Methods: Variance and Regression Analysis (in Portuguese). Atual LTDA, São Paulo, 147 pp.
- Cavalcante, E.H. (2002) Theoretical and Experimental Investigation on SPT (in Portuguese). DSc Thesis, COPPE, UFRJ, Rio de Janeiro, 430 pp.
- Costa Nunes, A.J. & Fonseca, A.M.M.C.C. (1959) Correlation Study Between the Cone Penetration Test and the SPT Sample Penetration (in Portuguese). Franki Brazil Report DT 37/59, Rio de Janeiro, 29 pp.
- Danziger, B.R. & Velloso, D.A. (1995) Correlations between the CPT and the SPT for some Brazilian soils. Proc. CPT'95, Linkoping, v. 2, pp. 155-160.
- Danziger, F.A.B.; Almeida, M.S.S.; Paiva, E.N.; Mello, L.G.F.S. & Danziger, B.R. (1998) The piezocone as a tool for soil stratification and classification. Proc. XI COBRAMSEG, Brasília, v. 2, pp. 917-926.
- Danziger, F.A.B. & Schnaid, F. (2000) Piezocone test procedure, recommendations and interpretation (in Portuguese). Proc. Conference SEFE IV/BIC I, São Paulo, v. 3, pp. 52-79.
- ISSMFE (1989) International Reference Test Procedure for the Standard Penetration Test (SPT). Report of the ISSMFE - TC 16 - Technical Committee on Penetration Testing of Soils, with Reference Test Procedures - CPT- SPT - DP - WST, pp. 17-19.
- Kayen, R.E.; Mitchell, J.K.; Seed, R.B.; Lodge, A.; Nishio, S. & Coutinho, R. (1992) Evaluation of SPT-CPT- and shear wave-based methods for liquefaction potential assessment using Loma Prieta data. Proc. 4th Japan-U.S. Workshop on Earthquake-Resistant Des. Of Life-line Fac. and Countermeasures for Soil Liquefaction, Honolulu, v. 1, pp. 117-204.
- Kasim, A.G.; Chu, M.Y. & Jensen, C.N. (1986) Field correlation of cone and standard penetration tests. J. of Geotechnical Engineering, ASCE, v. 112:3, p. 368-372.
- Kulhawy, F.H. & Mayne, P. W. (1990) Manual of Estimating Soil Properties for Foundation Design. Cornell University, Geotechnical Engineering Group, Research Project 1493-6, California, 308 pp.
- Meireles, E.B. (2002) Retrospective of the Fifteen Years of Piezocone Tests in Soft Clay at COPPE/UFRJ (in Portuguese). MSc. Thesis, COPPE, UFRJ, Rio de Janeiro, 210 pp.
- Mitchell, J.K. & Brandon, T.L. (1998) Analysis and use of CPT in earthquake and environmental engineering. Proc. Geotechnical Site Characterization, Atlanta, pp. 69-97.
- Odebrecht, E. (2003) Energy Measurements on SPT (in Portuguese). DSc Thesis, UFRGS, Porto Alegre, 230 pp.
- Odebrecht, E.; Schnaid, F.; Rocha, M.M. & Bernardes, G.P. (2005) Energy efficiency for standard penetration tests, J. of Geotechnical and Environmental Engineering, ASCE, v. 131:10, p.1252-1263.
- Oliveira, J.T.R. (1991) Piezocone Tests in a Soft Clay Deposit in Recife (in Portuguese). MSc. Thesis, COPPE, UFRJ, Rio de Janeiro, 187 pp.
- Palacios, A. (1977) Theory and Measurements of Energy Transfer During Standard Penetration Test Sampling. Ph.D. Thesis, University of Florida, Gainesville, 391 pp.
- Politano, C.F.; Danziger, F.A.B. & Danziger, B.R. (1998) CPT - SPT Correlations for some Brazilian residual soils. Proc. International Site Characterization ISC'98, Atlanta, pp. 907-912.
- Politano, C.F. (1999) CPT and SPT Correlations in Residual Soils (in Portuguese). MSc Thesis, COPPE, UFRJ, Rio de Janeiro, 210 pp.
- Politano, C.F.; Danziger, F.A.B. & Danziger, B.R. (2001) Correlations between results from CPT and SPT in residual soils (in Portuguese). Soils & Rocks, v. 24:1, p. 55-71.
- Robertson, P.K. & Campanella, R.G. (1983) Interpretation of cone penetration tests, part 1. Canadian Geotechnical Journal, v. 20:4, p. 718-745.
- Robertson, P.K.; Campanella, R.G. & Wightman, A. (1983) SPT CPT Correlations. ASCE Journal of Geot. Eng., v. 109:11, p. 1449-1459.
- Robertson, P.K.; Campanella, R.G.; Gillespie, D. & Greig, J. (1986) Use of piezometer cone data. Proc. In-Situ 86, Specialty Conf., ASCE, Blacksburg, pp. 1263-1280.
- Robertson, P.K. (1991) Soil classification using the cone penetration test: replay. Canadian Geotechnical Journal, v. 38:28, p. 176-178.

- Robertson, P.K.; Wride, C.E.; List, B.R.; Atukorala, U.; Biggar, K.W.; Byrne, P.M.; Campanella, R.G.; Cathro, D.C.; Chan, D.H.; Czajewski, K.; Finn, W.D.L.; Gu, W.H.; Hammamji, Y.; Hofmann, B.A.; Howie, J.A.; Hughes, J.; Imrie, A.S.; Konrad, J.M.; Küpper, A.; Law, T.; Lord, E.R.F.; Monahan, P.A.; Morgenstern, N.R.; Phillips, R.; Piché, R.; Plewes, H.D.; Scott, D.; Segó, D.C.; Sobkowicz, J.; Stewart, R.A.; Watts, B.D.; Woeller, D.J.; Youd, T.L. & Zavadni, Z. (2000) The CANLEX project: summary and conclusions. *Canadian Geotechnical Journal*, v. 37:3, p. 563-591.
- Schmertmann, J.H. (1976) Interpreting the dynamics of the standard penetration test. Final Report. Gainesville, Florida Department of Transportation – research division – Waldo Road, project D 636, No 32601. on Project D-636 to the Florida Department of Transportation, Research Division, Florida.
- Schmertmann, J.H. (1979) Statics of SPT. *ASCE Journal of the Geotechnical Engineering Division*, v. 105, p. 655-669.
- Schmertmann, J.H. (1978) Guidelines for Cone Penetration Test, Performance and Design. Federal Highway Administration, Report FHA - T5, Washington, pp. 78-209.
- Schnaid, F. (2000) Field Tests and its Applications to Foundation Engineering (in Portuguese). Oficina Textos, São Paulo, 189 pp.
- Seed, H.B. & Idriss, I.M. (1982) Ground Motions and Soil Liquefaction During Earthquakes. Earthquake Engineering Research Institute Monograph, Oakland, 134 pp.
- Senneset, K.; Sandven, R. & Janbu, N. (1989) The evaluation of soil parameters from piezocone tests. *Transportation Research Record*, No. 1235, Washington DC, pp. 24-37.
- Senneset, K. & Janbu, N. (1984) Shear strength parameters obtained from static cone penetration tests. *Proc. Symp. on Strength Testing of Marine Sediments: Laboratory and In-Situ Measurements*. ASTM 04-883000-38, San Diego, pp. 41-54.
- Souza, J.M.S. (2009) The Influence of Sand Density in the Correlations Between CPT and SPT Tests (in Portuguese). MSc Thesis, PGCIV, UERJ, Rio de Janeiro, 249 pp.
- Souza Pinto, C.S. (2000) Basic Course on Soil Mechanics (in Portuguese). 1ª ed. Oficina de Textos, São Paulo, v. 1, 247 pp.
- Terzaghi, K. & Peck, R.B. (1967) *Soil Mechanics in Engineering Practice*. John Willey & Sons, Inc., New York, 512 pp.
- Viana da Fonseca, A. & Coutinho, R.Q. (2008) Characterization of residual soils. Huang, An-Bin & Mayne, Paul (eds) Keynote Lecture, *Geotechnical and Geophysical Site Characterization*. Taylor & Francis, London, pp. 195-248.
- Wride, C.E.; Robertson, P.K.; Biggar, K.W.; Campanella, R.G.; Hofmann, J.M.O.; Hughes, J.M.O.; Kupper, A. & Woeller, D.J. (2000) Interpretation of in situ test results from the CANLEX sites. *Canadian Geotechnical Journal*, v. 37, p. 505-529.
- Youd, T.L.; Idriss, I.M.; Andrus, R.D.; Arango, I.; Castro, G.; Christian, J.T.; Dorby, R.; Finn, W.D.L.; Harder Jr., L.F.; Hynes, M.E.; Ishihara, K.; Koester, J.P.; Liao, S.S.C.; Marcuson III, W.F.; Martin, G.R.; Mitchell, J.K.; Moriwaki, Y.; Power, M.S.; Robertson, P.K.; Seed, R.B. & Stokoe II, K.H. (2001) Liquefaction resistance of soils: Summary Report from the 1996 NCEER and 1998 NCEER/ NSF Workshops on Evaluation of Liquefaction Resistance of Soils. *J. Geotechnical and Geoenvironmental Engineering, ASCE*, v. 127:10, p. 817-833.

# *SOILS and ROCKS*

An International Journal of Geotechnical and Geoenvironmental Engineering

## **Publication of**

**ABMS - Brazilian Association for Soil Mechanics and Geotechnical Engineering**

**SPG - Portuguese Geotechnical Society**

**Volume 35, N. 1, January-April 2012**

## **Author index**

Carvalho, C.A.B.	39, 51	Pacheco, M.	89
Conde de Freitas, A.	89	Pedrini, R.A.A.	75
Danziger, B.R.	89, 99	Portelinha, F.H.M.	51
Danziger, F.A.B.	99	Ribeiro, R.C.H.	31
Fontes, M.P.F.	39, 51	Sandroni, S.S.	31
Fontoura, S.A.B.	31	Sayão, A.S.F.J.	31, 65
Giacheti, H.L.	75	Sieira, A.C.C.F.	65
González de Vallejo, L.I.	1	Souza, J.M.S.	99
Lima, D.C.	39, 51	Velten, R.Z.	39
Oliveira, L.P.R.	75	Vitali, O.P.M.	75

# SOLOS MOLES?



# CPR<sup>®</sup>

## CONSOLIDAÇÃO PROFUNDA RADIAL

**O MAIS RÁPIDO E EFETIVO  
TRATAMENTO PARA SOLOS MOLES**

*Processo de adensamento de solo mole, eficientemente controlado, monitorando-se o grau de consolidação desejado.*



### Vantagens do CPR

- 100% específico para solos moles;
- Mobilização rápida;
- Ausência de transtornos à obra;
- Ampla gama de aplicações;
- Ausência de aterros, refugos e lama;
- Técnica não destrutiva;
- Alternativa super econômica, além de prazos extremamente curtos em relação à substituição de solos, aterros temporários, colunas granulares e estaqueamentos;
- Alcança profundidades de tratamento onde técnicas clássicas são limitadas;
- Acesso a locais restritos, limitados e difíceis, sem interferência com a rotina do cliente;
- Melhor custo benefício;
- Perfeito para reforço de fundação.

[www.engegraut.com.br](http://www.engegraut.com.br)

Simple drapery system



Surficial reinforcing systems

# ROCKFALL PROTECTION SYSTEMS

Rockfall protection systems have become a key element in the design and maintenance of infrastructure networks impacting directly on safety and necessitating thus, a new approach that encompasses the overall analysis of the rockfall structural system and not the individual components alone. The word "system", best describes the different structural components that interact with one another.

## MACCAFERRI

[www.maccafferri.com.br](http://www.maccafferri.com.br)

BRASIL

Phone: 55 (11) 4525-5000  
Fax: 55 (11) 4599-4275  
[maccafferri@maccafferri.com.br](mailto:maccafferri@maccafferri.com.br)  
[www.maccafferri.com.br](http://www.maccafferri.com.br)

PORTUGAL

Phone: (351) 263 858 030  
Fax: (351) 263 858 036  
[maccafferri@mail.telepac.pt](mailto:maccafferri@mail.telepac.pt)  
[www.maccafferri.pt](http://www.maccafferri.pt)



Rockfall barriers



Rockfall protection embankments

# SPECIALISTS IN GEOTECHNICAL IN-SITU TESTS AND INSTRUMENTATION

## GEOTECHNICAL SERVICES (onshore and offshore)

### IN-SITU TESTS

Seismic CPT  
Cone Penetration Testing Undrained-CPTu (cordless system)  
Vane Shear Testing (electrical apparatus)  
Pressuremeter Testing (Menard)  
Flat Dilatometer Test-DMT (Machetti)  
Standard Penetration Test-SPT-T

### INSTRUMENTATION

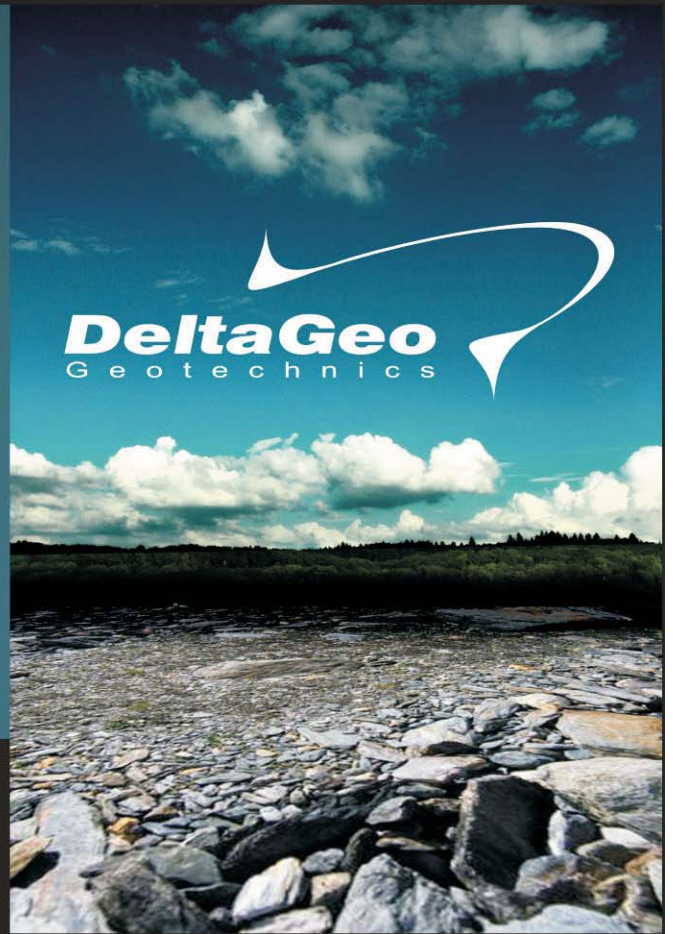
Instrumentation, installation and direct import  
Routine Monitoring  
Operation and Maintenance  
Engineering analyses  
Consultancy, design & geotechnical engineering services

### SAMPLING

Soil sampling and monitoring  
Groundwater sampling and monitoring  
Field and laboratory testing

### ENVIRONMENTAL

Environmental Services  
Soil and groundwater sampling and monitoring  
Field and laboratory testing



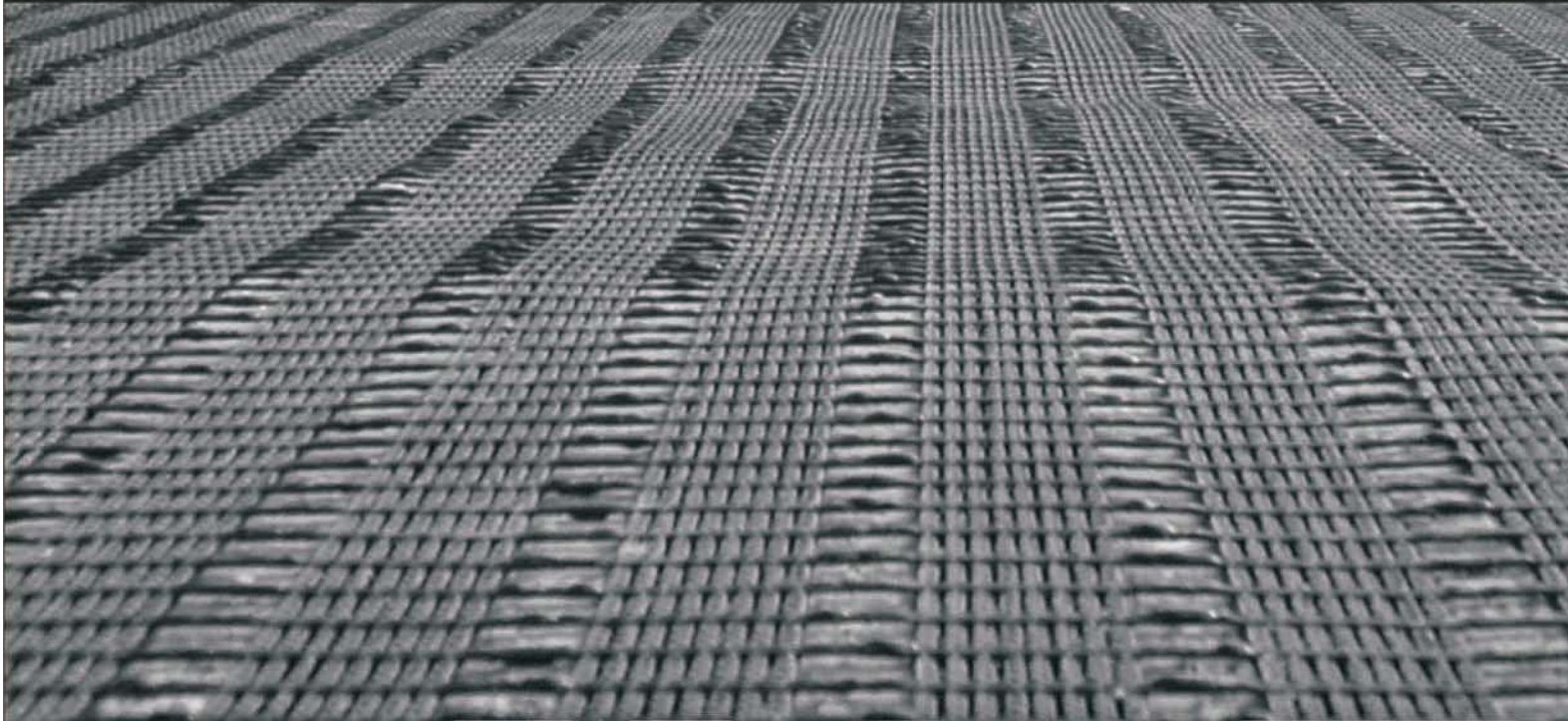
**0800 979 3436**

**São Paulo: +55 11 8133 6030**

**Minas Gerais: +55 31 8563 2520 / 8619 6469**

**[www.deltageo.com.br](http://www.deltageo.com.br) [deltageo@deltageo.com.br](mailto:deltageo@deltageo.com.br)**

» We're known for our strength «



**Fortrac®**

High tensile stiffness geogrid  
for soil reinforcement



**HaTelit® C**

Flexible grid for  
asphalt reinforcement



**Fornit®**

Flexible geogrid for  
base reinforcement



**HaTe®**

Fabric for separation,  
stabilization and filtration



**Ringtrac®**

Ring reinforcement for granular  
columns on soil improvement



**Stabilenka®**

High strength woven  
geosynthetic for soil reinforcement



**NaBento®**

Geosynthetic clay liner  
for sealing



**Incomat®**

Construction system for  
slope and bed protection

# **HUESKER**  
Engineering with Geosynthetics



**GEOLOGY - GEOTECHNICS - SUPERVISION OF GEOTECHNICAL WORKS**



**EMBANKMENT DAMS - UNDERGROUND WORKS - RETAINING STRUCTURES**



**SPECIAL FOUNDATIONS - SOIL IMPROVEMENT - GEOMATERIALS**

**CENOR GROUP**

PORTUGAL, ANGOLA, ALGERIA, MOROCCO, ROMANIA, TIMOR

**CENOR GEO** - Engenharia Geotécnica, Lda.

Rua das Vigias, 2. Piso 1 Parque das Nações 1990-506 LISBOA . PORTUGAL  
T. +351.218 437 300 F. +351.218 437 301 cenorgeo@cenor.pt

ISO 9001  
BUREAU VERITAS  
Certification





- > **Prospecção Geotécnica**  
*Site Investigation*
- > **Consultoria Geotécnica**  
*Geotechnical Consultancy*
- > **Obras Geotécnicas**  
*Ground Treatment-Construction Services*
- > **Controlo e Observação**  
*Field Instrumentation Services and Monitoring Services*
- > **Laboratório de Mecânica de Solos**  
*Soil and Rock Mechanics Laboratory*

Certificada ISO 9001 por



Parque Oriente, Bloco 4, EN10  
2699-501 Bobadela LRS  
Tel. 21 995 80 00  
Fax. 21 995 80 01  
e.mail: mail@geocontrole.pt  
www.geocontrole.pt

  
**Geocontrole**  
Geotecnia e Estruturas de Fundação SA



**COBA**



## GEOLOGY AND GEOTECHNICS

Hydrogeology • Engineering Geology • Rock Mechanics • Soil Mechanics • Foundations and Retaining Structures • Underground Works • Embankments and Slope Stability  
Environmental Geotechnics • Geotechnical Mapping



- Water Resources Planning and Management
- Hydraulic Undertakings
- Electrical Power Generation and Transmission
- Water Supply Systems and Pluvial and Wastewater Systems
- Agriculture and Rural Development
- Road, Railway and Airway Infrastructures
- Environment
- Geotechnical Structures
- Cartography and Cadastre
- Safety Control and Work Rehabilitation
- Project Management and Construction Supervision



### PORTUGAL

CENTER AND SOUTH REGION  
Av. 5 de Outubro, 323  
1649-011 LISBOA  
Tel.: (351) 210125000, (351) 217925000  
Fax: (351) 217970348  
E-mail: coba@coba.pt  
www.coba.pt

Av. Marquês de Tomar, 9, 6°.  
1050-152 LISBOA  
Tel.: (351) 217925000  
Fax: (351) 213537492

### NORTH REGION

Rua Mouzinho de Albuquerque, 744, 1°.  
4450-203 MATOSINHOS  
Tel.: (351) 229380421  
Fax: (351) 229373648  
E-mail: engico@engico.pt

### ANGOLA

Praceta Farinha Leitão, edifício nº 27, 27-A - 2º Dto  
Bairro do Maculusso, LUANDA  
Tel./Fax: (244) 222338 513  
Cell: (244) 923317541  
E-mail: coba-angola@netcabo.co.ao

### MOZAMBIQUE

Pestana Rovuma Hotel. Centro de Escritórios.  
Rua da Sé nº114. Piso 3, MAPUTO  
Tel./Fax: (258) 21 328 813  
Cell: (258) 82 409 9605  
E-mail: coba.mz@tdm.co.mz

### ALGERIA

09, Rue des Frères Hocine  
El Biar - 16606, ARGEL  
Tel.: (213) 21 922802  
Fax: (213) 21 922802  
E-mail: coba.alger@gmail.com

### BRAZIL

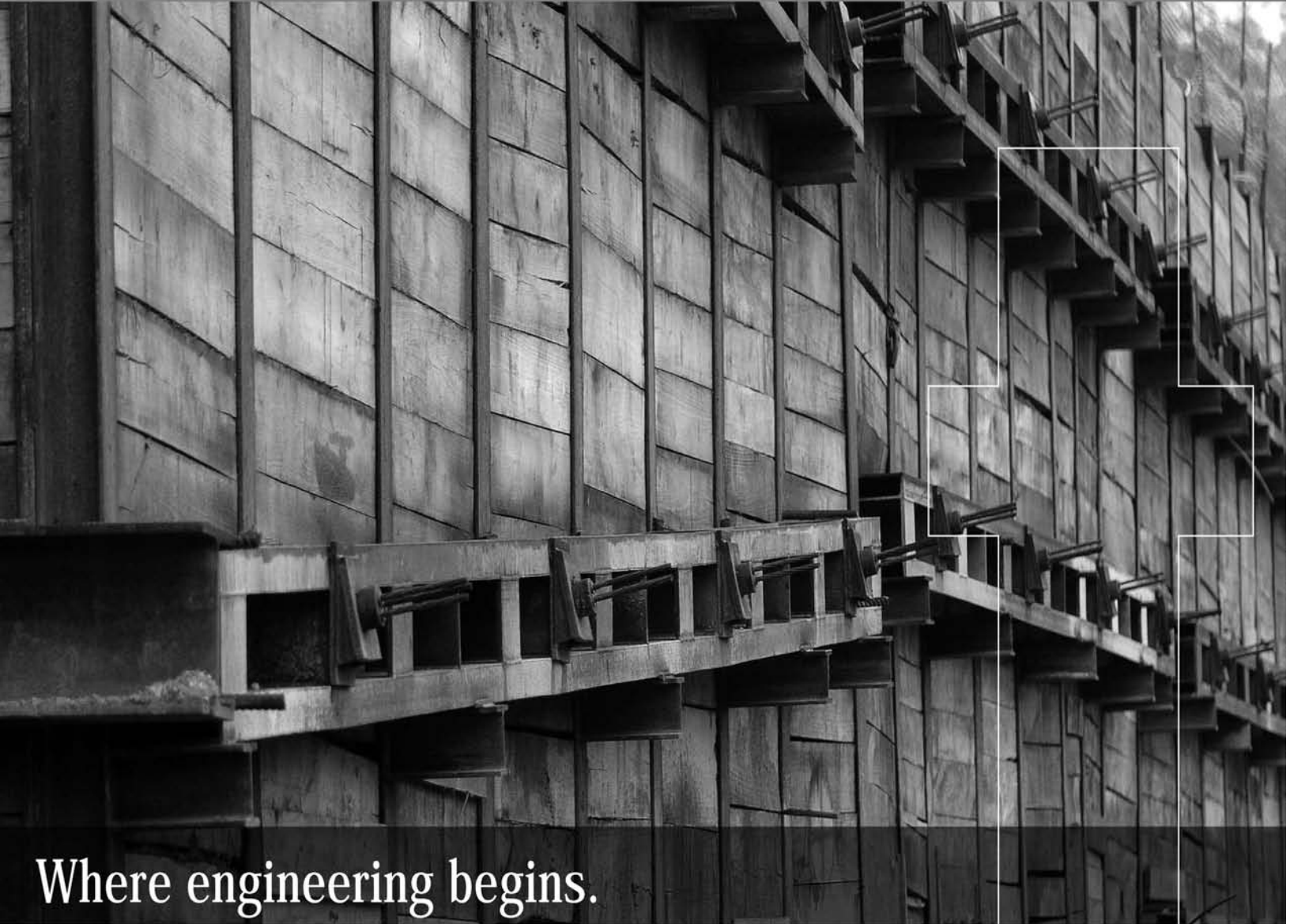
Rio de Janeiro  
COBA Ltd. - Rua Bela 1128  
São Cristóvão  
20930-380 Rio de Janeiro RJ  
Tel.: (55 21) 351 50 101  
Fax: (55 21) 258 01 026

### Fortaleza

Av. Senador Virgílio Távora 1701, Sala 403  
Aldeota - Fortaleza CEP 60170 - 251  
Tel.: (55 85) 3261 17 38  
Fax: (55 85) 3261 50 83  
E-mail: coba@esc-te.com.br

### UNITED ARAB EMIRATES

Corniche Road - Corniche Tower - 5th Floor - 5B  
P. O. Box 38360 ABU DHABI  
Tel.: (971) 2 627 0088  
Fax: (971) 2 627 0087



## Where engineering begins.

Behind a great work there's always a great company.

tgeotecnia enters in national and Spanish market with a wide range of solutions, with state of the art technology and qualified means necessary to engage geotechnical studies, projects and works.

Currently, tgeotecnia is specialised in all kinds of work, from geologic-geotechnical studies and project development to slope stabilisation, reinforcement, soil treatment and special foundations.

The works carried out and client satisfaction, as well as the growing number of projects, are the proof that it is worth making innovation the lever of development.

tgeotecnia  
In the origin of construction

a dst group company

ph + 351 253 307 285 | geral@tgeotecnia.pt | www.dstsgps.com



## Geotechnics and Foundation Engineering



**HEAD OFFICE**  
Edifício Edifer  
Estrada do Seminário, 4 - Alfragide  
2610 - 171 Amadora - PORTUGAL  
Tel. 00 351 21 475 90 00 / Fax 00 351 21 475 95 00

**Madrid**  
Calle Rodríguez Marín, Nº 88 1º Dcha  
28016 Madrid - ESPANHA  
Tel. 00 34 91 745 03 64 / Fax 00 34 91 411 31 87

**Angola**  
Rua Alameda Van-Dúnem, n.º 265 R/c  
Luanda - ANGOLA  
Tel. 00 244 222 443 559 / Fax 00 244 222 448 843

**Porto**  
Rua Eng. Ferreira Dias, nº 161 2º Andar  
4100-247 Porto - PORTUGAL  
Tel. 00 351 22 616 74 60 / Fax 00 351 22 616 74 69

**Barcelona**  
Calle Comte d' Urgell, 204-208 6.º A  
08036 Barcelona - ESPANHA  
Tel. 00 34 93 419 04 52 / Fax 00 34 93 419 04 16

**Madeira**  
Rampa dos Piornais, n.º 5 - Sala 1  
9000-248 Funchal - PORTUGAL  
Tel. 00 351 291 22 10 33 / Fax 00351 291 22 10 34

**Sevilha**  
Polígono Industrial de Guadalquivir, C/ Artesania, 3  
41120 Gelves (Sevilla) - ESPANHA  
Tel. 00 34 955 762 833 / Fax 00 34 955 76 11 75



Geotechnic and Rehabilitation

**TEIXEIRA DUARTE**  
ENGENHARIA E CONSTRUÇÕES, S.A.

• **Head Office**  
Lagoas Park – Edifício 2  
2740-265 Porto Salvo - Portugal  
Tel.: [+351] 217 912 300  
Fax: [+351] 217 941 120/21/26

• **Angola**  
Alameda Manuel Van Dunen 316/320 - A  
Caixa Postal 2857 - Luanda  
Tel.: [+34] 915 550 903  
Fax: [+34] 915 972 834

• **Algeria**  
Parc Miremont – Rua A, Nº136 - Bouzareah  
16000 Alger  
Tel.: [+213] 219 362 83  
Fax: [+213] 219 365 66

• **Brazil**  
Rua Iguatemi, nº488 – 14º - Conj. 1401  
CEP 01451 - 010 - Itaim Bibi - São Paulo  
Tel.: [+55] 112 144 5700  
Fax: [+55] 112 144 5704

• **Spain**  
Avenida Alberto Alcocer, nº24 – 7º C  
28036 Madrid  
Tel.: [+34] 915 550 903  
Fax: [+34] 915 972 834

• **Mozambique**  
Avenida Julyus Nyerere, 130 – R/C  
Maputo  
Tel.: [+258] 214 914 01  
Fax: [+258] 214 914 00

## Instructions to Authors

### Category of the Papers

*Soils and Rocks* is the scientific journal edited by the Brazilian Association for Soil Mechanics and Geotechnical Engineering (ABMS) and the Portuguese Geotechnical Society (SPG). The journal is intended to the divulgation of original research works from all geotechnical branches.

The accepted papers are classified either as an Article paper, a Technical Note, a Case Study, or a Discussion according to its content. An article paper is an extensive and conclusive dissertation about a geotechnical topic. A paper is considered as a technical note if it gives a short description of ongoing studies, comprising partial results and/or particular aspects of the investigation. A case study is a report of unusual problems found during the design, construction or the performance of geotechnical projects. A case study is also considered as the report of an unusual solution given to an ordinary problem. The discussions about published papers, case studies and technical notes are made in the Discussions Section.

When submitting a manuscript for review, the authors should indicate the category of the manuscript, and is also understood that they:

- assume full responsibility for the contents and accuracy of the information in the paper;
- assure that the paper has not been previously published, and is not being submitted to any other periodical for publication.

### Manuscript Instructions

Manuscripts must be written in English. The text is to be typed in a word processor (MS Word or equivalent), using ISO A4 page size, left, right, top, and bottom margins of 25 mm, Times New Roman 12 font, and line spacing of 1.5. All lines and pages should be numbered. The text should be written in the third person.

The first page of the manuscript is to include the title of the paper in English, followed by the names of the authors with the abbreviation of the most relevant academic title. The affiliation, address and e-mail is to be indicated below each author's name. An abstract of 200 words is to be written in English after the author's names. A list with up to six keywords at the end of the abstract is required.

Although alteration of the sequence and the title of each section may be required, it is suggested that the text contains the following sections: Introduction, Material and Methods, Results, Discussions, Conclusion, Acknowledgements, References and List of Symbols. A brief description of each section is given next.

**Introduction:** This section should indicate the state of the art of the problem under evaluation, a description of the problem and the methods undertaken. The objective of the work is to be clearly presented at the end of the section.

**Materials and Methods:** This section should include all information needed to the reproduction of the presented work by other researchers.

**Results:** In this section the data of the investigation should be presented in a clear and concise way. Figures and tables should not repeat the same information.

**Discussion:** The analyses of the results should be described in this section. **Conclusions:** The text of this section should be based on the presented data and in the discussions.

**Acknowledgements:** If necessary, concise acknowledgements should be written in this section.

**References:** References to other published sources are to be made in the text by the last name(s) of the author(s), followed by the year of publication, similarly to one of the two possibilities below:

“while Silva & Pereira (1987) observed that resistance depended on soil density” or “It was observed that resistance depended on soil density (Silva & Pereira, 1987).”

In the case of three or more authors, the reduced format must be used, e.g.: Silva *et al.* (1982) or (Silva *et al.*, 1982). Two or more citations belonging to the same author(s) and published in the same year are to be distinguished with small letters, e.g.: (Silva, 1975a, b, c.). Standards must be cited in the text by the initials of the entity and the year of publication, e.g.: ABNT (1996), ASTM (2003).

Full references shall be listed alphabetically at the end of the text by the first author's last name. Several references belonging to the same author shall be cited chronologically. Some examples are listed next:

Papers: Bishop, A.W. & Blight, G.E. (1963) Some aspects of effective stress in saturated and unsaturated soils. *Géotechnique*, v. 13:2, p. 177-197.

Books: Lambe, T.W & Whitman, R.V. (1979) *Soil Mechanics*, SI Version, 2<sup>nd</sup> ed. John Wiley & Sons, New York, p. 553.

Book with editors: Sharma, H.D.; Dukes, M.T. & Olsen, D.M. (1990) *Field measurements of dynamic moduli and Poisson's ratios of refuse and underlying soils at a landfill site*. Landva A. & Knowles, G.D. (eds) *Geotechnics of Waste Fills - Theory and Practice*, American Society for Testing and Materials - STP 1070, Philadelphia, p. 57-70.

Proceedings (printed matter or CD-ROM): Jamiolkowski, M.; Ladd, C.C.; Germaine, J.T & Lancellotta, R. (1985) *New developments in field and laboratory testing of soils*. Proc. 11<sup>th</sup> Int. Conf. on Soil Mech. and Found. Engr., ISSMFE, San Francisco, v. 1, pp. 57-153. (specify if CD – ROM)

Thesis and dissertations: Lee, K.L. (1965) *Triaxial Compressive Strength of Saturated Sands Under Seismic Loading Conditions*. PhD Dissertation, Department of Civil Engineering, University of California, Berkeley, 521 p.

Standards: ASTM (2003) *Standard Test Method for Particle Size Analysis of Soils - D 422-63*. ASTM International, West Conshohocken, Pennsylvania, USA, 8 p.

Internet references: *Soils and Rocks* available at <http://www.abms.com.br>.

On line first publications must also bring the digital object identifier (DOI) at the end.

Figures shall be either computer generated or drawn with India ink on tracing paper. Computer generated figures must be accompanied by the corresponding digital file (.tif, .jpg, .pcx, etc.). All figures (graphs, line drawings, photographs, etc.) shall be numbered consecutively and have a caption consisting of the figure number and a brief title or description of the figure. This number should be used when referring to the figure in text. Photographs should be black and white, sharp, high contrasted and printed on glossy paper.

Tables shall be numbered consecutively in Arabic and have a caption consisting of the table number and a brief title. This number should be used when referring to the table in text. Units should be indicated in the first line of the table, below the title of each column. Abbreviations should be avoided. Column headings should not be abbreviated. When applicable, the units should come right below the corresponding column heading. Any necessary explanation can be placed as footnotes.

Equations shall appear isolated in a single line of the text. Numbers identifying equations must be flush with the right margin. International System (SI) units are to be used. The symbols used in the equations shall be listed in the List of Symbols. It is recommended that the used symbols

be in accordance with Lexicon in 8 Languages, ISSMFE (1981) and the ISRM List of Symbols.

The text of the submitted manuscript (including figures, tables and references) intended to be published as an article paper or a case history should not contain more than 30 pages formatted according to the instructions mentioned above. Technical notes and discussions should have no more than 15 and 8 pages, respectively. Longer manuscripts may be exceptionally accepted if the authors provide proper explanation for the need of the required extra space in the cover letter.

#### **Discussion**

Discussions must be written in English. The first page of a discussion paper should contain:

- The title of the paper under discussion in the language chosen for publication;
- Name of the author(s) of the discussion, followed by the position, affiliation, address and e-mail. The discussor(s) should refer himself (herself, themselves) as “the discussor(s)” and to the author(s) of the paper as “the author(s)”.

Figures, tables and equations should be numbered following the same sequence of the original paper. All instructions previously mentioned for the preparation of article papers, case studies and technical notes also apply to the preparation of discussions.

#### **Editorial Review**

Each paper will be evaluated by reviewers selected by the editors according to the subject of the paper. The au-

thors will be informed about the results of the review process. If the paper is accepted, the authors will be required to submit a version of the revised manuscript with the suggested modifications. If the manuscript is refused for publication, the authors will be informed about the reasons for rejection. In any situation comprising modification of the original text, classification of the manuscript in a category different from that proposed by the authors, or refusal for publication, the authors can reply presenting their reasons for disagreeing with the reviewers' comments

#### **Submission**

The author(s) must submit for review:

1. A hard copy of the manuscript to Editors - Soils and Rocks, Av. Prof. Almeida Prado, 532 – IPT, Prédio 54 – DEC/ABMS, 05508-901 - São Paulo, SP, Brazil. The first page of the manuscript should contain the identification of the author(s), or

2. The digital file of the manuscript, omitting the authors' name and any information that eventually could identify them, should be sent to **abms@ipt.br**. The following must be written in the subject of the e-mail message: “*Paper submitted to Soils and Rocks*”. The authors' names, academic degrees and affiliations should be mentioned in the e-mail message. The e-mail address from which the digital file of the paper was sent will be the only one used by the editors for communication with the corresponding author.

#### **Follow Up**

Authors of manuscripts can assess the status of the review process at the journal website ([www.soilsandrocks.com.br](http://www.soilsandrocks.com.br)) or by contacting the ABMS secretariat.

**Volume 35, N. 1, January-April 2012****Table of Contents****XXVII MANUEL ROCHA LECTURE**

*Design with Geo-Hazards: An Integrated Approach from Engineering Geological Methods*  
L.I. González de Vallejo

1

**ARTICLES**

*Considerations on the Probability of Failure of Mine Slopes*

A.S.F.J. Sayão, S.S. Sandroni, S.A.B. Fontoura, R.C.H. Ribeiro

31

*Electroosmosis in the Remediation of Tropical Soils Contaminated with Cadmium:  
Effect of the Incubation Time*

R.Z. Velten, D.C. Lima, M.P.F. Fontes, C.A.B. Carvalho

39

*Modification of a Lateritic Soil with Lime and Cement:  
An Economical Alternative for Flexible Pavement Layers*

F.H.M. Portelinha, D.C. Lima, M.P.F. Fontes, C.A.B. Carvalho

51

*Evaluation of Direct Shear Tests on Geogrid Reinforced Soil*

A.S.F.J. Sayão, A.C.C.F. Sieira

65

*Developing a System for Down-Hole Seismic Testing Together with the CPTU*

O.P.M. Vitali, R.A.A. Pedrini, L.P.R. Oliveira, H.L. Giacheti

75

*Estimating Young Moduli in Sands from the Normalized N60 Blow Count*

A. Conde de Freitas, M. Pacheco, B.R. Danziger

89

*The Influence of the Relative Density of Sands in SPT and CPT Correlations*

J.M.S. Souza, B.R. Danziger, F.A.B. Danziger

99